PLUME AND PROBLEMS OF DEEP SOURCES OF ALKALINE MAGMATISM

Плюмы и глубинные источники щелочного магматизма

KHABAROVSK
2003

Russian Academy of Sciences
Vinogradov Institute of Geochemistry
Siberian Branch of RAS
Institute of Tectonics and Geophysics
Far East Branch of RAS
Russian Foundation of Basic Research

PLUMES AND PROBLEMS OF DEEP SOURCES OF ALKALINE MAGMATISM

(Плюмы и проблема глубинных источников щелочного магматизма)

PROCEEDING
of International Workshop
«Plumes and problems of deep sources of alkaline magmatism»

Edited by Dr. N.V. Vladykin

KHABAROVSK

2003

UDK 552.33+ 552.32

Plumes and problems of deep sources of alkaline magmatism. Proceedings of the Interntional Conference. Khabarovsk. Publishing House of the Irkutsk State Technical University, 2003, 200 p., ISBN 5-8038-025-4.

The proceedings of the International Seminar, which will be held at the Institute of tectonics and geophysics, Far East Branch of RAS, Khabarovsk are devoted to complicated formation of alkaline rocks. The invited reports consider the features of the alkaline and kimberlite magmatism. Detailed characteristics of the alkaline magmatism and magmatic sources are given for different provinces. The book provides new data on Aldan and Indian benstonite carbonatites, carbonatite complex of the Kovdor massif (Kola Peninsula), alkaline volcanics of Kamchatka, Primor'e and Japan. Experimental data on layering in alkaline systems are of great importance. A particular attention is given to studies of deep xenoliths and PT-conditions of their crystallization from kimberlite pipes "Yubileinaya", "Zarnitsa" (Siberia), Winter Shore (Arkhangelsk province), alkaline basalts (Japan) and of the significance of plume and plate tectonics in their formation.

The book is of great importance for petrologists, geochemists, and specialists studying deep alkaline and kimberlite magmatism, students and teaching staff of universities.

Published following the decision of the Scientific Council of Vinogradov Institute of Geochemistry, SB RAS

Editor: Prof. N.V. Vladykin

Reviewers: Prof. O.M. Glazunov and Prof. A.I. Al'mukhamedov
Original-model: A.B. Perepelov

ID№ 06560 26.12.01

Irkutsk State Technical University
664074, Irkutsk, Lermontov str. 83

ISBN 5-8038-025-4

TABLE OF CONTENTS

FOREWORD

Alkaline rocks are unique formation on the Earth. They have been of particular interest for researchers. Large Nb, Ta, Zr, Y, TR, Cu, P deposits, gemstones of charoite, Cr-diospide, dianite are associated with alkaline rocks. The Australian lamproites are connected with diamonds. The complicated processes of their formation provoked multi-year scientific disputes, which are still the case. The new methods of investigations provided much information on the composition of alkaline rocks. The data on geochemistry of isotopes confirm the mantle sources of the substance of alkaline rocks. The new stage of the plume tectonics deepened the interest of scientists to the alkaline rocks from the viewpoint of plate tectonics. The deep-seated Earth's geodynamics can be interpreted using these data.

The above problems were discussed during the 1st International Seminar "Alkaline magmatism and problems of the mantle sources", held at the Institute of Geochemistry, SB RAS (Irkutsk, 2001) and the 2nd seminar held at the Far East Geological Institute, Far East Branch of RAS (Vladivostok, 2002). The 3rd Seminar to be taken place at the Institute of Tectonics and Geophysics (Khabarovsk) will be also devoted to these problems.

This book includes the invited reports of the International Seminar "Plumes and problems of deep sources of alkaline magmatism" in English. The proceedings of the seminar will be published in Russian.

The invited reports consider the features of the alkaline and kimberlite magmatism. Detailed characteristics of the alkaline magmatism and magmatic sources are given for different provinces. The book provides new data on Aldan and Indian benstonite carbonatites, carbonatite complex of the Kovdor massif (Kola Peninsula), alkaline volcanics of, Primor'e, Japan and ultrapotassic rhyolites of Kamchatka. Experimental data on layering in alkaline systems are of great importance. A particular attention is given to studies of deep xenoliths and PT-conditions of their crystallization from kimberlite pipes "Yubileinaya", "Zarnitsa" (Siberia), Winter Shore (Arkhangelsk province), alkaline basalts (Japan) and of the significance of plume and plate tectonics in their formation.

The book is of great importance for petrologists, geochemists, and specialists studying deep alkaline and kimberlite magmatism.

Chief Editor Dr. N.V. Vladykin

Kimberlite xenoliths as evidence for subducted oceanic crust in the formation of the Siberian craton

Spetsius Z.V.[1] and Taylor L.A.[2]

[1]Institute of Diamond Industry, ALROSA Co. Ltd., Mirny, Russia,
E-mail: spetsius@yna.alrosa-mir.ru
[2]Planetary Geosciences Institute, Dept. of Earth & Planetary Sciences, Univ. of Tennessee, Knoxville, TN 37996, USA, E-mail: lataylor@utk.edu

The carbon isotopic ratios of diamonds from kimberlites reveal that many diamonds have $\delta^{13}C$ values distinct from typical mantle. The reasonable explanation for the high and very low $\delta^{13}C$ values involves an ultimate source from the crust. This crustal source is also supported by sulfur isotopes of sulfide diamond inclusions. In addition, oxygen isotopic data suggest that man, perhaps all, eclogite xenoliths, especially the group C eclogites, are representatives of subducted crust. The presence and preservation of coesite in eclogites from Udachnaya and other kimberlite pipes of Yakutia provides evidence of the development of the sub-continental lithospheric mantle (SCLM) by subduction of ancient oceanic crust.

Oxygen isotope data, obtained from more than 100 clean garnet mineral separates and about 20 clinopyroxene, by laser-fluorination techniques also provide additional evidence for the subduction theory. Cpx was analyzed from eclogite xenoliths, and Gt was separated from the other xenoliths, including peridotites, pyroxenites, and alkremites. The restricted range of $\delta^{18}O$ clinopyroxenes from eclogites is 2.8 to 6.7 ‰ and lie within the range reported for eclogite xenoliths from Siberian platform (between 2.8 and 8.0 ‰, Snyder et al., 1995). The majority of the garnet samples lie within the range of average mantle values (5.5±0.4 ‰, Mattey et al, 1994, based upon peridotitic Gt analyses. However, 10 Gt samples have high $\delta^{18}O$ values that lie well beyond the mantle average – i.e., they reflect a definite crustal origin.

These isotopic values permit speculation that many eclogites, and probably a portion of the ultramafic xenoliths as well, formed from protoliths of ancient oceanic crust that were subducted beneath the Siberian Craton. It is possible to grossly estimate the amount of crust added to the mantle under the Siberian Platform, based upon the isotopically light carbon of the diamonds.

INTRODUCTION

There exists a considerable amount of evidence that suggests that the lithospheric keel of the Siberian Platform was formed in the Archaean (e.g., [26, 27, 30]). This also applies to the Anabar and Aldan shields, as well. At the same time, several terranes are divided in the Yakutian kimberlite province on the east part of the Siberian platform. The dates of separation of the crustal portion of terranes from their mantle source are about 2.9-3.5 Ga. Subsequent evolution of the subcontinental lithospheric mantle (SCLM); subduction of oceanic crust under

different terrane; and later additions to the lithosphere probably took place during the period of sub-craton amalgamation and stabilization at 2.5-2.9 Ga.

The role of subduction early in history of the Earth, particularly in the formation of the old cratons and their underlying mantle keels, is not well constrained. Eclogite xenoliths and eclogitic diamonds are now routinely ascribed to origins from subduction [2, 15, 17-21, 24, 33, 36, 37, 39, 45-50], but there are not many studies that directly constrain the timing of ancient subduction and its relation to craton stabilization. New investigations of Re-Os systematics in mantle samples and diamonds show that the Re/Os isotope system holds the key to further progress in understanding of continental mantle evolution, not only with reference to mantle keel depletion [29, 35] but also to the addition of eclogitic components via subduction. Direct and indirect evidences show that subduction processes were involved in the origin of the mantle roots under old platforms, such as South African and Siberian [17, 18, 24, 34, 45, 46]. It is to be expected that this process would be reflected in compositions of mantle xenoliths and possibly diamonds and their inclusions, which may retain a history of their source rocks and subsequent evolution.

There is little reported on a real or model age of kyanite eclogites from kimberlite pipes, with the exception of a report by Jagoutz et al. [18] on dating xenoliths from the Orapa pipe with the age of about 2.5 Ga. Our preliminary results (WHERE?? REFERENCE???) on dating rutiles from kyanite eclogites show that some rocks were formed between 2.2 and 2.5 Ga. These data suggest that formation of subcontinental lithospheric mantle (SCLM) and the subduction of oceanic crust beneath the Siberian Platform took place within a long interval of time. This statement is supported by the extended period of time that has been determined for mantle xenoliths, according to Re-Os dating of sulfides included in coarse-grained olivine megacrysts from the Udachnaya kimberlite pipe [16]. This evidence points to a long period of time for the formation and stabilization of the mantle beneath the Siberian Platform, including the active subduction tectonics.

Kyanite and coesite eclogites occur in a number of kimberlite pipes of Yakutia, in the Udachnaya, Zagadochnaya, and other pipes of the Daldyn-Alakitsky region. Coesite was found to occur in more than 20 samples of kyanite eclogites and grospydites from the Udachnaya pipe ([43], and references therein). The presence and preservation of coesite in eclogites indicate both high-pressure formation of coesite-bearing xenoliths (not less than 30 kbar) and set limits on the timing of the cooling of the xenoliths, during their encapsulation and movement to the surface by the kimberlite. This is considered as evidence of the involvement of subducted oceanic crust as a contribution to the formation of the SCLM, also confirmed for coesite-bearing and diamondiferous eclogites from kimberlites of Yakutia (e.g., [18, 36]).

As was demonstrated by Sobolev V.S. and Sobolev N.V. [39], in rare cases, kyanite eclogites from Yakutian kimberlites contain cubic diamonds that are isotopically enriched in light C^{12} isotope. A probable cause for this would be that

they were formed in remnants of subducted oceanic crust or at least that the source of carbon for their formation have been from subducted former crustal rocks. Such carbon isotopic values of diamonds are present worldwide kimberlites, for example, from South Africa pipes (Orapa, Jwaneng, Bellsbank, Roberts Victor), as well in Siberian kimberlites (Udachnaya, Sytakanskaya, Zarnitsa, etc.). In most cases, kimberlite pipes, containing such cubic and isotopically light diamonds, are situated in central part of Yakutian kimberlite province that belongs to the Daldyn-Alaritsky region. Given the light-carbon isotope compositions of many eclogitic diamonds, in addition to the variable sulphur-isotopic compositions of eclogitic sulfide diamond inclusions [12], a recycled crustal component is also strongly suggested.

SAMPLES AND ANALYTICAL TECHNIQUES

More than 150 mantle xenoliths were studied from the different pipes of the Yakutian kimberlite province. Modal analyses have been performed on most of these xenoliths, as well as whole-rock chemistry. Major-element analyses were also conducted on the various minerals in these selected xenoliths. All samples were classified into different varieties of eclogites and peridotites according to their petrographic and chemical features.

Major-element compositions of silicate and oxide minerals in the xenoliths were determined with a CAMECA SX-50 electron microprobe at Institute of Geology (Yakutsk) and with a Superprobe JXA-8800R electron microprobe at the ALROSA Co Ltd. (Mirny, Russia). A portion of the garnets and clinopyroxenes were also investigated by ESM with EDS at the University of Western Australia (Perth). Analytical conditions included an accelerating voltage of 15 kV, a beam current of 20 nA, beam size of 5 μm, and 20 second-counting time for all elements. All EMP data underwent full ZAF corrections.

Fresh garnets and clinopyroxenes were selected from over a hundred peridotite and eclogite xenoliths collected from the Udachnaya and Obnazhennaya kimberlite pipes. These minerals were crushed and sieved to 200 μm and hand-picked for purity using a binocular microscope. After picking, the optically gem-quality garnet grains were washed with water and acetone. A split of each sample was used for EMP analyses. Another 10 mg portion was set aside for oxygen isotope analyses by laser-fluorination at the University of Wisconsin. The oxygen-isotope analyses were performed on the garnet and clinopyroxene separates, approximately 1-2 mg per run, using a 32 W CO2 laser, BF5, and a dual-inlet Finnigan MAT 251 mass spectrometer. Replicate analyses were performed on many samples, particularly those that had initial oxygen values outside that of the mantle range (5.4±0.4 ‰). These analytical procedures are discussed by Valley et al. [51]. All values are reported with respect to V-SMOW. The results of these oxygen analyses were previously reported by Taylor et al. [48, 49].

RESULTS

Oxygen isotopic values were determined on the garnets and clinopyroxenes from the selected xenoliths from the two well-known and contrasting kimberlite pipes of Yakutia: Udachnaya and Obnazhennaya. This study was conducted in order to estimate the possible presence of subducted crustal remnants in the upper mantle underlying the Siberian platform. The xenoliths include both eclogites and ultramafics as well, as reported by Taylor et al. [48, 49].

Oxygen isotope data were obtained from more than 100 clean garnet mineral separates and about 20 clinopyroxene separates by the laser-fluorination technique mentioned above [51]. Only clinopyroxene was analyzed from the eclogite xenoliths, and garnet was separated from the different types of mafic and ultramafic xenoliths including garnet peridotites, lherzolites, pyroxenites, and alkremites. A selected and representative array of analyses of oxygen isotopes and major-element compositions of garnets are given in Table 1. It should be noted that many of the investigated garnets were taken from ultramafic xenoliths. The petrography of these xenoliths, as well as the high-chromium content of garnets (>8 wt.% Cr_2O_3, Table 1) confirms that they belong to the lherzolite-dunite xenolith suite from these two kimberlite pipes [43].

The large spread of δ18O values for the eclogitic clinopyroxenes from 2.8 to 6.7 ‰ is within the range for eclogite xenoliths from the Siberian platform (between 2.8 and 8.0 ‰, Snyder et al., [36-37]). With reference to Figure 1, it appears that about 1/3rd of the whole eclogite pollution lies outside the mantle range. This not only indicates that these outlier eclogites are of crustal origin, but indicates that it is probable that most of the eclogites indeed, are of crustal origin [48]. This distribution of oxygen values is what is to be expected from the subduction of an ophiolite sequence. The majority of the garnets from the eclogite xenoliths are within the mantle range of 5.5±0.4 ‰ [23], also reported as 5.4±0.2 [11]. No very light values less than 4.0 ‰ are observed, as reported from Roberts Victor eclogites [22]. A total of 10 garnets have values higher that the 5.5±0.4‰ mantle range. However, these $\delta^{18}O$ values do not appear to show a correlation with the major-element chemistry of the garnets (e.g., FeO or CaO), as reported for eclogite diamondiferous xenoliths from the Udachnaya kimberlite pipe [18, 37].

The distribution of $\delta^{18}O$ values for garnets from the peridotite and pyroxenite xenoliths from the Udachnaya kimberlite pipe is shown in Figure 2. It is obvious that some of the $\delta^{18}O$ values of garnets are higher than the mantle range. It should be noticed that most of these garnets are from pyroxenite xenoliths or clinopyroxene-rich lherzholites. The range of $\delta^{18}O$ garnets from rare and unusual alkremite xenoliths was estimated for Gt-separates only in 6 samples from the Udachnaya pipe. Estimated values are vary from 5.28 to 7.30‰, and only in a half of these unique samples have oxygen isotopic values within the mantle range.

The distribution of $\delta^{18}O$ values of garnets from different mafic and ultramafic mantle xenoliths from the Obnazhennaya kimberlite pipe is shown in

Table 1.

Representative selected $\delta^{18}O$ values and garnet compositions in xenoliths from the Yakutian kimberlites. Oxygen values are from Taylor et al. [48, 49].

#	Sample	$\delta^{18}O$	SiO_2	TiO_2	Al_2O_3	Cr_2O_3	FeO	MnO	MgO	CaO	Na_2O	Total
1	**U-2247**	5.25	41.63	0.37	19.44	4.83	4.27	0.39	22.54	5.01	0.14	98.62
2	**U-2249**	4.88	41.11	0.20	17.03	8.70	7.01	0.42	20.59	6.45	0.00	101.51
3	**U-2283**	5.15	40.82	0.75	21.39	0.80	12.33	0.55	19.72	5.01	0.07	100.38
4	**U-2298**	5.40	42.25	0.33	22.12	2.26	7.06	0.26	21.60	4.43	0.08	100.39
5	**U-80-3**	5.04	40.99	0.42	21.38	1.65	8.05	0.49	20.93	6.06	0.09	100.06
6	**U-83-7**	5.18	41.78	1.11	20.97	1.42	6.54	0.36	22.07	4.61	0.16	99.02
7	**U-83-14**	4.93	41.65	0.21	17.15	8.54	7.50	0.39	19.65	6.24	0.10	101.43
8	**U-83-26**	5.41	41.88	0.82	21.64	1.81	6.10	0.41	21.90	4.52	0.13	99.21
9	**U-83-31**	5.19	41.68	0.09	20.26	4.06	7.99	0.33	21.44	5.04	0.02	100.91
10	**U-83-39**	5.34	41.15	0.58	21.76	2.12	7.14	0.29	23.09	4.23	0.03	100.39
11	**U-83-547**	6.28	40.64	0.06	24.48	0.40	8.93	0.36	21.51	4.05	0.09	100.52
12	**U-84-2**	5.17	41.19	0.00	20.56	4.85	7.68	0.49	19.92	6.16	0.00	100.85
13	**O-3127**	6.51	40.82	0.07	23.66	0.11	15.28	0.44	16.46	3.52	0.00	100.36
14	**O-3170**	6.38	41.71	0.14	23.80	0.43	9.65	0.31	20.01	4.21	0.00	100.28
15	**O-3177**	6.05	41.76	0.11	23.92	0.73	10.22	0.45	20.55	3.70	0.00	101.44
16	**O-3184**	6.19	41.08	0.16	23.32	1.77	4.50	0.32	24.86	4.57	0.03	100.61
17	**O-3198**	5.80	41.77	0.08	22.53	1.94	8.08	0.37	21.60	4.71	0.05	101.13
18	**O-3199**	5.28	40.77	0.06	22.17	2.06	8.71	0.33	21.24	4.98	0.06	100.38
19	**O-3312**	6.11	39.37	0.14	24.06	0.22	14.08	0.30	18.22	3.71	0.10	100.20
20	**O-3355**	5.48	39.51	0.12	24.92	0.10	7.57	0.20	23.32	4.36	0.00	100.10
21	**O-3460**	5.93	42.11	0.09	23.14	0.58	8.69	0.29	21.35	4.01	0.01	100.27

Note. *Samples labeled: U-Udachnaya and O-Obnazhennaya pipes. 1, 2, 4-10, 17, 18- Gt-peridotites, 3- Ilm-Gt peridotite, 11, 13, 14- Gt-pyroxenites, 12-Gt-dunite, 15,16, 21-Gt-lherzolites, 19, 20-eclogites.*

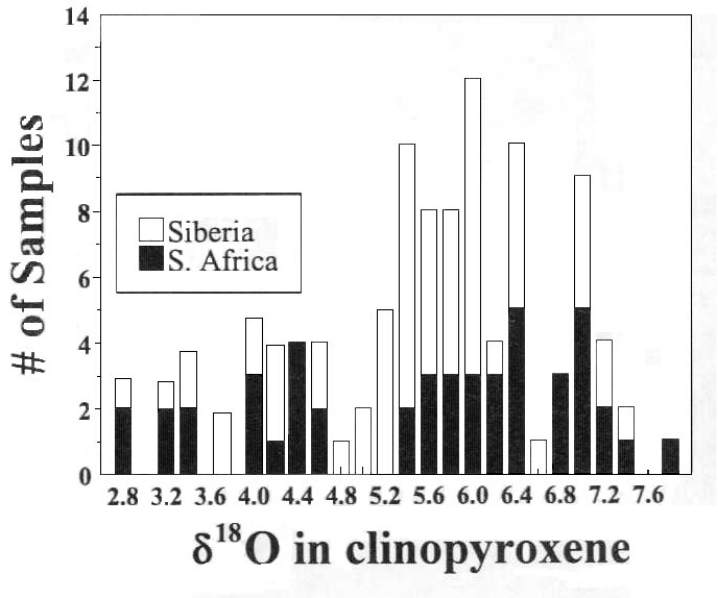

Fig. 1. *Oxygen isotope values for eclogitic clinopyroxenes from the Yakutian kimberlites (after Snyder at al., 1995 [36] with addition).*

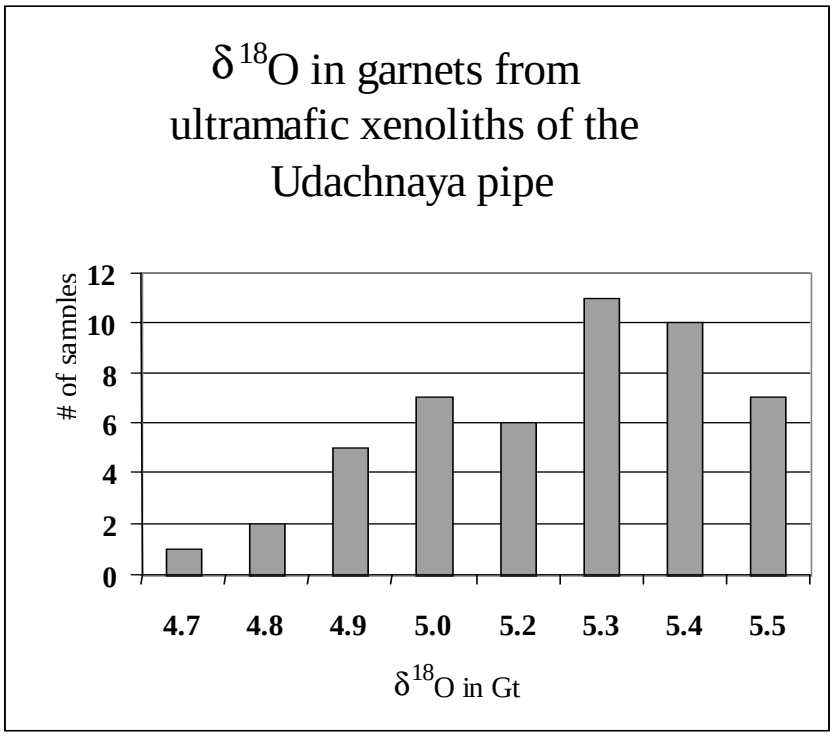

Fig. 2. *Oxygen isotope data of garnets in ultramafic xenolith from the Udachnaya kimberlite pipe (data from Taylor et al., 2003 [48, 49]).*

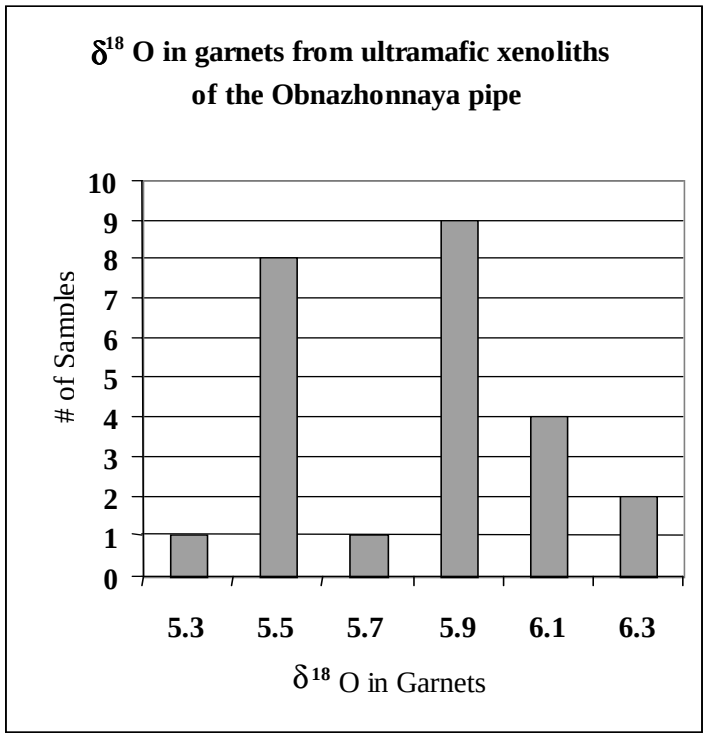

Fig. 3. *Oxygen isotope data of garnets in mantle xenolith from the Obnazhonnaya kimberlite pipe (data from Taylor et al. [48, 49]).*

Figure 3, as based upon the data from Taylor et al. [48, 49]. Similar to values from the garnets from xenoliths from the Udachnaya pipe, several oxygen isotopic $\delta^{18}O$ values are definitely outside the mantle range – about ~20% lies outside the mantle window, both above and below. All garnets with high $\delta^{18}O$ from this pipe belong to the xenoliths of mantle pyroxenites, some to the lherzolites (see Table 1). Based on these findings of oxygen values outside those of the mantle range, it can be concluded that, in addition to eclogites, some xenoliths of pyroxenites and peridotites may represent the remnants of subducted oceanic crust, a conclusion originally put forth by Taylor et al. [48, 49].

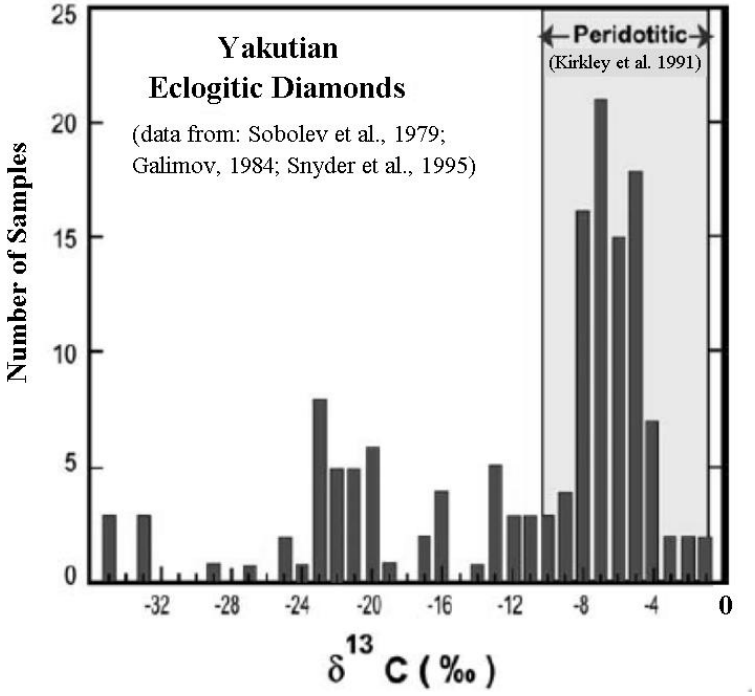

Fig. 4. *Carbon isotope values for eclogitic diamonds from the Yakutian kimberlites (copied from Taylor et al. [48]).*

It should be possible to use well-established and characterized samples from the mantle - xenoliths and diamonds - to estimate the distribution of subducted crustal remnants in the upper mantle underlying the Siberian platform. The data base involves the extensive populations of mantle xenoliths from the main kimberlite pipes of the Yakutian province. In addition, already published data were also compiled, such as the distribution of carbon isotopes reported from the diamonds from the various pipes [13, 14, 38]. These aggregated data show that many Yakutian E-type diamonds have light to very-light isotopic compositions (Fig. 4). This carbon with values outside the normal mantle range may also be indicative of a crustal source for the diamond chemnistry. These results show that in many pipes, where both kyanite- and coesite-eclogite xenoliths occur, isotopically light diamonds are also present. This is definite for the kimberlites of the central Daldyn-Alakitsky region. All these evidences can be interpreted as

indicating the involvement of crustal subduction in the formation of the SCLM beneath the Siberian platform.

DISCUSSION

Mantle xenoliths in kimberlites worldwide are represented by mafic and ultramafic rocks. It has been assumed that they probably formed in the different terranes (sub-continents) of the Yakutian kimberlite province, but are coupled in their ultimate origins. The lowest peridotite Os isotopic compositions require Re depletion in the mid-Archaean (3.2 Ga), according Pearson et al. [27], and this age is interpreted as the time of the differentiation of the Siberian lithospheric mantle. This ancient origin for the Siberian lithosphere is also supported by Re-Os and Sm-Nd model ages for eclogite and peridotite xenoliths from Udachnaya. The formation age of the parent mantle rocks, as represented by the xenoliths, and their differentiation in the mantle, based on isotopic data and other petrologic evidence, is not less than 3.0 Ga [16, 25-27, 41]. In addition, the Re/Os determinations from P-type diamonds from Yakutian kimberlites result in an age range from 2.8 to 3.4 Ga (e.g. [28]).

The long period of formation and evolution of the SCLM and subduction of oceanic crust beneath various terranes of the Siberian Platform is supported by the Re-Os dating of sulfides included in coarse-grained olivine megacrysts from the Udachnaya kimberlite pipe [16, 41]. Accordingly, the subduction and recrystallization of mantle protoliths are probably recorded by the 2.9 Ga events. In adition, several individual sulfide inclusions with low Re/Os have TMA=2.5-2.6 Ga and may represent a new addition to the lithosphere. Pearson et al. [27] reported Re-Os data for 18 peridotite xenoliths from Udachnaya, and for olivine separated from two of these xenoliths. Most of these samples have high $^{187}Os/^{188}Os$ ($\geq$0.12) and very high $^{187}Re/^{188}Os$ ($\geq$2). The samples scatter about a 490 Ma isochron, which is distinctly different from the overall array defined by the sulfide-inclusion data reported by Griffin et al. [16].

As presented above, kyanite- and coesite-eclogites occur several kimberlite pipes in Yakutia, mainly in Udachnaya, Zagadochnaya, and other pipes of the Daldyn-Alakitsky region. In fact, coesite is found in >20 samples of kyanite-eclogites and grospydites from the Udachnaya pipe [42-44]. The presence and preservation of coesite in eclogites is interpreted as additional evidence of the involvement of subducted oceanic crust in the formation of the SCLM. It appears from all the data [31, 41] that formation of the SCLM and subduction of oceanic crust beneath various terranes of the Siberian Platform took place over an extended period of time. This statement finds support in the large duration of time recorded for the formation of the mantle xenoliths, according to the Re-Os dating of sulfides included in coarse-grained olivine megacrysts from the Udachnaya kimberlite pipe [16]. This indicated the extended period of time for the formation and stabilization of the mantle beneath the Siberian Platform, accompanied by the subduction processes.

Mafic xenoliths from the Yakutian kimberlites are represented by different types of bi- and tri-mineralic eclogites and certain pyroxenites. The idea that some of these rocks represent the metamorphosed remenants of subducted oceanic crust is generally accepted, particularly for the group B and C eclogites. These include the coesite-bearing eclogites and many diamondiferous eclogites. Such rocks are from Udachnaya, Zagadochnaya, Sytykanskaya and other kimberlite pipes of the Daldyn-Alakitsky region, representative of the central part of the Yakutian kimberlite province, as well the central portion of the Siberian platform [40]. If the presence of coesite is an indication of crustal origin, this has major ramifications for the origins of diamonds beneath the Siberian Platform; there are numerous reports of coesite diamond inclusions from the Mir, Udachnaya, Zarnitsa, and other Yakutian kimberlites [4, 5]. These data are interpreted as additional evidence for a major contribution to the SCLM by the subduction of ancient oceanic crust, leading ultimately to the formation of eclogitic diamonds.

Another line of evidence supporting the proposition that subduction of oceaninc crust has played a major role in the formation of the mantle xenoliths containing diamonds can be found in the carbon isotopics for diamonds. The presence of light C^{12} in eclogitic diamonds is a long-standing observation of major significance [e.g., 6, 13]. Data on the carbon isotopes has been forthcoming from several classic studies, each pointing to the anomalous carbon isotopes for mantle products [6-10, 20]. The carbon isotopic ratios of diamonds from the Yakutian kimberlites have shown that many diamonds have $\delta^{13}C$ distinct from the typical mantle values [4, 13, 14, 39]. Such crystals are widespread in all of the well-studied kimberlite pipes of the Daldyn-Alakitsky region, as well as in the Mir and others pipes of the province. It should be emphasized that the proportion of isotopically light carbon in diamonds increases distinctly from the south to the north of the province. The most reasonable explanation for the very low and high δ13C is a contribution of carbon with subducted oceanic crust. A crustal source for the carbon of some eclogitic diamonds is also supported by sulfur isotopes from sulfide inclusions in diamonds [12, 32].

Oxygen-isotopic and trace-element data suggest that many eclogite xenoliths, especially the group B and C eclogites, are representatives of subducted crust. Detailed studies of diamondiferous eclogites from the Udachnaya kimberlite pipe [17, 18, 36, 37] and determination of oxygen-isotope compositions of their clinopyroxenes have demonstrated that over $1/3^{rd}$ of the xenoliths have values outside those of the accepted mantle range, evidence for a crustal component. This relationship for clinopyroxenes of diamondiferous eclogites from the Udachnaya pipe is illustrated on Figure 1, and it is probable that this this regularity for oxygen isotopes may well indicate that a large proportion of the eclogites from Udachnaya may be of ultimate crustal origin.

In a recent study of mafic and ultramafic xenoliths from the Obnazhennaya kimberlite, Taylor et al. [50] found similar oxygen evidence for Group A eclogites and websterites. They have proposed the most, if not all, eclogites from the

kimberlites of the world may be derived from crustal protoliths. It is obvious that the tectonics occurring during the early formation of cratons included considerable underplating by subducted oceanic crust, that ultimately returned to the Earth's surface in the form of kimberlitic xenoliths.

Taylor et al. [48, 49] have shown that oxygen isotopic values of certain ultramafic xenoliths from Udachnaya and Obnazhennaya, discussed above, would appear to indicate that a portion of these xenoliths also have crustal signatures. The role of subduction in the formation of the SCLM may have a more far-reaching effect than anyone ever imagined until now.

Thus, evidence taken from the studying of mantle xenoliths from the kimberlites of the Yakutian province confirm that the processes of subduction were operative during the early formation of the SCLM beneath the major eastern portion of the Siberian Platform, which occurred in the late Archaean.

If we assume that all isotopic light diamonds belong to the eclogitic paragenesis and were formed from carbon of remnants of subducted oceanic crust, we can use this criterion for estimation of the contribution of subducted rocks associated with the formation of cratonic croots under old cratons, such as that in Yakutia. It accord with such data, about 20% of the diamond population from the Yakutian kimberlites had an origin associated with subducted products, such as eclogites, and perhaps some pyroxenites. However, the connection between the percentage of eclogitic diamonds and the amount of subducted crust is tenuous at best.

Eclogites from kimberlites have been interpreted as former oceanic crust or may represent residues after melting and fractionation [2, 18, 22, 24, 33, 34]. Petrologic evidence suggest that at least two ways of the eclogite xenoliths formation are possible: (i) in the result of transformation of initial rocks of gabbro-anorthosite composition through the intermediate stage - eclogite-like rocks; (ii) in the result of fraction crystallization in deep-seated conditions of ultramafic composition primary melt. The first way is proved by petrographic, petrochemical and isotopic investigations that show genetic relationship of all the series of these rocks [24, 36, 43]. The second way is proved by the presence of subsolidus changes in eclogites and by continuous sets of high-aluminous line formations from kyanite eclogites up to alkremites, by linear trends of the differentiation [40]. The possibility to form the part of eclogites in the result of subduction and the following metamorphism of oceanic crust, that is proved by simplified isotopic composition of diamonds in separate eclogites [20, 39] and other evidences [22, 24, 36, 37, 46] is very probable. We cannot exclude possible formation of part of eclogite xenoliths through the process of delamination of the former gabbro-anortozite or ophiolite interlayered complexes [43, 49, 50] that also could explane their oxygen and some trace element characteristics. Such diversity of their origin and also the following evolution of eclogite rocks in the process of partial melting and global mantle metasomatism, which we have considered in details in a number

of papers ([36, 43, 44], and references therein) and, in their turn, determine the specific nature of their rocks and minerals composition in separate pipes.

Detailed studies of the mineral assemblages in the xenoliths from the Yakutian kimberlite pipes has revealed that there exists an obvious difference in their distribution in different pipes and fields [40, 43]. Comparison of eclogite-suite xenoliths along a traverse from south to north in the province revealed that there appears to be a linear heterogeneity in the mantle for over 1000 kilometers. This is present in the central part of province by a suite of high-aluminous rocks, which are represented by kyanite- and coesite-bearing eclogites in kimberlite pipes of then Daldyn-Alakitsky field. These xenoliths were found, in particular, at Udachnaya, Zagadochnaya, and Zarnitsa. It should be noted that these mantle xenoliths appear related to some crustal xenoliths of the granulite facies, such as eclogite-like rocks containing plagioclase and some kyanite, in addition to garnet and clinopyroxene [42]. Radiometric dating with Sm-Nds on mineral separates of granulite xenoliths demonstrate a significant range of ages from 2.9 to 3.3 Ga. Model ages from two samples of these eclogite-like rocks gave age 2.5 Ga. These ages correlate with the time of stabilization of the metamorphic series of the Anabar shield. The closing time for the Sm-Nd system in samples of such lower crustal xenoliths is 1.7-1.8 Ga [30, 31]. This appears to be indicative of the long-lasting cooling of the metamorphism. This is also evidenced by zircon dating in a pyroxenite xenolith from the Udachnaya pipe, where zircon is possibly related to phlogopitization of the rock. The zircon growth occurred at 1.8 Ga, according U/Pb dating by SHRIMP (unpublished data). The age of zircon in this xenolith would seem to be in agreement with the evolution of the SCLM of the Yakutian kimberlite province. It may reflect late-stage metasomatic events in subcontinental lithosphere beneath the central part of the Siberian platform.

EVOLUTION OF THE SIBERIAN CRATON

It is possible to summarize and outline the evidences that are important to an understanding of the formation and evolutionary processes for the Siberian Craton:

(1) Common occurrence and wide distribution of kyanite- and coesite-bearing xenoliths in most pipes of the Daldyn-Alakitsky region and rare occurrences of diamonds and xenoliths with these minerals in kimberlites of the Malo-Botuobinsky and Nakynsky fields.

(2) Presence of isotopically light carbon in diamonds from the pipes at Mir, Udachnaya, Yubileynaya, and others. The C isotopic contents of diamonds from the Yakutian kimberlites have shown that many diamonds have $\delta^{13}C$ distinct from the typical mantle value (e.g., [5, 13, 14]). A reasonable explanation for the low $\delta^{13}C$ is that the carbon had its ultimate origin in subducted oceanic crust. Cubic diamond crystals present in kyanite eclogites [40] may also have formed in such subducted crustal rocks.

(3) A complicated history of formation from sources enriched in subducted crustal material, such as an ophiolite sequence. This also applies to some garnet

pyroxenite xenoliths from the Udachnaya pipe, as suggested by the Sr-Sm-Nd isotope study of Agashev et al. [1].

Based upon some of the evidence discussed in this paper, and much more, it is definitely probable that many, if not most, eclogites, and possibly some pyroxenites are products of the subduction of ancient oceanic crust. This is confirmed for the coesite-bearing and some diamondiferous eclogites from kimberlites of Yakutia (e.g., [17, 18, 36, 37]). The oxygen-isotopic and trace-element data suggest that most eclogite xenoliths, particularly those of Group B and C, but also some of Group A, are representatives of subducted crust [22, 24, 46, 50]. According to the distribution of different types of eclogites and presence of isotopically light carbon in cubic crystals of diamonds in kimberlites of Yakutian province, it is possible to estimate the addition of crustal material to the mantle under the Siberian craton. In the central part of the craton, the remnants of subducted crust could be about 10-20 % of the upper mantle, in accordance with the distribution and abundances of xenoliths the various kimberlite pipes in Yakutia [40, 43]. If we assume that most isotopically light diamonds belong to the eclogitic paragenesis and were originated by their growth in remnants of subduction crust we could use this for the estimation of contribution of subducted oceanic crust in formation of the lithospheric roots under Siberian platform. It should be noticed that according these data about 20% of diamond population from kimberlites of Yakutia were originated in subducted rocks such as eclogites and probably partially pyroxenites.

CONCLUSION

Oxygen isotopic values of garnets from mafic and ultramafic xenoliths from the kimberlites of Yakutia would appear to indicate crustal protoliths, not only for many eclogites, but also some ultramafic xenoliths of the peridotite-pyroxenite suite and alkremites. These garnets have $\delta^{18}O$ values that are outside the acceptable mantle range, and are interpreted as indicative of the subduction of ancient oceanic crust.

The oxygen data is supported by the carbon isotope of diamonds and emphasizes the importance of the concept that the subduction of oceanic crust had a definite role in the formation of the SCLM beneath the Siberian craton.

It is suggested that the presence of kyanite- and coesite-bearing eclogites among the kimberlite xenoliths, in addition to the isotopically light carbon in both cubic and octahedral diamonds, may be used to estimate the degree of involvement of the subduction process in the formation of the SCLM.

There is an overwhelming amount of quality data from the xenoliths from the kimberlites of Yakutia that provides evidence that oceanic crust subducted beneath the Siberian Craton played a major part in the formation of eclogites, their diamonds, and perhaps, some of the peridotitic xenoliths, in time of stabilization and after main formation of the SCLM of the Siberian platform some 3.0-3.5 Ga ago [16, 31].

ACKNOWLEDGEMENTS

Portions of this study were supported by National Science Foundation (NSF) grants to LAT, for which we are grateful. ALROSA Co Ltd. is thanked for its continuing support of the senior author in his research endeavors. Many enthusiastic discussions with Galia Bulanova, Chris Smith, Greg Snyder, Mahesh Anand, Nick Sobolev, Jeff Harris, and others have proven to be most educational and have certainly added to the research presented in this paper.

REFERENCES

1. **Agashev, A.M., Watanabe, T., Kuligin, S.S., Pokhilenko, N.P., and Orihashi, Y.,** 2001. Rb-Sr and Sm-Nd isotopes in garnet pyroxenite xenoliths from Siberian kiberlites: an insight into litospheric mantle. Jorn. of Mineralogical and Petrological Sci, 96, 7-18.
2. **Beard, B. L., Fraracci, K. N., Taylor, L. A., Snyder, G. A., Clayton, R. N., Mayeda, T., Sobolev, N. V.,** 1996. Petrography and geochemistry of eclogites from the Mir kimberlite, Yakutia, Russia. Contributions to Mineralogy and Petrology 125, 293-310.
3. **Boyd, F. R., Pokhilenko, N. P., Pearson, D. G., Mertzman, S. A., Sobolev, N. V., and Finger, L. W.,** 1997. Composition of the Siberian cratonic mantle: evidence from Udachnaya peridotite xenoliths. Contrib. Mineral. Petrol. 128, 228-246.
4. **Bulanova, G.P., Griffin, W.L., Kaminsky, F.V., Davies, R., Spetsius, Z.V., Ryan, C.G., Andrew, A., and Zahkarchenco, O.D.,** 1999. Diamonds from Zarnitsa and Dalnaya kimberlites, their nature and lithospheric mantle source. Proc. 7th Int. Kimb.Conf., 49-56.
5. **Bulanova, G.P., Shelkov, D., Milledge, H.J., Hauri, E.N., and Smith, C.B.**, 1999. Nature of eclogitic diamonds from Yakutian kimberlites: Evidence from isotopic composition and chemistry of inclusions. Proc. 7th Int. Kimb. Conf., 57-65.
6. **Deines, P.,** 1980. The carbon isotopic composition of diamonds: relationship to diamond shape, colour, occurrences and vapour composition. Geochimica et Cosmochimica Acta 44, 943-961.
7. **Deines, P., Harris, J.W., and Gurney, J.J.,** 1991. The carbon isotopic composition and nitrogen content of lithosphere and asthenospheric diamonds from the Jagersfontein and Koffiefontein kimberlite, South Africa. Geochim. Cosmochim. Acta 55, 2615-2625.
8. **Deines, P., Harris, J.W., and Gurney, J.J.,** 1993. Depth-related carbon isotope and nitrogen concentration variability in the mantle below the Orapa kimberlite, Botswana, Africa. Geochim. Cosmochim. Acta 57, 2781-2796.
9. **Deines, P., Harris, J.W., and Gurney, J.J.,** 1997. Carbon isotope ratios, nitrogen content and aggregation state, and inclusion chemistry of diamonds from Jwaneng, Botswana. Geochim. Cosmochim. Acta 61, 3993-4005.
10. **Deines, P., Harris, J.W., Spear, P.M., and Gurney, J.J.**, 1989. Nitrogen and □13C content of Finch and Premier diamonds and their implications. Geochim. et Cosmochim.Acta 53, 1367-1378.
11. **Eiler, J.M.**, 2000, Oxygen isotope variations of basaltic lavas and upper mantle rocks. In Stable Isotope Geochemistry, Eds. Valley and Cole, Reviews in Mineral. Geochem., v. 43, Mineral. Soc. Amer., 319-364.
12. **Eldridge, C. S., Compston, W., Williams, I. S., Harris, J. W., and Bristow, J. W.**, 1992. Isotope evidence for the involvement of recycled sediments in diamond formation. Nature, 353, 649-653.
13. **Galimov, E.M.**, 1884. The relationship between formation conditions and variations in isotope composition of diamonds. Geokhimiya 8, 1091-1118 (in Russian).

14. **Galimov, E.M.**, 1991. Isotope fractionation related to kimberlite magmatism and diamond formation. Geochim. Cosmochim. Acta, 55, 1697-1708.
15. **Garlick, G.D., MacGregor, I.D., and Vogel, D.E.**, 1971. Oxygen isotope ratios in eclogites from kimberlites. Science 172, 1025-1027.
16. **Griffin, W.L., Spetsius, Z.V., Pearson, N.J., and Suzanne, Y. O'Reilly.**, 2002. In-situ Re-Os analysis of sulfide inclusions in olivine: New constraints on depletion events in the Siberian lithospheric mantle. Geochemistry, Geophysics, Geosystems 11-21, 1029/2001GC000287.
17. **Jacob, D., and Foley, S.F.**, 1999. Evidence for Archean oceanic crust with low high field strength element signature from diamondiferous eclogite xenoliths, Lithos 48, 317-336.
18. **Jacob, D., Jagoutz, E., Lowry, D., Mattey, D., and Kudrjavtseva, G.**, 1994. Diamondiferous eclogites from Siberia: Remnants of Archean oceanic crust. Geochim. Cosmochim. Acta, 58, 5191-5207.
19. **Jagoutz, E.**, 1988. Nd and Sr systematics in an eclogite xenolith from Tanzania: Evidence for frozen mineral equilibria in the continental lithsphere. Geochim. Cosmochim. Acta 52, 1285-1293.
20. **Kirkley, M.B., Gurney, J.J., Otter, M.L., Hill, S.J., Daniels, L.R.**, 1991. The application of C isotope measurements to the identification of the sources of C in diamonds: a review. Applied Geochem. 6, 477-494.
21. **Lowry, D., Mattey, D.P., and Harris, J.W.**, 1999. Oxygen isotope composition of syngenetic inclusions in diamond from the Finch Mine, RSA. Geochim. Cosmochim. Acta 63, 1825-1836.
22. **MacGregor, I.D., and Manton, W.I.**, 1986. Roberts Victor eclogites: ancient oceanic crust. J. Geophys. Res., 91, 14063-14079.
23. **Mattey, D., Lowry, D., and Macpherson, C.**, 1994. Oxygen isotope composition of mantle peridotite. Earth Planet. Sci. Lett. 128, 231-241.
24. **Neal, C.R., Taylor, L.A., Davidson, J.P., Holden, P., Halliday, A.N., Paces, J.B., Clayton, R.N., and Mayeda, T.K.**, 1990. Eclogites with oceanic crustal and mantle signatures from the Bellsbank kimberlite, South Africa, Part 2: Sr, Nd, and O isotope chemistry. Earth Planet. Sci. Lett. 99, 362-379.
25. **Pearson, D.G.**, 1999. The age of continental roots. Lithos 48, 171-194.
26. **Pearson, D.G., Kelley S.P., Pokhilenko N.P., and Boyd, F.R.**, 1997. Laser 40Ar/39Ar analyses of phlogopites from southern African and Siberian kimberlites and their xenoliths: constraints on eruption ages, melt degassing and mantle volatile composition. Russian Geology and Geophysics 38, 106-117.
27. **Pearson, D.G., Shirey, S.B., Carlson, R.W., Boyd, F.R., Pokhilenko, N.P., and Shimizu, N.**, 1995. Re-Os, Sm-Nd and Rb-Sr isotope evidence for think Archaean lithospheric mantle beneath the Siberia craton modified by multi-stage metasomatism. Geochim. Cosmochim. Acta 59, 959-977.
28. **Pearson, D.G., Shirey, S.B., Bulanova, G. P., Carlson, R.W., and Milledge, H.J.**, 1999. Re-Os isotopic measurements of single sulfide inclusions in a Siberian diamond and its nitrogen aggregation systematics. Geochim. Cosmochim. Acta 63, 703-711.
29. **Richardson, S.H., Shirey, S.B., Harris, J.W., and Carlson, R.W.**, 2001. Archean subduction recorded by Re/Os isotopes in eclogitic sulfide inclusions in Kimberley diamonds. Earth and Planetary Science Letters 191, 257-266.
30. **Rosen, O.M.**, 1995. Metamorphic effects of tectonic movements at the lower crust level, Protorozoic collision zones and terraines of the Anabar shield. Geothectonics, 29, 91-101.
31. **Rosen, O.M., Serenko, V.P., Spetsius, Z.V., Manakov, A.V., and Zinchuk, N.N.**, 2002. Yakutian kimberlite province: position in the structure of the Siberian craton and

composition of the upper and lower crust. Russian Geology and Geophysics 43, 3-26 (in Russian).

32. **Rudnick, R.L., Eldridge, C.S., and Bulanova, G.P.**, 1993. Diamond growth history from in situ measurement of Pb and S isotopic compositions of sulphide inclusions, Geology 21, 13-16.
33. **Shervais, J.W., Taylor, L.A., Lugmair, G.W., Clayton, R.N., Mayeda, T.K., Korotev, R.L.**, 1988. Early Proterozoic oceanic crust and the evolution of subcontinental mantle: Eclogites and related rocks from southern Africa. Geol Soc Amer Bull 100: 411-423
34. **Shirey, S.B., Carlson, R.W., Richardson, S.H., Menzies, A., Gurney, J., Pearson, D.G., Harris, J.W., and Wiechert, U.**, 2001. Archean emplacement of eclogitic components into the lithospheric mantle during formation of the Kaapvaal Craton. Geophys. Res. Lett. 28, 2509-2512.
35. **Shirey, S.B., and Walker, R.J.**, 1998. The Re-Os isotope system in cosmochemistry and high-temperature geochemistry. Ann. Rev. Earth Planet. Sci. 26, 423-500.
36. **Snyder, G.A., Taylor, L.A., Jerde, E.A., Clayton, R.N., Mayeda, T.K., Deines, P., Rossman, G.R., and Sobolev, N.V.**, 1995. Archean mantle heterogeneity and the origin of diamondiferous eclogites, Siberia: Evidence from stable isotopes and hydroxyl in garnet: Amer. Mineral. 80, 799-809.
37. **Snyder GA, Taylor LA, Crozaz G, Halliday AN, Beard BL, Sobolev VN, Sobolev NV**, 1997, The origins of Yakutian eclogite xenoliths. Jour. Petrol 38: 85–113
38. **Sobolev, N.V., Galimov, E.M., Ivanovskaya, I.N., and Yefimova, E.S.**, 1979. Carbon isotope composition of diamonds containing crystalline inclusions. Doak. Akad. Nauk. SSSR 249, 1217-1220 (in Russian).
39. **Sobolev, V.S., and Sobolev, N.V.**, 1980. New evidence for subduction on deep levels of eclogitized crustal rocks. Dokl. AN SSSR, 250, 683-685 (in Russian).
40. **Spetsius, Z. V.**, 1995. Occurrence of diamond in the mantle: a case from the Siberian Platform. Journal of Geochemical Exploration, 53, 25-39.
41. **Spetsius, Z.V.**, 2002, Evidence for the resemblance of the subcontinental lithospheric mantle in the areas of kimberlite-lamproite magmatism: constraints on the evolution of the Siberian craton. Proceeding of II Workshop: Deep-seated magmatism, magmatic sources and the problem of plumes. Vladivostock, 166-188.
42. **Spetsius, Z.V.**, 2003. Highly aluminous xenoliths from kimberlites of Yakutia: mantle petrology remarks. Ext. Abstracts of 8th Intern. Kimberlite Conference, Victoria. Canada.
43. **Spetsius, Z.V., and Serenco, V.P.**, 1990. Composition of continental upper mantle and lower crust beneath the Siberian platform. Nauka. Moscow. 272 pp. (in Russian).
44. **Spetsius, Z.V., and Taylor, L.A.**, 2003. Partial melting in mantle eclogite xenoliths: evidence from Yakutian kimberlites. Intern. Geol. Rev. 11, 983-987.
45. **Taylor, L. A., and Neal, C. R.**, 1989. Eclogites with oceanic crustal and mantle signatures from the Bellsbank kimberlite, South Africa, part 1: Mineralogy, Petrography, and whole rock chemistry. Jour. Geol. 97, 551-567.
46. **Taylor, L.A.**, 1993. Evolution of the subcontinental mantle beneath the Kaapvaal craton: a review of evidence for crustal subduction for Bellsbank eclogites. In V.S. Sobolev Memorial Volume, Russian Geol. Geophys., Geologiya Geofizika, 34, n. 12, 21-39.
47. **Taylor LA, Keller RA, Snyder GA, Wang W, Carlson WD, Hauri EH, McCandless T, Kim K-R, Sobolev NV, Bezborodov SM** (2000) Diamonds and their mineral inclusions and what they tell us: A detailed "pull-apart" of a diamondiferous eclogite. Internat Geol Review 42, No. 12, 959-983.
48. **Taylor, L. A., Spetsius, Z. V., Wiesli, R., Anand, M., Promprated, P., and Valley, J. W.**, 2003. The origin of mantle peridotites: crustal signatures from Yakutian kimberlites. Ext. Abstr. 8th International Kimberlite Conference, Victoria, Canada.

49. **Taylor, L.A., Spetsius, Z.V., Wiesli, R. Anand, M., Promprated, P., Spicuzza, M, and Valley, J.W.**, 2003, Ultramafic mantle xenoliths: Crustal signatures from Yakutian kimberlites. Contrib. Mineral. Petrol., submitted.
50. **Taylor, L.A., Snyder, G.A., Keller, R., Remley, D.A. Anand, M., Wielsi, R., Valley, J.W., and Sobolev, N.V.**, 2003. Petrogenesis of group A eclogites and websterites: Evidence from the Obnazhennaya kimberlite, Yakutia. Contrib. Mineral. Petrol. 145, 424-443. DOI 10.1007/s00410-003-0465-y.
51. **Valley, J.V., Kitchen, N.E., Kohn, M.J., Niendorf, C.R., and Spicuzza, M.J.**, 1995, Strategies for high precision oxygen isotope analysis by laser fluorination. Geochim. Cosmochim. Acta, 59, 5223-5221.

Yubileynaya pipe: from mineralogy to mantle structure and evolution

Ashchepkov I.V.[1], Vladykin N.V.[2], Logvinova A.M.[1], Nikolaeva I.V.[1], Palessky S.V.[1], Khmel'nikova O.S.[1], Saprykin A.I.,[1], Rotman A.Y.[3]

[1]*United Institute of Geology Geophysics and Mineralogy SD RAS, Novosibirsk*
[2]*Institute of Geochemistry SD RAS, Irkutsk*
[3]*Central Scientific Investigation Geological Exploration Institute, ALROSA , Mirny*

Concentrate from Yubileinaya kimberlite pipe (>800 analyses), Alakite field, Russia, was used for estimation of chemical composition thermal condition and construction of the mantle sequence using monomineral thermobarometry [4, 5, 26]. Cpx and Gar geotherm reveal divide at 35 kbar. Al – and Cr based thermobarometric models gives different structure of lower part of the section: three layer of the dunite –harzburgite – lherzolite sequence basing on Cr and more continuous depletion with the depth using Al-Cr model. From relatively heated 40 -35mv/ m^2 branch the inflection to 350^oC - 65 kbar was determined. The marble –cake structure (at least 7 units) was cut through by the metasomatic veins: amphiboles (< 35 kbar belong to) are Ca-rich while lower belong to richterite- kataforites. TRE for amphibole parental melts are close to kimberlites while clinopyroxenes were even more LREE enriched. Spinels (8 groups) are TiO_2 -rich in lower and uppermost parts. Cr-rich chromites differ in oxygen fugacity. Ilmenite trend consist from two units: >49% TiO_2 enriched in Al_2O_3 (~ 0.7 %) and Fe- rich ilmenites are Al-poor. Ilmenite megacrysts trace feeding vein system of fractionating pre- eruption kimberlite- carbonatite melts. Cr enrichment in ilmenites and Ti rise in Cr-spinelides suggest AFC interaction in veins and surrounding peridotites proved by similar W-type REE patterns. Division into two parts at 35-40kbar corresponds to dehydration peridotite line [38] in subduction stage. High degree of the metasomatism is in accord with high serpentinization degree of kimberlites. Amount of layers in mantle column of Yubileynaya pipe is close to that of Udachnaya pipe but the later contain more eclogites and less metasomatized peridotites. The Ni -rich chromite and olivine inclusions in diamonds agree with essentially peridotitic mantle keel structure.
Most enriched Cpx compositions are Th-U rich but low Rb-Cs and Nb-Ta low. Garnets vary in REE from S-shape to hampered patterns, having all high Pb and small Ta peaks. Mica is high in TRE. Geochemistry of minerals suggests continental type of subduction.

INTRODUCTION

Knowledge of mantle column structures under the kimberlite pipes give mantle petrology the record of the ancient subduction processes, plume impacts and developing of the kimberlite related processes [8, 12, 13, 24, 27, 28, 33] Diamond exploration also needs detail information for mantle structure which together with diamond inclusions may show their parental source because diamonds are mainly the xenoliths of the mantle diamondiferous rocks [8, 9, 19, 21, 32-35, 39]. The thermobarometric methods using the mineral associations are not applicable for some highly serpentinized pipes. In Yakutia the pipes belonging to the Daldyn field usually contain more preserved xenoliths while Alakite field accounting several large kimberlite pipes [19] usually do not reveal abundant fresh minerals except garnets, Cr-spinel, ilmenites and more scarce clinopyroxenes. Special attempts were made to receive the concentrate of pyroxenes and amphiboles using the magnetic separation and high density liquids developed in IGC SD RAS, Irkutsk. These minerals were used to reconstruct using mineral thermobarometry the structure, geochemistry and processes taking place beneath the Yubileinaya - the largest pipe in the Alakite field. The high amount of relatively small minerals were mounted polished and analyzed by EPMA (~800) and then by LAM ICP MS (24) and allowed to reconstruct the layered structure and geochemical features of the minerals their parental melts and kimberlites.

LOCATION AND GENERAL GEOLOGY

Alakite kimberlite field locate in the Alakit –Markha river basin in at the Vilyui – Kotui zone of the deep seated faults and account about 56 kimberlite pipes. Yubileynaya pipe located 15 km NW from Aikhal town is the largest in the region ~ 850 m in diameter. It is surrounded by satellite pipe and separate body possibly represented the crater bank. In section it is a funnel composed from autolitic kimberlites and the marginal dykes of massive porhyric kimberlites from stage 1. It is covered by volcanic sediments, tuffs and breccias in the upper part. The degree of the carbonatization and serpentinization is very high especially in the upper part [19].

METHODS

Concentrate used for the diamond exploration (fractions -0.25-0.1) was undergone to the electromagnetic separations. The clinopyroxens often within the serpentine cover and in intergrowth with amphibole were found mainly in non-magnetic fraction with pyrite, serpentine and mica. Mineral grains of clinopyroxenes (200), amphiboles (30), various garnets (200), and octahedral Cr-spinel grains (80), ilmenites (90), micas (40) and others were analyzed in Camebax Microbe in Analytic Center of UIGGM SD RASc (Analyst O.S. Khmel'nikova). The same mounts were used for the LAM ICP analyses (Analysts Palessky S.V.,

Nikolaeva I.V., Saprykin A.I.) scanned by the laser beam (UV Laser Probe, frequency 266 nm) and analyzed in high resolution ICP MS Finnegan Element.

MINERALOGY OF MAJOR PHASES

Garnets in Yubileynaya pipe concentrate pink, red, purple, violet and less frequent orange were separated to 10 clusters. Cr- less garnets vary in MgO- FeO content from megacrystic values ~10-11% FeO 12- 16% and more common for eclogites (Fig.1). Low Cr_2O_3 >1% garnets higher in TiO_2 to 2% belong to pyroxenites and to megacrystic suit. Garnets with 1-2 % Cr_2O_3 are common lherzolitic and Fe- Ti –enriched pyroxenitic garnets are found in 2-4 Cr_2O_3 interval. Three groups of lherzolitic (and pyroxenitic) garnets Cr_2O_3 >4 were divided from dunite-harzburgites by nearly continuous trend in lherzolite lower boundary. Rare subcalcic dunite harzburgites garnets reveal three clusters. Enrichment in TiO_2 concentration for Cr-rich garnets is correlating with rise TiO_2 for the Cr- spinels only in uppermost part of mantle. All Fe- rich (to 25% FeO) garnets is difficult definitely to attest as to be born in mantle conditions. The orange 'eclogitic' 12-15% FeO garnets are not frequent in concentrate.

Clinopyroxenes from Yubileinaya pipe contain high amount of Na_2O, Cr_2O_3. Al_2O_3 close to Cr_2O_3 in values are concurring for Na_2O in structure. Such pyroxenes are typical for the metasomatic peridotites [2, 12, 13, 21, 36, and 37]. These clinopyroxenes common for many localities: Colorado- Wyoming [12, 22] in Chmopolo kimberlite –like rocks [1, 6] usually contain nearly equal amount of Fe, Cr, Na Al. (Fig. 2). the clustering based on the Al_2O_3 is more realistic then those based on the Cr_2O_3 because the later produce several positive lineal Fe-Cr lines. On variation diagram for clinopyroxenes from the several Daldyn-Alakite pipes (Fig.4) they plot at the central part between the depleted clinopyroxenes from garnet peridotites from Udachnaya pipe [8, 20, 29] and those from spinel peridotites (Fig. 3). At least 4 correlation lines between FeO and Na_2O (Fig. 2-3) possibly reflect different processes of mantle metasomatism and enrichment of mantle peridotites by the melts. Positive good correlation Fe –Ti and Fe-Al and Fe -Cr - two large clots for Yubileinaya pipe definitely differ from the other groups of the kimberlitic clinopyroxenes from other Daldyn- Alakite kimberlites.

Amphiboles in the concentrate usually found as the intergrowth with the Cr-diopsides may be subdivided in to 5 groups (Fig. 4) (Mg- richterite – kataforite-pargasite hornblende- pargasite - kaersutite) with the general rise of Fe-Ca-Ti what reflect the sequence from the deep to upper mantle section and degree of the differentiation of the metasomatic agents (Fig. 4). In general Fe-in amphiboles is correlating with K2O and negatively with the Na_2O. Behavior of TiO_2 and Cr_2O_3 differ for this two amphibole groups rising with silica content for Ca- amphiboles Al_2O_3 fall with SiO_2 increase while Mg is rising for deeper amphiboles.

Micas form concentrates belongs to three groups: relatively large, Ti- biotites, reflect vein suits Cr – rich (to 2%) phlogopites containing crystalline inclusions

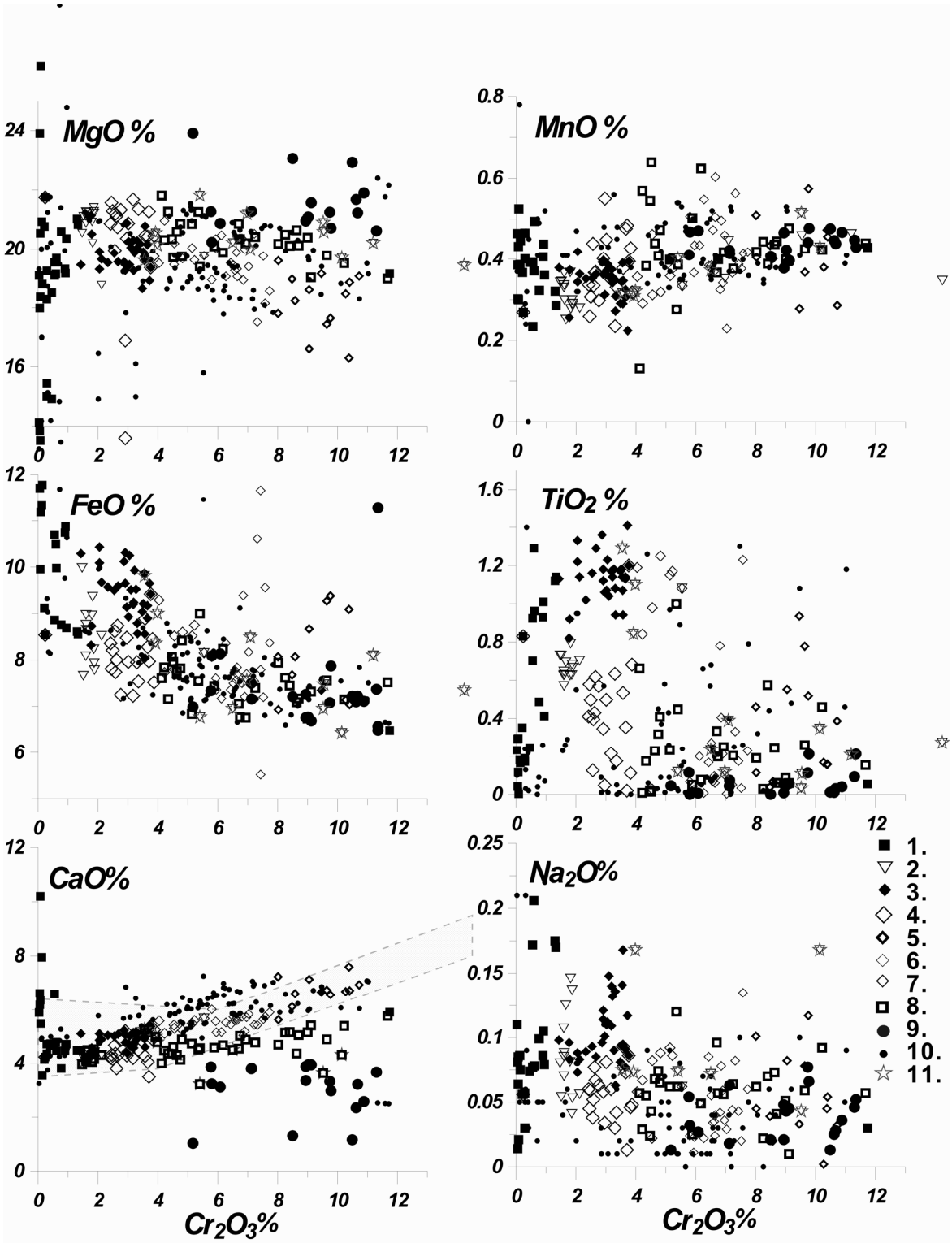

Fig. 1. *Variation diagram of garnet composition from the concentrate from Yubileynaya pipe. Variations of the garnet compositions*

1. megacrysts, eclogites, Fe-pyroxenites; 2. Ga-Sp –peridotites; 3. Ga-Sp –pyroxenites; 4. Ga- pyroxenites; 5. Ga- peridotites; 6. Ga – pyroxenites;7. peridotites from diamond facie; 8. depleted lherzolites; 9. Sub -Ca garnets (dunite); 10. Garnets from Udachnaya pipe; 11. Garnet analysed by ICP.

rutiles and Mg-rich low -Ti phlogopites. Most of micas fall at the field between istonite and phlogopite [24] (Fig. 5)

Spinel Cr- rich compositions (Fig. 6) reveal deviation from mantle array caused by different type of the isomorphic substitution. Ulvospinel enrichment is characteristic for Cr rich spinels while the middle parts common FeCr – MgAl trend dominates. V2O5 is correlating in general with the TiO_2 behavior and NiO with the MgO. All spinel sequence was divided on to 7 groups possibly reflecting mantle layering (Fig. 7).

Ilmenite compositional trends differ from the common schemes of the ilmenite fractionations found for the Africa [14, 24] and other kimberlites. General positive TiO_2- MgO and negative FeO correlations became more complicated in case for the minor components (Fig. 8). Several sub parallel lines of Cr_2O_3 enrichment suggests mechanism of the AFC interaction with the peridotites and possibly metasomatic trend associations for more magnesian compositions. Abrupt decrease of the Al in the central part possibly suggests the coeval garnet precipitation. The step by step decreasing Al trend due to different crystallization associations is also visible. Vanadium trend which rise in general together with FeO may be also divided on to two parts

THERMOBAROMETRY

Due to lack of abundant fresh polymineral xenoliths [19] except of several eclogites (Cr- bearing but more Fe–Na –rich close to Obnazhennaya nodules [36] we used three variants of the monomiteral *clinopyroxene thermobarometry* applicative for the Cr-Diopsides from the kimberlites [4, 5, 26]. Here we used also the new equation which is developed to account the influence of TiO_2, Fe2O3 for the metasomatic associations. Two barometers produced in general similar diagram but different layering based on Cr - Al minals associated with the

Na (Fig. 8 a, b). Mantle column is likely should be built up from at least 5 essentially clinopyroxene- bearing rocks (lherzolites), the depleted dunite – harzburgite [8] horizon in lower part and the heated bend giving the inflection to the hot field which for Udachnaya [8] and South Africa [9, 27] corresponds to the sheared (asthenospheric) lherzolites. The thermobarometric methods give relatively heated geotherm (to 40 mv/m2). In general the amount of the layers is close to those from the Udachnaya pipe though the composition of peridotite minerals and associations essentially differ.

Newly developed garnet thermobarometry [5] with two variants of equations based on Cr and Al-Cr combinations also give two variants of TP diagrams with nearly continuous changing of the associations with the depletion to the depths for the Al-Cr variant (Fig. 8 c) and sharp layering with the 3 horizons of the dunite – harzburgite – lherzolite (+ pyroxenite) bends.

GEOCHEMISTRY

The LAM ICP analyses of the minerals 20 for 30 components (Fig. 9) (tabl. 1) reveal rather specific TRE distributions. The LREE enrichment for CPx is so high that they REE patterns are nearly lineal with the more enriched patterns for

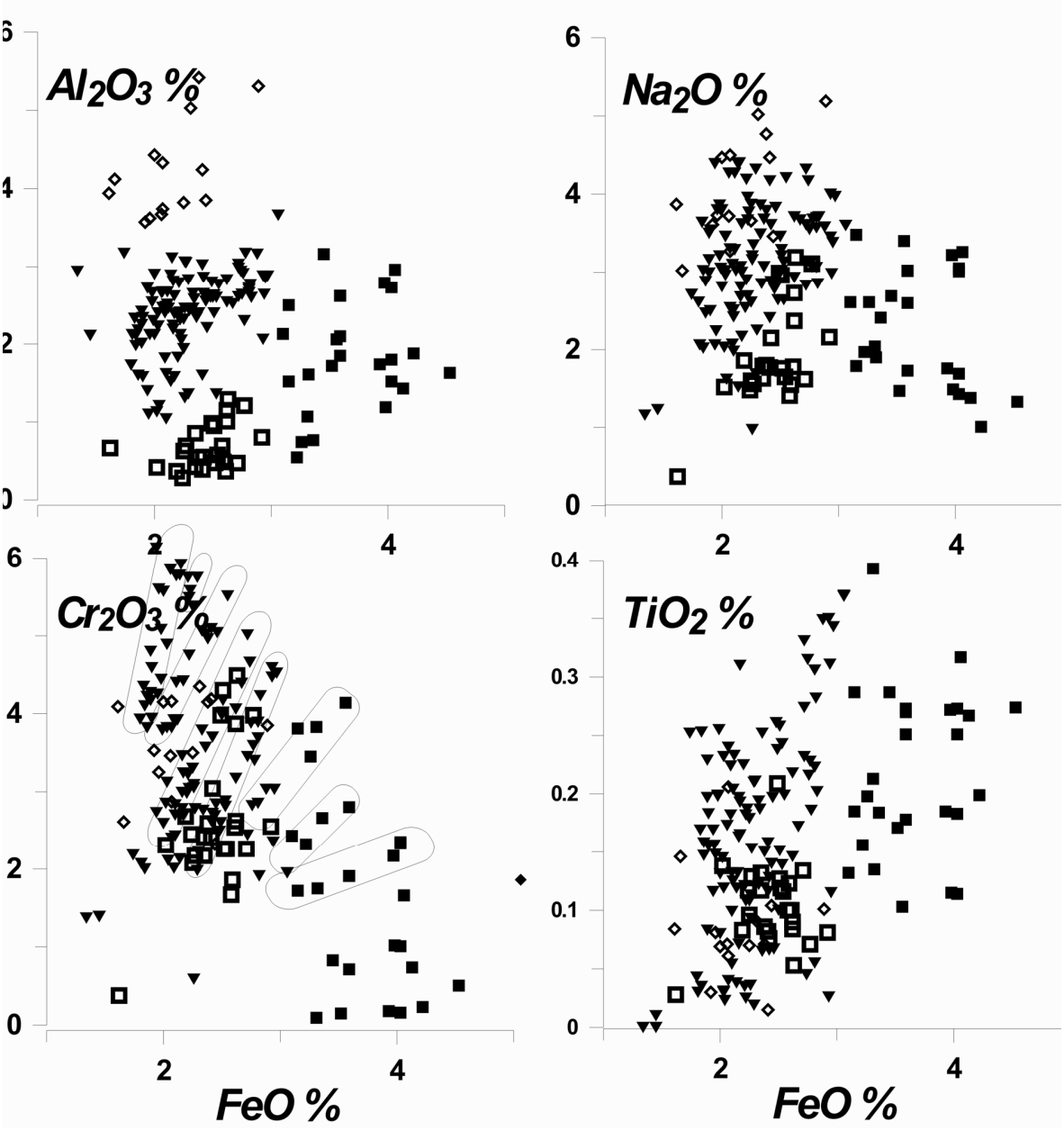

Fig. 2. *Variation of the clinopyroxene compositions with the subdivision to the major chemical groups.*

the deeper pyroxenes (see Fig. 8a, b) similar to Phl-richterite peridotites from Kimberly [14]. Amphibole has concave upward REE and is very close in TRE elements also for the composition of one kimberlite from Yubileynaya analyzed also by LAM ICP method. The garnets highly vary from S- type what is more common for the Cr- rich garnets to HREE - rich more rounded patterns with- and without Ce minima and even to hampered in middle part REE line found for

pyroxenite garnet [16]. Clinopyroxenes reveal Ti- Pb minima for most enriched compositions but elevated Th, Nb, U. Garnets an opposite reveal Pb, Ti peaks (possibly due to microinclusions).

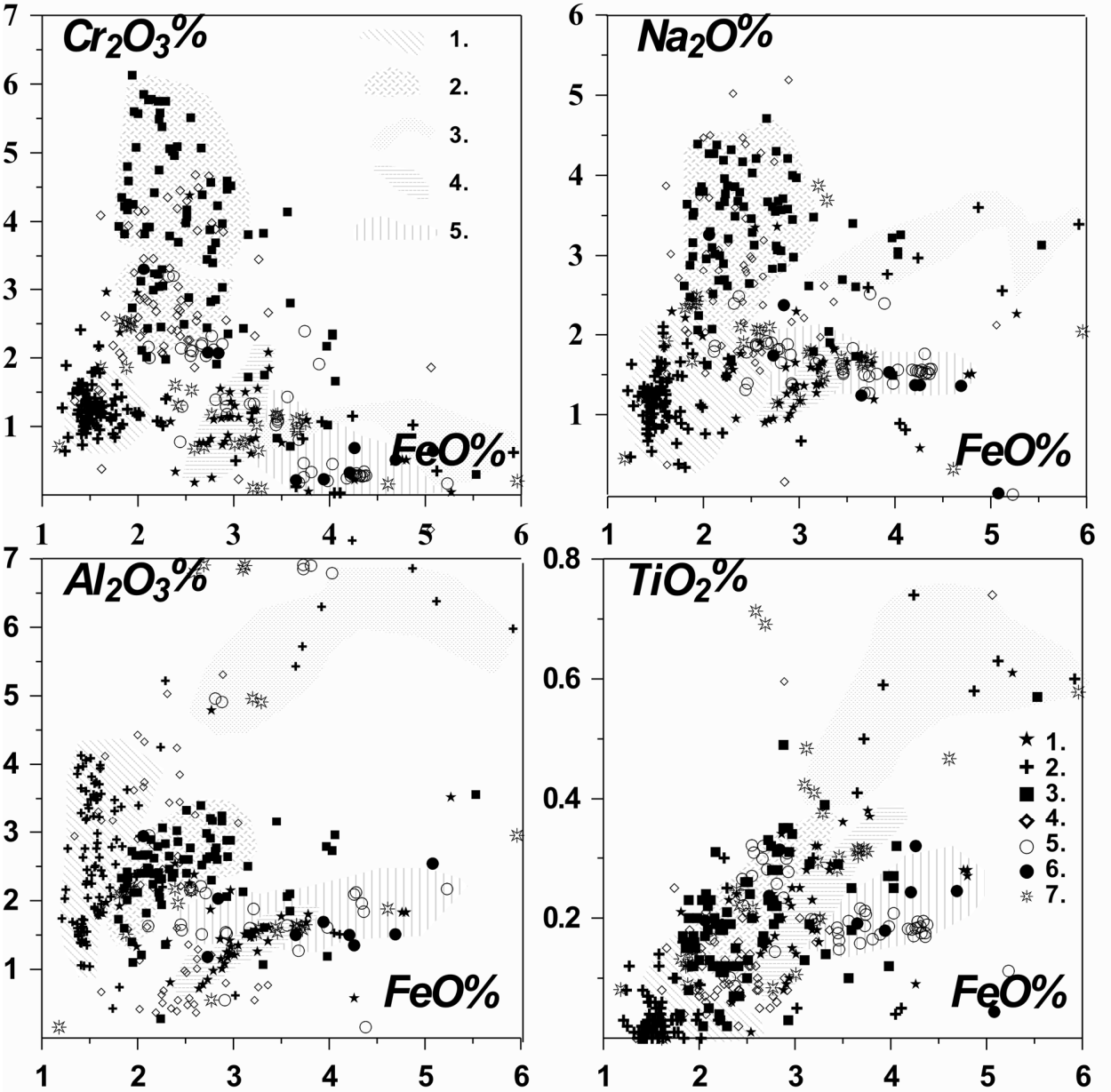

Fig. 3. *Variation of the clinopyroxene compositions from several pipes from Daldyn- Alakit kimberlites.*

1. Udachnaya, diamond facies; 2. Udachnaya, 3. Yubeleinaya, diamond facie; 4.Yubileinaya, garnet facie; 5. Irelyahskaya; 6. Dolgozhdannaya; 7. Zarnitsa. Shaded areas. 1- primary depleted; 2. eclogitic and hibridic; 3. metasomatic; 4. sheared 5. melt interaction.

Spinels and ilmenite both reveal rather specific W-type REE distributions.

TRE spidergrams for ilmenites display very high Nb-Ta-Ti peaks rising with the degree of REE depletion. In spinels Nb –Ta are correlating with LREE but Hf-

Ti-Zr correlate negatively. Mica reveal very high the REE and TRE patterns with the HFSE LILE (Rb, Cs) high concentrations what is in accord with the rutile co-precipitation.

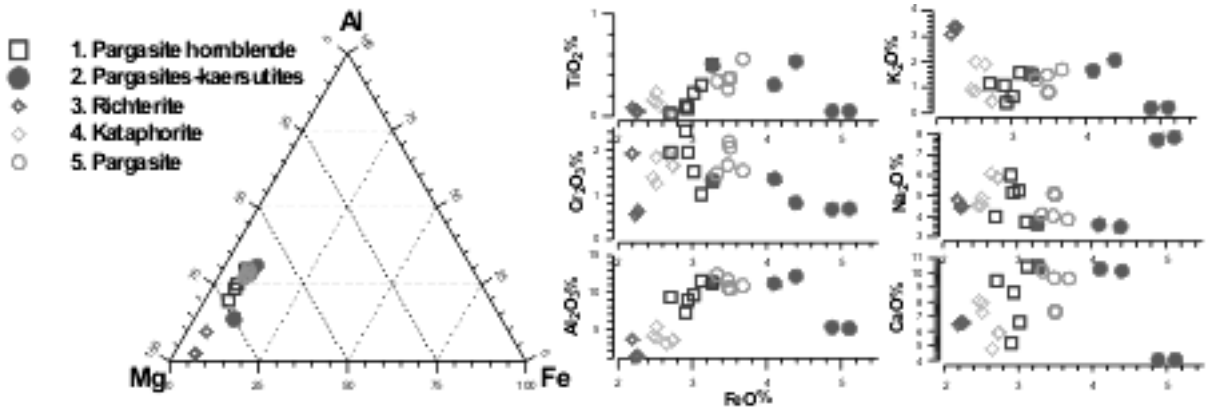

Fig. 4. *Variation of the amphibole compositions.*

1. pargasite hornblende, 2. kaesutite, 3. richterite, 4. kataforite, 5. pargasite.

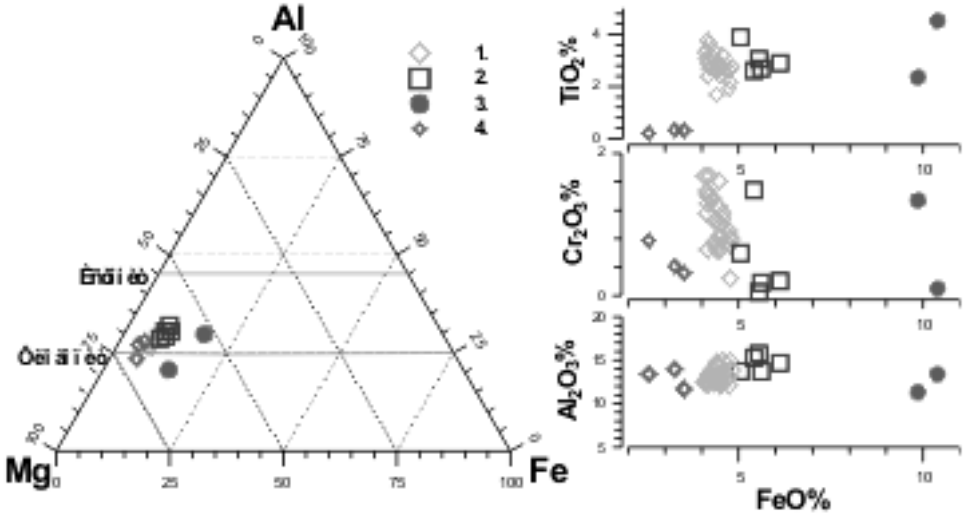

Fig. 5. *Variation of the mica compositions.*

1. Mg- phlogopite, 2-3. Cr-Ti bearing– phlogopite – istonite, 4.Ti- biottite.

The TRE compositions of three samples of kimberlites scanned by laser (1-2mm^2) reveal the distributions close to the other kimberlites from the central part of Yakutian diamond province [1] with the small Zr- Ti- Hf minima. The more serpentinized samples reveal general and especially LILE decrease.

DISCUSSION

Suggestions about the composition of the mantle column. Comparing the mineralogy of the clinopyroxenes and garnets from Yubileinaya with the data base on the minerals from published works [7, 8, 11-13, 19, 24, 26, 27, 32-36, 40] and

analyzed other pipes it possible to receive the imagination about the compositions of the rocks. Alkaline clinopyroxene Cr rich peridotite associations are typical for the Wyoming kimberlites [3, 12, 22] concentrate from the kimberlitic pipes from Amga (Chompolo) [1, 6], Obnazhennaya pipe [36], Nikos kimberlites, Finland, diamond inclusions in Sputnik pipe [35] and form Molodo [19]. Modal composition of these rocks vary from depleted coarse lherzolites – harzburgites to pyroxenites. Frequent intergrowth with the Ca – and alkaline amphiboles is similar

Table1.

Major and trace element composition of the minerals from the concentrate of Yubileinaya pipe

Comp.	GrY1	GrY2	GrY3	GrY4	GrY5	GrY6	GrY7	Am1Y	YCpx1	Yb Cpx2
SiO2	41.00	41.21	41.63	40.65	41.30	41.09	41.47	46.62	54.61	54.64
TiO2	0.03	0.24	0.84	1.10	1.29	0.12	0.35	0.50	0.03	0.27
Al2O3	16.34	18.30	19.28	18.33	18.87	19.36	15.56	11.31	2.23	2.62
Cr2O3	9.52	6.50	3.92	3.98	3.55	5.40	10.14	1.30	4.89	1.91
FeO	6.95	6.95	8.36	9.00	9.81	6.77	6.43	3.27	2.03	3.59
MnO	0.52	0.37	0.31	0.32	0.32	0.40	0.43	0.02	0.09	0.11
MgO	20.90	20.22	20.55	20.13	19.61	21.82	19.70	18.74	14.83	14.67
CaO	3.64	4.50	4.99	4.78	5.25	3.23	4.31	10.40	16.66	17.81
Na2O	0.04	0.07	0.07	0.17	0.08	0.07	0.17	3.65	3.46	3.02
K2O					0.01			1.51	0.03	0.01
Сумма	98.94	98.36	99.96	98.46	100.08	98.27	98.56	97.33	98.85	98.66
Ba	0.89	0.45	0.79	0.81	0.22	0.43	0.67	79.1	385	35
La	0.15	0.05	0.03	0.04	0.01	0.02	0.16	4.8	150	15
Ce	0.61	0.14	0.10	0.10	0.07	0.11	0.29	15.2	261	22
Pr	0.13	0.03	0.02	0.03	0.02	0.02	0.08	2.6	26.8	4.3
Nd	1.00	0.41	0.23	0.29	0.17	0.27	0.47	13	86	15
Sm	0.37	0.27	0.20	0.26	0.17	0.16	0.51	2.7	10.2	2.4
Eu	0.10	0.10	0.07	0.11	0.08	0.07	0.27	0.8	2.6	0.6
Gd	0.25	0.44	0.30	0.51	0.32	0.21	1.14	2.1	6.3	1.6
Tb	0.01	0.07	0.05	0.09	0.06	0.04	0.20	0.2	0.6	0.18
Dy	0.08	0.42	0.31	0.87	0.36	0.15	1.12	1.1	2.7	0.7
Ho	0.01	0.10	0.06	0.18	0.09	0.02	0.18	0.1	0.4	0.10
Er	0.04	0.29	0.15	0.56	0.27	0.05	0.35	0.3	0.8	0.2
Tm	0.01	0.05	0.02	0.08	0.03	0.005	0.04	0.03	0.1	0.02
Yb	0.07	0.25	0.17	0.48	0.23	0.06	0.26	0.2	0.4	0.1
Lu	0.01	0.05	0.03	0.07	0.03	0.02	0.04	0.02	0.1	0.0
Hf	0.17	0.10	0.22	0.35	0.32	0.10	0.31	1.7	2.1	1.4
Ta	0.02	0.01	0.02	0.01	0.00	0.00	0.02	3.1	0.3	0.4
Pb	0.30	0.16	0.27	0.14	0.03	0.10	0.33	0.50	0.59	12.2
Th	0.068	0.017	0.019	0.022	0.005	0.011	0.08	0.10	13.3	1.0
U	0.025	0.006	0.005	0.006	0.003	0.007	0.02	0.015	0.424	0.07
V	27	45	39	58	44	36	73	165	267	140
Sc	28.8	24.3	16.5	25.0	15.7	22.1	51.1	27.3	32.2	24.6
Co	29.8	27.7	22.7	24.8	20.0	19.5	23.2	28.2	24.6	25.7
Cu	7.0	6.6	6.6	6.5	7.9	6.7	7.1	9.8	8.4	17.8
Rb	40.0	20.0	5.12	4.60	3.90	0.33	0.38	5.0	1.17	1.95
Sr	1.80	1.09	0.96	0.74	0.59	0.72	3.65	171	664	0.57
Y	0.30	2.73	1.61	4.84	2.59	0.59	4.72	3.92	10.02	2.25
Zr	2.2	3.7	7.9	14.1	10.3	6.0	24.5	67	38	29
Nb	0.21	0.10	0.10	0.10	0.14	0.07	0.25	30	4	3
Cs	0.008	0.008					0.004	0.01	0.05	0.02

Table 1. *(end)*

Comp.	YCpx3	YCpx4	YIlm1	YIlm2	YIlm3	YChr2	YChr3	YChr1	YbMic1
SiO2	54.86	54.73				0.04	0.10		40.39
TiO2	0.37	0.01	48.09	51.42	44.45	0.06	0.38	0.04	3.41
Al2O3	3.66	2.11	0.45	0.65	0.16	18.37	21.27	19.05	12.49
Cr2O3	1.95	1.39	0.91	0.78	5.53	52.76	48.28	47.25	1.47
FeO	3.06	1.45	39.80	33.12	39.32	17.05	14.81	21.43	4.14
MnO	0.08	0.01	0.27	0.30	0.28	0.29	0.26	0.58	0.01
MgO	14.88	16.25	9.21	12.19	8.13	11.25	13.91	10.51	22.46
CaO	16.28	22.32	0.02	0.04	0.01	0.00	0.06	0.00	0.02
Na2O	3.60	1.23				0.07	0.03		0.36
K2O			0.05	0.10	0.13			0.08	9.88
Сумма	98.74	99.50	98.81	98.60	98.00	99.89	99.11	98.95	94.62
Ba	194	59	0.44	0.48	0.20	1.1	0.54	0.83	291
La	60	36	0.03	0.02	0.00	0.33	0.024	0.05	2.1
Ce	102	51	0.04	0.04	0.01	0.16	0.052	0.25	5.7
Pr	14.2	7.3	0.01	0.01	0.00	0.01	0.009	0.01	0.52
Nd	54	31	0.06	0.04	0.01	0.05	0.035	0.14	1.7
Sm	8.2	5.0	0.06	0.03	0.02	0.01	0.025	0.07	0.26
Eu	2.3	1.37	0.03	0.01	0.01	0.02	0.024	0.02	0.11
Gd	5.4	3.5	0.07	0.05	0.02	0.05	0.081	0.09	0.20
Tb	0.7	0.41	0.02	0.01	0.00	0.007	0.010	0.01	0.02
Dy	3.1	1.7	0.07	0.02	0.02	0.014	0.025	0.07	0.13
Ho	0.4	0.24	0.01	0.00	0.00	0.003	0.006	0.01	0.02
Er	0.9	0.45	0.03	0.01	0.003	0.004	0.025	0.02	0.02
Tm	0.1	0.06	0.004	0.001	0.001	0.003	0.003	0.004	0.01
Yb	0.7	0.25	0.02	0.02	0.01	0.007	0.014	0.02	0.03
Lu	0.1	0.03	0.00	0.01	0.004	0.002	0.004	0.01	0.01
Hf	1.8	1.73	4.1	5.0	7.7	0.010	0.017	0.07	0.32
Ta	0.6	0.26	58.1	72.9	110	0.027	0.038	0.74	2.2
Pb	10.7	0.48	0.12	0.10	0.002	0.04	0.06	0.20	0.37
Th	2.0	2.3	0.006	0.004	0.002	0.049	0.003	0.005	0.47
U	0.1	0.277	0.014	0.006	0.011	0.054	0.009	0.004	0.32
V	308.4	174	628	363	595	314	294	240	219
Sc	25.4	18.8	14.8	11.9	17.0	2.0	3.9	5.7	6.2
Co	34.0	18.8	82.7	53.8	60.9	108	70	65.0	59
Cu	9.5	8.5	14.1	10.3	9.6	7.5	8.5	7.2	11.0
Rb	3.0	3.810	0.44	0.009	0.004	0.167	0.167	0.56	289
Sr	502	278	0.69	0.78	0.54	1.2	1.3	1.35	11.0
Y	13.26	7.29	0.338	0.034	0.036	0.06	0.17	0.430	0.57
Zr	64.7	37	126	155	228	0.46	0.85	3.0	11.61
Nb	15.3	4	415	541	887	0.82	0.42	4.7	20.52
Cs	0.2	0.17	0.002	0.004					2.04

Notes. *Analyses were made in Analytical Center of UIGGM SB RAS, Novosibirsk. Major components are determined by CamebaxMicro (O.S. Khmelnikova, January, 2003). Trace elements are determined using ICP MS "ELEMENT" (Finnigan) with laser UV LaserProbe (S.V. Palessky, I.V. Nikolaeva, A.I. Saprykin, Febrary, 2003).*

to Namibia [13] and Zimny Bereg, Zimbabve kimberlites. Such compositions mineralogy and petrography corresponds to the motley mantle sequence with wide distribution metasomatites, anatexic pyroxenites as well depleted harzburgite-dunites. For the and Kl-1 kimberlite pipe Wyoming [12] is suggested the

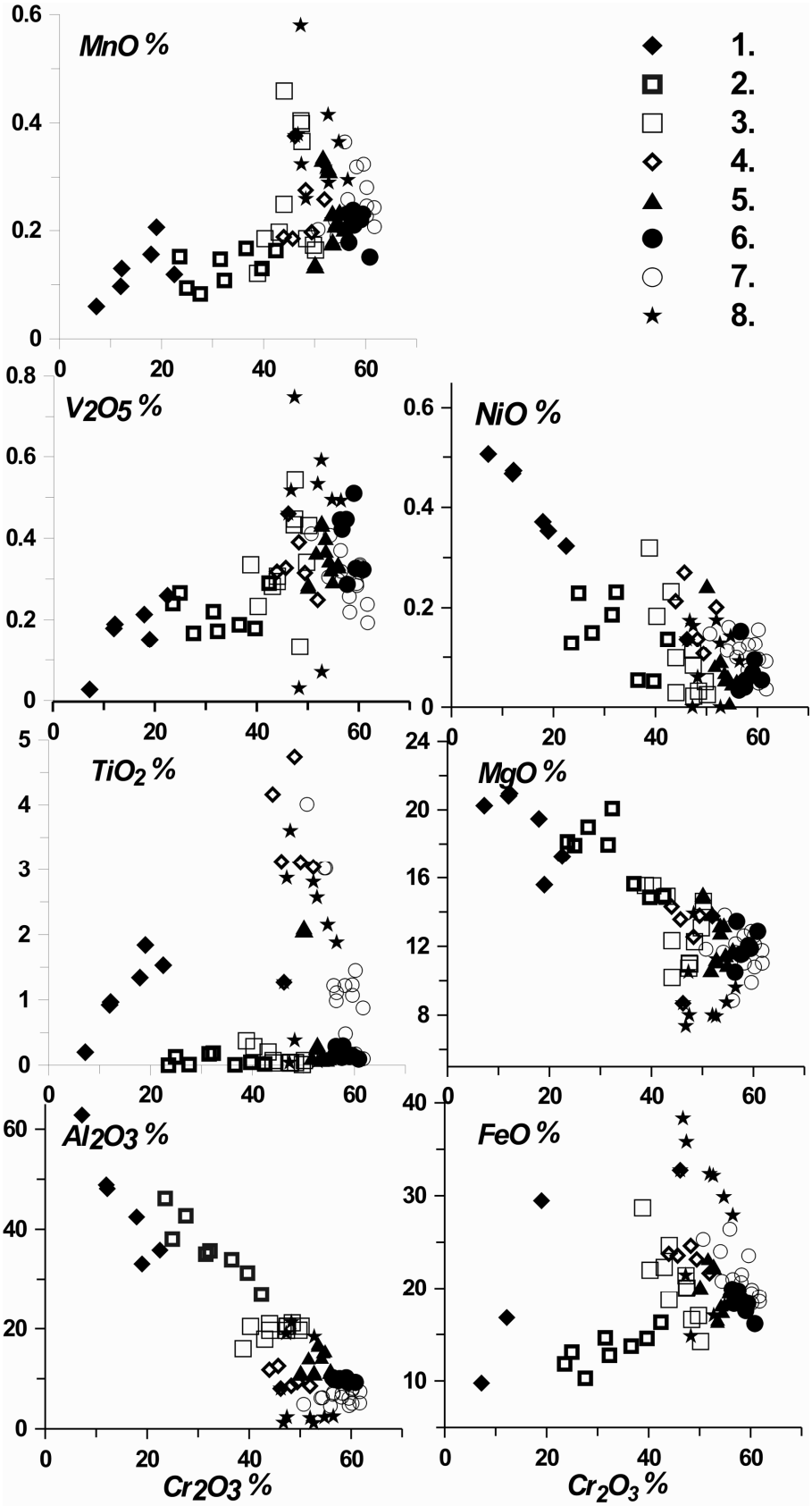

Fig. 6. *Variation of the spinel compositions. Division om groupth is close to Fig1.*

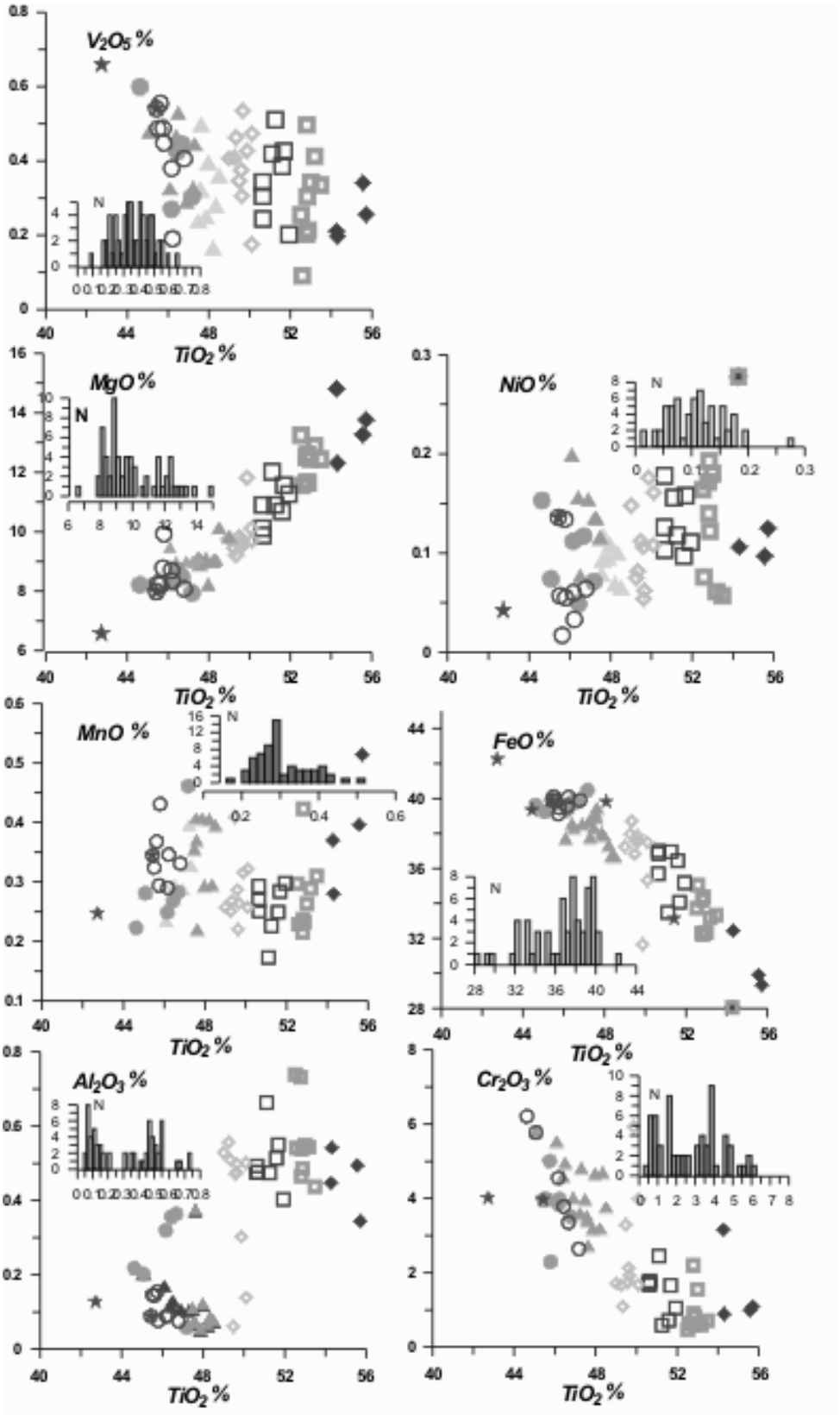

Fig. 7. *Variation of the ilmenite compositions.*

Division om groupth is close to Fig1. Variation of the ilmenite compositions. Division om groups is close to Fig1.

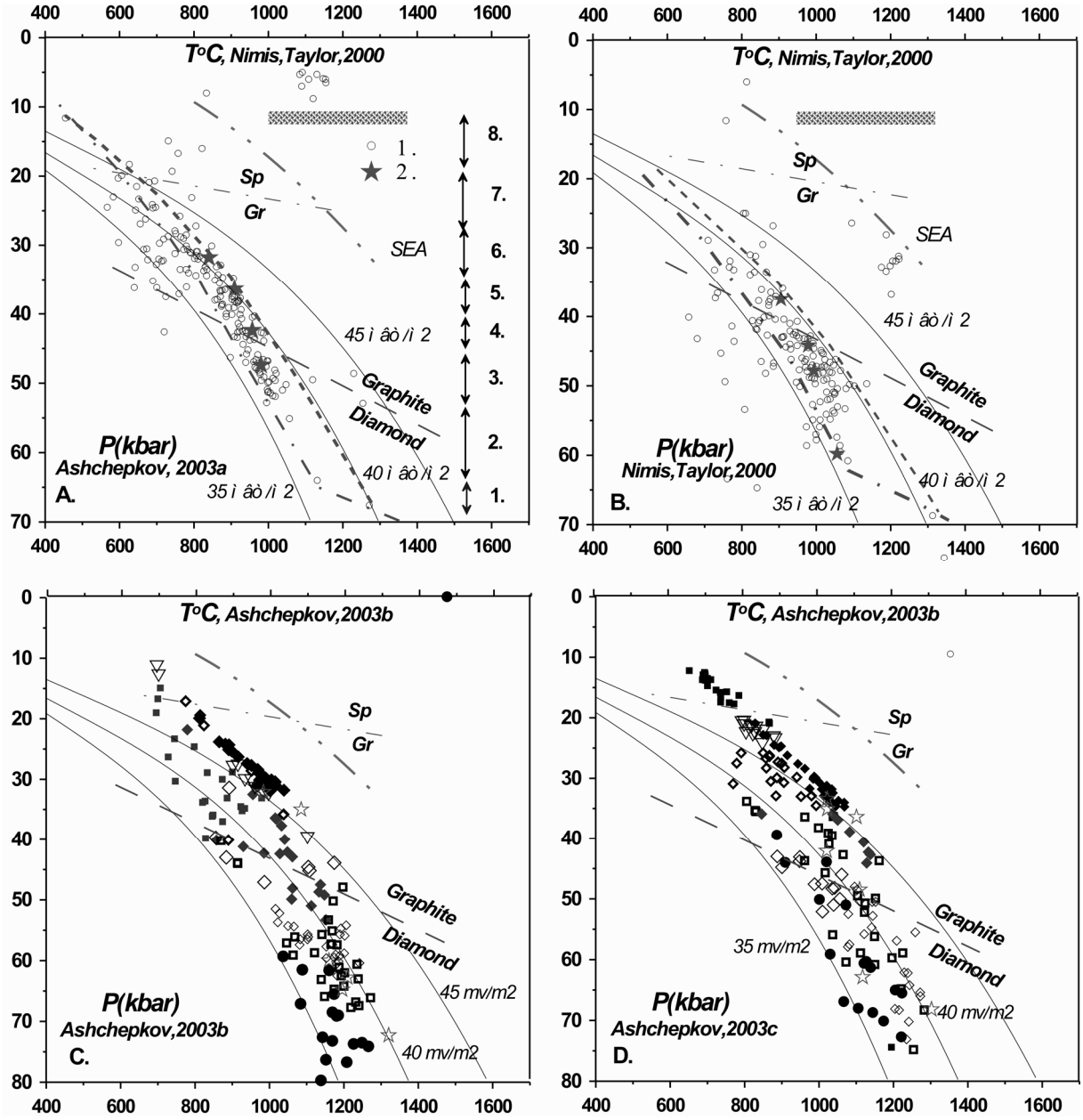

Fig. 8. *TP estimations using the clinopyroxene concentrate form Yubileynya pipe.*

Groups the same as for the Fig.1

influenceof the subduction related silica- rich fluids what is the common for the mantle keel of craton.

Construction of the mantle column in PT diagram 5 major peridotites (Cpx rich) units in the mantle section of the Yubileynaya pipe may be suggested. Depleted hot horizon should exist in the basement dividing essentially pyroxene- bearing asthenospheric mantle peridotites. In spinel facie Fe- enriched Gar – pyroxenites should exist. The Cr based models give the same but even more sharp layering The middle layer in 35 kbar coincides with the inflection of the garnet trends near 4 % of Cr_2O_3.This level in mantle (fluctuating between the 35 and 40 kbar) in PT diagrams correspond to the crossing of the path of the subducting slabs with the

water bearing peridotite solidus [39, 41] and is also close to the crossing of the subduction gradients with the dehydration line of peridotites ca 35 kbar 750^{o}C [38]. Presence of H_2O rich layer is responsible for the LT melting and

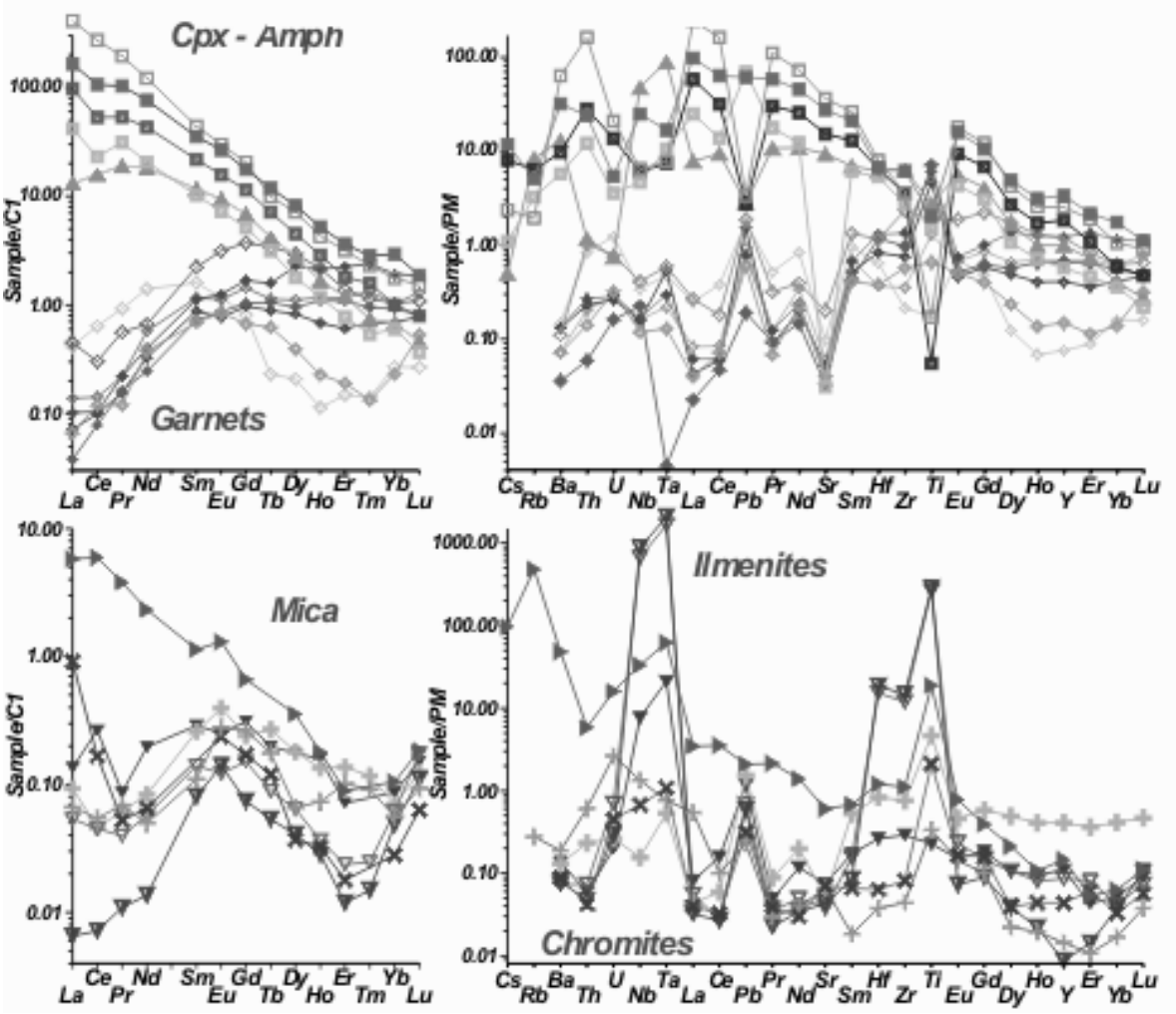

Fig. 9. *TRE compositions of the minerals from Yubileinaya pipe*

producing of anatexic and hybrid (with eclogite admixture) pyroxenites. But judging by the presence of the richterite garnets that are typical for the metasomatites from 60 kbar in Kimberly [14] the mantle column beneath Yubileinaya was all subjected to the fluid interaction and K- enrichment at the more deep level probably due to the continental type subduction and decomposition of the phlogopites.

Reasons of layering most probably originally were in the subduction [28]. Layering should be the common feature of lithospheric mantle. It was proved that is growing from the bottom by the underplating of the subducting layers. Mantle convection has the cycles multiplied to 32 (16) ma and in each new cycle new subducting possibly may couple to the lithiospheric keel. The amount of the layers for this pipe is very close to Udachnaya pipe [8] what evidence for the same stages of the craton growth in the adjacent areas. Physicochemical reasons - phase

transitions that usually accumulate melts and pyroxenites due to the density melt/solid difference changes [29], regulations of the fluid flow etc also play essential role. The waves of the melt fluid percolations like it suggested for Horoman and some orogenic massifs may be the next reason.

Metasomatism determined by wide spreading of the hydrous phases and the long and continuous trends of the mineral compositions may be explained by the interaction of the mantle peridotites with the hydrous alkaline and silica rich melts and fluids. Positive correlation of K with the Fe suggests that the metasomatic agencies were of different and independent types – these are deep fluids (K-Fe) and rich carbonatite melts [39]. The most probable candidate source of the Na-Al metasomatism are the subducted slabs where Na-Al eclogites are associated with the hydrated mantle peridotites of the subduction mantle wedge. The K-Fe-Ti metasomatic agents may have subduction nature (Ti-low) with the involvement of continental sediments. It is likely also that K-Ti agent represent the plum sources. The K metasomatism is more deep then Na-Al.

Trace element also evidence about the different nature of the metasomatic agents. Reconstructed with the KD for Cpx [15], garnet [16], spinels, ilmenites [40] and mica parental melts display the evidence for the difference for the mineral forming mater for some of them. Analyzed alkaline Cpx are formed by more enriched melts then garnets even assuming the possibly T- depended variation in the scale by the order of 1 at least. The melts parent for the chromites are close for those formed ilmenites being lower for the later. Micas – born melt has more enriched are and HFSE –high compositions probably due to partial dissolution of ilmenites. These facts evidence for the multistage mineral growth in the mantle column beneath Yubileynaya pipe possibly in the different vein environment and depth levels (Fig. 10).

Joint evolution of the megacrystic and peridotite suits is the possible explanation of the similarity of the geochemistry of the spinels and ilmenites. Some silicates including garnets also may be products of such crystallization. In rare nodules in Colorado kimberlite concentrate [3] it possible to find the associations of Cr- rich garnets, ilmenites, Ti-rich spinels. The growth of the Cr – garnets and Na-Cr clinopyroxenes in micaceous kimberlites from Daldyn field from the kimberlites was suggested. The assumption seems to be partly realistic because such associations do not reflect all the varieties and spectrums of the mineral compositions. Megacrystalline associations that similar to the alkaline basalts trace the feeding pre- eruption vein system are lower in Cr content. But some high temperature metasomatic veins and apophyses may contain the material with the hybrid peridotite and kimberlite (carbonatite features).

Metasomatism. Highly volatile and fluid rich melts like kimberlites and carbonatites may penetrate through the rather vast system forming high scale metasomatic changes in surrounding peridotites and change their compositions also due to the intensive exchange with the peridotites. The contact rock halo possibly may change their characters in time and space accounting the interaction

of the rising system with metsomatics that should be created at the previous subduction stages. The units and mantle wedges coupling with the cratonic keel may differ and include the metasomatites formed by Na-enriched fluid system in

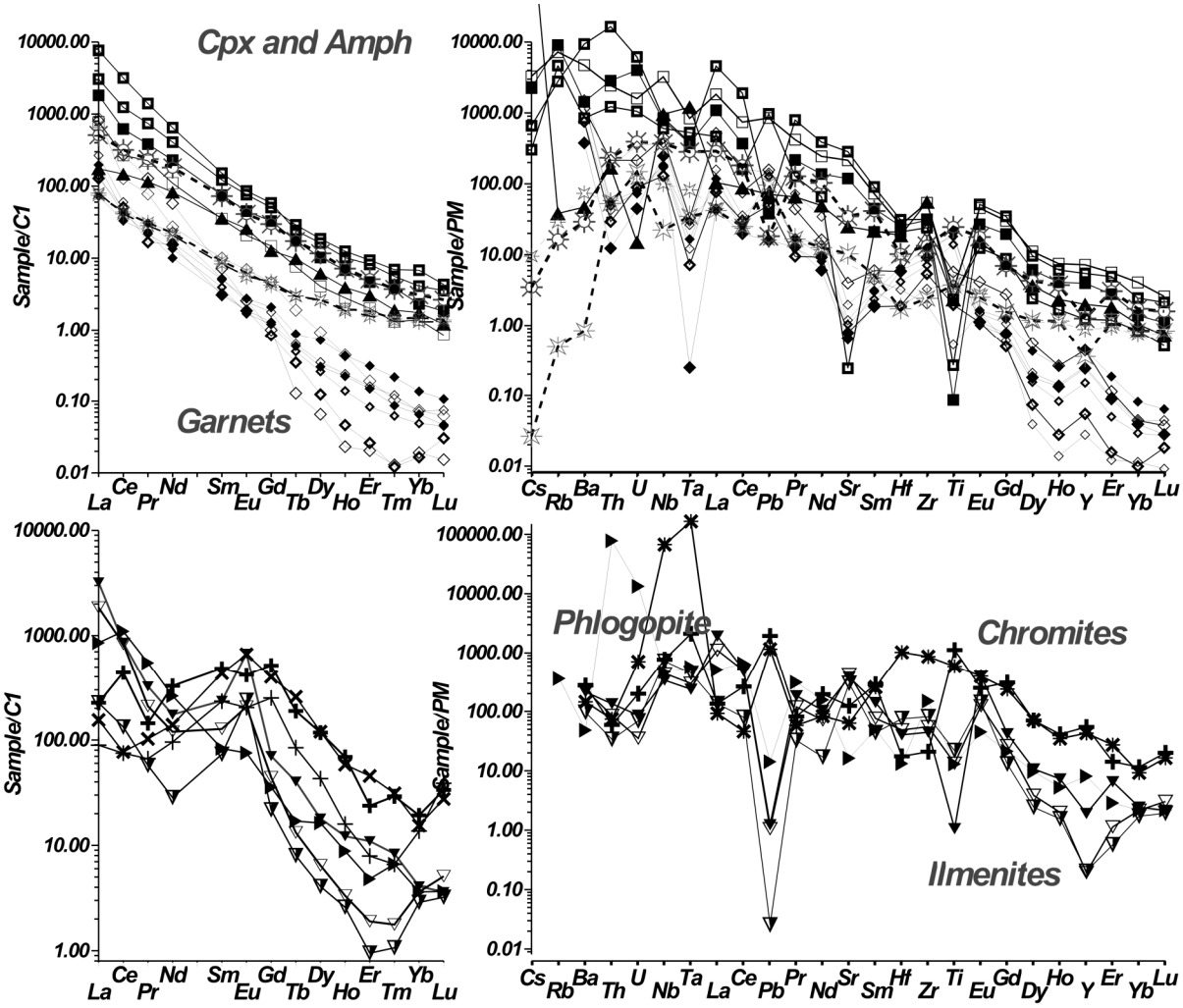

Fig. 10. *TRE compositions of the melts parental for the minerals and some kimberlite samples from Yubileinaya pipe.*

oceanic mantle and by more deep and K-rich melt/fluids derived from the continental slabs.

Comparison with Udachnaya shows that mineral concentrates from Yubileynaya pipe sharply differ from those of Udachnaya in chemical features. Garnets from Yubileynaya are relatively more Mg-rich and Ca poor comparing to Udachnaya. The trend for the garnets and amount of the independent groups is much higher though some varieties are close.

Alkali -rich pyroxenes in Udachnaya are rare (1%) but Hi- Alumina eclogitic pyroxenes are more widely met in the concentrate. For the chromites from Udachnaya the ulvospinels as well as the abundant sub trends are not characteristic while Yubileynaya spinels demonstrate complicated branching trends. In general

for Yubileynaya primary subduction eclogites are not so characteristic as well as Fe- rich garnet websterites that are common in shallow mantle in Udachnaya [20] while metasomatic associations are very typical. Ilmenite trend in the Yubileynaya pipe suggest intensive exchange of the parental magma with the peridotites column. The difference also appeared in the high developing of the Ti-Na rich pyrope population which should correspond to garnet anatexic pyroxenes while for Udachnaya in the shallow level the hot Fe- harzburgites and lherzolites are more typical.

CONCLUSIONS

1. Mantle beneath Yubileynaya pipe is layered like beneath Udachnaya pipe. Degree of the depletion rise with the depths. Middle part concentrate pyroxenites The heat flow corresponds to 35-40 mvt/m2
2. Peridotites are represented by the fragments of metasomatic associations. Analyzed pyroxenes were not in equilibrium with the garnets sometimes. The type of metasomatism changes from the Fe-K to Na- Al in shallow mantle
3. Ilmenite trends at least at the last stages were produced by the polybaric fractionation of protokimberlite – (carbonatite) melt within during the creation of vein feeding system.

ACKNOWLEDGMENTS

To the geologists of Amakinskaya expedition for the allowing to receive the concentrate. To stuff of the laboratory of microanalyses and ICP MS of UIGGM SD RASc. To Pokhilenko N.P, Kuligin S.G. Malygina E.M. for the giving the analyses from Udachnaya pipe.

Supported by RBRF grants: 99-05-65688, 00-05-65288, 03-05-64146.

REFERENCES

1. **Agashev A.M., Orihashi Y., Watanabe T.** Isotopic –geochemical characteristics of the Siberian platform kimberlites and the problem of their origin.// Russ.Geol.Geophys., 2000. v. 41., N1., pp. 90-99.
2. **Ashchepkov I, Vladykin N., Pokhilenko N., Sobolev N., Malygina E., Kuligin S., Ovchinnikiv Yu, Afanasiev V., Mkrtychan G., Rotman A., Kostrovitsky S. Tolstov A., Khmel'nikova1 O., Pokhilenko L, Logvinova A.** Clinopyroxene geotherms for the mantle columns beneath kimberlite pipes from Siberian craton. //Extended Abstracts of the 8International Kimberlite Conference. 2003.
3. **Ashchepkov I. V., Vladykin N. V., Mitchel R. H.l, Coopersmith H., Garanin V. G., Saprykin A. I., Khmel'nikova O. S., Anoshin G. N.** Mantle Evolution beneath the Colorado Plateau: Interpretation of the Study of Mineral Concentrates from KL-1 Kimberlite Pipe.// Trans. RAS ESS v385 pp. 721-726.
4. **Ashchepkov I.V.** Jd-Di barometer for mantle peridotites and eclogites.// Experiment in Geosciences 2002, v.10, N1, 137-138.
5. **Ashchepkov I.V.** Empirical garnet thermobarometer for mantle peridotites. //Seattle Annual Meeting (November 2-5, 2003). Abstract ID: 65507.

6. **Ashchepkov I.V., Vladykin N.V., Saprykin A.I., Khmelnikova O.S.** Composition and thermal structure of the mantle in peripheral parts of the ancient shields within Siberian craton. //Revista Brasileira de Geociencias, 2001, 31(4): 527-636.
7. **Boyd F.R., Pearson D.G., Nixon P.H., Mertzman S.A.** Low-calcium garnet harzburgites from southern Africa: their relations to craton structure and diamond crystallization. //Contrib. Mineral. Petrol. 1993, V.113, pp. 352±366
8. **Boyd F.R.; Pokhilenko N.P.; Pearson D.G.; Mertzman S.A.; Sobolev N.V.; Finger L.W.** 1996. Composition of the Siberian cratonic mantle: evidence from Udachnaya peridotite xenoliths. //Contrib. Mineral. and Petrol. 1997., V. 128. N 2-3. P. 228-246.
9. **Boyd F.R. & Finnerty A.A.** Conditions of origin of natural diamonds of peridotite affinity. //J. Geophys. Res. 1980. v. 85, 6911-6918.
10. **Brey G.P., Kohler T.** Geothermobarometry in four-phase lherzolites. II. New thermobarometers, and practical assessment of existing thermobarometers. //J. Petrol. 1990. V.31, pp. 1353±1378.
11. **Dawson, J.B., Stephens, W.E.** Statistical classification of garnets from kimberlite and associated xenoliths. //J. Geol. 1975, v. 83, pp. 589-607.
12. **Eggler, D.H., Mccallum, M.E.** A geotherm from megacrysts in the Sloan kimberlite pipes, Colorado. // Carnegie Inst. Wash. Yearb. 1976. v.75, pp. 538-541.
13. **Franz L, Brey G.P.,Okrusch M.** 1996. Reequilibration of ultramafic xenoliths from Namibia by metasomatic processes at the mantle boundary.// J. Geol. v.104, pp.599 –615
14. **Gregoire M., Bell, D.R.; Le Roex, A.P.** Trace element geochemistry of phlogopite-rich mafic mantle xenoliths: their classification and their relationship to phlogopite-bearing peridotites and kimberlites revisited. //Contrib. Mineral. Petrol. 2002, v.142(5) pp. 603-625.
15. **Griffin, W.L., Moore, R.O., Ryan, C.G., Gurney, J.J., Win, T.T.** Geochemistry of magnesian ilmenite megacrysts from Southern African kimberlites. // Russian Geol. Geophys. 1997. v.38(2). pp.398-419
16. **Griffin, W. L., N. I. Fisher, J. H. Friedman, S. Y. O'Reilly, and C. G. Ryan,** Cr-pyrope garnets in the lithospheric mantle, 2. Compositional populations and their distribution in time and space, Geochem. Geophys. Geosyst., 20023(12), 35 p.
17. **Hart, S.R., Dunn, T.** Experimental cpx/melt partitioning of 24 trace ele-ments. Contrib. Mineral. Petrol., 1993, v.113, pp.1-8.
18. **Harte, B. M.B., Kirkley, M.B.,** 1997. Partitioning of trace elements between clinopyroxene and garnet: data from mantle eclogites. //Chem. Geol., v.136. pp. 1-24.
19. **Khar'kiv A.D. Zinchuk N.N., Kr'ychkov A.I.** /Primary deposits of the diamonds in the World. Moscow. Nedra. 1998. 545p.
20. **Kuligin, S.S., Pokhilenko, N.P.** Mineralogy of xenoliths of garnet pyroxenites from kimberlite pipes of Siberian platform. //Extended Abstracts 7IKC. 1998. Cape Town. pp. 480- 482.
21. **Leost I., Stachel T., Brey G.P. Harris J.W. Ryabchikov I.D.** Diamond formation and source carbonation: mineral associations in diamonds from Namibia. Contrib Mineral Petrol. 2003, v.145, pp. 12-24.
22. **Mccallum, M.E., Eggler, D.H.** Diamonds in an upper mantle peridotite nodule from kimberlite in southern Wyoming. // Science.1976. v.192, pp.253-256.
23. **McGregor I.D.** The system MgO- SiO_2- Al_2O_3: solubility of Al_2O_3 in enstatite for spinel **and garnet peridotite compositions. //Am.Miner.,1974, v.59, P.110-119.**
24. **Mitchell R.H.** 1995. Kimberlites, orangeites and related rocks. /New York: Plenum, 500 P.
25. **Moor, R.O., Griffin, W.L. Gurney et al.** Trace element geochemistry of ilmenites megacrysts from the Monastery kimberlite, South Africa. 1992. Lithos. 29, pp.1-18.

26. **Nimis P., Taylor W.** Single clinopyroxene thermobarometry for garnet peridotites. Part I. Calibration and testing of a Cr-in-Cpx barometer and an enstatite-in-Cpx thermometer. //Contrib. Mineral. Petrol. 2000. V. 139. N5. P.541-554
27. **Nixon, P.H., Boyd, F.R.** Petrogenesis of the granular and sheared ultrabasic nodule suite in kimberlites. /In Lesotho Kimberlites (P.H. Nixon, ed.). Lesotho National Development Corporation, Maseru, Lesotho. 1973. (48-56).
28. **O'Reilly S.Y., Griffin W.L., Poudium Diomany, Morgan P.** Are lithospehers forever? //GSA Today. 2001. N11, pp.4-9
29. **Pokhilenko, N. P., Sobolev, N.V., Kuligin, S. S., Shimizu, N.** Peculiarities of distribution of pyroxenite paragenesis garnets in Yakutian kimberlites and some aspects of the evolution of the Siberian craton lithospheric mantle.// Proceedings of the VII International Kimberlite Conference. 2002. The P.H. Nixon volume. pp. 690-707.
30. **Pokhilenko, N.P., Pearson, D.G., Boyd, F.R., Sobolev N.V.** Megacrystalline dunites: sources of Siberian diamonds. //Carnegie Inst. Wash. Yearb. 1991.v. 90, pp. 11-18
31. **Rudnick G., McDonough W.F., Chappell B.W.** Carbonatite metasomatism in the northern Tanzanian mantle // Earth Planet. Sci. Lett. 1993. V.114. pp. 463-475.
32. **Ryan C. G.; Griffin W. L.; Pearson N. J**. Garnet geotherms: Pressure-temperature data from Cr-pyrope garnet xenocrysts in volcanic rocks// J. Geophys. Res. B. 1996. V. 101. N 3. P. 5611-5625
33. **Sobolev, N.V.** Deep-Seated Inclusions in Kimberlites and the Problem of the Composition of the Upper Mantle.// Am. Geophys. Union, Washington, D.C. 1977. 264p.
34. **Sobolev, N.V., Botkunov, A.I., Lavrent'ev, Y.G. & Usova, L.V.** New data on the minerals associated with the diamonds in the "Mir" kimberlite pipe in Yakutia. // Sov. Geol. Geophys. 1976. v.17, 1-10.
35. **Sobolev, N.V., Kaminsky, F.V., Griffin, W.L., Yefimova, E.S., Win, T.T., Ryan, C.G. & Botkunov, A.I.** Mineral inclusions in diamonds from the Sputnik kimberlite pipe, Yakutia.// Lithos. 1997, v. 39, 135-157.
36. **Taylor L.A., Gregory A., Snyder A., Keller R., Remley D.A., Anand M., Wiesli R., Valley J., Sobolev N.V.** Petrogenesis of group A eclogites and websterites: evidence from the Obnazhennaya kimberlite, Yakutia . Contrib Mineral Petrol. 2001, v.145 pp.424-443.
37. **Van Achterberg E., Griffin W.L., Steinfenhofer J.** Metasomatism in mantle xenoliths from Letlhakane kimberlites estimation of element fluxes.// Contrib. Mineral. Petrol. 2001. v. 141, pp.397-414.
38. **Van Keken P. E. , Kiefer B., Peacock S.M.** High-resolution models of subduction zones: Implications for mineral dehydration reactions and the transport of water into the deep **mantle. //Geochemistry, Geophysics, Geochemistry. 2002, v. 3, N 10**
39. **Wallace M.E.,Green D.H.** Experimental determination of primary carbonatite magma composition. //Nature. 1988. v. 335, pp.343 –346
40. **Wang, W.Y. & Gasparik, T.** Metasomatic clinopyroxene inclusions in diamonds from the Liaoning province, China. //Geochim. Cosmochim. Acta. 2001. v.65, pp. 611-620.
41. **Wyllie P.J., Huang W.L.** Carbonation and melting reactions in the system CaO –MgO – SiO_2 –CO_2 at mantle pressures with geophysical and petrological applications. //Contrib. Mineral.Petrol. 1976, v. 54, pp.79 –107
42. **Zack, T., Brumm, R.** Ilmenite/ liquid partition coefficients for 26 trace elements determined through ilmenite/clinopyroxene partitioning in garnet pyroxenites. //7th International Kimberlite Conference. Extended abstracts. Cape town. 1998. pp.986-988.
43. **Zhang H.F., Menzies M., MAttey D.P, Hinton R.W., Gurney J.J.** Petrology, mineralogy abdnd geochemistry of oxide minerals in polymict xenoliths from the Bultfontein kimberlites, South Africa: implications for bulk rock oxygen isotopic ratios. //Contrib Mineral Petrol 2001. v.141; pp. 367 –379

Noble gases in mantle-derived xenocrysts in an alkali basalt from Japan Trench oceanward slope

Junji Yamamoto[1,2,3], Naoto Hirano[2,4], Takeshi Hanyu[5], Hiroyuki Kagi[3] & Ichiro Kaneoka[4]

[1]Centre de Recherches Pétrographiques et Géochimiques, 15 rue Notre Dame des Pauvres 54501 Vandoeuvre les Nancy, France, E-mail: jyama@eqchem.s.u-tokyo.ac.jp
[2]Department of Earth and Planetary Sciences, Tokyo Institute of Technology, 2-12-1 Ookayama, Meguro-ku, Tokyo 152-8551, Japan, E-mail: nhirano@geo.titech.ac.jp
[3]Laboratory for Earthquake Chemistry, University of Tokyo, 7-3-1 Hongo, Bunkyo-ku, Tokyo 113-0033, Japan, E-mail: kagi@eqchem.s.u-tokyo.ac.jp
[4]Earthquake Research Institute, University of Tokyo, 1-1-1, Yayoi, Bunkyo-ku, Tokyo 113-0032, Japan, E-mail: kaneoka@eri.u-tokyo.ac.jp
[5]Japan Marine Science & Technology Center, 2-15 Natsushima, Yokosuka 237-0061, Japan, E-mail: hanyut@jamstec.go.jp

We measured noble gas isotopic ratios of olivine xenocrysts in an alkali-basalt sampled from a northwest pacific seamount. The xenocrysts are reported to be derived from upper-mantle from major element compositions [12]. The depth where the xenocrysts were entrained by the host magma was estimated to be 10-14 km under the sea bottom from the density of co_2 in fluid inclusions; thereby they originated from the uppermost mantle. By applying both vacuum crushing and stepwise heating extraction of the noble gases, uncontaminated $^{3}he/^{4}he$ ratios range between 7.2 and 7.7 r_a (r_a is the atmospheric $^{3}he/^{4}he$ ratio of 1.4×10^{-6}) and $^{40}ar/^{36}ar$ ratios are up to 5000 in the xenocrysts. These observations demonstrate that the upper mantle beneath the oceanward slope of the japan trench has a similar isotopic composition to the morb (mid-ocean ridge basalt) source, suggesting a uniform morb source is largely distributed in the upper mantle.

INTRODUCTION

The source of MORB has generally been regarded to be derived from the suboceanic mantle, and to be located in the upper-mantle (e.g., [14]). The $^{3}He/^{4}He$ ratio in MORB shows quite uniform values of (8 +/- 1) R_A. MORB-like $^{3}He/^{4}He$ ratios have often been observed in mantle-derived rocks from island arcs and subcontinental mantle [18, 19, 22, 25, 33]. There is a widespread consensus that the source of MORB is a ubiquitous component of the upper-mantle.Recently, however, occurrences of $^{3}He/^{4}He$ ratios lower than that of MORB have been reported for some subcontinental and island arc ultramafic xenoliths [5, 7, 16, 22, 36]. Several possibilities are proposed to explain these low ratios including mixing with an atmospheric component; the influence of radiogenic ^{4}He ingrowth attributed to metasomatic enrichment of incompatible elements such as U and Th,

or reduction of He/U ratio caused by preferential depletion of helium. These discussions depend greatly on the implicit assumption that the source of MORB is a unique and uniform component in the upper-mantle.

The aim of this paper is to investigate whether the noble gas characteristics like MORB has a wide distribution over the upper-mantle. For this purpose, upper-mantle-derived minerals sampled far from mid-oceanic ridge are used to identify the distribution of the source of MORB. We analyzed all noble gas compositions in olivine xenocrysts from the Japan Trench oceanward slope. In addition, we tried to determine internal pressures of trapped fluids by micro-Raman spectroscopic analyses. The investigation of the internal pressure of the fluid inclusions in the xenocrysts can provide an extremely important constraint on the origin of the xenocrysts.

SAMPLES AND GEOLOGICAL BACKGROUND

Pillow alkali-basalt outcrops were sampled at depth of 7324 to 7360 m on the oceanward slope of the northern Japan Trench (39˚23' N, 144˚16' E) during JAMSTEC (Japan Marine Science and Technology Center) R/V Kairei/ROV KAIKO cruise KR97-11. The Ar-Ar age of the alkali-basalt is 5.95 +/- 0.31 Ma and is reported as a new form of intra-plate volcanism where decompression and magmatic activity occurs off the fore bulge of the downgoing Pacific slab [12]. Two basalt samples, 10K#56 R-001 and R-002, were collected from the pillow basalt at around 7360 m depth.

There are two compositionally distinct olivines in the alkali-basalts; large olivine megacrysts with a reaction rim and small olivine phenocrysts. The average size of the large olivine megacrysts and the small olivine phenocrysts is about 2 mm and less than 0.2 mm in diameter, respectively. The large olivine megacrysts (Fo values, 90-93, and NiO contents, 0.3-0.5 wt%) are more primary in origin than small olivine phenocrysts (Fo values, 80-90, and NiO contents, 0.1-0.5 wt%), and have compositions in disequilibrium with the host basalt [12]. Therefore, the large olivine megacrysts are considered to be xenocrysts derived from the upper-mantle. In the present study, the xenocrysts were used for micro-Raman spectroscopic analysis and noble gas study.

EXPERIMENTAL

Micro-Raman spectroscopic analyses

The basalt rock wafers were carefully prepared and doubly polished to about 500 micrometer in thickness, ensuring no resin was on the section to be analyzed. The resin used for polishing was completely removed by acetone. The fluorescent light from the mineral separates were negligible in this study.

Raman spectra were measured using a Raman spectrometer equipped with an optical microscope (Olympus, BX60) installed at the Laboratory for Earthquake

Chemistry, University of Tokyo. The excitation laser beam was focused on a spheroidal spot of approximately 1 x 1 x 5 μm^3 using an Olympus 100x objective lens (N.A. = 0.95) with a confocal arrangement that allows us to pick up signals exclusively from fluid inclusions. Though the spectral resolution of our spectrometer is approximately 1.5 cm^{-1} per pixel at the present experimental condition, more than 20 data points are collected along CO_2 Raman line, so the center of the fitted Lorentzian curve could be determined with much higher precision, typically +/- 0.10 cm^{-1} [15]. Spectra were accumulated with an exposure time of 150 seconds per point with laser power of 12-14 mW on the sample. Raman shift was calibrated with a standard sample of naphthalene. More detailed analytical conditions for Raman spectroscopy at the Laboratory for Earthquake Chemistry have been reported by Yamamoto et al. (2002) [35] and Kawakami et al. (2003) [15].

Noble gas analyses

The large olivine megacrysts were separated from the small olivine phenocrysts using a sieve. Furthermore, the olivine grains were carefully separated by handpicking, removing altered parts and impurities. Grains were soaked in 2N HNO_3 for half an hour at 70˚C, and washed ultrasonically in distilled water, ethanol and acetone.

Noble gases were extracted by both vacuum crushing and stepwise heating methods for olivine separates. Before crushing, a crushing vessel was preheated at 150˚C overnight. During crushing, the crushed sample together with the vessel was heated at 120˚C. Gases extracted were exposed to a cold trap at liquid N_2 temperature in order to remove gases adsorbed on newly created powder surfaces. The crushing yield, defined as the fraction of the crushed material (150 micrometer), was 45% in this study. Preliminary stepwise heating experiments for mantle-derived olivine suggest that degassing of intrinsic gases occurs at 1000-1200˚C, but adsorbed atmospheric gases are degassed at less than 700˚C and the remaining component (radiogenic and intrinsic) degassed at 1900˚C due to melting of olivine. Therefore, for the stepwise heating procedure, noble gases were extracted with three temperature steps (700˚C, 1200˚C and 1900˚C), using a resistance furnace. Duration of heating is 40, 30 and 20 minutes for the fraction of 700, 1200 and 1900˚C, respectively.

Noble gas analyses were performed on a sector-type mass spectrometer (VG-5400) installed at the Earthquake Research Institute (ERI), University of Tokyo. Procedural crushing blanks for ^{3}He, ^{4}He, ^{20}Ne, ^{36}Ar, ^{84}Kr and ^{132}Xe were less than 3.0 x 10^{-15}, 2.0 x 10^{-11}, 2 x 10^{-12}, 1 x 10^{-12}, 2 x 10^{-14} and 4 x 10^{-15} cm^3STP, respectively. Procedural heating blanks for ^{3}He, ^{4}He, ^{20}Ne, ^{36}Ar, ^{84}Kr and ^{132}Xe at each temperature step were less than 9.0 x 10^{-15}, 2.0 x 10^{-10}, 6 x 10^{-12}, 1 x 10^{-11}, 5 x 10^{-13} and 1 x 10^{-13} cm^3STP, respectively. Consistency of the helium isotope ratio with the ^{3}He content was guaranteed down to the range of 1 x 10^{-15} cm^3 STP (after blank correction) by repeated analyses of the diluted air standard and two types of

standard gases (artificial helium standard gas (20.63 +/- 0.10 R_A; [17, 32]) and Kaminoyama well gas, Yamagata, Japan (6.04 +/- 0.29 R_A; [11])). The uncertainties in the precision (1 sigma include those for the sensitivity and blank corrections for isotope ratios. Sensitivities of the other kinds of noble gas isotope were checked by repeated analyses of different amounts of diluted air standard. Analytical conditions for noble gases at the ERI have been reported by Hanyu et al. (1999) [11].

RESULTS AND DISCUSSION

Micro-Raman spectroscopic analyses of fluid inclusion

The xenocrysts include abundant fluid inclusions. Two compositionally distinct groups of fluid inclusion are observed (Fig. 1). One is a liquid inclusion having a negative crystal shape, a type of inclusion reflecting the crystal form of the host mineral, with partly spherical shape. The liquid inclusions are usually less than 10 micrometer in diameter. The liquid inclusion trails have been observed in most of the xenocrysts. The other inclusion group is solid (silicate melt) inclusions, which are elongated and vermicular. A large number of the solid inclusions were observed in all xenocrysts. Bubbles are often observed in the solid inclusions, which have been formed by shrinkage of the melt during cooling. Based on micro-Raman spectroscopic analyses, CO_2 was identified in both the liquid inclusions and shrinkage bubbles in the solid inclusions. No other components such as H_2O, CH_4, N_2 and CO were detected using micro-Raman spectroscopy.

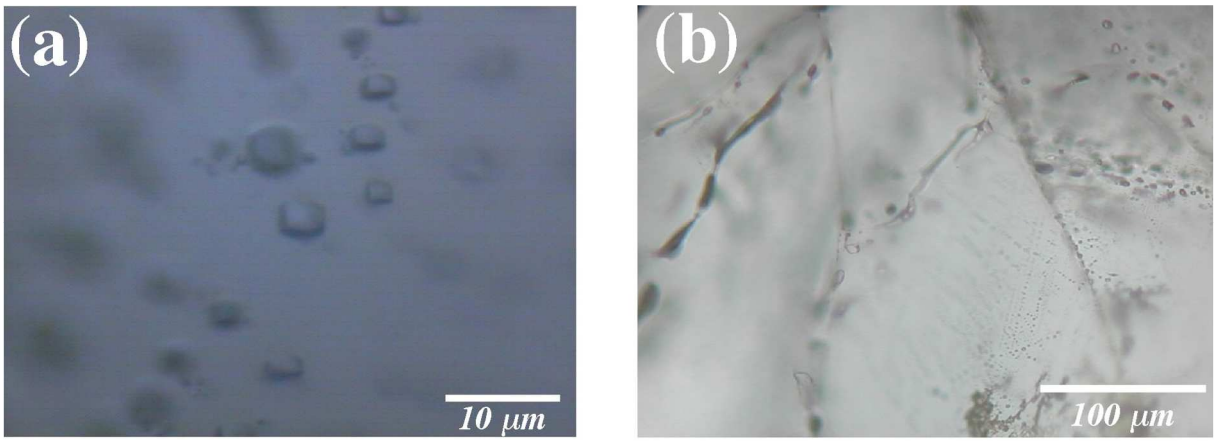

Fig. 1. *Photomicrographs of fluid inclusions in a xenocryst thick section (~500 micrometer thickness) from Japan Trench oceanward slope: (a) Negative crystal liquid inclusions. (b) Solid inclusions with a dendritic or vermicular form. They often include shrinkage bubbles.*

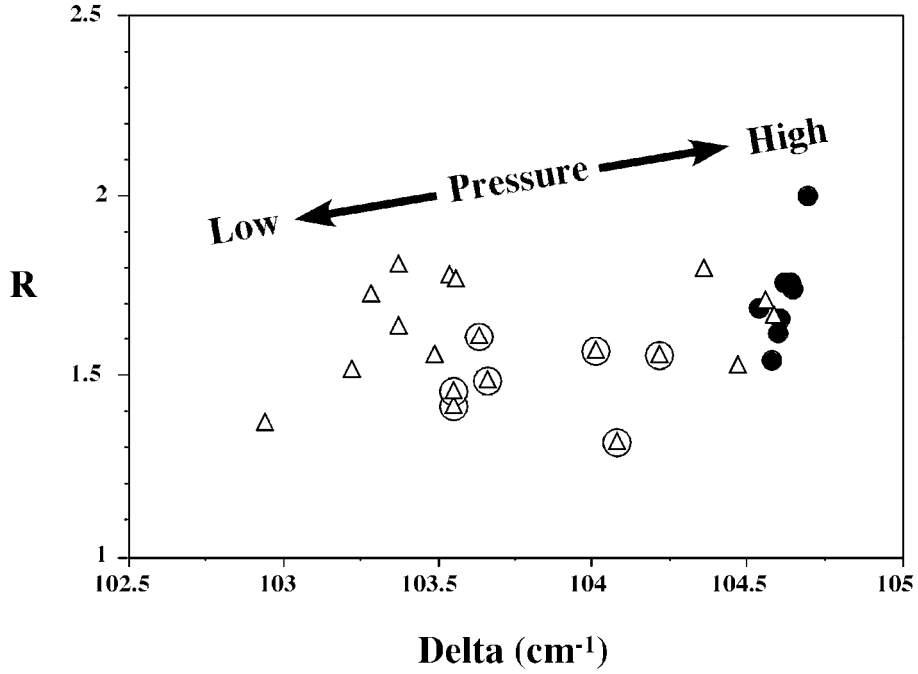

Fig. 2. *R-Delta plot for CO_2 Fermi diad of CO_2 inclusions in some xenocrysts.*

R means intensity ratio of the CO_2 Fermi diad. Delta means separation of wavenumber of the CO_2 Fermi diad. Circle: liquid inclusion; triangle: solid inclusion; triangle + circle: solid inclusion with vapor bubble. The reproducibility of the Delta and R for data with moderate intensity (counts) is typically ~0.15 cm^{-1} and ~0.2 cm^{-1}, respectively. Because the inclusions with low Delta-value have lower density than that of high Delta-value, the data tend to show wide variation particularly in the R-value.

Depth where xenocrysts was entrained by host magma

For mantle-derived xenoliths, residual pressure in fluid inclusions has often been used to estimate the depth where the xenolith was entrained by host magma [1, 4, 9, 23, 26, 27, 29, 30, 35]. If the density of CO_2 in the fluid inclusions is determined, the P-T condition where the fluid inclusions were equilibrated with the host minerals can be determined using the equation of state for CO_2 and a temperature estimated from a geothermometer. Raman spectra of CO_2 can provide density of CO_2 in fluid inclusions in the following way. Raman spectrum of CO_2 has two main peaks. Figure 2 shows plots of R (intensity ratio) vs. Delta (separation of wavenumber between the higher and the lower frequency peaks) for two kinds of fluid inclusion in the present study. As the density of CO_2 increases, both R and Delta are elevated, thereby high-density CO_2 inclusions plot upper-right in the figure. The liquid inclusions cluster around a Delta-value of about 104.6 cm^{-1}. Bubbles in solid inclusions have a wide distribution over Delta-values lower than those of liquid inclusions. The highest Delta-value for both inclusion morphologies are fairly similar to each other within the experimental uncertainty at the 1 sigma level, typically +/- 0.10 cm^{-1}. The internal pressure of fluid inclusions with negative crystal morphologies were in equilibrium with ambient pressure in their mantle source region. The liquid inclusions have therefore had CO_2 density

corresponding to the depth where the host olivines were entrained by magma. On the other hand, as a melt inclusion cools below its temperature of entrapment, it is depressurized along the isochore until it becomes saturated with a volatile phase such as CO_2, and then a shrinkage bubble nucleates. Olivine is not strong enough to withstand the pressure differential between the inclusion's internal pressure and the external environmental pressure. The melt inclusion will change in volume due to plastic deformation of host olivine, or due to interdiffusion of Mg or Fe between host olivine and melt inclusion until the shrinkage bubble has an internal pressure equivalent to the ambient pressure (averaged over a long time period). Therefore, Delta and R-values of liquid inclusions record the depth where the xenocrysts were entrapped in the host magma whereas those of bubbles in solid inclusions provide the minimum limit of the entrainment depth.

Yamamoto et al. [35] simulated the volume change of minerals caused by decompression and temperature decrease during the the ascent of mantle-derived minerals entrained by host magmas based on "Birch-Murnaghan's equation of state", "thermal expansivities of minerals" and "constitutive equations". During transport of xenocrysts to near the Earth's surface, CO_2-dominant liquid inclusions preserve internal pressure up to around 1 GPa [2]. Thus, a differential stress of around 1 GPa would have occurred between the CO_2-dominated liquid inclusion and the surrounding crystal lattice when the xenocrysts were near the Earth's surface. In the case of mantle-derived xenoliths from Far East Russia, CO_2-dominated liquid inclusions in olivine expand by 10 vol% by plastic deformation during ascent of the xenoliths. In present study, the density of CO_2 in the liquid inclusions would be also reduced. Assuming a temperature of the host basalt of 1200˚C and a differential stress of 1GPa, liquid inclusions expand by 25% in volume in only 10 hours. If the internal pressure of the liquid inclusions was partly released by plastic deformation, the density had never been greater than 1.2 g/cm^3 prior to entrainment. A CO_2 density of 1.2 g/cm^3 in fluid inclusions would approximate to the maximum for olivine to withstand decrepitation, which occurs when the internal pressure within the fluid inclusion exceeds the strength of the host mineral. Indeed, a CO_2 density of more than 1.2 g/cm^3 has not been reported so far on fluid inclusions in mantle-derived minerals [2]. To put it briefly, CO_2 inclusions having CO_2 densities of more than 1.2 g/cm^3 decrepitate during entrainment. In the present xenocrysts, possible decrepitation-induced texture such as fracture and darkening of fluid inclusions was not observed. Therefore, the initial CO_2 density in liquid inclusions prior to entrainment would fall somewhere in the range 0.9 to 1.2 g/cm^3.

Trapping pressures of xenocrysts were estimated by the intersection of the CO_2 isochore and the geothermal gradient around this region (Fig. 3). Extrapolation of a density of 1.2 g/cm^3 (the maximum possible) to it's interaction with the geothermal gradient indicates that the internal pressure of the inclusions were up to 0.4 GPa. Such a pressure corresponds to 14 km in depth under the sea bottom. Obviously, this confirms that these xenocrysts are not deep mantle

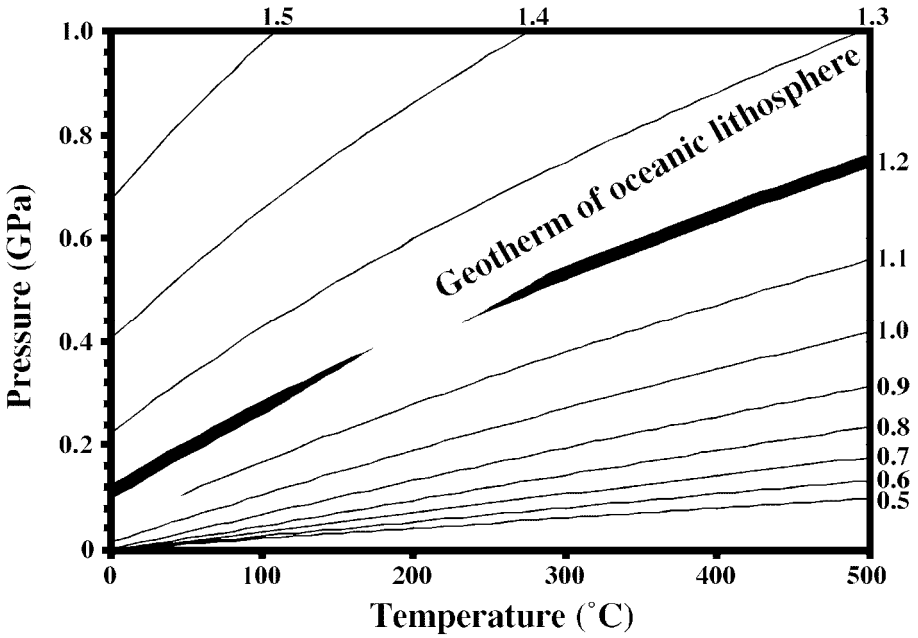

Fig. 3. *P-T phase diagram of CO_2 with geotherm for old oceanic lithosphere at 120 Ma.*

The geotherm is estimated after a geothermal model (CHABLIS) proposed by Doin and Fleitout (1996) [6]. CO_2 equation of state is after Pitzer and Sterner (1994) [24]. Contours represent density, in g/cm^3 (i.e. isochors).

material such as the source of ocean island basalt. Furthermore, the xenocrysts show primary major element composition of upper mantle-derived olivine. It is clear that the xenocrysts are samples derived from mantle. Crustal thickness in this region is ~10 km (e.g., [20]). Thus, it is concluded that the xenocrysts were entrapped by the host magma at the depth ranging from 10 to 14 km.

Noble gas compositions in xenocrysts

Noble gas isotope results are summarized in Table 1. It is noteworthy that the amount of gas extracted by crushing made up a large proportion (more than 50% for helium) of the gas extracted by total fusion, despite that the crushing yield, which is usually defined as the fraction of the crushed material (< 150 micrometer), is only 45%, this is unusual because the amount of gas extracted by crushing depends mainly on inclusion density and efficiency of extraction. Since the inclusions are ~5 micrometer in diameter, the gases in the crushing experiment should be almost exclusively extracted from fluid inclusions. It is impossible to release a significant proportion of the lattice-trapped noble gases with such a low crushing yield. In the previous section, we reported the high density of CO_2 in CO_2-dominated liquid inclusions. Generally, the $CO_2/^3He$ ratio in the upper-mantle is recognized to be uniform (e.g., [28]). Thus, abundance of noble gases in mantle-derived xenoliths should be correlated with the number of CO_2-dominated liquid inclusions. The present xenocrysts, therefore, have a large number of fluid inclusions or fluid inclusions enormously rich in noble gases.

Table 1. Noble gas isotopic compositions in large olivine xenocrysts from Japan Trench oceanward slope

		weight (g)	^{3}He	error	^{4}He	error	^{20}Ne	error	^{36}Ar	error	^{40}Ar	error	^{84}Kr	error	^{132}Xe	error
Crushing		0.245	6.5E-12	8.8E-13	7.6E-07	9.9E-08	1.2E-10	1.5E-11	1.4E-10	8.6E-12	2.4E-07	1.4E-08	5.4E-12	3.8E-13	4.0E-13	2.7E-14
Heating	**700°C**	1.384	1.9E-13	4.4E-14	5.0E-08	6.5E-09	8.0E-11	1.0E-11	1.5E-10	9.0E-12	4.8E-08	2.9E-09	4.8E-12	2.9E-13	2.7E-13	1.8E-14
	1200°C		4.2E-12	5.7E-13	4.7E-07	6.1E-08	2.3E-11	4.1E-12	3.1E-11	1.9E-12	1.5E-07	9.1E-09	1.4E-12	9.5E-14	1.8E-13	1.3E-14
	1900°C		7.7E-12	1.0E-12	8.9E-07	1.2E-07	2.3E-10	2.9E-11	3.8E-10	2.3E-11	5.1E-07	3.0E-08	1.8E-11	1.1E-12	1.6E-12	1.1E-13
	total		1.2E-11	1.2E-12	1.4E-06	1.3E-07	3.4E-10	3.1E-11	5.7E-10	2.5E-11	7.1E-07	3.2E-08	2.4E-11	1.1E-12	2.0E-12	1.1E-13

		weight g	^{3}He/^{4}He R/Ra	error R/Ra	^{20}Ne/^{22}Ne	error	^{21}Ne/^{22}Ne	error	^{40}Ar/^{36}Ar	error	^{38}Ar/^{36}Ar	error	^{4}He/^{40}Ar*	error
Crushing		0.245	7.20	0.31	9.70	0.30	0.0306	0.0040	1647	30	0.1891	0.0027	3.9	0.6
Heating	**700°C**	1.384	3.02	0.57	9.66	0.27	0.0272	0.0028	320	4	0.1885	0.0008	13.7	3.2
	1200°C		7.70	0.27	9.82	1.36	0.0271	0.0107	4945	71	0.1892	0.0015	3.2	0.5
	1900°C		7.36	0.13	9.75	0.11	0.0304	0.0008	1331	19	0.1895	0.0011	2.3	0.3
	total		7.30	0.12	9.73	0.23	0.0294	0.0020	732	10	0.1887	0.0007	5.7	0.6
	1200°C+1900°C								1963	27	0.1895	0.0010		

Units of noble gas data are ccSTP/g. The noble gas data were analyzed by J. YAMAMOTO in 2002 using a sector-type mass spectrometer (VG-5400).

For gases extracted by crushing, the helium isotopic ratio is 7.3 R_A, which is within the range of MORB value (8 +/- 1 R_A). Argon isotopic ratios are also high ($^{40}Ar/^{36}Ar$=1650) compared to that of air (295.5). Neon, krypton and xenon isotopic ratios are indistinguishable from the atmospheric values within the experimental uncertainty of 1 sigma level for both crushing and heating methods.

For gases extracted by heating, the $^{3}He/^{4}He$ ratios obtained in both 1200 and 1900˚C fractions roughly correspond to that detected by crushing. Although low a $^{3}He/^{4}He$ ratio was obtained in the 700˚C fraction, a rough agreement is observed between $^{3}He/^{4}He$ ratios by total heating and by crushing. This indicates that He should be located in a phase that can be extracted by the crushing method, that is, in fluid inclusions. Low $^{40}Ar/^{36}Ar$ ratios were obtained in the 700˚C fraction. The most likely source of the low $^{40}Ar/^{36}Ar$ ratio gases is attributed to material with an atmospheric component. The gases in the 700˚C fraction could be affected by possible atmospheric contaminants such as adsorbed atmospheric gases or hydrous mineral caused by low temperature alteration. The $^{40}Ar/^{36}Ar$ ratios in the 1200 and 1900˚C fraction are higher than that of the atmosphere, and that in 1200˚C fraction is far higher than by crushing. This may be due to post-eruptive accumulation of radiogenic ^{40}Ar by decay of ^{40}K within sample. The $^{4}He/^{40}Ar^{*}$ ratio may be a useful indicator for examining accumulation of radiogenic components, where $^{40}Ar^{*}$ indicates ^{40}Ar corrected for air-addition. The instantaneous $^{4}He/^{40}Ar^{*}$ production ratio in the mantle is estimated to be approximately 5 to 20 (e.g., [3, 36]) depending on the assumed K/U ratio ranging from 12700 to 3000. The $^{4}He/^{40}Ar^{*}$ ratios of the total furnace gas release (5.7 +/- 0.6) are higher than that of crushing experiment (3.9 +/- 0.6). This may be due to post-eruptive ingrowth of radiogenic nuclides. We examined whether the high $^{40}Ar/^{36}Ar$ ratios can be explained by accumulation of radiogenic ^{40}Ar. The influence of the post-eruptive accumulation of radiogenic ^{40}Ar on $^{40}Ar/^{36}Ar$ depends on both the age when the xenocrysts were transported to the surface and the ratio of K content to the initial ^{40}Ar content. If the xenocrysts have a K content as observed in most mantle-derived rocks, which is approximately 100 ppm [8, 10, 13, 21, 31, 34], then 2.3 x 10^{-9} cm^3STP/g of radiogenic ^{40}Ar accumulated since the xenocrysts were transported to the surface at around 6 Ma. The total $^{40}Ar^{*}$ content extracted by fusion is 5.3 x 10^{-8} cm^3STP/g greater than that extracted by crushing. Although the crushing method can not completely extract all the trapped gases, it is difficult to explain this excess $^{40}Ar^{*}$ content (5.3 x 10^{-8} cm^3STP/g) only by post-eruptive accumulation (2.3 x 10^{-9} cm^3STP/g). This estimation indicates that there may be another noble gas host phase present in these xenocrysts. However, on the whole, a rough agreement is observed between the amounts of gases extracted by total heating and those by crushing method. Also, helium and argon isotopic ratios extracted by crushing correspond to those extracted by fusion. The noble gas composition in the sample is strongly controlled by the occurrence of fluid inclusions with compositions similar to those observed in MORB.

The $^{3}He/^{4}He$ ratios of the subcontinental and island arc mantle are more variable compared to those of MORB. The $^{3}He/^{4}He$ ratios in MORB, however, show quite uniform values of around 8 R_A. MORB-like $^{3}He/^{4}He$ ratios have often been observed in such samples from island arcs and subcontinental mantle xenoliths (e.g., [18, 19, 22, 25, 33]. Furthermore, these results indicate that upper-mantle with a helium isotopic composition fairly similar to that of MORB-source exists beneath the oceanward slope of the northern Japan Trench. The argon isotopic ratio is also high ($^{40}Ar/^{36}Ar$=1650), which is consistent with the value found in MORB. After all, MORB-source has a worldwide distribution and it may be a ubiquitous component of upper-mantle.

SUMMARY

Petrologic and petrographic observations confirm that there are two compositionally distinct olivines in an alkali-basalt from Japan Trench oceanward slope; large olivine xenocrysts with reaction rims, and small olivine phenocrysts. Based on micro-Raman spectroscopy, CO_2 was identified in fluid inclusions in the large olivines xenocrysts. The CO_2 Raman spectra indicate that these CO_2 inclusions represent a sample of volatiles from the uppermost part of the upper-mantle (10-14 km depth under the sea bottom), consistent with an uppermost mantle origin for the xenocrysts.

For gases extracted by crushing, the helium isotopic ratio is 7.3 R_A, within the range of the MORB value (8 +/- 1 R_A). The argon isotopic ratio is also high ($^{40}Ar/^{36}Ar$=1650) compared to that of air (295.5). This indicates that an upper-mantle with noble gas compositions like MORB exists beneath the Japan Trench oceanward slope, which might reflect a more ubiquitous character of the upper-mantle as a whole.

ACKNOWLEDGMENTS

We appreciate Dr. Y. N. Miura and Dr. H. Kumagai for their help in analyzing noble gases. Dr. Y. Lai gave us suggestions on description of fluid inclusion. We would like to acknowledge Prof. T. Fujii, Dr. A Yasuda and Dr. Y. Kido for valuable suggestion on estimation of geotherm for oceanic lithosphere. This study has been financially supported in part by the Research Fellowships of the Japan Society for the Promotion of Science for Young Scientists to J. Y.

REFERENCES

1. **Andersen T., O'Reilly S. Y. and Griffin W. L. The** trapped fluid phase in upper mantle xenoliths from Victoria, Australia: implications for mantle metasomatism. *Contrib. Mineral. Petrol. 88*, 72-85, 1984
2. **Andersen T. and Neumann E.-R.** Fluid inclusions in mantle xenoliths. *Lithos 55*, 301-320, 2001
3. **Burnard P. G., Farley K. A. and Turner G.** Multiple fluid pulses in a Samoan harzburgite. *Chem. Geol. 147*, 99-114, 1998

4. **De Vivo B., Frezzotti M. L., Lima A. and Trigila R.** Spinel lherzolite nodules from Oahu island (Hawaii): a fluid inclusion study. *Bull. Mineral. 111*, 307-319, 1988
5. **Dodson A. and Brandon A. D**. Radiogenic helium in xenoliths from Simcoe, Washington, USA: implications for metasomatic processes in the mantle wedge above subduction zones. *Chem. Geol. 160*, 371-385, 1999
6. **Doin M. P. and Fleitout L.** Thermal evolution of the oceanic lithosphere: an alternative review. *Earth Planet. Sci. Lett. 142*, 121-136. 1996
7. **Dunai T. J. and Baur H**. Helium, neon, and argon systematics of the European subcontinental mantle: Implications for its geochemical evolution. *Geochim. Cosmochim. Acta 59*, 2767-2783, 1995
8. **Ebihara M.** Determination of ppm level contents of potassium in silicate materials by means of neutron activation analysis. *BUNSEKI KAGAKU 34*, 761-765, 1985
9. **Frezzotti M. L., Burke E. A. J., De Vivo B., Stefanini B. and Villa I. M.** Mantle fluids in pyroxenite nodules from Salt Lake Crater (Oahu, Hawaii). *Eur. J. Mineral. 4*, 1137-1153, 1992
10. **Funkhouser J. G. and Naughton J. J.** Radiogenic helium and argon in ultramafic inclusions from Hawaii. *J. Geophys. Res. 73*, 4601-4607, 1968
11. **Hanyu T., Kaneoka I. and Nagao K.** Noble gas study of HIMU and EM ocean island basalts in the Polynesian region. *Geochim. Cosmochim. Acta 63*, 1181-1201, 1999
12. **Hirano N., Kawamura K., Hattori M., Saito K. and Ogawa Y.** A new type of intra-plate volcanism; young alkali-basalts discovered from the subducting Pacific Plate, northern Japan Trench. *Geophys. Res. Lett. 28*, 2719-2722, 2001
13. **Ionov D. A., Prikhod'ko V. S. and O'Reilly S. Y.** Peridotite xenoliths in alkali basalts from the Sikhote-Alin, southeastern Siberia, Russia:trace-element signatures of mantle beneath a convergent continental margin. *Chem. Geol. 120*, 275-294, 1995
14. **Kaneoka I.** Noble gas constraints on the layered structure of the mantle. *Nature 302*, 698-700, 1983
15. **Kawakami Y., Yamamoto J. and Kagi H.** Micro-Raman densimeter for CO_2 inclusions of mantle-derived minerals. Applied Spectroscopy, 2003 (in press)
16. **Kyser T. K. and Rison W.** Systematics of rare gas isotopes in basic lavas and ultramafic xenoliths. *J. Geophys. Res. 87*, 5611-5630, 1982
17. **Matsuda J., Matsumoto T., Sumino H., Nagao K., Yamamoto J., Miura Y., Kaneoka I., Takahata N. and Sano Y.** The $^3He/^4He$ ratio of the new internal He standard of Japan (HESJ). *Geochem. J. 36*, 191-195, 2002
18. **Matsumoto T., Honda M., McDougall I., Yatsevich I. and O'Reilly S. Y.** Plume-like neon in a metasomatic apatite from the Australian lithospheric mantle. *Nature 388*, 162-164, 1997
19. **Matsumoto T., Honda M., McDougall I. and O'Reilly S. Y.** Noble gases in anhydrous lherzolites from the Newer Volcanics, southeastern Australia: A MORB-like reservoir in the subcontinental mantle. *Geochim. Cosmochim. Acta 62*, 2521-2533, 1998
20. **Mooney W. D., Laske G. and Masters T. G.** CRUST 5.1: a global crustal model at 5' x 5'. *J. Geophys. Res. 103*, 727-747, 1998
21. **Morgan J. W. and Goode A. D. T.** Potassium abundances in some ultra-basic and basic rocks. *Earth Planet. Sci. Lett. 1*, 110-112, 1966
22. **Nagao K. and Takahashi E.** Noble gases in the mantle wedge and lower crust: an inference from the isotopic analyses of xenoliths from Oki-Dogo and Ichinomegata, Japan. *Geochem. J. 27*, 229-240, 1993
23. **Pasteris J. D. and Wanamaker B. J.** Laser Raman microprobe analysis of experimentally re-equilibrated fluid inclusions in olivine: some implications for mantle fluid. *Am. Mineral. 73*, 1074-1088, 1988

24. **Pitzer K. S. and Sterner S. M.** Equations of state valid continuously from zero to extreme pressures for H_2O and CO_2. *J. Chem. Phys. 101*, 3111-3116, 1994
25. **Porcelli D., O'Nions R. K. and O'Reilly S. Y.** Helium and strontium isotopes in ultramafic xenoliths. *Chem. Geol. 54*, 237-249, 1986
26. **Roedder E.** Liquid CO_2 inclusions in olivine-bearing nodules and phenocrysts from basalts. *Am. Mineral. 50*, 1746-1782, 1965
27. **Roedder E.** Geobarometry of ultramafic xenoliths from Loihi Seamount, Hawaii, on the basis of CO_2 inclusions in olivine. *Earth Planet. Sci. Lett. 66*, 369-379, 1983
28. **Sano Y. and Marty B.** Origin of carbon in fumarolic gas from island arcs. *Chem. Geol. 119*, 265-274, 1995
29. **Schwab R. G. and Freisleben B.** Fluid CO_2 inclusions in olivine and pyroxene and their behaviour under high pressure and temperature conditions. *Bull. Mineral. 111*, 297-306, 1988
30. **Seitz J. C., Pasteris J. D. and Chou I. -M.** Raman spectroscopic characterization of gas mixtures. II. Quantitative composition and pressure determination of the CO_2-CH_4 system. *Am. J. Sci. 296*, 577-600, 1996
31. **Stueber A. M. and Murthy V. R.** Potassium-rubidium ratios in the ultramafic rocks: Differentiation history of the upper mantle. *Science 153*, 740-741, 1966
32. **Sumino H., Nagao K. and Notsu K.** Highly sensitive and precise measurement of helium isotopes using a mass spectrometer with double collector system. *J. Mass Spectrom. Soc. Jpn. 49*, 61-68, 2001
33. **Sumino H., Nakai S., Nagao K. and Notsu K.** High $^3He/^4He$ ratio in xenoliths from Takashima: evidence for plume type volcanism in southwestern Japan. *Geophys. Res. Lett. 27*, 1211-1214, 2000
34. **Wakita H., Nagasawa H., Uyeda S. and Kuno H.** Uranium, thorium and potassium contents of possible mantle materials. *Geochem. J. 1*, 183-198, 1967
35. **Yamamoto J., Kagi H., Kaneoka I., Lai Y., Prikhod'ko V. S. and Arai S.** Fossil pressures of fluid inclusions in mantle xenoliths exhibiting rheology of mantle minerals: implications for the geobarometry of mantle minerals using micro Raman spectroscopy. *Earth Planet. Sci. Lett. 198*, 511-519, 2002
36. **Yamamoto J., Kaneoka I., Nakai S., Kagi H., Prikhod'ko V. S. and Arai S.** Extremely low $^3He/^4He$ and relatively low $^{40}Ar/^{36}Ar$ ratios observed in ultramafic mantle xenoliths from Far Eastern Russia: evidence for incorporation of recycled components into the subcontinental mantle. 2003 (submitted to *Chem. Geol.*)

Minerals from Zarnitsa pipe kimberlite: the key to enigma of the mantle composition and constuction

Ashchepkov I.V.[1], Vladykin N.V.[2], Rotman A.Y.[3], Nikolaeva I.A.[1], Palessky V.S.[1], Saprykin A.I.[1], Anoshin G.N.[1], Khmel'nikova O.S.[1]

[1]*United Institute of Geology Geophysics and Mineralogy SD RAS*
[2]*Novosibirsk Institute of Geochemistry SD RAS, Irkutsk*
[3]*Central Scientific Investigation Geological Exploration Institute, ALROSA , Mirny*

Analyzed mineral concentrate from Zarnitsa pipe show that the compositions of all major minerals are more clustered then for nearest pipes in Daldyn and Alakit kimberlite fields. The ilmenite trend and the histograms for the major minerals show 7 peaks in the compositions with the 3 major maximums. The 2/3 garnets represent the material from the upper part of mantle. The TP conditions determined by the pyroxenes [6,12,23,25] give inflected geotherm with three separate levels. Newly developed garnet thermobarometry [4] produces more continuous geotherm with the heating 35-43 mv/m2 at the lower level - 70-50 kbar. The gap between 50-45 kbar, coincides with the 8-9%Cr_2O_3 gap for the garnets. Relatively heated conditions were determined for the section upper then 30 kbars. The local enrichment in Fe and several trends of the Ti enrichment most likely reflects several pulses of the melt percolation in the mantle what was accompanied by the heating. It possible to suggest heating in the deep part of section coursed the dissolution of the fine diamond grains and growth of the larger more isometric crystals. Thrace element for the Zarnitsa pipe comparing to the Yubileinaya display the Pb –U enrichments without high LILE increase what probably means the influence of the melts/fluids derived from subducted oceanic plates in the stage of the lithoslhere growth.

INTRODUCTION

Zarnitsa is the first kimberlite pipe found in Siberia by L.Popugaeva. One of the largest pipes in Daldyn field with the not properly determined potential due to the very irregular distributions of the diamonds reveal rather low concentration of small octahedral grains common in Udachnaya pipe what is compensated partly by presence of rare large high quality crystals [20]. Decoding the real composition and structure of the mantle column may partly solve this problem and to help for developing of the exploration program in the Daldyn region because ore supply of the Udachnaya pipe is not endless. Previous detail study of the concentrate from the different parts and probes of the pipe have shown relatively homogeneous mixing and coincidence of compositions for pyropes and picroilmnites. [1-3, 20] Here the compositions of the minerals separated from the two kimberlite small drilling samples and concentrate from larger probe of autolitic kimberlite was used to detail the variability of the minerals and compare with those from pipes

Yubileynaya and Udachnaya (this volume). EPMA and LAM ICP MS analyses made in UIGGM SD RAS characterized the mantle material and are the base for geochemistry models and PT reconstructions.

MINERALOGY

Garnets. Variations on Cr_2O_3 –CaO (and Cr_2O_3 vs. Feo, MgO, Na_2O, NiO) show in general the structure of mantle section since Cr_2O_3 is pressure dependent [23, 28] and lithology may be determined by CaO, TiO_2, FeO, Na_2O [10, 15, 17, 30]. In analyzed drill sample all garnets represent 7 clots with the near lineal Cr_2O_3-CaO correlations. Small arrays with the negative slopes represent the isobaric variations [22] in large disintegrated samples or groups of similar rocks. The large probe reveal large scale variations of mineral compositions close to those estimated by [1, 2] for Cr_2O_3-CaO. Most of garnets continuously trace the lower boundary of the lherzolite field [1, 30]. In 4 series with different inclination in Cr_2O_3-CaO diagram, two with higher CaO values are similar to Udachnaya pipe garnets [8] coinciding with lherzolite – pyroxenite zonation [22]. The sub- vertical arrays at the Cr-(Na-Fe-Mg) probably reflect the grain zonation and compositional rock variations for the same domains in the mantle. The garnets from Zarnitsa continue trends from Udachnaya to more FeO -CaO rich pyroxenitic compositions [22, 27]. The N_2O content is higher in pyroxenitic shallow garnets but with the depth it rises [29] forming the 4 compositional arrays. Garnet population is more clustered and split sharper in the Cr-rich part on to depleted dunite- harzburgite [9] and enriched pyroxenite compositions. The gaps in 8-9 % Cr_2O_3 visible on the previous diagrams [1-2, 21] suppose missed interval or essentially elclogitic or deeply depleted garnet -less compositions of the rocks near 50kbars. Cubcalcic garnets [10] are found at Cr_2O_3%. The 4 positive arrays Cr_2O_3-TiO_2 (shaded in fig.1) for the Cr rich peridotite compositions suggest through enrichment processes while negative slopes for the low- Cr, Fe-rich garnets represent megacrystalline and shallow pyroxenite -enriched lherzolie suites. The wehrlitic garnets near 4%Cr_2O_3 are not abundant. Degree of the TiO_2 enrichment is close to Udachnaya garnets but higher in Cr- rich part. Frequency Cr2O3 histograms for the garnets with 7 peaks show gentle decrease to the left and maximum at ~2.7 Cr_2O_3 close to found earlier [1].

Cr- Spinels. long trend from typical diamond bearing associations >60% Cr2O3 content to 25% Cr_2O_3 demonstrates the sharp splitting from the most Cr rich samples to ulvospinel (with the enrichment with $FeTiO_3$ and V_2O_5) and common CrFe-MgAl mantle array. Most Cr- rich samples deviate from mantle array to Mg –rich compositions.

Chromites demonstrate bimodal distribution with the peaks near 55 and 30% Cr_2O_3 and more rare intermediate compositions. The gap between two major groups represents mainly two horizons in the mantle but some intermediate

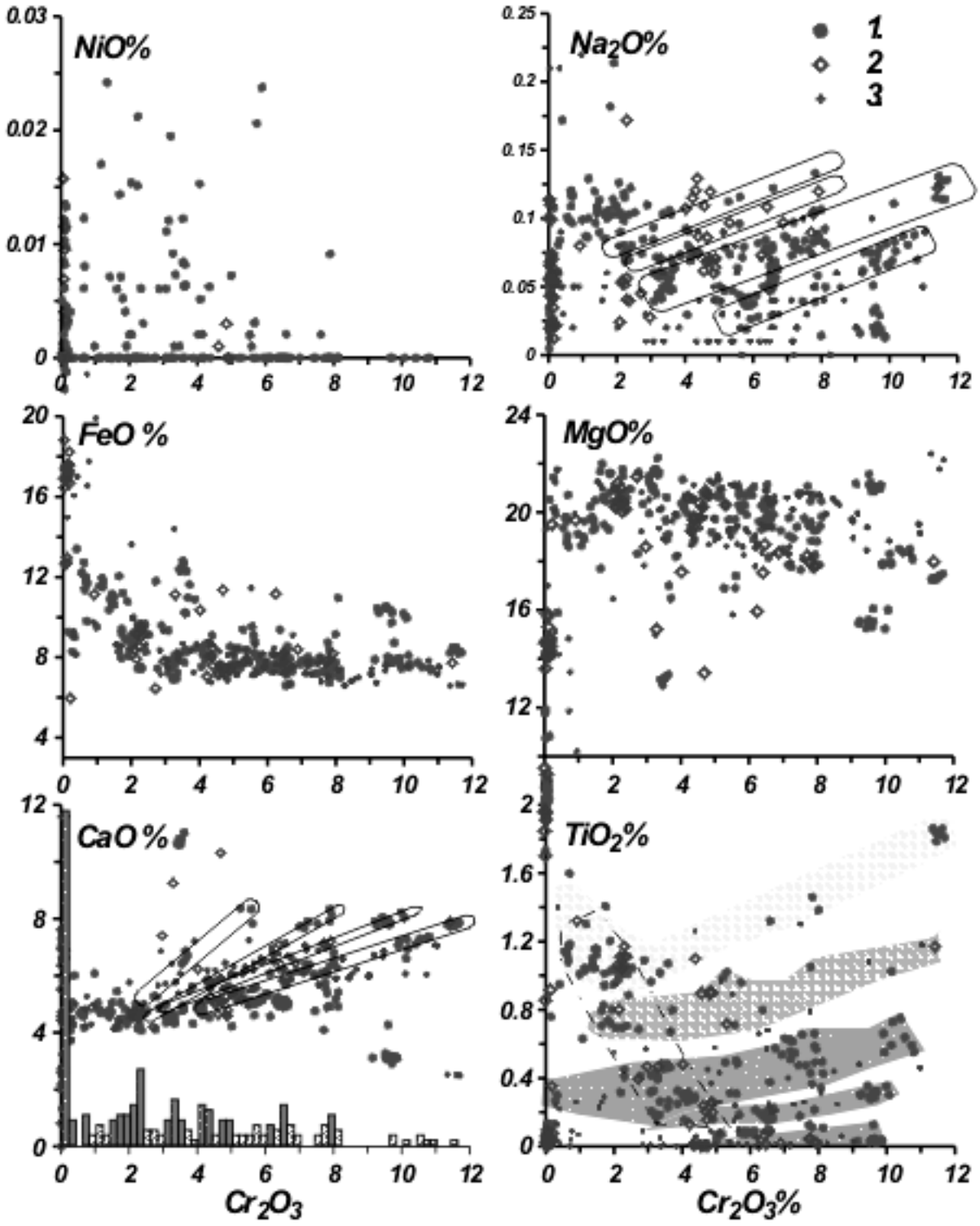

Fig. 1. *Variation diagram for the Garnets from Zarnitsa.*

peridotite compositions need higher statistics, 7 groups are identified by rare grains (Fig.2).

Clinopyroxenes. Mantle clinopyroxenes with the content Fe 1-4 % reveal rather diverse compositions which identified using the analogy with those from

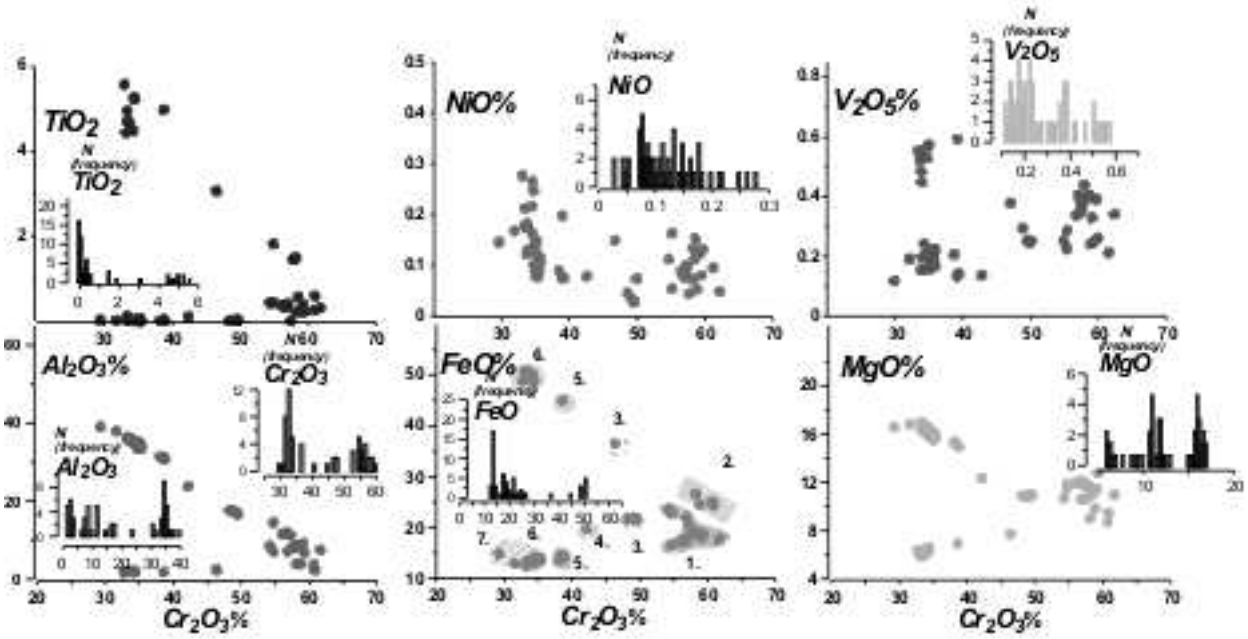

Fig. 2. *Variation diagram for Cr-spinels. Shaded are 7 possible groups form different pressure intervals.*

other pipes. Pyroxenes form (field 1 in fig .3) are close to the most primitive for Yubileynaya pipe Cr-diopsides common in Udachnaya peridotites [10, 21, 27] relatively low in Al_2O_3 and Na_2O (probably primary compositions). The group 2 between 2.5-3.5 Na_2O directly trace the trend of the sheared lherzolites determined for Udachnaya pipe [10]. Most Cr-Al-Na –rich pyroxenes (3) are close to 40 kbar what corresponds to 4 % Cr_2O_3 inflection on Cr_2O_3 CaO diagram for lherzolitic field [31] and refer to metasomatics - garnet pyroxenites in Daldyn – Alakit field [19], Aldan [8], in Colorado [7, 19] and other kimberlites being higher in Al_2O_3 content then metasomatic pyroxenes from Yubileynaya pipe (this volume). Field 4 grain – represents hybrid pyroxenite composition. Ferriferous assemblages (5-6) 7-11% FeO, ~1% are close mostly salites from the lower crust cumulates. Other (7) are shallow crust assemblages.

Orthopyroxenes from Zarnitsa representing 3 groups (Fig.4) are more Fe-rich then in Udachnya. The depletion in Al for deep pyroxenes extreme enrichment for garnet- spinel are found, Ti fluctuations are close to Udachnaya orthopyroxenes.

Ilmenites demonstrate more continuous in TiO_2 crystallization line [16, 24]. Similar to Yubileinaya trend is divided into 7 separate clots (Fig.5). Three major were found to be relatively constant for both small grains and large ilmenite nodules [1, 3]. The variation (150 analyses) of the most TiO_2- MgO (and Cr_2O_3) - rich are close to those from the mica veins and marids and glimmerites [13]. The large grains reveal more discrete compositions. Fine grains are higher in Cr_2O_3 and represents fragment of metasomatic peridotites [13, 31]. The break with the

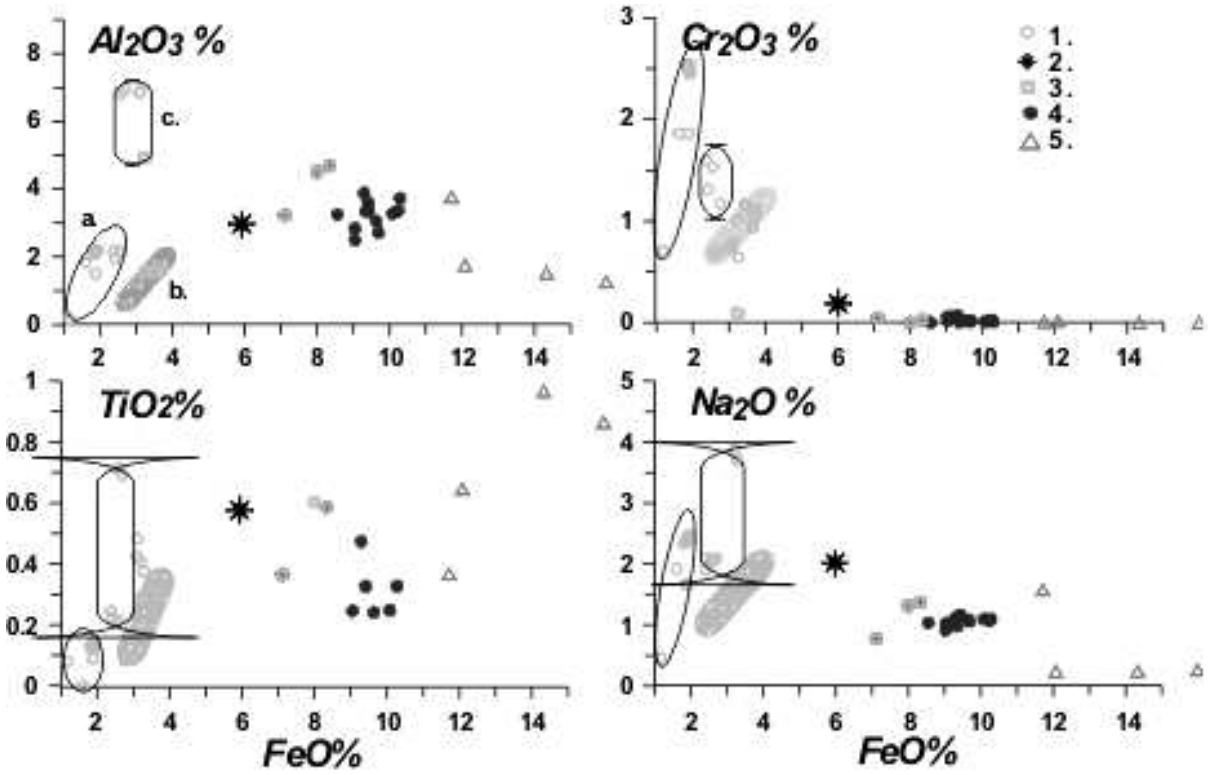

Fig. 3. *Variation diagram for clinopyroxens. 1.- Cr- diopsides; 2- hybrid HT pyroxenite; 3 – salites low crust ; 4. 5. Ti – augites.*

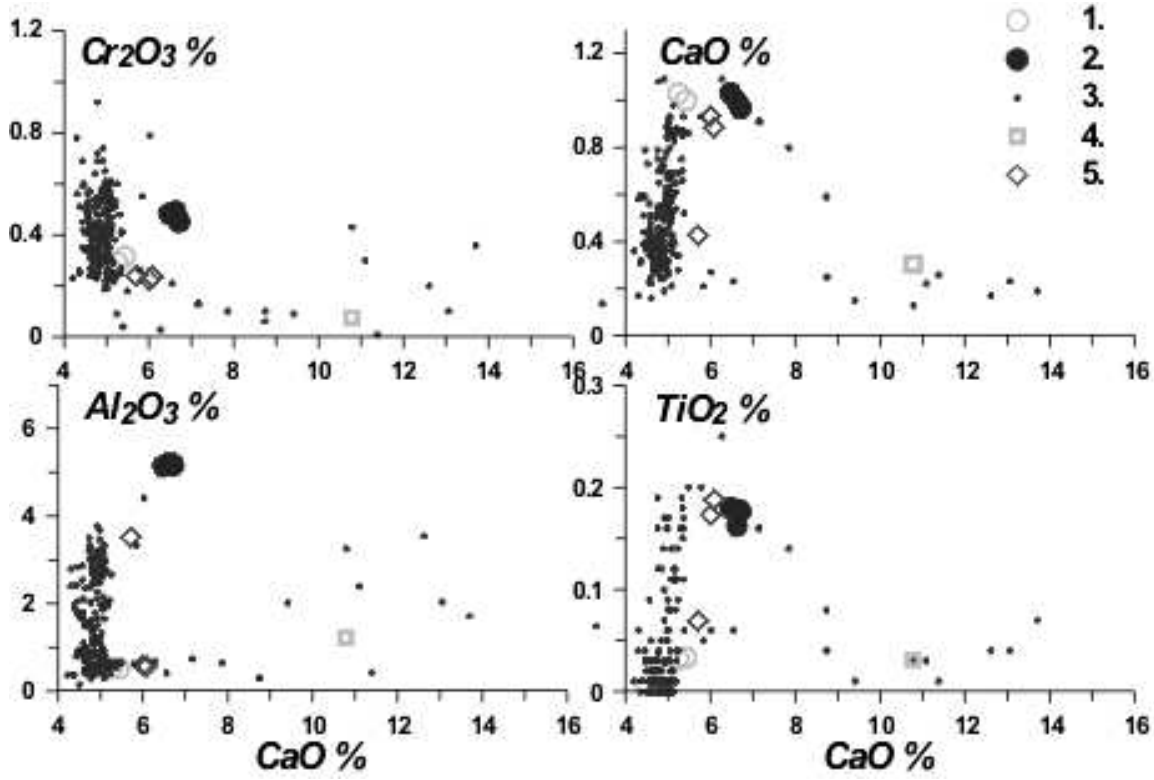

Fig. 4. *Variation diagram for orthopyroxens in comparison with those from Udachnaya pipe.*

1. primitive deep seated peridotites; 2.sheared. 3- Udachnaya peridotites; 4.- cumulates; 5. garnet – spinel lherzolites.

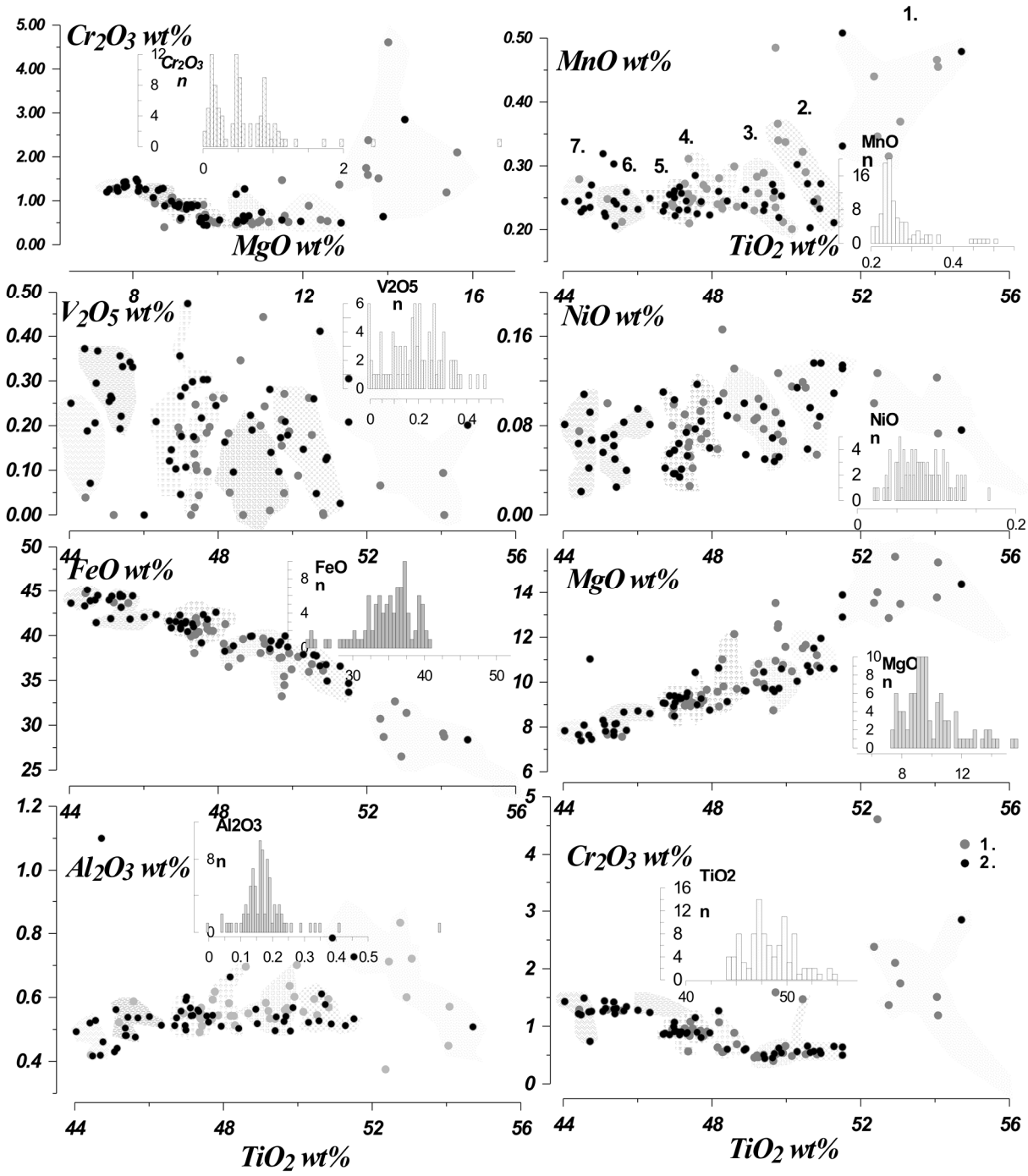

Fig. 5. *Variations for the picroilmenites.*

1. whole population variations; 2. the autolitic kimberlites

growth of FeO -Cr_2O_3 visible in Mg-Cr and Ti-Cr diagrams means changing crystallizing assemblage or way of the differentiation (from chamber or large vein fractionation to AFC).

Micas from Zarnitsa pipe belong to 4 groups (Fig.6). Analyzed mantle phlogopites are close to the most wide spread in Yubileynaya pipe (this volume). The other Ti – rich and Cr – low represents mantle veins and glimmerites and Cr-less are from crust cumulates.

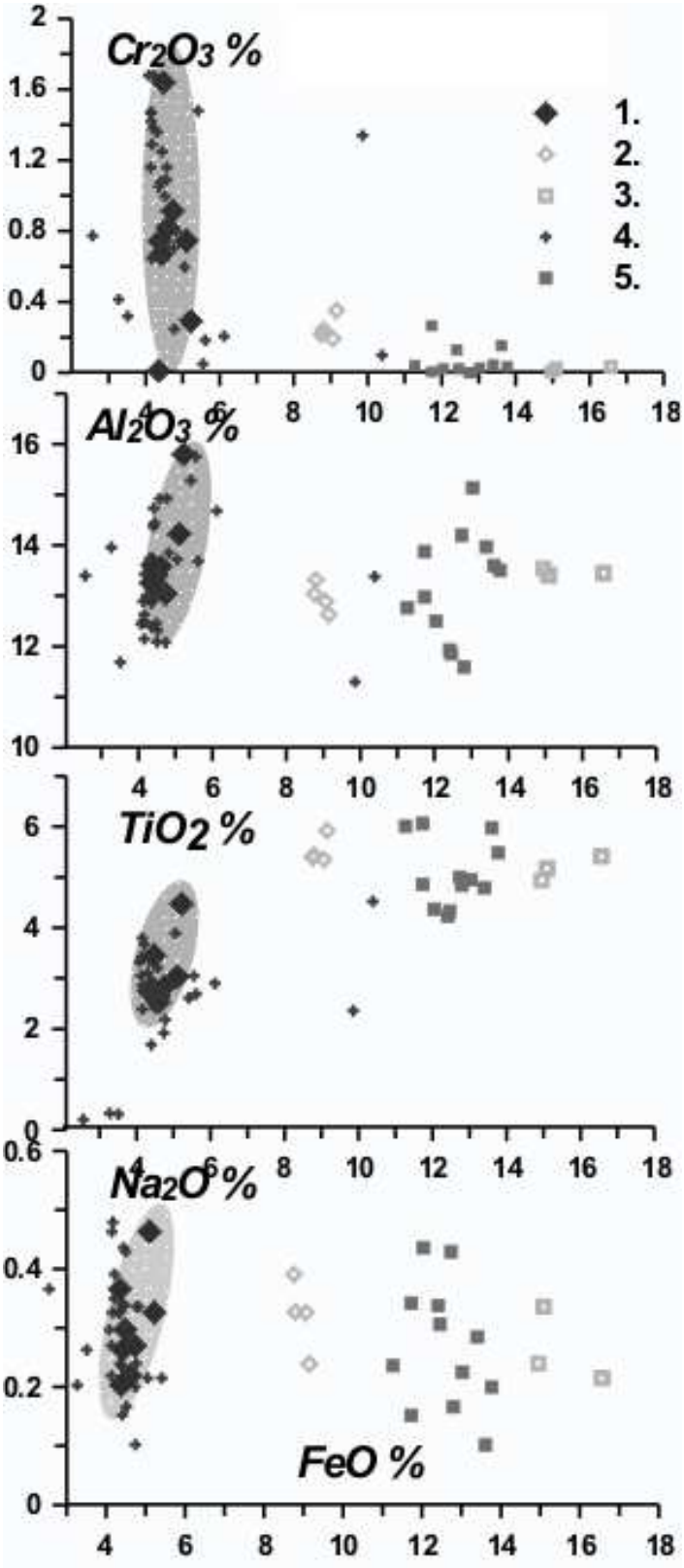

Fig.6. *Diagram for the micas from Zarnitsa.*

1. peridotitic lherzolitic type; 2. vein and glimmerites; 3,5 megacrysts; 4. lherzolite micas from Yubileinaya.

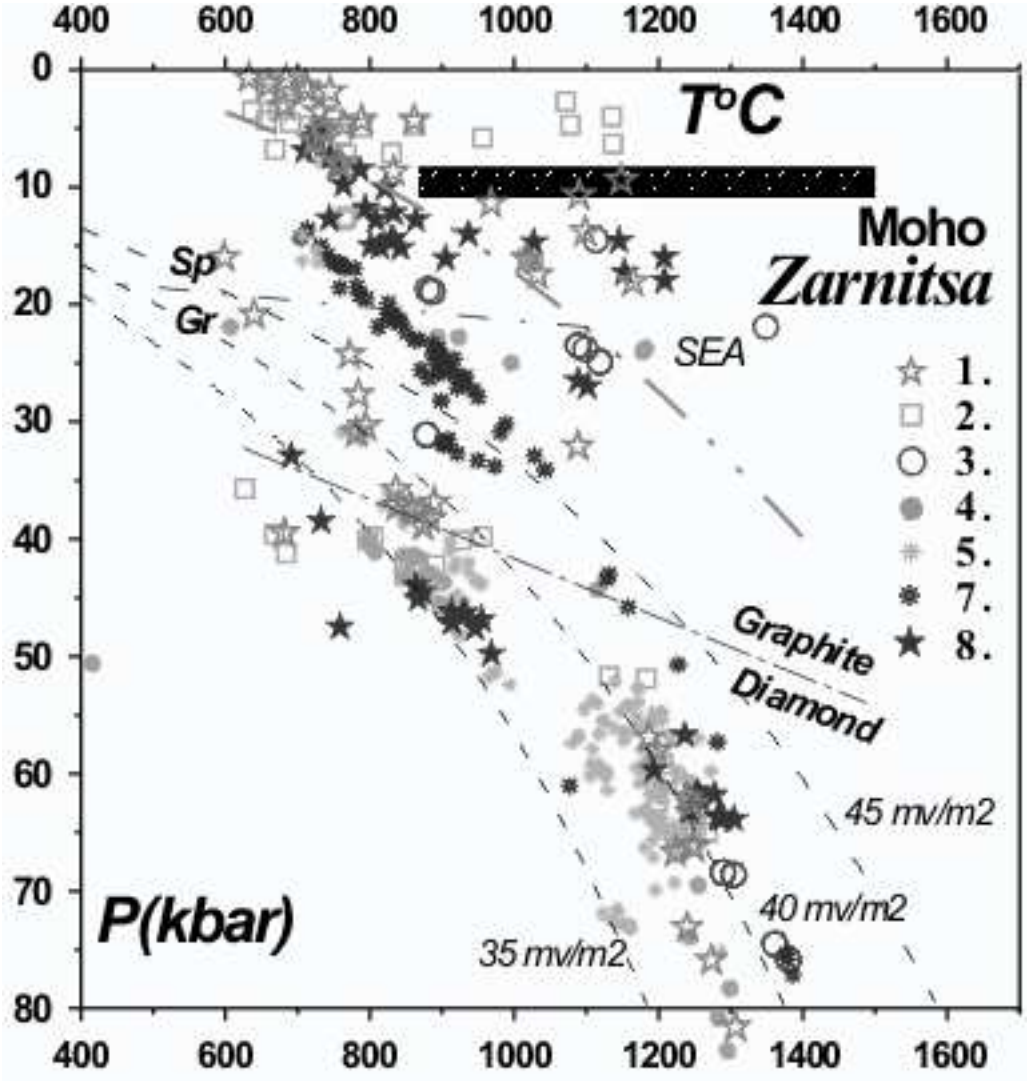

Fig. 7. *TP diagram for Zarnitsa pipe.*
Different combinations of methods: 1. [26]-[6].2. [26]-[6a]; 3.[13]-[24];4 [26]; 5 [4] for deep mantle; 6. [4] for shallow mantle; 7. [26] –[6]c.

THERMOBAROMETRY

The TP diagram for the Zarnitsa pipe determined using 31 Cr-diopsides and 17 enstatites show clear coincidence of the results of clinopyroxene and orthopyroxene barometry (Fig.7). Lower horizon 50-70 kbar is relatively heated to 40 mv/m2. The gap between the 40-50 kbar probably refers to dunite (heated) rocks without pyroxenes, eclogites or is not sampled by the magma during the rise to the surface. The middle part usually represented by mica lherzolites, hydrous anatexic websterites and metasomatites [14, 20, 22, 27, 30] well mapped by pyroxene and garnet TP estimates near 40 kbar is irregular heated from 35 to 45 what is common [7, 18, 26]. Shallower garnet-spinel part seems to be close in geothermal gradients to the other pipes. The black pyroxenes and some Cr - diopsides trace SEA geotherm starting from 30 kbar to crust level. The orthopyroxene and clinopyroxene TP estimates are very close in upper part also.

Compositions of the major and trace elements in the minerals from Zarnitsa concentrate. ***Table 1***

Compo-nent	Cpx1	Cpx2	Cpx3	Gr1	Gr2	Gr3	Ilm1	Ilm2	Cr1	Cr2
SiO_2	53.95	52.41	53.71	41.72	41.55	40.51				
TiO_2	0.467	0.691	0.578	0.237	1.11	0.003	47.71	49.71	0.09	0.026
Al_2O_3	1.88	6.91	2.95	19.47	19.54	18.59	0.593	0.56	23.77	34.61
Cr_2O_3	0.159	0.704	0.203	4.62	2.37	6.24	0.89	0.509	42.17	35.13
FeO	4.61	2.69	5.96	7.61	9.15	11.16	40.73	37.56	19.63	13.39
MnO	0.147	0.107	0.146	20.9	0.295	0.838	0.242	0.235	0.346	0.22
MgO	16.68	13.98	17.29	0.289	20.16	15.94	9.43	10.95	12.36	16.07
CaO	22.22	20.36	17.56	4.62	4.61	6.54	0.068	0.052	0.017	0.015
Na_2O	0.318	2.09	2.04	0.024	0.133	0.035	0.097	0.213		
K_2O	0.008	0.015	0.017		0.016					
Total	100.439	99.957	100.454	99.49	98.934	99.856	99.76	99.789	98.383	99.461
Ba	2.2	89	5.5	0.1	2.6	6.48	2.9	23.0	17	276
La	17.9	7.8	1.5	0.088	2.6	1.03	8.9	25.1	1.7	2.5
Ce	71.9	21.3	5.0	0.2	4.22	4.16	12.2	61.2	5.9	12.3
Pr	13.7	3.39	2.11	0.08	0.15	0.46	1.17	3.25	0.93	0.32
Nd	74.7	17.1	5.5	0.76	1.21	3.32	4.4	15.5	3.7	1.1
Sm	19.9	4.3	2.2	0.76	1.10	1.58	0.8	4.0	0.7	0.2
Eu	4.4	1.00	0.8	0.32	0.25	0.73	0.504	0.37	0.37	0.036
Gd	16.0	2.70	3.15	1.20	1.06	2.24	0.28	0.90	0.68	0.06
Tb	1.84	0.43	0.60	0.22	0.23	0.40	0.03	0.12	0.07	0.01
Dy	7.59	2.00	4.49	1.84	1.12	2.22	0.24	0.59	0.41	0.06
Ho	1.29	0.40	1.09	0.48	0.27	0.47	0.04	0.09	0.09	0.01
Er	2.25	1.02	3.12	1.25	0.65	1.36	0.16	0.29	0.13	0.06
Tm	0.22	0.06	0.36	0.16	0.06	0.12	0.00	0.04	0.03	0.01
Yb	1.0	0.7	3.4	1.4	0.7	1.1	0.1	0.6	0.1	0.1
Lu	0.15	0.07	0.34	0.20	0.08	0.17	0.00	0.05	0.03	0.03
Hf	13.0	4.2	1.4	1.0	1.2	2.1	31.6	13.2	0.6	0.4
Ta	0.14	0.04	0.03	0.05	0.05	0.11	297	97	0.03	0.14
Pb	1.6	4.2	2.5	3.4	4.5	9.2	4.1	9.8	45.3	319
Th	0.26	0.22	0.17	0.02	0.06	0.65	0.04	1.02	0.11	0.84
U	0.04	0.12	0.78	0.06	0.02	0.06	0.30	1.80	0.07	0.09
V	968	660	316	179	180	312	1947	1178	417	2085
Sc	182	44	87	79	85	131	43	21	12	5
Co	28.9	15.2	4.2	6.9	5.9	11.7	35.1	24.3	160	162
Cu	0.01	6.09	5.21	0.11	3.74	5.09	8.09	16.9	0.38	5.40
Ni	26	118	71	14	23	49	156	133	443	236
Rb	0.4	6.0				0.1		0.8	1.4	1.9
Sr	37.58	609	120		4.37	2.75	1.32	15.8	8.06	27.8
Y	25.9	8.3	23.6	9.67	5.10	9.28	0.68	3.12	1.22	0.30
Zr	344.1	66.6	41.4	29.1	45.4	75.4	824.8	349.2	16.9	11.1
Nb	0.9	4.1	0.3	0.3	1.4	1.7	2731	845	1.6	4.5
Cs		6.95	0.16	0.04	0.03	0.03	0.02	0.04	0.011	

Note. *Analyses were made in Analytic Center, UIGGM Sd RAS,.Novosibirsk. Major components are determined on CamebaxMicro, analyst O.S.Khmelnikova, January, 2003. Trace elements are made by LAM ICP MS using mass-spectrometer, "Finigan Element" and laser microprobe "Finigan UV LaserProbe" n=266., analysts: S.V.Palessky, I.V.Nikolaeva, A.I. Saprykin, Febrary,14, 2003*

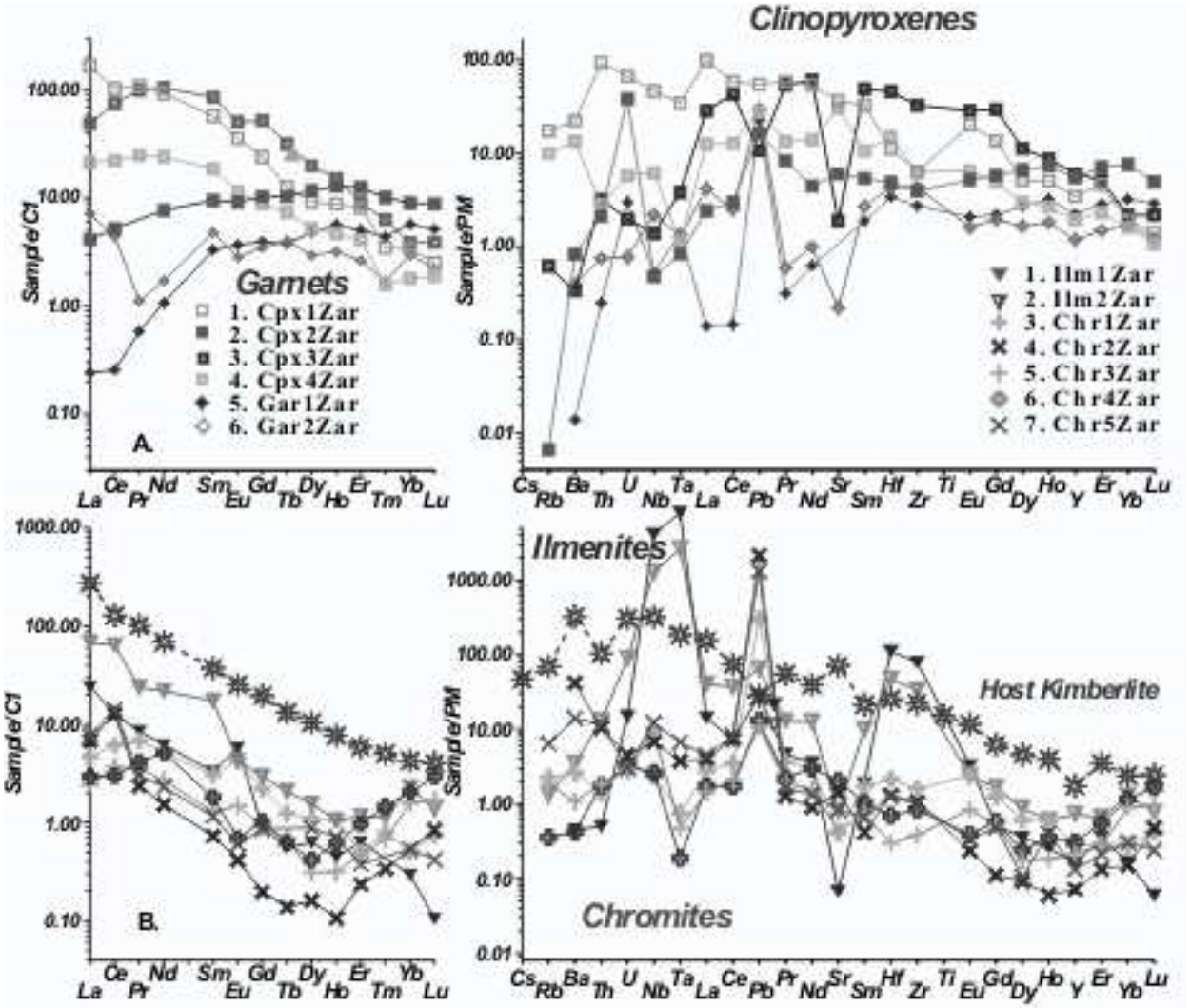

Fig. 8. *TRE spectrums of the mineral from Zarnitsa pipe.*

Results of the garnets thermobarometry [4] show that TP estimates by garnets coincides but give more broad TP range at the HP level ~70 kbar with the dispersion from the 35 to 40 mv/m2 geotherms for garnets probably due to the heating. Most estimates coincide with pyroxene geotherm. Upper 30 kbar garnet geotherm splits on two several branches probably reflecting the way of the melt percolation. The branched geotherm for Zarnitsa and other pipes differ from the suggested relatively smooth in middle part Siberian geotherm [9].

GEOCHEMISTRY

LAM ICP analyses were made for clinopyroxenes, garnets, orthopyroxene spinels and ilmenites.

Analyzed garnets are relatively low in Cr and do not show S patterns (tabl. 1). The REE and TRE patterns for the analyzed mantle garnets and clinopyroxenes do

not display strong extremes in HFSE – LILE typical for the ilmenites from some other pipes in as well as the strong REE fractionation (Fig.8). Deep Cr-Di pyroxenes are not highly depleted in HREE possibly due to low abundance of garnets in the deep horizons. But all garnets and chromites display strong Pb peaks. Chromites reveal strongly LREE rich incline patterns with depression in MHREE. Rise of the Nb, Ta in ilmenites is accompanied by the HREE decrease, suggesting garnet co-precipitation. Black clinopyroxens occurred in concentrate reveal smooth pattern and were derived from the primitive mantle melt as well as the composition of the matrix in the debris of basaltic kimberlites determined by LAM ICP MS.

The TRE elements determined by laser for the dark olivine – bearing fragments in the kimberlite without the visible xenoliths show also unusual for the Yakutian kimberlite pattern less depleted in HREE.

DISCUSSION

Garnets concentrate histogram for Zarnitsa pipe defines the major captured interval rather shallow. The material diamond facie compile not more the 1/4 of all garnet population. But Cr-Spinels define near ½ of deep seated compositions. The ilmenite trend also gives rather high volume of deep material.

Thermobarometry suggest the heating at the lower part of the sections what is probably responsible for the dissolution of the small garnets and growth of the HT rounded type of the diamond grains. Not continuous type of the capturing or the layering with the marble cake eclogite –peridotite structure may be responsible for the separate clots of the mineral compositions and TP estimates Very irregular and sometimes discontinuous mineral trends and TP values are higher then in Udachnaya [8]. Fe content of minerals possibly means presence of the melts in several levels of mantle just before the eruption and local interaction with the peridotites. One can suggest the 4 levels of melt concentration. The 4 trend of the Ti enrichment possibly reflect the enrichment near the conduit of the rising melt and 4 stages of the melt intrusion in pre- eruption stage possibly during creation of the feeding system and rising of kimberlitic melts. Coincidence with the Na-enrichment trends proves the polybaric natures of this process.

Comparing to the Yubileinaya pipe the geochemistry of the minerals define this type of mantle sections to be formed by the influence of the oceanic type subduction. Similarity of the TRE patterns for the spinels and ilmenites means crystallization from the similar mater probably near the rising kimberlite masses.

CONCLUSIONS

1. The gap in the compositions of the chromites and garnets is also supported by the pyroxene thermobarometry. It means either eclogite bend not supported by clinopyroxene compositions or missed interval not captured by magma.

2. Mantle column is more ferriferous and more heated at the lower part what is corresponded to the degree of the heating.

3. Ilmenite megacryst are crystallizing from the large portions of magma in the first step and then according to the AFC most likely in the polybaric vein system.

4. The amount of the large diamonds in the pipe probably is depended from the relatively high heating degree in all lower par what may brings to the dissolution of small crystals.

Supported by RBRF grants: 99-05-65688, 00-05-65288, 03-05-64146.

REFERENCES

1. **Amshinsky A.N.** Minerals – diamond-fellows form the kimberlites of the Daldyn – Alakite field. Dissertation for the degree of doctor (candidate) of geological – mineralogical sciences. Novosibirsk. 1985. 174 p.
2. **Amshinsky A.N., Blinchik T.M., Kuligin S.S.** Comparative characteristic of the minerals diamond -fellows in the kimberlites of the Daldyn field. In book: Problems of the kimberlite origin. Novosibirsk. Nauka . 1989. pp. 126-131.
3. **Amshinsky A.N., Pokhilenko N.P.** Characteristic features of the picroilmenite compositions from the kimberlite pipe Zarnitsa. Russian Geol Geophys. 1983. N11.pp .116-119.
4. **Ashchepkov I.V.** Empirical garnet thermobarometer for mantle peridotites. Seattle Annual Meeting (November 2-5, 2003). Abstract ID: 65507.
5. **More precise equation of the Jd-Di Barometr.** Herald ff of the Earth department RAS.2003, N1. pp.45-46.
6. **Ashchepkov I.V.** Jd-Di barometer for mantle peridotites and eclogites. Experiment in Geosciences v.10, N1, 137-138.
7. **Ashchepkov I. V., Vladykin N. V., Mitchel R. H.l, Coopersmith H., Garanin V. G., Saprykin A. I., Khmel'nikova O. S., Anoshin G. N.** Mantle Evolution beneath the Colorado Plateau: Interpretation of the Study of Mineral Concentrates from KL-1 Kimberlite Pipe Trans. RAS ESS v385 pp. 721-726.
8. **Ashchepkov I.V., Vladykin N.V., Saprykin A.I., Khmelnikova O.S.** Composition a thermal structure of the mantle in peripheral parts of the ancient shields within Siberian craton. Revista Brasileira de Geociencias (2001), 31(4): 527-636.
9. **Boyd F.R.; Pokhilenko N.P.; Pearson D.G.; Mertzman S.A.; Sobolev N.V.; Finger L.W.** 1996. Composition of the Siberian cratonic mantle: evidence from Udachnaya peridotite xenoliths. //Contrib. Mineral. and Petrol. 1997., V. 128. N 2-3. P. 228-246.
10. **Boyd FR, Pearson DG, Nixon PH, Mertzman SA** (1993) Low-calcium garnet harzburgites from South Africa: their relations to craton structure and diamond crystallization. Contrib Mineral Petrol 113:352 –366.
11. **Boyd, F.R.,** 1984. A Siberian geotherm based on lherzolite xenoliths from the Udachnaya kimberlite, U.S.S.R. Geology 12, 528–530.

12. **Brey GP, Kohler T** (1990) Geothermobarometry in four-phase lherzolites II: new thermobarometers, and practical assessment of existing thermobarometers. J Petrol 31:1353 –1378

13. **Gregoire M., Bell, D.R.; Le Roex, A.P.** 2002. Trace element geochemistry of phlogopite-rich mafic mantle xenoliths: their classification and their relationship to phlogopite-bearing peridotites and kimberlites revisited. Contrib Mineral Petrol. 142(5) pp. 603-625.

14. **Griffin W.L., Ryan C.G., Kaminsky F.V., O'Reilly S.Y., Natapov L.M., Win T.T., Kinny P.D., Ilupin I.P.** The Siberian lithosphere traverse: mantle terranes and the assembly of the Siberian Craton. // Tectonophysics. 1999. V.310. P. 1–35.

15. **Griffin, W. L., N. I. Fisher, J. H. Friedman, S. Y. O'Reilly, and C. G. Ryan**, Cr-pyrope garnets in the lithospheric mantle, 2. Compositional populations and their distribution in time and space, Geochem. Geophys. Geosyst., 20023(12), 35 p.

16. **Griffin, W.L., Moore, R.O., Ryan, C.G., Gurney, J.J., Win, T.T.**, 1997. Geochemistry of magnesian ilmenite megacrysts from Southern African kimberlites. Russian Geol. Geophys. 38(2). pp.398-419

17. **Dawson, J.B., Stephens, W.E.**, 1975. Statistical classification of garnets from kimberlite and associated xenoliths. J. Geol. 83, 589-607.

18. **Hearn B.C. Jr.** Upper-Mantle Xenoliths in the Homestead Kimberlite, Central Montana, USA: Depleted and Re-Enriched Wyoming Craton Samples. 8th International Kimberlite Conference Extended Abstracts.

19. **Kostrovitsky S.I. , De Bruin D.** Garnets from the ultramafic associations in the groups Zagadochnaya and Bukovinskaya kimberlite pipes. Alkaline magmatism and the problem of mantle sources. Irkutsk, IGTU, 2001. pp. 170- 187.

20. **Khar'kiv A.D. Zinchuk N.N., Kr'ychkov A.I.** Primary deposits of the diamonds in the World. Moscow Nedra. 1998. 545p.

21. **Kuligin S., Malkovets V., Pokhilenko N., Vavilov M., Griffin W., O'Reilly S.** Mineralogical and geochemical characteristic of a unique mantle xenoliths from the Udachnaya kimberlite pipe. Depleted and Re-Enriched Wyoming Craton Samples. 8 th International Kimberlite Conference Extended Abstracts.

22. **Malinovsky I.Y., Godovikov A.A., Doroshev A.M. et al.** Silicate systems under high pressures and temperatures and application to the petrology of the upper mantle and the low part of the Earth's crust. In: Physics – chemistry conditions of the processes of the mineral origin according to the theoretic and experimental data. Novosibirsk. Nauka. 1976. p. 136 - 146.

23. **McGregor I.D.** 1974.The system MgO- SiO2-Al2O3: solubility of Al2O3 in enstatite for spinel and garnet peridotite compositions. Am.Miner ., V.59, P.110-119.

24. **Moor, R.O., Griffin, W.L. Gurney et al.** 1992 Trace element geochemistry of ilmenites megacrysts from the Monastery kimberlite, South Africa. Lithos. 29, pp.1-18.

25. **Nimis P., Taylor W.** Single clinopyroxene thermobarometry for garnet peridotites. Part I. Calibration and testing of a Cr-in-Cpx barometer and an enstatite-in-Cpx thermometer. //Contrib. Mineral. Petrol. 2000. V. 139. N5. P.541-554

26. **O'Reilly S.Y., Griffin W.L., Poudium Diomany, Morgan P.**, 2001. Are lithospehers forever? GSA Today. 11, pp.4-9

27. **Pokhilenko, N. P., Sobolev, N.V., Kuligin, S. S., Shimizu, N.** 2000. Peculiarities of distribution of pyroxenite paragenesis garnets in Yakutian kimberlites and some aspects of the evolution of the Siberian craton lithospheric mantle. Proceedings of the VII International Kimberlite Conference. The P.H. Nixon volume. Pp. 690-707.

28. **Ryan C. G.; Griffin W. L.; Pearson N. J.** Garnet geotherms: Pressure-temperature data from Cr-pyrope garnet xenocrysts in volcanic rocks. J. Geophys. Res. B. 1996. V. 101. N 3. P. 5611-5625

29. **Sobolev NV, Lavrent'yev YG** (1971) Isomorphic sodium admixture in garnets formed at high pressures. Contrib Mineral Petrol 31:1 –12

30. **Sobolev, N.V.** (1977): Deep-Seated Inclusions in Kimberlites and the Problem of the Composition of the Upper Mantle. Am. Geophys. Union, Washington, D.C.

31. **Zhang H.F., Menzies M., MAttey D.P, Hinton R.W., Gurney J.J.** Petrology, mineralogy abdnd geochemistry of oxide minerals in polymict xenolithsfrom the Bultfontein kimberlites, South Africa: implications for bulk rock oxygen isotopic ratios. Contrib Mineral Petrol 2001.

Petrography and mineral chemistry of mantle xenoliths and xenocrysts from the Grib pipe, Zimny Bereg area, Russia

Sablukova L.I.[1], Sablukov S.M.[1], Verichev E.M.[2], Golovin N.N.[3]

[1]TsNIGRI, Moscow, E-mail: S.Sablukov@g23.relcom.ru
[2]ZAO "Arkhangelskgeolrazvedka", Novodvinsk
[3]OAO "Arkhangelskgeoldobicha", Arkhangelsk

The Grib pipe is to date the only deposit of its kind of flat-faced diamonds in the Zimny Bereg district of Russia. Mantle xenoliths are abundant (by Zimny Bereg pipe standards) in rocks that comprise the Grib pipe; these vary in size from 1-2 cm to 22 cm. These deep-seated inclusions in the kimberlites represent a broad spectrum of rock varieties. The Grib pipe xenoliths are dominated by nodules of various types of pyrope peridotite and pyroxenite of differing depth facies; chrome spinel ultramafic xenoliths are few. Among the Fe-Ti series ultramafic rocks, peculiar ilmenite-rutile and pyrope-rutile lithological varieties are present, together with more typical ilmenite-bearing and pyrope-ilmenite rocks. Rather abundant are eclogite-like rocks and Group A, Group B and, more rarely, Group C-type eclogites. Megacrysts are abundant in rocks of the Grib pipe. A peculiar feature of the Grib pipe is the presence of rutile megacrysts along with "ordinary" megacrysts of ilmenite, garnet, phlogopite, pyroxenes and olivine. The abundance of various clinopyroxene-phlogopite and phlogopite rocks may either be evidence of mantle hydrous-calc-alkali (K-Ca) metasomatism, or of crystallization from volatile-rich residual melts. The presence of diversified nodules of combined rocks is an indication of a complex, multistage history of mantle substrate formation, including cumulus-type magma segregation, development of vein-type metasomatic domains, and intrusive rock relationships, resulting in the formation of zones of "hot" contact metasomatism ("skarnoids"). In general, the variation of TP formation parameters for the examined nodules of various peridotites and eclogites is quite well approximated by a 42-43 mW/m^2 conductive geotherm. The set of mantle rock varieties present in the Grib pipe is very distinct from that characteristic of kimberlite pipes of the Lomonosov deposit (Zimny Bereg Al-series kimberlites), being most similar to that of pipe An-688 from the Pachuga group (Zimny Bereg Fe-Ti series kimberlites). The Grib pipe differs from pipe An-688 by its higher mantle nodule content and abundance of clinopyroxenites, clinopyroxene-phlogopite rocks and megacrysts of clinopyroxene, orthopyroxene, deformed phlogopite and rutile. In general, based on the essential varieties of mantle xenoliths, their large size and high concentration in rock samples, the predominance of pyrope rock varieties among the xenoliths, and taking into account the geochemical and Nd-Sr characteristics of the rocks themselves, the Grib pipe kimberlites can be classified with the Fe-Ti series Zimny Bereg kimberlites, as similar to Group 1 South African kimberlites and diamondiferous kimberlites of the Southern fields of the Yakutian diamond province (excluding the Nakyn field). The predominance of flat-faced octahedra among the diamonds is another common feature that the kimberlites of the Grib pipe and Yakutian kimberlites share.

INTRODUCTION

The Zimny Bereg diamond-bearing region of Russia is globally unique; it has two full Late Devonian kimberlite series (Al-series and Fe-Ti series) that are distinct in structure and composition, and differentiated from highly diamondiferous kimberlites to barren melilitites and picrites occurring together with basaltic volcanic pipes of the same age. Rounded, "Uralian-type" diamond crystals [28] predominate in all the Zimny Bereg diamondiferous and poorly diamondiferous pipes, with the exception of the Grib pipe discovered in February 1996 [27], which is characterized by a predominance of flat-faced octahedral diamonds [19]. This distinction in diamond morphology may reflect a number of factors, while the Grib kimberlite pipe still is a member of a complex and diversified yet single and common Late Devonian volcanic system, with local volcanites having similar age, tectonic controls, structural and textural features and regularly varying petrological, mineralogical, geochemical and isotope characteristics [17]. This general similarity of Zimny Bereg volcanites suggests that particular structural and compositional features of the mantle substrate, from which different local volcanites formed, are crucial in controlling diamond morphology. Some peculiarities of the mantle substrate characteristic of the Lomonosov deposit [dominated by rounded diamonds (the Zolotitsky group of pipes)] and of the Pachuga group of pipes have been already analyzed in our previous studies [16,18]. Accordingly, direct examination of mantle rock fragments from the Grib pipe as a deposit dominated by flat-faced diamonds is of great interest both for determining the main factors governing diamond morphology and for more precise mantle substrate mapping in the Zimny Bereg region, that is considered a world-class kimberlite province.

AREA DESCRIPTION, METHODS AND MATERIALS STUDIED

The Zimny Bereg kimberlite district is situated on the southeastern White Sea coast, in the joint zone of the Russian plate and the Baltic shield (Fig. 1). In all, 61 Late Devonian volcanic bodies (pipes, dikes and sills) are known in this region [14,15,20]. 26 of these occurrences are composed of ***Fe-Ti series*** kimberlites rocks similar to Group 1 South African kimberlites [9,22], and another 23 bodies are made up of ***Al-series*** kimberlite rocks, which are quite peculiar, being most similar in composition to the so-called "isotopical transitional type" kimberlites that are "intermediate" in isotopic composition between Group 1 and Group 2 South African kimberlites [21,22]. The rocks of both Zimny Bereg kimberlite series vary in composition from diamondiferous kimberlites (Al-series in the Lomonsov deposit and Fe-Ti series in the Grib pipe) to poorly diamondiferous and barren melilitites and picrites [14,15,27]. Another 12 volcanic bodies are made up of tholeiitic and subalkaline basalts. The Grib pipe is located in the northwestern part of the study region. Being spatially isolated from all other local igneous rock

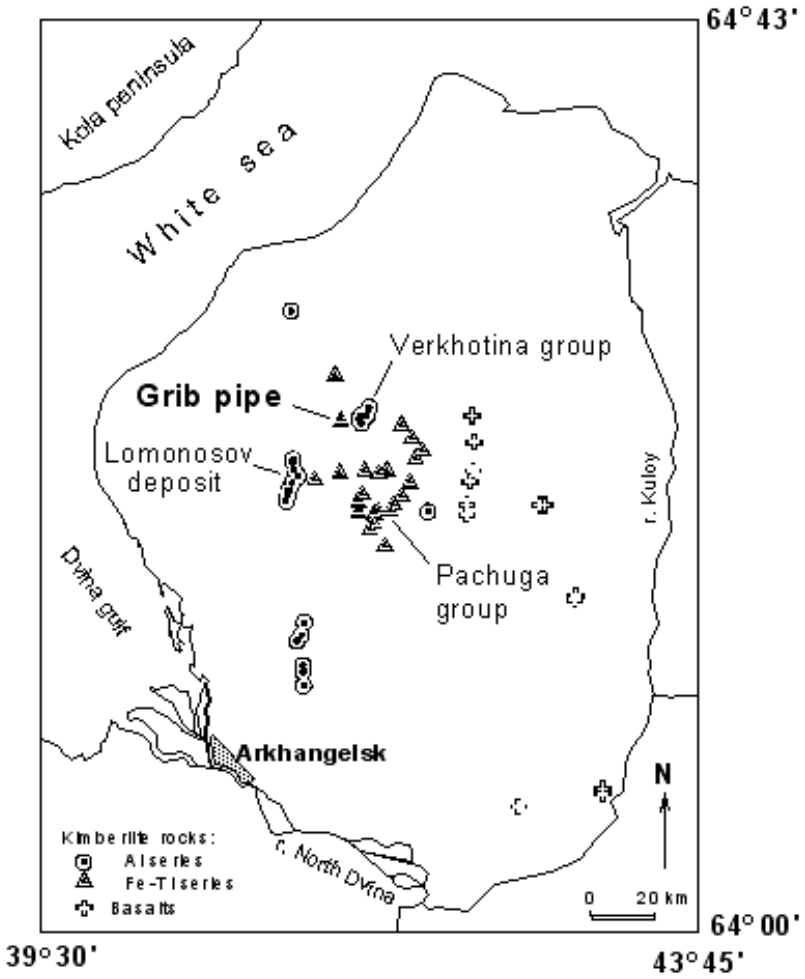

Fig. 1. *Location of volcanic bodies in the Zimny Bereg area.*

occurrences, this pipe also differs from them according in respect to mantle rock xenoliths.

Mantle xenoliths occurring in the Grib pipe are much more abundant, significantly larger and more weakly altered than in all other Zimny Bereg pipes. The concentration of xenoliths in the Grib pipe occasionally ranges up to 3-5 nodules per meter of drill core. Neck tuffisites are most enriched with mantle nodules, whereas neck porphyritic kimberlites show a significantly lower concentration of nodules, which are therewith much more heavily altered. Crater volcanites are characterized by a very low concentration of nodules, which are quite small and almost completely saponitized and carbonatized.

Deep-seated inclusions are mostly oval and oval-flattened and, more rarely, irregular and subangular, some with autolith rims. The inclusions vary in size from 0.5 to 22 cm, with a prevailing size of 3-5 cm (Fig. 2). Larger size is characteristic of almost all petrological xenolith varieties present in the examined rocks, pyrope peridotite nodules being generally the largest (judging by the curvature radii of their fragments in core samples, the actual size of these nodules may be approximately 50 cm or even larger). Most of the nodules are partially

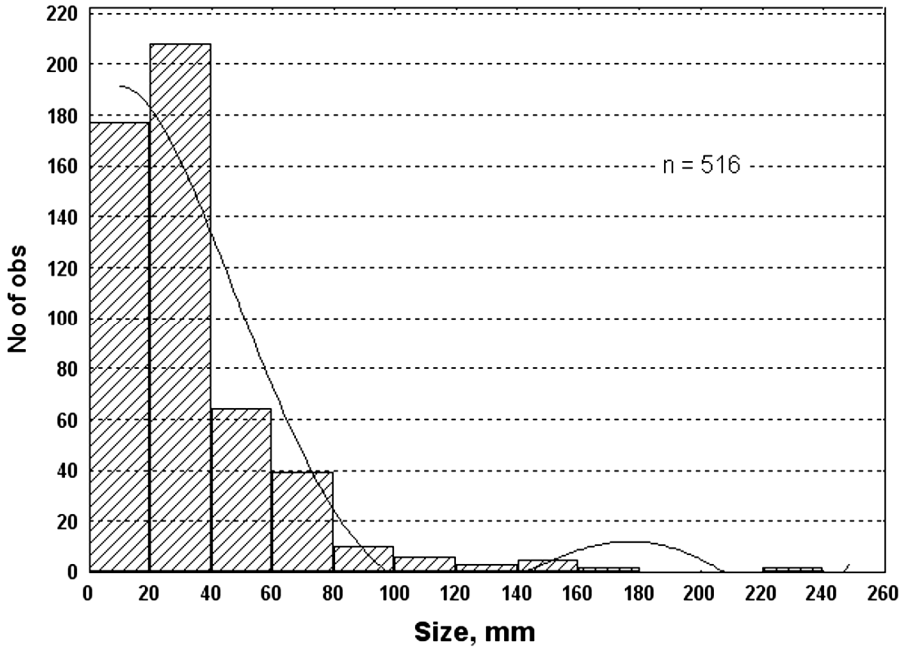

Fig. 2. *Histogram for the sizes of mantle nodules in the Grib pipe kimberlites.*

serpentinized, but fresh (occasionally, very fresh) nodules also occur, although these are only found in tuffisites from deeper that 250 m.

Our collection of mantle nodules from the Grib pipe consists of more than 500 samples, not counting numerous xenocrysts. This set of samples was collected from more than 6000 m of drill core during 1996-2002. Studying the deep-seated inclusions, we have performed some 450 X-ray spectral microanalyses of minerals, including the examination of 60 thin and polished sections of the deep-seated rocks. Mineral chemistry was studied using a Camebax X-ray spectral microanalyzer (MicroBeam Cameca) in an optimum mode (U = 15 kV, I = 15 nA), Laboratory of IGEM RAN, analyzer Borisovsky S.E., 2003 year.

PETROLOGICAL VARIETIES OF MANTLE NODULES

When subdividing mantle nodules into groups by petrology (see the scheme in Fig. 3), we used a number of classification principles proposed by different researchers [2,3,10,24]. Deep-seated inclusions were subdivided into ***deep-seated rock inclusions*** (including their disintegration products: xenoliths, microxenoliths, intergrowths, oikocrysts and xenocrysts) and ***megacrysts***. The spectrum of deep-seated inclusion varieties present in Grib pipe kimberlites is very wide (Fig. 3), from various ultramafic rock types (including metasomatites and combined rocks with a complex structure and composition), mafic rocks, xenocrysts and megacrysts.

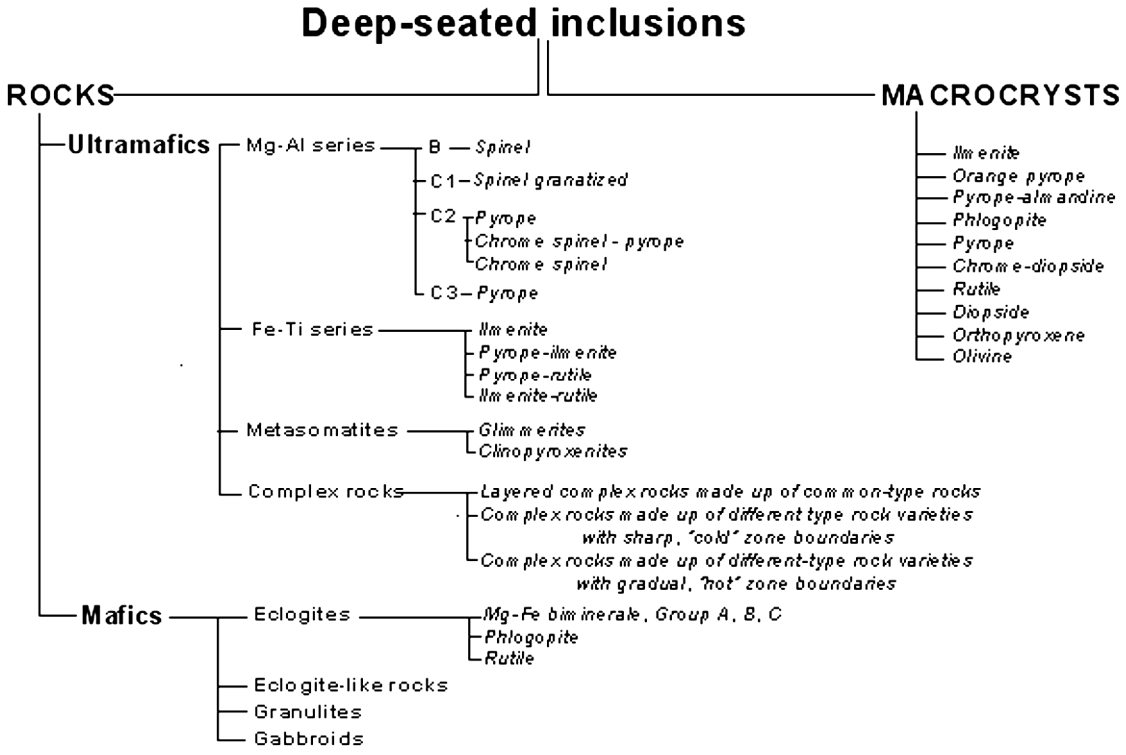

Fig. 3. *Classification of the deep-seated inclusions from the Grib pipe kimberlites.*

MG-AL SERIES ULTRAMAFIC ROCKS

Ilmenite-free ultramafic rocks of the Mg-Al magmatic series [10] are represented essentially by pyrope-bearing rock varieties: lherzolites, dunites, harzburgites, clinopyroxenites and websterites. Rocks of the grospydite depth subfacies "C_2" (22-34 kbar, [24]) predominate, and rocks of the coesite subfacies "C_3" (34-40 kbar) are minor. The texture of these rocks varies from fine-grained to coarse-grained, with allotriomorphic, hypidiomorphic, panidiomorphic (or protogranulose) textural varieties. Typical cataclastic rocks are rare, although some of these have picroilmenite co-existing with violet high-Cr pyrope. Spinel- and chrome spinel-bearing ultramafic rock varieties are few, all of them being dunites and harzburgites of the spinel-pyroxene facies "B" (7-17 kbar), grospydite and coesite subfacies. In addition, there are single inclusions of garnetized spinel lherzolites of the spinel-pyrope subfacies "C_1" (17-22 kbar). In general, many of the Mg-Al series nodules contain phlogopite. At the same time, not one of the xenoliths studied to date shows any evidence of metasomatic amphibolization so typical of similar Mg-Al series mantle ultramafic xenoliths from the Zolotitsky and Pachuga pipe groups of Zimny Bereg.

FE-TI SERIES ULTRAMAFIC ROCKS

Xenoliths of Fe-Ti series ultramafic rocks [10] are very diversified, while less abundant than the Mg-Al series ones. Ilmenite-containing rock varieties: dunites,

lherzolites, harzburgites, orthopyroxenites and clinopyroxenites, are predominant. Pyrope-ilmenite dunites and lherzolites occur somewhat more rarely, most of them containing irregular segregations of low-Cr orange Ti-pyrope (G1 and G2 group garnets, after Dawson and Stephens, [5]). The texture of these rocks varies as widely as in the Mg-Al series rocks, however, with a somewhat greater abundance of cataclastic rocks and rocks with hypidiomorphic-granular to sideronitic texture, reflecting the irregular ilmenite segregations. A separate group includes as-yet single pyrope-rutile peridotite inclusions with a panidiomorphic-granular structure, where Cr-rutile develops instead of ilmenite, and orange pyrope is identical in composition to pyrope in pyrope-ilmenite peridotites. In addition, there are "mixed-type" rocks (pyrope-rutile-ilmenite peridotites) and ore-dunites composed of medium-crystalline panidiomorphic-granular ilmenite + rutile aggregates with relatively large segregations of altered olivine.

METASOMATITES

A separate and widespread group of ultramafic rocks includes xenoliths of inferredly metasomatic (?), predominantly clinopyroxene-phlogopite rocks. These inclusions are dominated by glimmerites (phlogopite-, clinopyroxene-phlogopite- and olivine-phlogopite-bearing) and phlogopite clinopyroxenites. More rarely, they contain some ilmenite, rutile, chrome spinel or pyrope. Rock texture varies from fine-grained to coarse-grained, with allotriomorphic, hypidiomorphic, panidiomorphic, poikilitic and, rarely, graphic varieties. The structure of these rocks is heterogeneous, and occasionally taxitic.

COMBINED ROCKS

Owing to the large size of the examined nodules, we have discovered that some of them consist of combined (complex) rocks with a complicated structure. These inclusions have a zoned, banded structure, incorporating several (usually two) different petrological rock varieties [7]. The analyzed complex rocks were subdivided into three types based on the set and composition of minerals in different zones within a xenolith and on the characteristics of the boundaries between these zones.

Common-type layered rocks

In xenoliths of this type, different zones are made up of rocks belonging to a common petrological type, with only quantitative petrographic differences and unclear boundaries between them. Two distinct varieties of this complex rock type were identified: (1) massive pyrope dunite + zone of alternating pyrope clinopyroxenite and pyrope-olivine websterite layers, or pyrope dunite + zone of pyrope websterite; (2) pyrope orthopyroxenite + olivine-pyrope clinopyroxenite, and banded pyrope clinopyroxenite (websterite?) with very dissimilar pyrope and clinopyroxene proportions in different bands. Common mineral species in

different zones of these rock samples are almost identical, both in appearance and in mineral chemistry. Complex rocks of this type resemble fragments of cumulus-type rocks from layered plutons or fragments of metamorphic rocks of the same type.

Different-type rocks with a sharp, "cold" interface

In xenoliths of his type, individual zones are made up of rocks with radically dissimilar petrology and mineralogy, with one of these zones (and, occasionally, both of them) consisting of a metasomatic rock. The boundary (interface) between the zones is sharp, well defined and "cold", with no structural and compositional changes evident in both rocks away from the interface. Two distinct varieties of this complex rock type were identified: (1) massive pyrope lherzolite + phlogopite clinopyroxenite layered subparallel to the interface, consisting of thin alternating layers with a predominance of phlogopite or clinopyroxene, or massive dunite + rutile-olivine-phlogopite glimmerite; (2) massive fine-crystalline pyrope-olivine-phlogopite glimmerite + phlogopite-bearing clinopyroxenite with a druse-like structure. Complex rocks of this type are similar to fragments of veinlets and/or segregations of various metasomatic rocks, including those with preserved fragments of replaced or partitioned rocks.

Different-type rocks with a gradual, "hot" interface

In xenoliths of this type, individual zones are made up of rocks with distinct petrology and mineralogy, with a gradual change in mineralogy and mineral chemistry away from the interface. Just a single variety of this complex rock type was identified: protogranular Mg-Al series pyrope wehrlite + Fe-Ti series ilmenite-pyrope clinopyroxenite. A 4 cm wide zone extending along the interface consists of an olivine-clinopyroxene-pyrope rock (with some elements of subparallel banding), where purplish-red medium-Cr pyrope (G9 group, according to the classification scheme of Dawson and Stephens, [5]) grades into orange low-Cr G1 Ti-pyrope, and emerald-green clinopyroxene becomes enriched in FeO and TiO_2 and impoverished in Cr_2O_3, gradually changing its color to grass-green. Complex rocks of this type resemble fragments of rocks that underwent "hot" contact metasomatism ("skarnoids" of a sort"). In the case in point, the appearance of the rock likely reflects the action of an ilmenite-pyrope ultramafic intrusion on a pyrope ultramafic massif. In another large (approximately 15 cm) sample of pyrope-ilmenite lherzolite, most of the minerals (ilmenite, pyrope, olivine and clinopyroxene) are chemically similar to respective minerals occurring in ilmenite rocks, whereas enstatite from this sample shows a composition typical of enstatite from pyrope peridotite, and some orange Ti-pyrope grains contain preserved relicts of violet pyrope. In most nodules of this type, only some features of similar rock transformation are usually found, predominantly manifested as gradual purplish-red pyrope replacement by orange pyrope, or as the co-existence of purplish-red

and orange pyrope in different zones of a single sample. All these features reflect inequal intensities of Fe-Ti metasomatism, from high-gradient contact metasomatic replacement ("skarnitisation") to quite homogeneous, slow "steaming".

MAFIC MANTLE NODULES

Among mafic mantle nodules, most abundant are typical bimineral Mg-Fe eclogites with a medium-to-coarse-crystalline texture (grain size up to 3 cm), consisting of red-orange, orange or orange-yellow pyrope-almandine and light green omphacite or omphacite-diopside. On the basis of mineral chemistry (see below), among these eclogites are representatives of all three groups identified by Coleman et al. [2]: types A, B and C, with a predominance of relatively high-Mg Group A eclogites grading into pyrope clinopyroxenites. Many of the eclogites contain variable amounts of phlogopite. Rutile- and ilmenite-bearing eclogite varieties occur more rarely.

Also abundant among the mantle nodules are ***eclogite-like rocks and granulites*** consisting of orange garnet, pale green clinopyroxene, plagioclase and variable amounts of biotite, amphibole and opaque minerals (rutile and ilmenite). Xenoliths of these rocks frequently have a well-defined banded structure and very diversified proportions of rock-forming minerals, from almost bimineral garnet-pyroxene rocks (with a minor admixture of plagioclase) to garnet- and pyroxene-containing, essentially plagioclase rocks. In addition, there are "black series" gabbroic rocks (olivine websterites) consisting of a fine-crystalline aggregate of tobacco-green diopside and bronzite with some admixture of olivine, amphibole, magnetite and, occasionally, plagioclase. Many of these inclusions appear to be fragments of crystalline basement rocks and rocks of lower crustal horizons, probably unrelated to any mantle formations.

XENOCRYSTS AND MEGACRYSTS (MACROCRYSTS)

Xenocrysts and megacrysts are abundant in Grib pipe rocks. They occur mostly as oval or subangular, rather large grains of violet and purplish-red pyrope (up to 2 cm), pyrope-almandine (up to 2 cm), chrome-diopside (up to 3 cm), picroilmenite (up to 4 cm), orange Ti-pyrope (up to 5 cm), phlogopite (up to 5 cm), rutile (up to 2 cm), pale green diopside (up to 5 cm) and omphacite (up to 6 cm), pale yellow orthopyroxene (up to 5 cm) and yellowish olivine (up to 3 cm). In addition, there occur picroilmenite inclusions in orange garnet, orange garnet inclusions in picroilmenite, and mutual intergrowths of garnet, clinopyroxene, phlogopite and rutile.

It is quite difficult to draw a dividing line between xenocrysts and megacrysts in Grib pipe rocks. Minerals from deep-seated inclusions (olivine, pyrope, chrome-diopside, picroilmenite, diopside, phlogopite and rutile) are identical, both in their mineral chemistry and in appearance, to respective minerals occurring as individual, isolated grains in the kimberlite matrix. Most probably, these minerals

occurring in two distinct modes reflect different degrees of disintegration and melting of deep-seated rocks.

MINERAL CHEMISTRY

The fact that mantle xenoliths in Grib pipe rocks are relatively well preserved enabled us to examine and compare mineral chemistry characteristics for most of the petrological rock varieties present (in all other Zimny Bereg pipes, this would be possible for just a few xenolith types).

Olivine

Olivine relicts are transparent; the relatively highest-Mg varieties are colorless, and a faint greenish-yellow shade appears with increasing iron index. Olivines with maximum magnesium index (Fo_{91-94}) are typical of coarse-grained chrome-spinel- and pyrope-bearing peridotites (Table 1), whereas somewhat lower Mg index (Fo_{90-91}) are characteristic of olivines from cataclastic pyrope peridotites, pyrope websterites and megacrysts (Fig. 4). Olivine porphyroblasts in cataclastic peridotites are less magnesian than recrystallized olivine from the mosaic matrix (Fo_{90} against $Fo_{91,5}$). Olivines from ilmenite-bearing and pyrope-ilmenite peridotites, containing a sizable TiO_2 admixture (up to 0.07 wt. %), are relatively low-Mg (Fo_{87-90}). At the same time, the relatively high-Fe (Fo_{86}) olivines from the "black series" olivine websterites (gabbroic rocks) are noteworthy for their lack of zero TiO_2 and with above average NiO content (0.53 wt. %), highlighting their relationship to a separate igneous rock series.

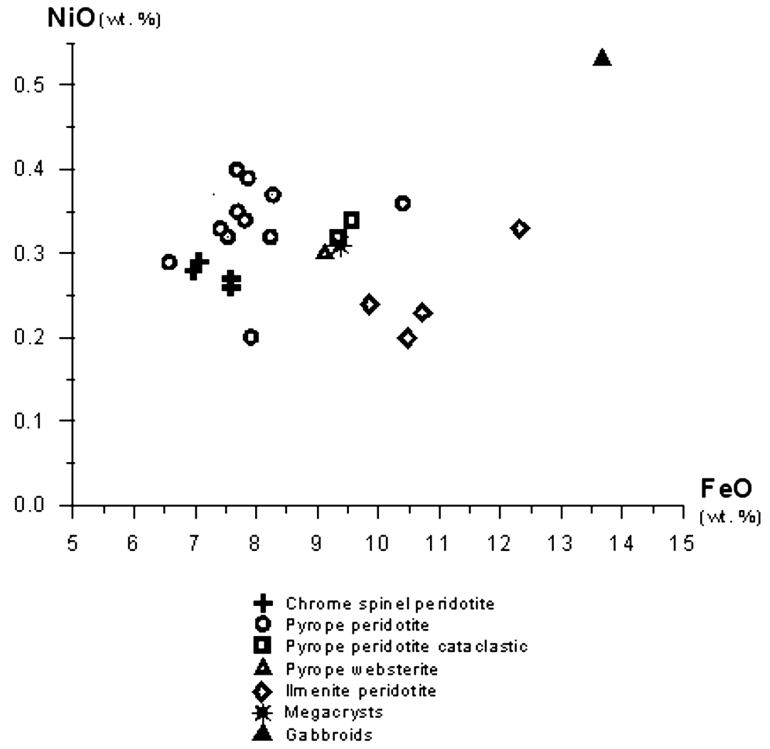

Fig. 4. *Compositional variation, NiO versus FeO of olivine from Grib pipe mantle nodules.*

Table 1. *Electron microprobe data for the olivine from mantle nodules (wt. %)*

No	Rock	Sample No	SiO_2	TiO_2	Al_2O_3	Cr_2O_3	FeO	MnO	MgO	CaO	NiO	Total
1	**pyrope websterite**	114/277.7	40,84	0,03	0,01	0,00	9,12	0,08	50,27	0,00	0,30	100,65
2	**chrome spinel harzburgite**	102/498.4	40,74	0,02	0,03	0,00	6,97	0,15	50,93	0,00	0,28	99,12
3	**chrome spinel harzburgite**	114/291.5	40,83	0,00	0,00	0,00	7,06	0,09	51,09	0,00	0,29	99,36
4	**garnetized spinel lherzolite**	122/234.5	40,68	0,02	0,00	0,00	7,58	0,09	51,27	0,00	0,27	99,91
5	**pyrope clinopyroxenite**	102/490.1	40,97	0,02	0,00	0,01	7,41	0,06	51,26	0,00	0,33	100,06
6	**pyrope lherzolite**	73/205	40,71	0,00	0,00	0,00	8,27	0,08	50,00	0,01	0,37	99,44
7	**pyrope lherzolite**	102/356	41,23	0,00	0,00	0,00	7,86	0,07	50,49	0,00	0,39	100,04
8	**sheared pyrope lherzolite (porphyroblaste)**	102/489.4	40,49	0,00	0,00	0,03	9,56	0,10	48,95	0,03	0,34	99,50
9	**sheared pyrope lherzolite (mozaic matrix)**	102/489.4	41,03	0,03	0,00	0,03	8,25	0,08	49,35	0,03	0,32	99,12
10	**sheared pyrope harzburgite**	85/213.1	40,73	0,07	0,00	0,03	9,34	0,08	49,15	0,03	0,32	99,75
11	**ilmenite harzburgite**	92/374	40,88	0,07	0,00	0,01	9,86	0,10	49,08	0,03	0,24	100,27
12	**pyrope-ilmenite lherzolite**	106/454	40,58	0,05	0,00	0,03	10,72	0,09	48,56	0,03	0,23	100,29
13	**pyrope-ilmenite lherzolite**	114/272.1	40,70	0,02	0,00	0,04	10,48	0,14	48,83	0,27	0,20	100,68
14	**megacryste**	106/384.6	40,54	0,03	0,00	0,01	9,37	0,12	49,03	0,03	0,31	99,44
15	**gabbroids**	106/421	40,21	0,00	0,02	0,00	13,68	0,19	45,88	0,01	0,53	100,52

Orthopyroxene

Orthopyroxene relicts are mostly colorless, rarely with a pale yellowish shade. Among the orthopyroxenes from the examined nodules are representatives of two distinct compositional groups. The relatively high-Mg enstatites with 4-4.5 wt. % FeO occur in coarse-grained chrome spinel-bearing and pyrope peridotites (Table 2). They are characterized by generally low concentrations of all admixture species, including Al_2O_3, which is never present in amounts of greater than 0.8 wt. % (with the exception of a garnetized spinel lherzolite with 1.2 wt. % Al_2O_3). Another orthopyroxene group includes relatively high-Fe enstatites (5.5-7.3 wt. % FeO) with above average CaO (0.55-0.7 wt. %), Na_2O (0.09-0.34 wt. %) and TiO_2 contents (0.12-0.18 wt. %), which occur in cataclastic pyrope peridotites, ilmenite-bearing and pyrope-ilmenite peridotites and megacrysts (Fig. 5). Bronzites from "black series" olivine websterites (gabbroic rocks) with 9.66 wt. % FeO stand out as having a high Al_2O_3 content (2.64 wt. %), moderate amounts of CaO (0.37 wt. %), TiO_2 (0.03 wt. %) and Cr_2O_3 (0.1 wt. %), and a lack of Na_2O.

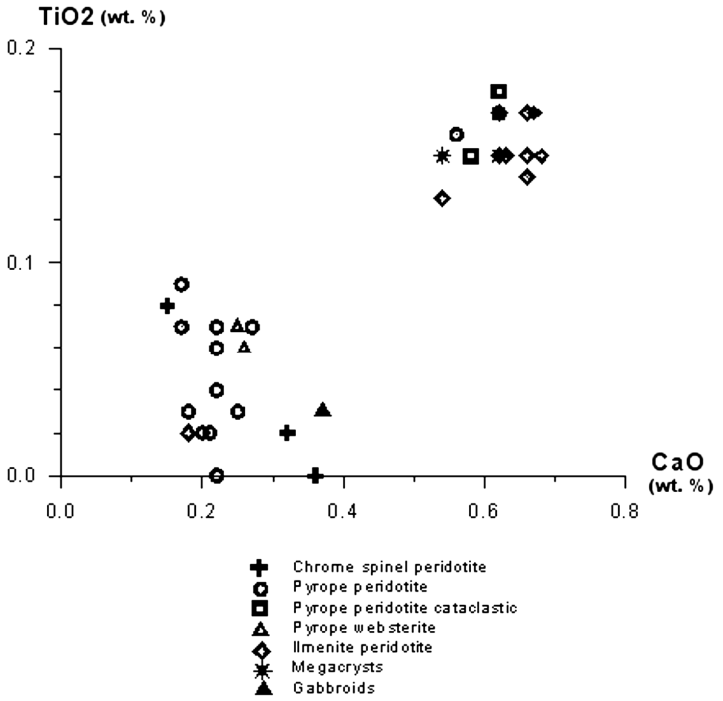

Fig. 5. *Compositional variation, TiO_2 versus CaO of orthopyroxene from Grib pipe mantle nodules.*

Clinopyroxene

Clinopyroxene occurs in most of the examined nodule types, showing a wide variation in mineral chemistry (Table 3). Clinopyroxenes from Mg-Al series pyrope peridotites are mostly chrome-diopsides with a high calcic index (Ca# generally varying between 47 and 50 %); subcalcic pyroxenes with Ca# between 43 and 44 % occur just in a few samples of nodules related to the "C_3" coesite subfacies. These clinopyroxenes are characterized by a high Cr_2O_3 content(1-3

Table 2. *Electron microprobe data for the orthopyroxene from mantle nodules (wt. %)*

No	Rock	Sample No	SiO_2	TiO_2	Al_2O_3	Cr_2O_3	FeO	MnO	MgO	CaO	Na_2O	K_2O	Total
1	**pyrope websterite**	114/277.7	57,50	0,06	0,50	0,00	5,93	0,11	34,82	0,26	0,06	0,02	99,26
2	**chrome spinel harzburgite**	102/498.4	57,51	0,02	0,74	0,28	4,45	0,13	36,13	0,32	0,01	0,01	99,60
3	**chrome spinel harzburgite**	114/291.5	57,79	0,00	0,77	0,30	4,40	0,13	36,42	0,36	0,04	0,00	100,21
4	**garnetized spinel lherzolite**	122/234.5	56,79	0,08	1,28	0,29	5,15	0,19	35,43	0,15	0,00	0,00	99,36
5	**pyrope clinopyroxenite**	102/490.1	58,28	0,07	0,49	0,16	4,49	0,08	36,30	0,25	0,09	0,00	100,21
6	**pyrope lherzolite**	73/205	57,50	0,07	0,82	0,24	5,00	0,10	35,62	0,17	0,04	0,00	99,56
7	**pyrope lherzolite**	102/356	57,86	0,17	0,57	0,16	5,58	0,10	34,61	0,62	0,19	0,00	99,86
8	**sheared pyrope lherzolite**	102/489.4	57,56	0,15	0,65	0,21	6,18	0,14	34,08	0,58	0,22	0,00	99,77
10	**sheared pyrope harzburgite**	85/213.1	57,61	0,18	0,42	0,20	5,62	0,10	34,61	0,62	0,19	0,00	99,55
11	**ilmenite harzburgite**	92/374	57,74	0,15	0,59	0,19	5,74	0,13	34,33	0,63	0,15	0,00	99,65
12	**pyrope-ilmenite lherzolite**	106/454	58,38	0,02	0,68	0,18	4,61	0,14	36,31	0,18	0,04	0,00	100,54
13	**pyrope-ilmenite lherzolite**	114/272.1	57,31	0,13	0,64	0,23	6,29	0,17	33,83	0,54	0,13	0,00	99,27
14	**megacrysts**	106/436.1	57,61	0,15	0,57	0,16	5,73	0,10	34,29	0,62	0,15	0,00	99,38
15	**megacrysts**	106/454.4	57,81	0,15	0,57	0,16	5,55	0,14	34,64	0,54	0,20	0,00	99,76
16	**gabbroids**	106/421	55,65	0,03	2,64	0,10	9,66	0,19	31,69	0,37	0,01	0,00	100,34

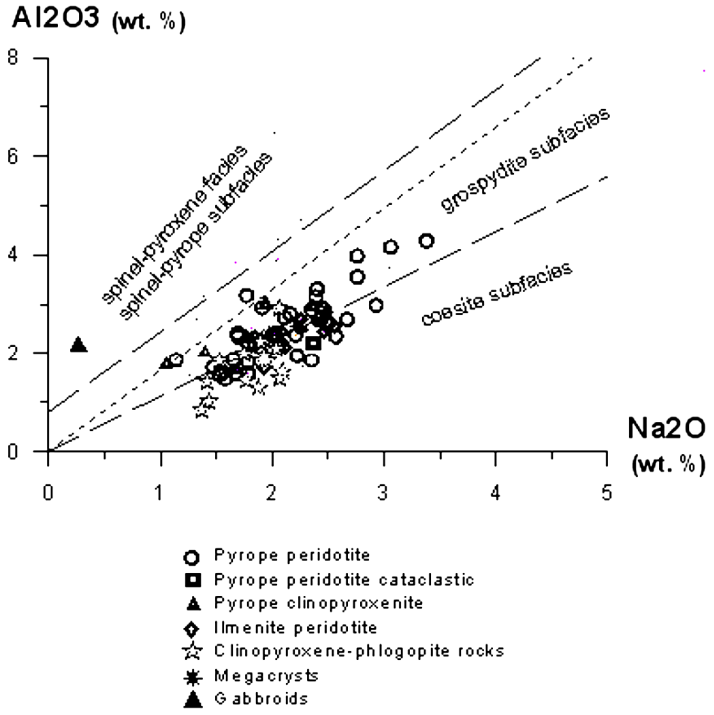

Fig. 6. *Compositional variation, Al_2O_3 versus Na_2O of clinopyroxene from Grib pipe mantle nodules.*

wt. %), a low Al_2O_3/Na_2O ratio and a moderate FeO admixture. Not one aluminous pyroxene related to low-pressure depth facies (B and C_1) was found (Fig. 6). Clinopyroxenes from ilmenite peridotites are mostly subcalcic diopsides (Ca# between 42 and 44 %, rarely up to 47 %) with above average FeO contents and lower than average Cr_2O_3 contents. Clinopyroxenes from megacrysts are generally (in the majority of compositional parameters) similar to low-Cr calcic diopsides from ilmenite peridotites. Clinopyroxenes from metasomatic clinopyroxene-phlogopite rocks are calcic chrome-diopsides with mineral chemistry variations wide enough to overlap the major oxide ranges characteristic of clinopyroxenes from pyrope-bearing and ilmenite peridotites. This might be evidence that these clinopyroxenes formed relatively late, as a result of replacement of various deep-seated rocks. Distinctive features of these clinopyroxenes are their lower than average Al_2O_3 and Na_2O contents.

Clinopyroxenes from mafic nodules also vary in composition. Clinopyroxenes from eclogite series rocks are dominated by medium-Na omphacites similar in composition to low-Cr sodic diopsides, with a minor proportion of omphacites and omphacite-jadeite [26] with very high Al_2O_3 (13.15 wt. %) and Na_2O contents (7.36 wt. %). In addition, a large (> 5 cm) omphacite-jadeite megacryst with 10.52 wt. % Al_2O_3 and 7.52 wt. % Na_2O was found. (These highly sodic and aluminous clinopyroxenes are also somewhat similar to clinopyroxenes from grospydites). On the basis of mineral chemistry, among the clinopyroxenes found in Grib pipe rocks are representatives of all three main eclogite groups [2,25]: A, B and C, with a predominance of relatively higher-Mg Group A eclogites (Fig. 7).

Table 3. *Electron microprobe data for the clinopyroxene from mantle nodules (wt. %)*

No	Rock	Sample No	SiO_2	TiO_2	Al_2O_3	Cr_2O_3	FeO	MnO	MgO	CaO	Na_2O	K_2O	Total
1	**pyrope websterite**	114/277.7	55,35	0,12	2,02	0,25	2,23	0,09	17,74	20,94	1,40	0,00	100,14
2	**garnetized spinel lherzolite**	122/234.5	54,55	0,18	3,18	1,25	1,35	0,10	16,24	20,91	1,77	0,00	99,53
3	**pyrope clinopyroxenite**	102/490.1	55,19	0,18	2,83	1,77	1,62	0,06	15,64	20,34	2,44	0,00	100,07
4	**pyrope lherzolite**	73/205	54,68	0,25	3,55	2,24	1,81	0,05	14,22	19,79	2,76	0,00	99,35
5	**pyrope lherzolite**	102/356	55,06	0,05	1,87	2,02	1,46	0,07	16,01	21,78	1,65	0,01	99,98
6	**sheared pyrope lherzolite**	102/489.4	54,93	0,27	2,21	2,39	2,69	0,10	15,14	19,39	2,37	0,02	99,51
7	**ilmenite clinopyroxenite**	79/274.5	55,65	0,35	2,69	0,38	3,66	0,12	16,00	19,31	2,26	0,01	100,43
8	**pyrope-ilmenite lherzolite**	106/454	55,73	0,39	2,50	0,96	3,76	0,12	16,63	18,01	2,26	0,02	100,38
9	**pyrope-ilmenite lherzolite**	114/272.1	54,67	0,35	2,44	0,88	3,67	0,15	17,36	17,80	2,46	0,00	99,78
11	**eclogite group A**	134/285.2	54,55	0,23	2,63	0,41	3,42	0,09	15,80	20,08	2,20	0,02	99,43
13	**eclogite group A**	79/226.5	54,79	0,20	3,10	0,13	3,34	0,06	15,09	20,60	2,31	0,00	99,62
12	**eclogite group B**	43/234.5	55,51	0,38	7,75	0,16	5,38	0,07	11,04	13,77	5,86	0,04	99,96
10	**eclogite group C**	106/460.1	56,38	0,32	13,15	0,22	1,85	0,01	8,87	12,48	7,36	0,05	100,69
14	**eclogite-like rok**	47/207	52,41	0,34	3,85	0,07	8,47	0,03	12,44	20,32	1,67	0,00	99,60
15	**megacrysts**	106/393.5	54,95	0,30	2,29	0,41	3,33	0,10	16,18	19,73	1,91	0,02	99,22
16	**megacrysts**	106/398.1	55,40	0,31	2,57	0,49	3,67	0,12	16,08	19,18	2,23	0,01	100,06
17	**megacrysts**	9ц/578.0	56,60	0,37	10,52	0,65	3,57	0,13	9,97	10,33	7,52	0,00	99,66
18	**clinopyroxene-phlogopite rock**	106/464.4	54,56	0,19	1,61	2,56	2,30	0,09	15,96	20,16	2,09	0,02	99,54
19	**clinopyroxene-phlogopite rock**	106/466.4	54,63	0,12	2,23	1,34	2,54	0,11	16,24	20,83	1,90	0,00	99,94
20	**pyrope-clinopyroxene-phlogopite rock**	47/181.2	54,60	0,13	1,98	0,95	2,29	0,09	16,10	21,37	1,75	0,00	99,26
21	**gabbroids**	106/421	53,25	0,07	2,15	0,07	3,30	0,10	15,97	23,88	0,27	0,01	99,07

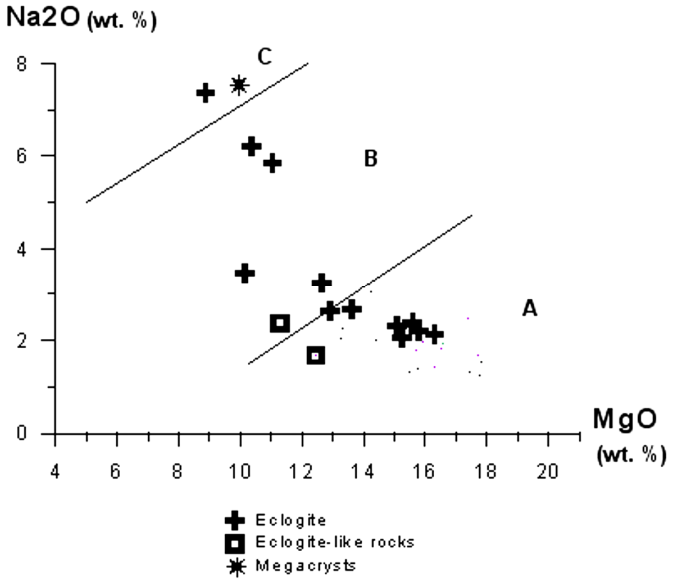

Fig. 7. *Compositional variation, Na_2O versus MgO of clinopyroxene from Grib pipe mantle nodules (diagram after Taylor and Neal, 1989).*

Diopsides from the "black series" olivine websterites (gabbroic rocks) features a high calcic index (Ca# 52 %), somewhat higher than average Al_2O_3 (2.64 wt. %) and FeO contents (3.3 wt. %), and nearly zero Na_2O, Cr_2O_3 and TiO_2 contents.

Garnet

Garnets from pyrope peridotites show a variable Cr_2O_3 content (1-11 wt. %), the overwhelming majority of them being of lherzolite suite, with just single grains of wehrlite and dunite-harzburgite association garnet (Table 4, Fig. 8). Pyrope from cataclastic ilmenite-containing peridotite contains approximately 10 wt. % Cr_2O_3, with almost zero TiO_2 contents. Garnets from clinopyroxenites and websterites are characterized by a low Cr_2O_3 content (not more than 1 wt. %) and above average FeO and TiO_2 contents. Orange pyropes from ilmenite-bearing and rutile peridotites have moderate Cr_2O_3 contents (2.2-3.6 wt. %) with some TiO_2 admixture (0.6-1.0 wt. %), much like the orange-red pyrope megacrysts. Pink pyrope from clinopyroxene-phlogopite metasomatites have a composition typical of C_2 grospydite subfacies pyropes, with 2.31 wt. % Cr_2O_3 and somewhat above average FeO content (10 wt. %).

Garnets from eclogite series rocks are characterized by a generally higher than average Mg index, being similar in composition to garnets from Group A and Group B eclogites, including garnet from the Group C omphacite-jadeite paragenesis (some of the garnets may be similar in composition to garnets from grospydite, although no disthen was found in these samples). Garnets from eclogite-like rocks are characterized by an exceedingly high iron index (*f* = 45-50%)

Table 4. *Electron microprobe data for the garnet from mantle nodules (wt. %)*

No	Rock	Sample No	SiO_2	TiO_2	Al_2O_3	Cr_2O_3	FeO	MnO	MgO	CaO	Na_2O	Total
1	**garnetized spinel lherzolite**	122/234.5	41,56	0,06	21,72	1,86	10,12	0,76	19,28	4,72	0,00	100,08
2	**pyrope clinopyroxenite**	102/490.1	41,72	0,12	22,22	2,53	7,44	0,40	20,38	4,44	0,05	99,30
3	**pyrope spinel harzburgite**	106/291.3	41,22	0,07	19,83	5,27	8,27	0,57	18,16	6,06	0,05	99,50
4	**pyrope websterite**	114/277.7	41,83	0,12	22,87	0,38	9,37	0,43	20,91	3,91	0,05	99,87
5	**pyrope lherzolite**	73/205	42,05	0,24	21,91	2,82	9,03	0,52	19,40	4,49	0,07	100,53
6	**pyrope lherzolite**	102/356	41,34	0,10	18,74	7,09	8,47	0,55	17,65	6,56	0,04	100,54
7	**pyrope lherzolite**	47/207.6	41,52	0,21	19,25	5,71	6,32	0,29	21,03	4,99	n.a.	99,32
8	**pyrope lherzolite**	47/226.4	40,61	0,11	16,50	9,35	7,09	0,34	19,55	6,46	n.a.	100,01
9	**sheared pyrope lherzolite**	102/489.4	40,80	0,05	16,32	9,79	7,00	0,42	18,17	6,71	0,01	99,27
10	**pyrope-ilmenite lherzolite**	106/454	41,84	0,81	21,20	2,49	9,33	0,38	19,80	4,25	0,12	100,22
11	**pyrope-ilmenite lherzolite**	114/272.1	41,75	0,85	19,35	2,81	9,72	0,40	20,15	4,37	0,19	99,59
12	**granatite**	79/223.7	41,86	0,76	20,17	3,57	8,07	0,33	21,31	3,28	0,05	99,40
13	**sheared pyrope harzburgite**	85/213.1	41,18	0,97	18,97	4,90	8,56	0,34	19,78	5,04	0,11	99,85
15	**eclogite group A**	134/285.2	41,50	0,53	22,90	0,15	9,88	0,43	18,49	5,60	0,08	99,56
17	**eclogite group A**	79/226.5	40,88	0,12	23,28	0,19	13,68	0,39	16,52	4,46	0,04	99,56
16	**eclogite group B**	43/234.5	40,90	0,36	22,19	0,23	14,93	0,26	15,90	4,76	n.a.	99,53
14	**eclogite group C**	106/460.1	41,35	0,23	23,30	0,09	9,91	0,19	13,86	10,80	0,11	99,84
18	**eclogite-like rok**	47/207	39,05	0,03	20,96	0,00	25,00	0,75	8,60	5,91	n.a.	100,30
19	**megacryste**	106/351.21	41,52	1,18	19,89	2,91	9,49	0,37	19,50	4,89	0,11	99,86
20	**megacrysts**	43/219.1	41,61	0,75	20,37	2,19	8,86	0,27	20,00	4,55	n.a.	98,60
21	**megacrysts**	48/297.5	41,87	0,90	19,82	3,11	8,31	0,34	20,56	4,99	n.a.	99,90
22	**pyrope-clinopyroxene-phlogopite rock**	47/181.2	41,27	0,13	21,92	2,31	10,01	0,54	18,61	4,70	0,05	99,54

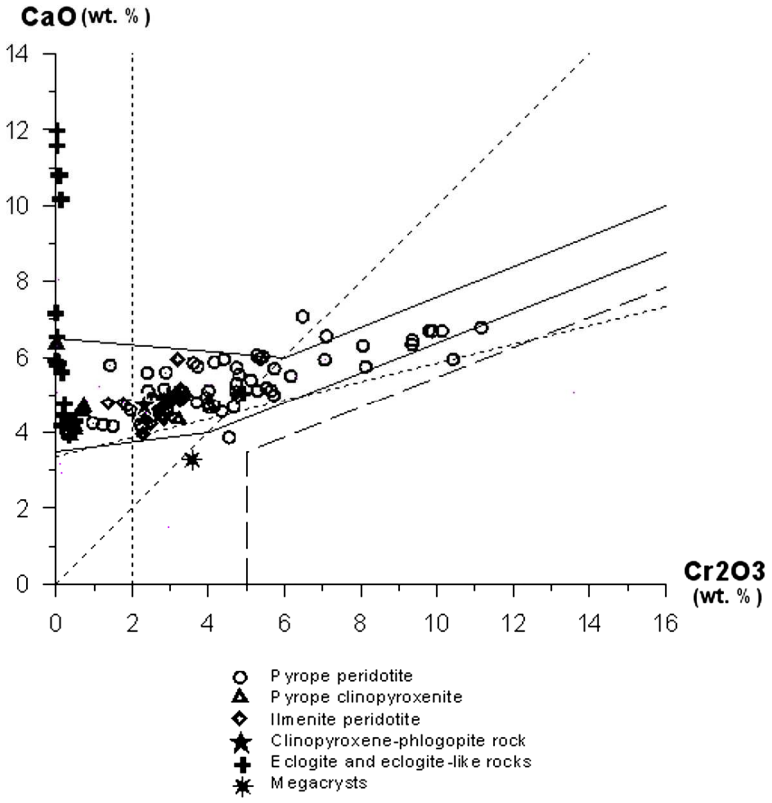

Fig. 8. *Compositional variation, CaO versus Cr_2O_3 of garnets from Grib pipe mantle nodules (diagram, after Sobolev, 1974; Gurney 1984).*

Table 5. *Electron microprobe data for the ilmenite from mantle nodules (wt. %)*

No	Rock	Sample No	TiO_2	Al_2O_3	Cr_2O_3	FeO	MnO	MgO	Total
1	**sheared pyrope lherzolite**	102/489.4	53,84	0,60	1,26	28,50	0,28	14,36	98,84
2	**ilmenite clinopyroxenite**	79/274.5	52,88	0,43	0,90	31,09	0,32	13,23	98,85
3	**ilmenite harzburgite**	92/374	53,78	0,58	2,62	27,01	0,28	14,83	99,10
4	**ilmenite-rutile peridotite**	48/248	54,60	0,62	2,16	29,59	0,27	13,29	100,53
5	**pyrope-ilmenite lherzolite**	106/454	53,03	0,28	2,57	29,44	0,27	13,36	98,95
6	**pyrope-ilmenite lherzolite**	114/272.1	53,36	0,49	2,30	30,54	0,28	12,56	99,53
7	**granatite**	79/223.7	52,44	0,98	4,09	26,70	0,23	14,39	98,83
8	**eclogite group A**	106/404	51,17	0,38	0,10	39,01	0,27	8,00	98,93
9	**granulite**	47/179	53,22	0,20	0,00	44,22	0,24	1,89	99,77
10	**megacrysts**	43/219.1	53,99	0,91	2,29	26,98	0,36	14,04	98,57
11	**megacrysts**	43/250	52,78	0,68	2,21	27,76	0,27	14,58	98,28
12	**clinopyroxene-phlogopite rock**	106/404.2	52,70	0,03	1,39	32,71	0,31	12,45	99,59
13	**olivine-phlogopite rock**	106/184	51,82	0,31	6,02	26,82	0,36	14,67	100,00

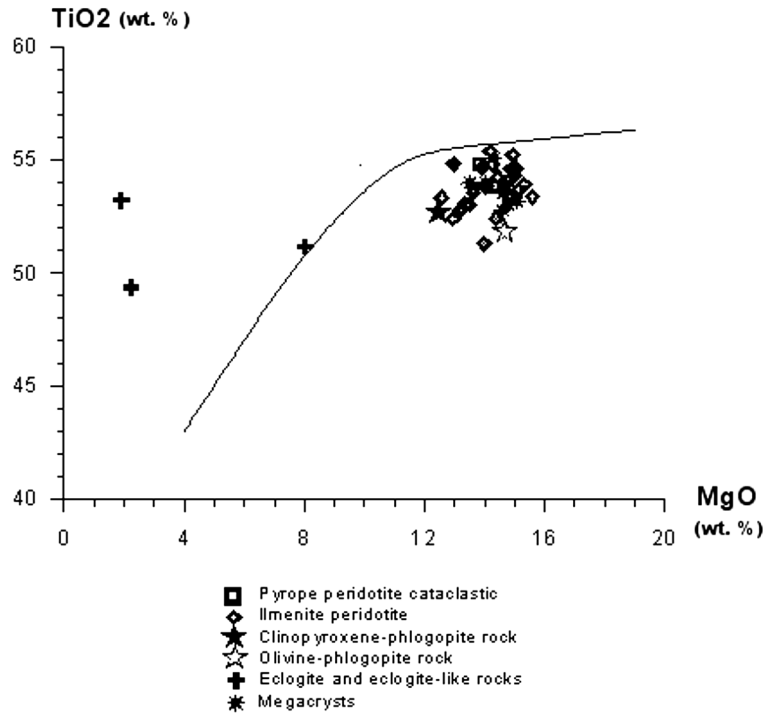

Fig. 9. *Compositional variation, TiO_2 versus MgO of ilmenite from Grib pipe mantle nodules. Curve shows boundary between kimberlitic and non-kimberlitic ilmenites (unpublished diagram after I.P. Ilupin).*

Ilmenite

Ilmenite from different Fe-Ti series ultramafic rocks (pyrope-bearing and pyrope-free ilmenite peridotites, clino- and orthopyroxenites, and ilmenite-rutile ultramafic rocks) is characterized by a quite constant composition, with rather high MgO (12-16 wt. %) and Cr_2O_3 contents (0.7-4 wt. %) (Table 5, Fig. 9). Ilmenite megacrysts and ilmenite from cataclastic pyrope peridotite have much the same composition. Ilmenite from clinopyroxene and olivine-phlogopite metasomatites is distinguished by its somewhat higher Cr_2O_3 content (up to 6 wt. % and, in some cases, up to 9 wt. %). Eclogites contain some Cr-free picroilmenite with approximately 8 wt. % MgO, and eclogite-like rocks contain some ordinary, low-Mg ilmenite. Decay lamellae in rutile segregations from ilmenite-rutile peridotites consist of medium-Mg (7-10 wt. % MgO) and high-Cr ilmenite.

Rutile

Rutile is rather abundant in Grib pipe kimberlite rocks. It occurs predominantly as black megacrysts, similar in appearance to picroilmenite grains. Megacrystic rutile is characterized by high Cr_2O_3 (3-7 wt. %) and FeO contents (0.4-1.7 wt. %), with minor Al_2O_3, MgO, Nb and Ta admixtures (Table 6). Large rutile segregations in phlogopite megacrysts have the same composition. Rutile from rutile-bearing and ilmenite-rutile ultramafic rocks contains 2-3 wt. % Cr_2O_3 and 0.3 wt. % FeO, being characterized by the presence of solid-solution decay structures with lamellar picroilmenite segregations (see above). Prismatic rutile segregations from olivine-phlogopite metasomatites also contain above average Cr_2O_3 (4 wt. %), whereas eclogites contain some pure rutile, almost free of any admixtures.

Table 6. *Electron microprobe data for the rutile from mantle nodules (wt. %)*

No	Rock	Sample No	TiO_2	Al_2O_3	Cr_2O_3	FeO	MnO	MgO	ZrO_2	Nb_2O_5	Ta_2O_5	Total
1	**ilmenite-rutile peridotite**	48/248	97,19	0,24	2,39	0,29	0,00	0,00	0,21	0,31	0,04	100,67
2	**pyrope-rutile peridotite**	46/239.6	96,02	0,05	3,16	0,43	0,00	0,01	0,00	0,53	0,17	100,37
3	**eclogite group B**	85/274.5	99,51	0,19	0,00	0,22	0,00	0,00	0,05	0,00	0,06	100,03
4	**megacrysts**	106/454.11	93,91	0,01	5,17	0,39	0,00	0,07	0,03	0,84	0,05	100,47
5	**megacrysts**	57-1/428	90,07	0,36	7,21	1,68	0,01	0,34	0,00	0,90	0,12	100,69
6	**megacrysts**	89/172.2	95,28	0,25	2,94	1,30	0,03	0,02	0,13	0,40	0,22	100,57
7	**inclusion in megacrysts phlogopite**	86/182.6	88,68	0,25	6,85	1,98	0,03	0,45	0,11	0,15	1,18	99,68
8	**rutile-olivine-phlogopite rock**	102/500.4	95,36	0,03	3,86	0,07	0,02	0,00	0,00	0,83	0,06	100,23

Table 7. *Electron microprobe data for the chrome spinel from mantle nodules (wt. %)*

No	Rock	Sample No	TiO_2	Al_2O_3	Cr_2O_3	FeO	MnO	MgO	ZnO	Total
1	**spinel dunite**	43/243	0,07	42,24	25,30	14,33	0,15	16,88	n.a.	98,97
2	**chrome spinel harzburgite**	102/498.4	0,20	13,58	55,44	19,70	0,38	9,52	0,06	98,88
3	**chrome spinel harzburgite**	114/291.5	0,11	15,50	54,06	18,54	0,37	10,37	0,51	99,46
4	**schrome spinel dunite**	79/252.5	0,12	17,59	49,35	18,24	0,30	11,89	0,20	97,69
5	**chrome spinel dunite**	89/235	0,09	29,65	39,91	16,15	0,27	13,29	0,00	99,36
6	**garnetized spinel lherzolite**	122/234.5	0,23	28,28	39,77	17,35	0,22	13,07	0,41	99,33
7	**pyrope spinel harzburgite**	106/291.3	0,48	14,31	54,33	17,52	0,32	12,13	0,15	99,24
8	**pyrope lherzolite**	102/356	0,50	14,72	53,70	17,70	0,37	12,19	0,15	99,33
9	**chrome spinel dunite**	106/448.1	0,25	6,22	61,08	19,73	0,31	11,54	0,10	99,23
10	**clinopyroxene-phlogopite rock**	114/497	3,24	3,91	54,58	26,11	0,45	10,38	0,09	98,76

Chrome spinel

Chrome spinel occurs in rare spinel-bearing and chrome spinel harzburgite and dunite nodules and in pyrope peridotite nodules. Chrome spinel generally shows a continuous $Cr^{3+} \Leftrightarrow Al^{3+}$ isomorphous series, from Mg-picotite from a spinel-pyroxene B facies nodule to Mg-chromites of C_3 cohesite subfacies (Table 7), and is characterized by a low TiO_2 content (not more than 0.8 wt. %). A similar composition is characteristic of chrome spinel from zones of fusion in ultramafic nodules. At the same time, high-Cr chrome spinels from pyrope-phlogopite wehrlites and phlogopite-clinopyroxene metasomatites features a lower than average Al_2O_3 content (not more than 5 wt. %) and above average FeO (25 wt. %) and, particularly, TiO_2 contents (up to 3 wt. %). A similar composition is characteristic of chrome spinel from pyrope kelyphitic rims, which might be evidence that the three last mentioned chrome spinel varieties formed as a result of relatively late, secondary processes.

Phlogopite

Phlogopite is abundant in Grib pipe nodules, where it occurs as isolated megacrysts and in association with primary mineral phases of the pyrope peridotites, pyroxenites and eclogites. In addition, phlogopite occurs as a "superimposed", metasomatic mineral, which replaces the primary mineralogy of the nodules and thus plays the role of a rock-forming mineral in olivine-phlogopite and clinopyroxenite-phlogopite rocks (metasomatites?). The overwhelming majority of phlogopite xenocrysts and megacrysts are characterized by moderate Al_2O_3 (11-14 wt. %), TiO_2 (0.3-1 wt. %) and Cr_2O_3 contents (up to 1 wt. %), being similar in composition to primary phlogopite from lherzolites and megacrysts (Table 8, figures 10, 11) [1,4,11]. A similar composition is also characteristic of phlogopite from the pyrope-phlogopite pyroxenites, websterites and wehrlites, and from olivine-phlogopite and clinopyroxene-phlogopite rocks (presumably metasomatites), which are – in this respect – similar to primary rocks rather than to metasomatic ones. Phlogopite from rutile-phlogopite metasomatites and from phlogopite-clinopyroxenite metasomatites in association with Fe-diopside is characterized by comparatively higher TiO_2 and Cr_2O_3 contents, which may suggest a secondary nature. The undoubtedly secondary phlogopites from zones of fusion in the nodules and from kelyphitic rims on pyropes, are characterized by high TiO_2 and Cr_2O_3 contents (up to 3.2 wt. %). Eclogitic phlogopite has above average TiO_2 (2.2 wt. %) and moderate Cr_2O_3 contents (0.7 wt. %), whereas mica from samples of eclogite-like rocks is high-Ti (5.5 wt. % TiO_2) and Cr-free phlogopite.

Table 8. *Electron microprobe data for the phlogopite from mantle nodules (wt. %)*

No	Rock	Sample No	SiO_2	TiO_2	Al_2O_3	Cr_2O_3	FeO	MnO	MgO	CaO	Na_2O	K_2O	BaO	Total
1	**pyrope wehrlite**	102/485	39,56	0,61	13,10	0,86	3,30	0,00	23,47	0,01	0,25	9,99	0,90	92,05
2	**pyrope clinopyroxenite**	102/490.1	41,37	0,80	12,96	0,58	2,44	0,03	24,16	0,00	0,63	9,30	2,69	94,96
3	**pyrope websterite**	114/277.7	40,25	0,54	14,30	0,14	3,25	0,06	25,66	0,00	0,46	8,95	2,42	96,03
4	**zone fusion in clinopyroxenite**	79/274.5	41,27	2,12	13,04	0,95	4,02	0,01	23,56	0,01	0,29	10,23	0,07	95,57
5	**eclogite group A**	134/285.2	40,91	2,27	12,65	0,73	4,41	0,01	22,51	0,01	0,30	10,65	0,18	94,63
6	**eclogite-like rock**	47/207	38,68	5,45	14,29	0,09	10,84	0,03	16,81	0,00	0,08	9,97	n.a.	96,24
7	**megacrysts**	86/182.6	40,90	0,97	14,61	0,98	3,84	0,00	24,09	0,01	0,66	9,63	0,53	96,22
8	**megacrysts**	43/241	42,03	0,59	11,63	0,63	3,35	0,06	25,32	0,00	0,05	10,66	n.a.	94,32
9	**megacrysts**	43/260	42,10	0,49	11,98	0,68	2,95	0,03	25,46	0,00	0,09	10,56	n.a.	94,34
10	**megacrysts**	43/285	42,35	0,50	11,95	0,61	2,99	0,06	25,38	0,00	0,90	10,72	n.a.	95,46
11	**clinopyroxene-phlogopite rock**	106/354.4	41,29	0,45	12,24	0,35	3,24	0,02	24,14	0,00	0,42	11,10	n.a.	93,25
12	**clinopyroxene-phlogopite rock**	106/404.2	40,45	0,68	12,23	0,47	3,40	0,02	24,72	0,05	0,85	10,24	n.a.	93,11
13	**clinopyroxene-phlogopite rock**	106/441	41,42	0,82	12,70	0,23	3,44	0,04	24,40	0,03	0,61	11,06	n.a.	94,75
14	**clinopyroxene-phlogopite rock**	106/464.4	41,14	0,70	11,94	0,74	3,14	0,01	25,78	0,00	0,26	11,39	n.a.	95,10
15	**clinopyroxene-phlogopite rock**	114/497	42,35	0,67	12,60	0,71	3,39	0,00	24,99	0,01	0,10	10,77	0,08	95,67
16	**olivine-phlogopite rock**	106/184	39,89	0,67	13,34	0,37	3,67	0,02	24,65	0,00	0,20	10,77	n.a.	93,58
17	**rutile-olivine-phlogopite rock**	102/500.4	41,04	1,80	14,35	1,54	3,58	0,04	23,63	0,00	0,32	10,08	0,04	96,42

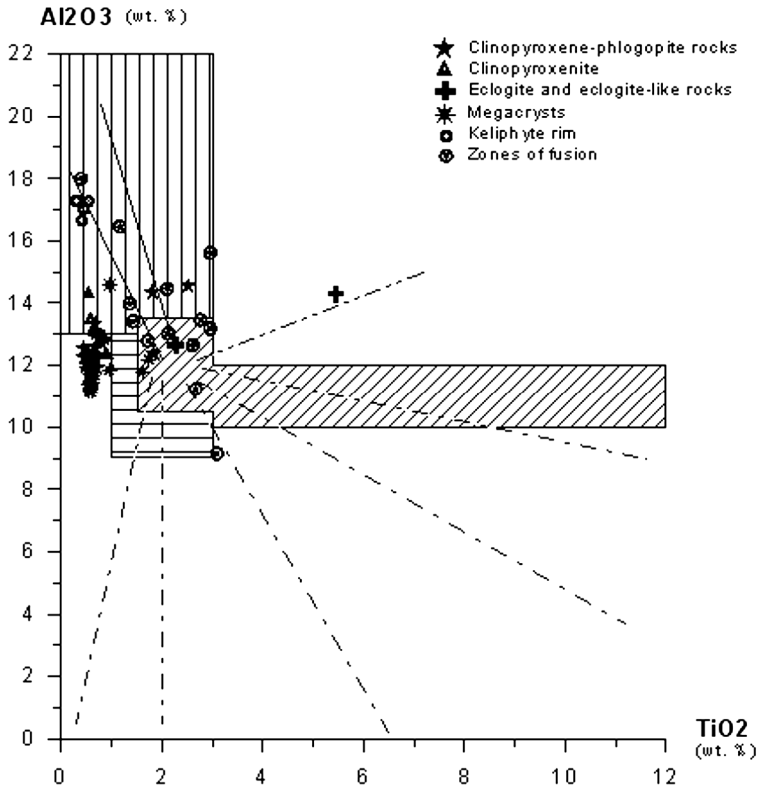

Fig. 10. *Compositional variation, Al_2O_3 versus TiO_2 of phlogopite from Grib pipe mantle nodules (diagram after Mitchell, 1995).*

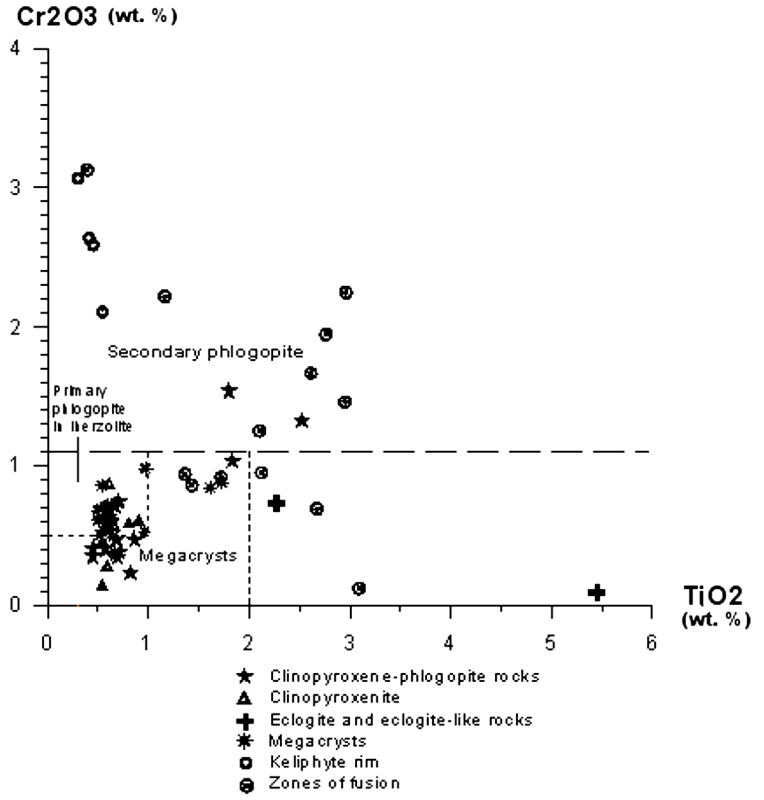

Fig. 11. *Compositional variation, Cr_2O_3 versus TiO_2 of phlogopite from Grib pipe mantle nodules (diagram, after Carswell, 1975 and Dawson and Smith, 1975).*

TEMPERATURE - PRESSURE FORMATION PARAMETERS OF MANTLE NODULES

To calculate the Temperature - Pressure (TP) formation parameters for the mantle xenoliths being studied, we utilized mineral chemistry data obtained for the two mineral associations that are most abundant in different nodule types: clinopyroxene + garnet (Cpx + Ga) and orthopyroxene + garnet (Opx + Ga). For the Cpx + Ga association, temperature values were determined by a NS94T thermometer, and pressure values were obtained using a NS94P barometer [12], both modified for peridotites and eclogites. For the Opx + Ga paragenesis, we used a NI92T thermometer and a NI92P barometer. The quite good convergence of the results obtained by different methods and the fact that these results are not contradictory to the petrological characteristics of the analyzed xenoliths, confirms the validity of using these methods.

Among Mg-Al series ultramafic rocks, garnetized spinel peridotites of the C1 spinel-pyrope subfacies are characterized by the lowest formation temperature and pressure values (713°C, 22.6 kbar), and peridotites of the C_3 coesite subfacies have the highest TP parameters (1234°C, 49 kbar) (Fig. 12). Most of the pyrope peridotites and various pyrope clinopyroxenites and websterites formed within an 800-1150°C temperature range and 25-45 kbar pressure range. Fe-Ti series ilmenite peridotites are generally characterized by relatively high TP parameters (1000-1250°C and 40-53 kbar), much like that found for combined rocks from "hot" contact zones (see section 7.3), which occasionally feature certain mineral associations that appear to be 'in equilibrium'. In particular, in the aforementioned pyrope-ilmenite lherzolite sample (# 106/464), the Opx + Ga and Cpx + Ga associations show very dissimilar formation parameters (737°C, 29.9 kbar and 1206°C, 49.9 kbar, respectively), which highlights the metasomatic nature of this rock. At the same time, the abundant clinopyroxene-phlogopite "matasomatites" (some of them containing pyrope) are characterized by moderate TP formation parameters (945°C, 33.9 kbar) typical of the grospydite depth subfacies [24]. Eclogite series rocks also differ in formation conditions. Group B eclogites [2,25] have the highest TP parameters (1170°C, 54 kbar); TP ranges of Group A eclogites are 900-1080°C, 27-44 kbar; lastly, TP parameters of the examined eclogite-like rocks vary between 838-873°C, 28.5-29.7 kbar. In general, the variation of PT parameters for different types of examined mantle nodules is quite closely approximated by a 42-43 mW/m^2 conductive geotherm [13].

DISCUSSION

The Grib pipe contains a large variety of deep-seated xenoliths, including rather large xenoliths with weak secondary alteration. Direct petrological examination of such xenoliths, together with a thorough analysis of their mineral

chemistry, would make for a more unbiased and detailed determination of the structural and compositional features of different igneous rock and, consequently,

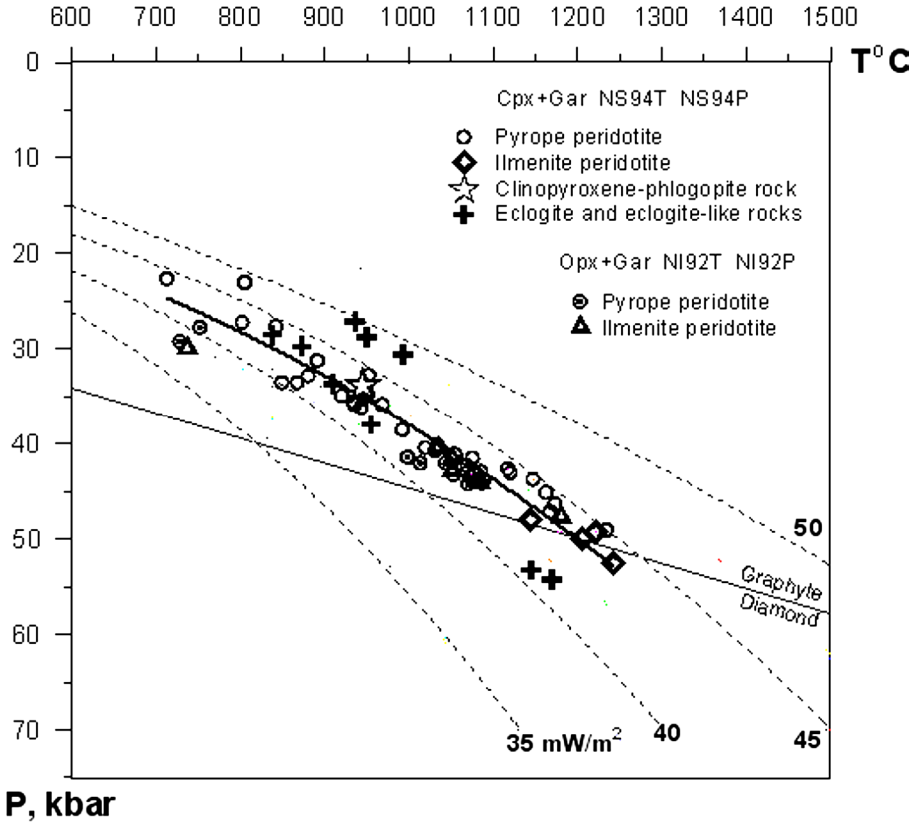

Fig. 12. *Temperatures and Pressures of equilibration of Grib pipe mantle nodules, calculated using the Nikitina and Simakov (1994) thermometer and barometer, and Nikitina and Ivanov (1992) thermometer and barometer. Diamond-graphite curve after Kennedy and Kennedy (1976); conductive geotherm curves after Pollack and Chapman (1977).*

facilitate a more reliable interpretation of their formation, transformation and relationship features.

Indications of igneous rock origin

Ultramafic xenoliths present in the Grib pipe are dominated by nodules of the Mg-Al igneous rock series (after Marakushev, 1984): various pyrope peridotites and pyroxenites of the grospydite and coesite depth subfacies ("C_2" and "C_3", [24]), whereas nodules of chrome spinel-bearing ultramafic rocks of the same facies are very rare (dunites and harzburgites only), and nodules of typical low-pressure spinel peridotites are few. These rock types show allotriomorphic, hypidiomorphic, protogranular and, rarely, mosaic-porphyroblastic textures, which may infer an igneous origin and dissimilar degrees of metamorphism. Moreover, complex rocks of this type (peridotites and pyroxenites), with characteristic parallel-banded structures, resemble fragments of igneous rocks of cumulus origin, typically formed in layered intrusions. In addition, there are rare garnetized spinel

(chrome spinel) lherzolite nodules, with chrome spinel replaced by pyrope, either related to an increase in pressure (during sinking of individual rock masses) or, more likely, due to cooling at a constant pressure [3]. The bulk of mantle within a depth range of 70 and 130 km beneath the Grib pipe consists of pyrope peridotites with varying degree of metamorphism, probably, of magmatic origin.

Two groups of rocks with apparently distinct formation conditions can be identified among the Fe-Ti ultramafic igneous rock series [10]. Most of these rocks are ilmenite- and pyrope-ilmenite-bearing (more rarely, peculiar rutile-, pyrope-rutile- and ilmenite-rutile-bearing) dunites, peridotites and pyroxenites with allotriomorphic, hypidiomorphic to sideronitic and, in some cases, mosaic-porphyroblastic textures, which (much like for the nodules of Mg-Al series rocks) is an indication of their probable igneous origin, and dissimilar degrees of metamorphism. In general, these rocks are of a higher-temperature and higher-pressure origin than the pyrope peridotites (according to our calculations: 1000-1250°C and 40-53 kbar). This is in good agreement with the relationships of rocks representing these two series in unique complex rock samples (see section 7.3) bearing evidence of "hot" contact metasomatic action of an ilmenite-pyrope clinopyroxenite intrusion on a pyrope wehrlite massif, owing to which banded pyrope-clinopyroxene rocks with varying mineral chemistry ("skarnoids" of a sort) formed in the 'contact-zone'. In this unique case, we are dealing with a manifestation of high-gradient, contact metasomatic replacement. Much more frequently, the process of Fe-Ti metasomatism manifests itself as partial transformation of pyrope peridotites (in the form of a gradual replacement of purplish-red pyrope by orange pyrope, or a co-existence of purplish-red and orange pyrope in different zones within a single sample), up to almost complete replacement of pyrope peridotites by ilmenite association minerals, with only rare relicts of violet pyrope and enstatite preserved. Complete replacement results in the formation of pyrope-ilmenite peridotites and pyroxenites (essentially, metasomatites with a set of minerals typical of ilmenite peridotites), which may be considered as the second group of ilmenite rocks, which formed as a result of metasomatic action of igneous ilmenite peridotites (first group) on host rocks (i.e., as a result of their slow, homogeneous "steaming"). A characteristic (indicative) feature of these rocks is the presence of veinlet-like and poikilitic textural elements. On the basis of our calculated TP parameters, pyrope-ilmenite peridotites must be widespread at depths of ~120-150 km.

Mantle metasomatism

The abundance of various clinopyroxene-phlogopite, olivine-phlogopite and phlogopite rocks may be evidence of intense mantle hydrous-calc-alkali (K-Ca) metasomatism in deep-seated substrate rocks parental to the Grib pipe kimberlites. However, the lack of any visible evidence of replacement of undoubtedly primary mantle rock minerals by the above listed phases, the presence of characteristic deformed clinopyroxene and phlogopite grains with fracture bands or "pseudo-

twinning" along tree cleavage joint systems, and mineral chemical peculiarities of these rocks (clinopyroxene, phlogopite and pyrope are all identical in composition to respective primary minerals), indicates that at least many of such olivine- and clinopyroxene-phlogopite rocks may be of primary magmatic, rather than metasomatic, origin. Rocks of this type could have formed from residual melts (enriched by volatiles) as vein-like bodies, similar to pegmatite and lamprophyre formations (bodies) in the apical parts of intrusions. On the basis of the calculated TP parameters (945°C, 33.9 kbar), clinopyroxene-phlogopite pyrope-containing rocks of this type, likely formed at a depth of ~100-119 km, in the zone of the grospydite depth subfacies. The as-yet single case of a sharp, "cold" contact (interface) between a rock of this type and a pyrope peridotite confirms the assumption about their vein-type (intrusive) origin. On the other hand, the essential minerals of this vein somewhat differ in composition from respective minerals in typical clinopyroxene-phlogopite rocks (higher-Fe and lower-Cr clinopyroxene, and higher-Ct and higher-Ti phlogopite), and hence there is justification in classifying this rock as a distinct variety. Nevertheless, the fact that the contact of two mantle rocks can be so sharp, crossing and "cold", is interesting and indicative by itself.

At the same time, there is strong evidence in support of hydrous-calc-alkali (K-Ca) metasomatism (with the prevailing development of small phlogopite and clinopyroxene segregations) in different rock types (in pyrope-bearing and chrome spinel peridotites, pyrope-ilmenite peridotites, eclogites, and even in the aforementioned clinopyroxene-phlogopite rocks). Structural features of mineral aggregates formed as a result of this process, their relationships with primary minerals (gradual replacement of primary xenolithic minerals by an aggregate of neogenic phlogopite and clinopyroxene in "zones of fusion" and by phlogopite in kelyphitic rims) and their compositional features unambiguously indicate that this metasomatism is superimposed, and, thus, its resultant metasomatic minerals, secondary.

Signs of well-defined, superimposed metasomatic phlogopitization of this type are also evident in mantle rock xenoliths (peridotites of the B, C_1 and C_2 facies) from kimberlite pipes of the Zolotitsky and Pachuga pipe groups of Zimny Bereg. However, much more widespread in these pipes are hydrous-alkali (K-Na) metasomatic processes manifested as superimposed amphibolization (gradual replacement of diopside and pyrope by Cr-pargasite). It is noteworthy that, to date, there is no indications of this kind of hydrous-sodic metasomatism found in any of the Grib pipe xenoliths (probably, mantle rocks beneath the Grib pipe were not affected by this type of metasomatic amphibolization).

Eclogitic series rocks and other mafic rocks

Together with xenoliths of various ultramafic rock-types in the Grib pipe, are abundant nodules of mafic rocks with differing origins and formation conditions. Most widespread are eclogite-like rocks grading by composition into granulites.

These rocks probably make up the horizons of lower crust and, partially, upper mantle zones (on the basis of the calculated TP parameters of 838-873°C and 28.5-29.7 kbar). The "black series" gabbroic rocks (olivine websterites) might also be related to these rock types. Eclogite xenoliths are also rather diversified: along with the most abundant Group A eclogites [2], which commonly occur as interlayers in ultramafic rock massifs, there are Group B eclogites (characteristic of magmatized gneissic complexes) and Group C eclogites (typically forming zones and lenses within Alpine-type metamorphic rock complexes, e.g., glaucophane-schists). Xenoliths of Group C eclogites may be interpreted as fragments of old oceanic crust, subducted under a continental platform [3] (i.e., as crustal fragments from the subduction zone of the Russian continental platform).

Megacrysts

The diversity of megacrysts, which are widespread in the Grib pipe, corresponds well with the diversity of mantle rock xenolith types present. The most abundant, ilmenite, rutile and Ti-pyrope megacrysts are similar in composition to respective minerals from ilmenite and rutile peridotites; clinopyroxene, orthopyroxene and olivine megacrysts are similar in composition to respective minerals from ilmenite-bearing and cataclastic pyrope peridotites; lastly, chrome-diopside and phlogopite megacrysts are similar in composition to corresponding minerals from the clinopyroxene-phlogopite metasomatic (?) rocks. Even in the case of Group C eclogites, which are very rare in the Grib pipe, megacrystic analogues were found in our collection (a single omphacite-jadeite megacryst of size 6 cm). Accordingly, it is difficult to draw a dividing line between xenocrysts and megacrysts in the Grib pipe rocks. It is likely, therefore, that minerals of deep-seated inclusions and respective minerals occurring as individual grains in kimberlite matrix are related to different degrees of disintegration and melting (fusion) of the deep-seated rocks.

Distinctions from xenoliths occurring in other Zimny Bereg pipes

The distribution of different deep-seated xenolith varieties in Grib pipe kimberlites is shown in figure 13. The set of mantle rock varieties present in the Grib pipe is very distinct from that typical of the kimberlite pipes of the Lomonosov deposit (Al-series Zimny Bereg kimberlites), being most similar to that of pipe Anomaly-688, in the Pachuga pipe group (Fe-Ti series Zimny Bereg kimberlites). The Grib pipe differs from the Lomonosov deposit pipes not only because it contains xenoliths of ilmenite and rutile peridotites, clinopyroxene-phlogopite rocks ("metasomatites" ?), eclogites, and various megacrysts (rarely if at all occurring in Lomonosov deposit kimberlites), but also in the essential characteristics of generally common-type ilmenite-free ultramafic rocks. In contrast to the Lomonosov deposit, the Grib pipe is dominated by pyrope peridotites, with a complete absence of spinel- and chrome spinel-bearing

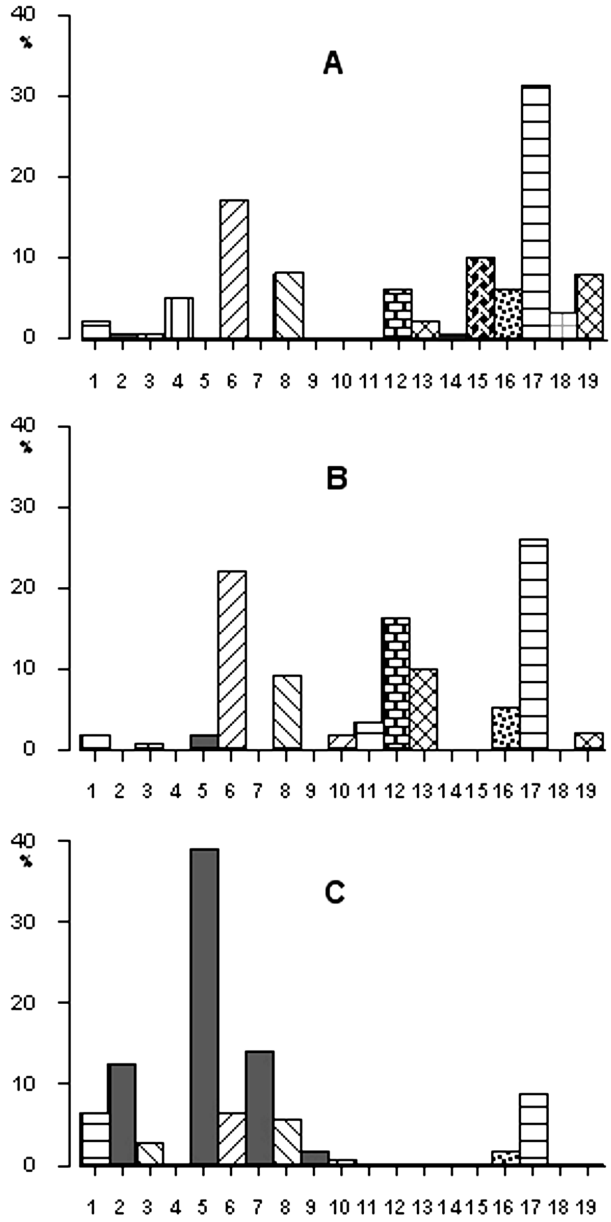

Fig. 13. *Distribution of various mantle nodules in the kimberlites of the Zimny Bereg area: A - Grib pipe; B - Anomaly-688 pipe; C - name M. Lomonosov deposit pipes.*

1 – dunites, 2-10 – ultramafic rocks of the Mg-Al-series (Marakushev, 1984): 2 - spinel-pyroxene "B" facies, 3 - spinel-pyropic "C1" subfacies, 4 - pyrope clinopyroxenites, 5,6 - grospydite "C2" subfacies, 7,8 - coesite "C3" subfacies, 9,10 - diamond-pyrope "D" facies, 11 - garnetized orthopyroxenites (3, 4, 6, 8, 10, 11 – pyrope-bearing varieties); 12-14 – ultramafic rocks of the Fe-Ti-series (Marakushev, 1984): 12 - ilmenitic rocks, 13 - pyrope-ilmenitic rocks; 14 - rutile rocks, 15 - clinopyroxene-phlogopite metasomatites, 16 - eclogites, 17 - eclogite-like rocks and granulites;18 - gabbros; 19 - megacrysts.

peridotites, i.e., the relationships between pyrope-bearing and chrome spinel rock varieties are directly opposed.

As regards kimberlites of the Pachuga group of pipes, the Grib kimberlites differ from them in mantle material characteristics quantitatively (with the greater diversity of mantle xenoliths reflecting their greater abundance and larger size), and by the fact that they are characterized by an abundance of clinopyroxenites and clinopyroxene-phlogopite rocks, and the presence of rutile, deformed phlogopite, clinopyroxene and orthopyroxene megacrysts. The presence of rutile in a variety of occurrence modes (as megacrysts, as a rock-forming mineral in peridotites and as an accessory mineral in various deep-seated rocks) appears to be one of the most spectacular and interesting mantle material features of the Grib pipe. However,

this may simply be a mantle substrate feature, not unique to this pipe: indeed, in all Fe-Ti series kimberlite pipes and sills of Zimny Bereg (the Grib pipe, pipes Anomaly-688, 693, 751, 748 and 734) idiomorphic phenocrysts of second generation olivine (crystallized from kimberlite melt) quite commonly contain microinclusions of rutile crystals. At the same time, in all Zimny Bereg Fe-Ti series picrites and kimpicrites all inclusions in olivine phenocrysts are opaque Ti-chrome spinels, whereas in the olivine phenocrysts of Zimny Bereg Al-series kimberlites and melilitites all inclusions are brown, aluminous chrome spinels. The presence of rutile microinclusions in olivine phenocrysts may be indirect evidence for the existence of rutile peridotites in the mantle substrate of the local Fe-Ti series kimberlite pipes.

Another spectacular and, probably, fundamental feature of the Grib pipe is the lack of any evidence of mantle metasomatic amphibolization of peridotites, which is so typical of nodules from the Lomonosov deposit and pipes of the Pachuga group, where the overwhelming majority of diamonds are rounded, "dissolved" crystals of "Uralian-type" [28]. There is reason to suggest that the absence of any ingress of the highly active, dissolving sodic component into the kimberlitic melt of the Grib pipe could make for the preservation of flat-faced octahedral habit in the majority of diamond crystals occurring in this pipe.

CONCLUSIONS

The Grib pipe xenoliths are dominated by nodules of various pyrope peridotites and pyroxenites of different depth facies, whereas chrome spinel ultramafic xenoliths are few. Rather abundant are eclogite-like rocks and Group A, Group B and, more rarely, Group C eclogites. Among Fe-Ti series ultramafic rocks, peculiar ilmenite-rutile and pyrope-rutile rock varieties are present together with more typical ilmenite-bearing and pyrope-ilmenite rocks. A peculiar feature of the Grib pipe is the presence of rutile megacrysts along with "ordinary" megacrysts of ilmenite, garnet, phlogopite, pyroxenes and olivine. The abundance of various clinopyroxene-phlogopite and phlogopite rocks may either be evidence of mantle hydrous-calc-alkali (K-Ca) metasomatism or of crystallization from volatile-rich residual melts. The presence of diversified nodules of combined rocks is an indication of a complex, multistage history of mantle substrate formation, including cumulus-type magma segregation, development of vein-type metasomatic domains, and intrusive rock relationships resulting in the formation of zones of "hot" contact metasomatism ("skarnoids"). In general, the variation of TP formation parameters for the examined nodules of various peridotites and eclogites is quite well approximated by a 42-43 mW/m^2 conductive geotherm.

The set of mantle rock varieties present in the Grib pipe is very distinct from that characteristic of kimberlite pipes of the Lomonosov deposit (Zimny Bereg Al-series kimberlites), being most similar to that of pipe An-688 from the Pachuga group (Zimny Bereg Fe-Ti series kimberlites). The Grib pipe differs from pipe An-688 by its higher mantle nodule content and abundance of clinopyroxenites,

clinopyroxene-phlogopite rocks and megacrysts of clinopyroxene, orthopyroxene, deformed phlogopite and rutile.

In general, based on the essential varieties of mantle xenoliths, their large size and high concentration in rock samples, the predominance of pyrope rock varieties among the xenoliths, and taking into account the geochemical and Nd-Sr characteristics of the rocks themselves, the Grib pipe kimberlites can be classified with the Fe-Ti series Zimny Bereg kimberlites, similar to Group 1 South African kimberlites and diamondiferous kimberlites of the Southern fields of the Yakutian diamond province (excluding the Nakyn field). The predominance of flat-faced octahedra among the diamonds is another common feature that the kimberlites of the Grib pipe and Yakutian kimberlites share.

The petrographic and mineralogical examination of mantle xenoliths performed in this study enable us to approximate the structure and composition of the upper mantle beneath the Grib pipe and to identify the formation peculiarities of, and relationships between, different mantle rock types, i.e., to create a necessary factual basis (framework) and develop a system of working hypotheses for further, more detailed investigation.

This study was supported by the Russian Foundation for Basic Research, grant 01-05-64257.

REFERENCES

1. **Carswell, D.A.**, 1975. Primary and secondary phlogopites in garnet lherzolite xenoliths. Phys. Chem. Eart 9, 417-430.
2. **Coleman, R.G., Lee, D.E., Beatty, L.B. and Brannock, W.W.**, 1965. Eclogites and eclogites: their differences and similarities. Bull. Geol. Soc. Amer. 76, 3, 483-508.
3. **Dawson, J.**, Kimberlites and their xenoliths, 1980. Springer-Verlag, Berlin-Heidelberg.
4. **Dawson, J.B. and Smith, J.V.**, 1975. Chemistry and origin of phlogopite megacrysts in kimberlite. Nature, 253, pp. 336-338.
5. **Dawson, J.B. and Stephens, W.E.**, 1975. Statistical analysis of garnets from kimberlites and associated xenoliths. J. Geol. 83, pp. 589-607.
6. **Gurney, J.J.,** 1984. A correlation between garnets and diamonds in kimberlites. In: J.E. Glover and P.G. Harris (Eds.), Kimberlite occurrence and origin. University of Western Australia, Geol. Dept., Publ., 8, pp. 143-166.
7. **Harte, B., Cox, K.G. and Gurney, J.J.,** 1973. Petrography and geological history of upper mantle xenoliths from the Matsoku kimberlite pipe. In: Physics and chemistry of the Eart, vol. 9 (First Int. Kimb. Conf. Cape Town, 1973). Pergamon Press, New York, pp. 477-506.
8. **Kennedy, C.S. and Kennedy, G.C**., 1976. The equilibrium boundary between graphite and diamond. J. Geophys. Res. 81, pp. 2467-2470.
9. **Makhotkin, I.L. and Zhuravlev, D.Z.,** 1993. Sr and Nd isotope composition of diamondiferous kimberlites and melilitites of the Arkhangelsk region, Dokl. Ross. Akad. Nauk, 332, 4, pp.491-495 (in Russian).
10. **Marakushev, A.A.** 1984. Peridotite nodules in kimberlites and basalts as indicators of deep litosphere structure. Proc. 27th IGC, Petrol., Sect. S.09, vol.9, Moscow, Nauka, p.153-161 (in Russian).

11. **Mitchell, R.H.,** 1995. Compositional variation of micas in kimberlites, orangeites, lamproites and lamprophires. Extended Abstracts 6 IKC, Novosibirsk, Russia, pp.390-392.
12. **Nikitina, L.P. and Simakov, S.K.,** 1994. TERRA nova. Fifth International EMPG Symposium, 6, p.34.
13. **Pollack, H.N. and Chapman, D.S.,** 1977. On the regional variation of heat flow, geotherms, and lithospheric thikness. Tectonophysics, 38, pp. 279-296.
14. **Sablukov, S.M.,** 1990. Petrochemical series of the kimberlite rocks. Dokl. Akad. Nauk SSSR 313 (4), pp. 935-939 (in Russian).
15. **Sablukov, S.M.,** 1995. Petrochemical series of kimberlite rocks of Arkhangelsk Province. Exstented Abstracts 6th IKC. Russia, Novosibirsk, pp. 481-483.
16. **Sablukov, S.M., Sablukova, L.I. and Shavirina, M.V.,** 2000. Mantle xenoliths in the Zimny Bereg kimberlite deposits of rounded diamonds, Arkhangelsk diamondiferous province. Petrologiya, 8 (5), pp. 466-494.
17. **Sablukov, S.M., Sablukova, L.I. and Verichev, E.M.** 2002. Essential types of mantle substrate in the Zimny Bereg region in connection with the formation of kimberlite hosting rounded and flat-faced diamonds. In: Proceedings of Int. Workshop "Deep-seated magmatism, magmatic sources and the problem of plumes", Vladivostok, Russia, pp. 185-202.
18. **Sablukova, L.I.,** 1995. Mantle nodules in kimberlite rocks of Arkhangelsk, Exstented Abstracts 6th IKC. Russia. Novosibirsk, pp. 484-486.
19. **Sergeeva, O.S.,** 2000. Morphological peculiarity of diamonds from Grib pipe. In: Material on geology and mineral deposits of Arkhangelsk district, Arkhangelsk, pp.97-102 (in Russian).
20. **Sinitsyn, A.V., Dauev, Yu.M. and Grib, V.P.,** 1992. The structure, position and productivity of kimberlites of the Arkhangelsk province, Geol. Geofiz. 10, pp. 74-83.
21. **Skinner, E.M.W, Smith, C.B., Viljoen, K.S. and Clark, T.C.,** 1994. The petrography, tectonic setting and emplacement ages of kimberlites in the south-western border region of the Kaapvaal craton, Prieska area, South Africa. Proceedings of the Fifth IKC, Araxa, Brazil, 1, pp. 80-97.
22. **Smith, C.B., Gurney, J.J., Skinner, E.M.W., Clement, C.R. and Ebrahim, N.,** 1985. Geochemical character of Southern African kimberlites. A new approach based on isotopic contents. Trans. Geol. Soc. S. Afr. 88, pp. 267-280.
23. **Sobolev, N.V.,** 1974. The deep seated inclusions in kimberlites and the problem of the upper mantle composition. Publishing House "Nauka", Siberian Branch, Novosibirsk (in Russian).
24. **Sobolev, V.S, Dobretsov, N.L. and Sobolev, N.V.,** 1972. Classification of the deep-seated xenoliths and types of the upper mantle. Geol. and Geoph.12, pp.37-42 (in Russian).
25. **Taylor, L.A. and Neal, C.R.,** 1989. Eclogites with oceanic crustal and mantle signatures from the Bellsbank kimberlite, South Africa, Part I: mineralogy, petrography and whole rock chemistry. J. Geol. 95, pp. 551-567.
26. **Udovkina, N.G.,** 1985. Eclogites of the USSR. Moscow, "Nauka" Public House.
27. **Verichev, E.M., Sablukov, S.M., Sablukova, L.I and Zhuravlev, D.Z.,** 1999. A new type of diamondiferous kimberlites of the Zimny Bereg, Arkhangelsk diamondiferous province, Dokl. Ross. Akad. Nauk, 368, 2, pp.226-229. (in Russian).
28. **Zakharchenko, O.D, Blinova, G.K., Botova, M.M. et al.,** 1990. Diamonds from kimberlite pipes of the Arkhangelsk Diamondiferous District. Final. Proc. VI All-Union meeting "The basic directions of increase of efficiency and quality of prospecting works on diamonds", Irkutsk, SSSR, pp.282-284 (in Russian).

Mantle plumes as a determining factor of vertical migration of magma generation zones, fixed from the bulk kimberlite compositions

Vasilenko V.B.[1], Zinchuk N.N.[2]

[1]Institute of Mineralogy and Petrography SB RAS, Novosibirsk,
E-mail: titan@uiggm.nsc.ru
[2]Joint-stock company "ALROSA", Yakutian research exploration enterprise, Mirnyi,
E-mail: adm.cnigri@alrosa-mir.ru

A problem of relation between kimberlite formation and mantle plumes was examined for kimberlite fields of the Yakutian Kimberlite Province, South Africa, and provinces of Lesotho and Wood Guinea. The database includes original 6997 bulk rock compositions of Yakutian kimberlites, as well as 169 bulk rock compositions of African unaltered kimberlites from literature sources. The petrochemical populational model, earlier dveloped by the authors, was used as an methodological approach. As a result of conducted investigation, it was established that the infiltration of mantle plumes in lithosphere is a principal requirement for the beginning of selective melting of mantle peridotites and generation of protokimberlite melts. The melting of lithosphere rocks takes place at gradual uplift of magma generation zones. Intrusive bodies within the kimberlite fields were formed successively from those which were generated from the deepest melts to those which were generated from the least deep melts. The kimberlite fields are usually zonal. The deepest kimberlites are successively surrounded by zones of less deep kimberlites. The least deep rocks are natural boundaries of kimberlite fields. The kimberlite fields differ in their sets of chemical rock types, or differ in lithosphere thickness under these fields. For an explanation of originating of linear elongation of the fields in the Yakutian Kimberlite Province, the hypothesis on plate motion above a hot spot is attracted.

INTRODUCTION

Mantle plumes represent rather narrow columns of heated substance, rising from mantle depths. The proposed dimensions of plumes range up to thousand kilometers. The connection of genesis of diamondiferous kimberlites with mantle plumes is recognized by all researchers. Three hypotheses are the most actual: differentiation, xenogenic hypothesis and selective melting. According to differentiation hypothesis (for example, in interpretation by V.A. Milashev [8]), kimberlite and picrite melts originated in rising convective streams of heated and decompressed substratum at a depth, where temperature of composing garnet peridotites becomes equal to temperature of their melting at corresponding pressure. Following this hypothesis, the kimberlites can be represented as differentiates of these melts, or as the most mobile part of these melts, saturated by

fluids. The adherents of the considered hypothesis believe that a source of diamonds in kimberlites is the astenosphere. The xenogenic hypothesis explains genesis of diamonds, rather than kimberlites. According to this hypothesis, the important source of information on diamonds genesis are mantle rocks, containing diamonds. Let's remember an essence of the xenogenic hypothesis by Taylor et al.: "the majority of diamonds are produced from kimberlites, but it reflects only how diamonds were transported to the surface. Mantle rocks, in which diamonds really grew (peridotites and eclogites), were mostly decomposed by turbulent fluid flow in kimberlite magma, whereby diamonds were liberated in them" [16]. The differentiation and xenogenic hypotheses ignore completely mineralogical and chemical peculiarities of kimberlites. Moreover, from the xenogenic hypothesis follows that the primary mineralogical and chemical peculiarities kimberlites cannot be ascertained as a result of intensive contamination of kimberlite melts by desintegrated lithosphere rocks. However, this is not the case. The kimberlite compositions, as well as all other magmatic rocks, can be surely determined. Furthermore, it is possible to trace evolutional variations of chemical compositions of kimberlites in connection with change of conditions of kimberlite melts generation. The connection between kimberlite compositions and conditions of their melts generation fits nicely in hypothesis on selective melting lithosphere at saturation of peridotites by fluids of mantle plumes. This hypothesis is based on physico-chemical experiments, which have shown that the melting of peridotite, saturated by carbonic acid, proceeds as successive melting of clinopyroxene-olivine, orthopyroxene-olivine and orthopyroxene-garnet-olivine cotectics. The melting of clinopyroxene-olivine cotectics gives rise the basic mass of protokimberlite melts, the crystallization of which results in the formation of rocks, mainly containing variable amounts of magmatic calcite and olivine. Despite that the presence of magmatic calcite in kimberlites was described in detail by Scott [14], Vasilenko et al. [18], many researchers of mineralogy and geochemistry of kimberlites ignore this fact. As a consequence, their works are separated from actual properties of kimberlites. Over a long time the authors of the present work examined chemical peculiarities of kimberlites from different provinces, using hundreds and thousands bulk rock analyses. As a result, the petrochemical populational model of kimberlite formation was formulated [19]. On the basis of this model, many characteristic features of structure and petrology of kimberlites were detected, including phenomenon of vertical zonality of compositions of kimberlite bodies for separate kimberlite fields. This phenomenon is described in the present work for the first time.

PETROCHEMICAL POPULATIONAL MODEL

A base for constructing of this model were the results of detailed investigations of chemical compositions of Yakutian diamondiferous kimberlites. These investigations were conducted with a wide use of methods of mathematical

statistics on the basis of system approach [19]. As a result, it has become possible to establish reliably positions of principal and supplementary minima of empirical distributions, which divide the statistical sampling including 1100 analyses into taxons of three-level hierarchy, and to propose a model of classification of kimberlites. Based on this model, each sample described by silicate analysis, obtains three-level taxonomic characteristic, which has a particular petrological sense. Petrochemical populations were distinguished as taxons of the first rank. The term "population" was chosen by us as an index of objective existence of 7 kimberlite groups, independent of the researcher and bounded among themselves by principal minima of empirical distributions. Only 7 populations of kimberlites are known. The average compositions of the populations ranked in TiO_2 and K_2O contents, form a complete succession of bulk compositions from minimum up to maximal values of TiO_2, that, according to the experimental data, reflects decreasing depths, where these populations were generated. The baric nature of this succession is confirmed also by a series of geologic observations. Each distinguished population originates only at a certain depth level, and all populations series (from 1 up to 7 populations) characterize a whole range of formation of kimberlite melts. Taxon of the second rank in the populational model was named as variety. The kimberlite populations are subdivided into varieties with successively varying contents of CaO and MgO, which inversely correlated each other. The formation of populations begins from melting of calcite varieties, which give place to more magnesian varieties with increasing temperature of melting. All varieties related to the same population are characterized by close contents of TiO_2. The considered model describes variation of kimberlite melt compositions depending on thermodynamic conditions of their formation and peculiarities of clinopyroxene composition in substratum at different pressures. As clinopyroxene is present at all peridotites, kimberlite melts are characterized by similar compositions and can differ only in volumes of selective smeltings at close values of P-T conditions. Just these circumstances have stipulated proximity of kimberlite compositions from different regions. If fragments of subducted oceanic lithosphere are present in magma generation zones, the compositions of kimberlite varieties will be remarkable for higher contents of potassium (at presence of pyroxenite xenoliths) and sodium (at presence of eclogite xenoliths). These primary peculiarities of kimberlites, as well as any other features, form the third taxonomic level of the model, i.e. variations of varieties. For practical using, including for petrochemical mapping of kimberlite diatremes and kimberlite fields, the authors propose the classification scheme (Table 1). Based on this scheme, the petrochemical populational models were constructed for kimberlite diatremes from different regions. These models represent average compositions of varieties or their variations for each population of the kimberlites, found in the same pipe. The petrochemical mapping of many imberlite bodies using the hierarchical scheme (Table 1), has shown that within the diatremes the assemblages of chemical rock

Table 1. *Scheme of petrochemical classification of kimberlite rocks*

1 level. Subdivision in to populations. The typochemical indication is TiO_2.												
Boundary values	<0.4		0.41-0.60		0.61-1.00		1.01-1.40		1.41-1.80		1.81-2.20	2.21-2.80
Population number	1		2		3		4		5		6	7
2 level. Subdivision into varieties. The typochemical indications are: SiO_2 и CaO/MgO												
Boundary contents of SiO_2	<30.0									>30.0		
Boundary values of CaO/MgO (from... to...)	>8,20 6.40	6.39 3.81	3.80 2.50	2.49 1.76	1.75 1.21	1.20 0.83	0.82 0.58	0.57 0.39	0.38 0.36	0.35 0.33	0.32 0.18	<0.18
Variety number	1	2	3	4	5	6	7	8	9	10	11	12
The varieties can be united into the following groups: Σ(1-4) – kimberlite carbonatites (Crb); Σ(5-6) – carbonatitic kimberlites (Ca-kmb); Σ(7-9) – kimberlites (Kmb); Σ(10-12) – magnesian kimberlites (Mg-kmb).												
3 level. Subdivision into variations of varieties A. Distinguishing of potassium variations: Ultrabasic variations (1) – K_2O<0.75 wt.%; micaceous (2) – 0.75-1.19 wt.% of K_2O; sublamprophyric + lamprphyric (3) – 1.20-2.20 wt.% of K_2O. B. Distinguishing of sodium variations: 1 – Na_2O <0.50 wt.%; 2 – Na_2O >0.50 wt.%												
Classification characteristic of kimberlite analysis can be expressed by four-positional formula h.k.l.m, where h is a population number, k is a variety number, l is a variation number by potassium content, m is a variation number by sodium content.												

compositions, named as populations, are mapped as vertical dike-like bodies. The diatremes are usually composed of several populations, represented in successively varying volumes. It is possible to distinguish modal populations (occupying the dominant volumes in the diatreme) and submodal populations, immediately adjoining to modal ones. The such approach allowed to reveal peculiarities of compositions of kimberlite bodies within the different kimberlite fields in the Yakutian and South African Provinces.

Yakutian Kimberlite Province. The province occupies a northeast part of the Siberian Platform (Fig. 1). The province extends for 1500 km from Malobotuobinsky region on the south to nearly beaches of Laptev Sea on the north, and for 850 km west-to-east. The Yakutian Kimberlite Province is generally subdivided into Vilyui and Anabar-Olenek subprovinces. Within the subprovinces kimberlite bodies are distributed irregularly and are grouped together in kimberlite fields. All kimberlite fields in the Vilyui subprovince include diatremes with high diamond grade. In fields of the Anabar-Olenek subprovince alkaline picrites occur together with kimberlites. For petrochemical mapping of alkaline picrites we constructed petrochemical model of these rocks (Table 2). As follows from the considered model, alkaline picrites, similar to the kimberlites, are subdivided into populations. An indicator element for the populations are the TiO_2 contents. Similar to the kimberlites, CaO and MgO contents are inversely proportional. The increased TiO_2 contents are characteristic for more magnesian varieties. The described picrites differ from kimberlites in higher contents of TiO_2, total iron and in lack of correlation between iron and titanium. The last circumstance is apparently explained by higher contents of picroilmenite and magnetite.

Petrochemical models of fields and populational successions of diatremes

Within the Vilyui subprovince there are five kimberlite fields: Nakyn, Mirny, Alakit-Markhin, Daldyn and Verkhne-Muna.

Table 2. *Petrochemical model of compositions of alkaline picrites from the Anabar and Olenek field groups*

Oxides	**Population**					
	1 (10)*	2 (71)	3 (74)	4 (47)	5 (41)	6 (5)
SiO_2	23.68	27.61	27.15	27.26	28.82	30.52
TiO_2	1.10	3.03	3.65	4.14	4.90	6.84
Al_2O_3	3.87	4.04	4.08	4.03	4.61	3.38
Fe_2O_3	10.50	7.24	7.36	7.70	7.44	10.16
FeO	3.57	4.56	4.71	4.42	5.29	4.51
MgO	16.46	20.52	21.13	22.11	22.25	24.39
CaO	19.22	14.99	14.46	12.85	11.32	7.16
Na_2O	0.43	0.21	0.19	0.19	0.22	0.13
K_2O	1.30	1.22	1.17	1.39	1.60	1.14
P_2O_5	1.53	0.74	0.84	0.75	0.62	0.39
LOI	19.50	16.00	15.11	14.45	11.86	11.14

Note. ** the number of analyses.*

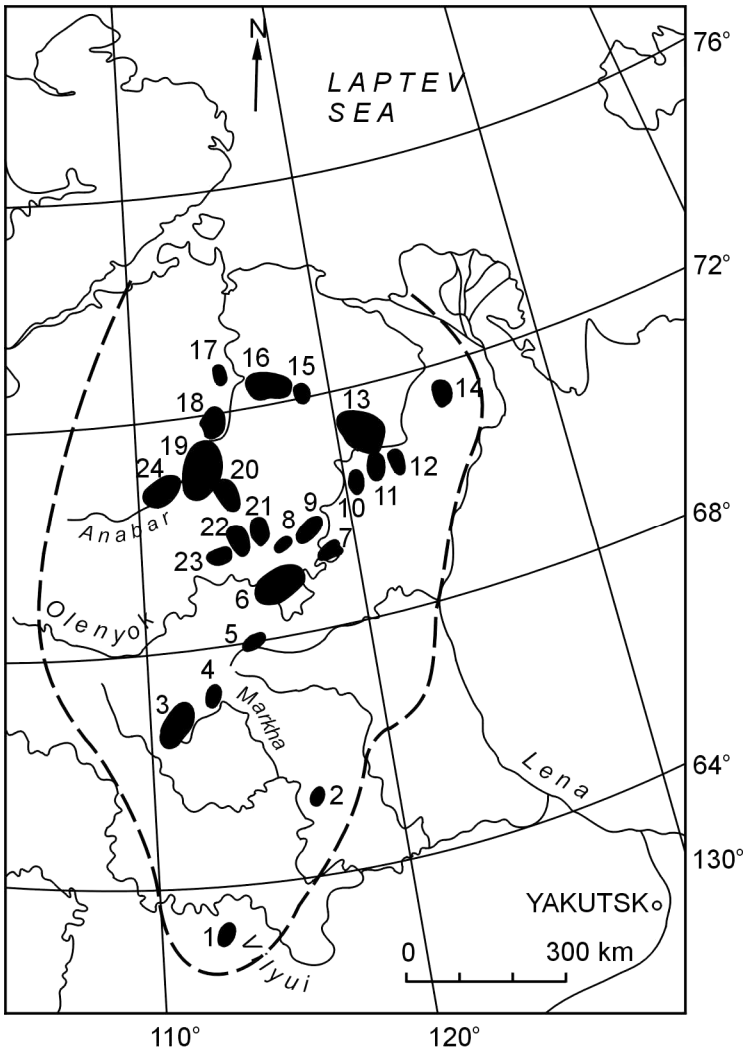

Fig. 1. *Location of kimberlite fields of the Yakutian kimberlite province.*

1 - Mirny, 2 - Nakyn, 3 - Alakit-Markha, 4 - Daldyn, 5 - Verkhne-Muna, 6 - Chomurdakh, 7 - Ogoner-Yuryakh, 8 - West Ukukit, 9 - East Ukukit, 10 - Merchimden, 11 - Molodo, 12 - Toluop, 13 - Kuoik, 14 - Khorbusuon, 15 - Tomtor, 16 - Ebelyakh, 17 - Yargin, 18 - Starorechenskoe, 19 - Ary-Mastakh, 20 - Dyuken, 21 - Luchakan, 22 - Birigindin, 23 - Kuranakh, 24 - Anabar.

Nakyn field. Within this field the Botuobinskaya and Nyurbinskaya diatremes, spaced 3 kilometers apart, are located. Structures of these diatremes and composing kimberlites are characterized by close similarity.

The petrochemical model (Table 3) suggests that diatremes within the field contain more than 9 % of the most plutonic and most diamondiferous kimberlites of populations 1 and 2. The population succession of diatremes within the field (Table 4) is not established in this case because of the similarity of population compositions for Botuobinskaya and Nyurbinskaya diatremes. The differences of these diatremes are detected only in compositions of varieties: Botuobinskaya diatreme contains a greater amount of carbonate rocks. A close location of these diatremes and their compositional similarity allow to assume that they are

Table 3.

Petrochemical populational model of kimberlites from the Nakyn field (based on 889 analyses)

Oxides	Population							
	1				2			
	Groups of varieties							
	Crb* (6.8)**	Ca-kmb (14.6)	Kmb (18.4)	Mg-kmb (6.0)	Crb (3.0)	Ca-kmb (13.8)	Kmb (20.3)	Mg-kmb (8.7)
SiO_2	17.20	22.78	29.33	32.72	22.70	24.80	29.67	32.78
TiO_2	0.32	0.35	0.35	0.37	0.44	0.45	0.47	0.49
Al_2O_3	4.07	3.78	3.32	3.29	5.59	4.53	3.66	3.38
Fe_2O_3	3.27	4.26	5.35	6.19	3.68	4.59	5.67	6.75
MgO	9.33	17.74	24.47	29.90	10.51	17.67	24.86	29.65
CaO	32.05	21.36	14.01	8.29	25.71	19.46	13.18	8.13
Na_2O	0.01	0.01	0.01	0.01	0.01	0.01	0.02	0.02
K_2O	1.15	1.17	0.78	0.57	2.11	1.50	1.00	0.73
P_2O_5	0.48	0.43	0.40	0.39	0.45	0.52	0.52	0.50
LOI	32.18	28.73	22.03	18.12	28.73	23.70	21.02	17.37

Oxides	Population					
	3				5	7
	Groups of varieties					
	Crb (0.2)	Ca-kmb (1.31)	Kmb (2.2)	Mg-kmb (4.5)	Mg-kmb (0.2)	Mg-kmb (0.4)
SiO_2	17.33	22.28	29.28	32.85	35.53	32.09
TiO_2	0.73	0.73	0.67	0.68	1.42	2.61
Al_2O_3	2.91	3.46	3.93	3.58	4.33	4.15
Fe_2O_3	3.43	5.63	6.17	6.77	7.90	6.63
MgO	5.64	17.96	24.76	31.78	29.35	28.00
CaO	36.81	21.67	13.17	6.94	6.38	8.97
Na_2O	0.01	0.01	0.01	0.03	0.17	0.03
K_2O	0.74	1.46	1.38	0.78	0.69	2.00
P_2O_5	0.99	1.03	0.79	0.65	0.47	2.31
LOI	31.69	25.55	20.12	15.85	13.62	13.27

Note. ** Crb – kimberlite carbonatites, Ca-Kmb – carbonatitic kimberlites, Kmb - kimberlites, Mg-kmb – magnesian kimberlites (see Table 1); ** -The number in brackets is a relative amount of analyses (%).*

represented by rocks of the same kimberlite sill, lying on the pipes. This explains the lack of evolutionary changing of compositions of the diatremes.

Mirny field. Within the field the most examined diatremes are Internationalnaya and Mir, which are the well known deposits of diamonds. The petrochemical populational model of the field suggests that kimberlites related to all seven populations, occur here. A characteristic feature of the field is the sharp decrease of relative amounts of rocks related to the populations 1 and 2, compared to the Nakyn field. It should be noted that the greatest abundance of kimberlites is related to the population 2.

Table 4.

Succession of relative contents (%) of modal populations in separate kimberlite bodies in fields of Vilyui subprovince

Diatreme	Population						
	1	2	3	4	5	6	7
Nakyn field (889 analyses)							
Nyurbinskaya	*16**; 31	*12*; 34					
Botuobinskaya	*27*; 17	*22*; 24					
Mirny field (704 analyses)							
A-21							75
Mir				28	31	13	
Amakinskaya				90			
Taezhnaya			36	24			
XXIII congress of CPSU		40	60				
Sputnik		46	46				
Dachnaya		61	33				
Internationalnaya	51	31					
Alakit-Markha field (2987 analyses)							
Marshrutnaya							70
Kira						46	35
Baytakhskaya						68	
Moskvichka					27	27	
Lipa					30	30	
Suvenir					33	33	
Molodost'					40	30	
Sytykanskaya					40	30	
Komsomolskaya					48	30	
Talisman				18	72		
Markhinskaya				30	68		
Magistralnaya				77			
Snezhinka				70			
Vostok				63			
Makatoyskaya			15	61			
Fineshtein			30	44			
Yubileynaya			40	34			
Krasnopresnenskaya			54	31			
Aikhal	49	42					
Alakitskaya	73	27					
Verkhne-Muna feld (286 analyses)							
Poiskovaya							42
Legkaya					36	36	
Novinka				25	38		
Zapoliarnaya				52	26		
325 years of Yakutia			25	75			
Komsomolskaya-Magnitnaya			29	37			

Table 4. *(end)*

Diatreme	Population						
	1	2	3	4	5	6	7
Daldyn field (2071 analyses)							
Molodezhnaya							30
Dal'naya						27	33
Geofizicheskaya						35	22
Zarnitsa					27	59	
Yakutskaya					24	58	
Leningradskaya					23	50	
Ozernaya					91		
Prognoznaya				4	81		
Ireliakhskaya				56	35		
Dolgozhdannaya			21	49			
Udachnaya-East			27	51			
Udachnaya-West			56	16			
Geokhimicheskaya		18	75				

Note. **Calcium kimberlites are shown in italics, kimberlites are shown by Roman type.*

The population 5 is also modal in the field. The succession of diatremes in the field, reflecting gradual variation of volumes of modal populations of kimberlites (Table 4), suggests the individuality of diatreme compositions and their gradual variation beginning with population 1 and ending with population 7. It is remarkable that the Internationalnaya diatreme contains the greatest amount of kimberlites related to population 1 in comparison with the other diatremes of the subprovince. A typochemical indication of the Mirny field is the higher relative abundance of kimberlites related to population 2.

Alakit-Markha field. More than 20 intrusive bodies of kimberlites were examined in this field. They include such known deposits of diamonds as Aikhal, Yubileinaya, Sytykanskaya diatremes. Diamond grade of these diatremes decreases with increase in number of modal populations (contents of TiO_2). The petrochemical model of the field allows to designate a further decreasing (after Nakyn and Mirny fields) of abundance of populations 1 and 2 and a predominance of kimberlites of populations 4 and 5 as the petrochemical signs. The population succession of intrusive bodies (Table 4) in sequence of gradual change of modal and submodal populations them is present here in full measure. It is remarkable that the populations 1 and 2 are represented in Aikhal diatreme almost as much as in Botuobinskaya and Nyurbinskaya diatremes in the Nakyn field. The Alakit-Markha field (Fig. 2) is a good example of zonal distribution of kimberlite bodies: the bodies containing modal populations 1 and 2, as well as population 3, are surrounded by bodies with modal populations 4 and 5. The peripheral zones of the field are composed of kimberlite bodies with modal populations 6 and 7. The deepest kimberlites are located in the center of the field. The least deep kimberlites occur in the periphery of the field.

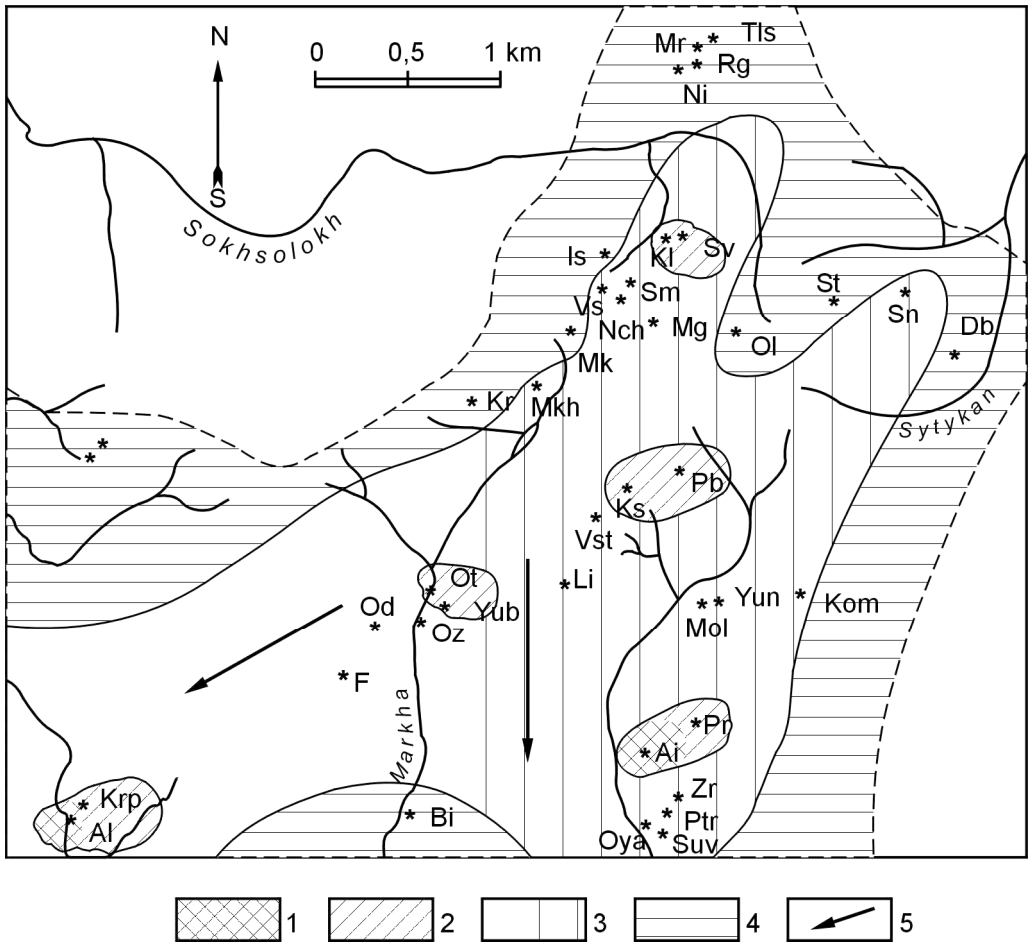

Fig. 2. *The schema of occurrence of modal populations of kimberlites in the Alakit-Markha field.*

Zones of occurrence: 1 – populations 1+2; 2 – population 3; 3 – populations 4+5; 4 – populations 6+7; 5 - most probable directions for searching diatremes of productive kimberlites.

Symbols of diatremes: Al - Alakitskaya, Ai - Aikhal, Bi - Baytakhskaya, Db - Druzhba, F - Fineshtein, Is - Iskorka, Kl - Kollektivnaya, Kom - Komsomolskaya, Kr - Kira, Krp - Krasnopresnenskaya, Ks - Kismet, Li - Lipa, Mg - Magistralnaya, Mkh - Markhinskaya, Mk - Moskvichka, Mol - Molodost, Mr - Marshrutnaya, N - Niva, Ni - NIIGA, Nch - Nachalnaya, Od - Odintsova, Ol - Olimpiyskaya, Oya - Oktyabrskaya, Oz - Ozernaya, Pb - Pobeda, Ptr - Podtrappovaya, Rg - Radiogeodezicheskaya, Sl - Slavutich, Sm - Smezhnaya, Sn - Snezhinka, St - Sytykanskaya, Sv - Svetlaya, Suv - Suvenir, Tls - Talisman, Vs - Veselaya, Vst - Vostok, Yun - Yunost ', Yub - Yubileinaya, Zr - Zarya,

Daldyn field. A major feature of this field is the presence of the well known diamond deposit, namely, the duplex diatreme Udachnaya. According to the petrochemical model, there are no kimberlites of population 1 in diatremes of the field, and kimberlites of population 2 are found to a smaller extent. Kimberlites of populations 4 and 5 are in abundance in the Daldyn field. The population succession (Table 4) of intrusive bodies in the field manifests itself in full measure. As in the case of the earlier considered fields, there are no bodies with an identical set of kimberlite populations. In this connection, a change of modal population 3 in Udachnaya-West diatreme for population 4 in Udachnaya-East diatreme is rather

remarkable. This fact allows to state that the Udachnaya-East diatreme is composed of less deep kimberlites, which were formed after kimberlites of Udachnaya-West.

Verkhne-Muna field. This field is lacking in kimberlites of population 1, and kimberlites of population 2 are present in small proportion. The majority of kimberlite compositions are related to populations 3, 4 and 5. The population succession of kimberlite bodies with gradual change of modal populations proportions is expressed in full measure (Table 4). All studied bodies are characterized by individual sets of populations.

Let's consider the Kuranakh field (Anabar group of fields) and the West-Ukukit field (Olenek group of fields) as representative examples of fields of the Anabar-Olenek subprovince. The study of these fields differs in the methodical attitude from descriptions of the fields of the Vilyui subprovince, because the intrusive bodies of the north subprovince are described by a few analyses. However, and in these cases the key features of kimberlite fields are detected with necessary completeness.

Kuranakh field. The deepest kimberlites here belong also to population 3. Moreover, typochemical indications of the field are the higher content of kimberlites of populations 6 and 7 and the presence of alkaline picrites. The succession of intrusive bodies according to population belonging of compositions of a small quantity of samples (Table 5) displays the same regularities, as succession of fields in the Vilyui subprovince. The alkaline picrites are sequential to the succession of kimberlite bodies. It should be noted that alkaline picrites can occur together with kimberlites in separate bodies (Universitetskaya diatreme).

West-Ukukit field. A characteristic feature of petrochemical model of the field is the distinct predominance of kimberlites of population 7 and alkaline picrites, with small amounts of kimberlites of populations 3 and 6. A population succession of intrusive bodies in the field (Table 5) and an individuality of their compositions in picritic part of the table are expressed more distinctly and more reliably, rather than in some kimberlite fields in the south of the province.

General regularities of evolution of average compositions of kimberlites

As follows from the aforecited data, the two directions of evolution of chemical compositions of kimberlites: within the fields and between them are of important value. The evolution of average compositions of kimberlites between the fields is well illustrated by Table 6. In the table the fields are ranked according to variations of proportions of populations 1 and 2. In the Vilyui subprovince the decrease of proportion of these populations is accompanied by increasing of proportions of other populations. As a whole, the total contents of populations 6 and 7 and alkaline picrites increase successively from the Nakyn field to the West-Ukukit field.

Table 5. *Distribution of bulk rock compositions throughout the populations in separate bodies of the Anabar-Olenek subprovince*

Kimberlite body	n*	Population											
		Kimberlites							Picrites				
		1	2	3	4	5	6	7	1	2	3	4	5
Kuranakh field (17 analyses)													
Los'	1									1			
Chita	1								1				
Universitetskaya	4			1	1	1			1				
Komarov	1							1					
Senkyu-North	2						1	1					
Kuranakh	1						1						
Senkyu-South	2					1	1						
Malokuonapskaya	5			1	2	1	1						
West-Ukukit field (43 analyses)													
An-72	1												1
An-22	2											1	1
An-23	2											2	
An-19, 44, 68	3											3	
Egientey	1											1	
An-15	2										1	1	
An-62n	3										2	1	
An-46a, 53, 57, 61	4										4		
An-45a, 62	2									2			
An-64	2								1	1			
An-11, 45, 54	3								3				
Severnaya	1								1				
Yuzhnaya	1								1				
An-65	2							1		1			
An-48	2							1	1				
An-18a, 46, 66	3							3					
KEPPES	1						1						
An-12	1						1						
An-71	2				1		1						
An-55	1					1							
Ruslovaya	1				1								
Omonos	1			1									
Leningrad	2			2									

Note. ** number of analyses*

It is remarkable that the succession from the Mirny field up to the West-Ukukit field coincides with a succession of geographic position of the fields in meridional direction. The evolution of kimberlite compositions within the fields as the succession of intrusive bodies depending on increasing numbers of their modal populations remains in all the fields, independent on their average compositions and geographic position.

Table 6. *Relative abundance (%) of kimberlite populations in the fields*

Field	Kimberlite population							Picrite
	1	2	3	4	5	6	7	
Nakyn	46	46	8	-	0.7	-	0.4	-
Mirny	12.7	26	16	12	20	9	7	-
Alakit-Markha	11	11	15	22	22	11	7.8	-
Daldyn	-	9.2	16	17	26	14	11	-
Verkhne-Muna	-	5	20	29	23	14	7	-
Kuranakh	-	-	11	15	21	21	15	15
West-Ukukit	-	-	7	5	2	7	12	67

The important characteristics of kimberlite fields are also peculiarities of compositions of kimberlite varieties. In this connection, it should be marked that the distributions of values of all examined analyses in coordinates population - variety (Fig. 3) display nearly rectangular form for Mirny and Verkhne-Muna fields. It means that the increase of numbers of populations was not accompanied by essential variation of a set of varieties. The distribution, similar to parallelepiped in its appearance (Alakit-Markha field), suggests that the compositions of variaties in populations become more magnesian with increasing the number of population. The distribution of compositions in the Daldyn field displays an intermediate pattern. The distribution patterns for all studied compositions of kimberlites from the Vilyui subprovince is characterized by continuos decrease of carbonate varieties and close proportions of magnesian varieties in going from deeper populations to less deep ones. Such distributions can originate, if the extent depletion of lithosphere peridotites increases from bottom to top.

African kimberlites

The chemical compositions of African kimberlites were described, using the analyses published by the different authors. The compositions of kimberlites with contents SiO_2 > 39 % were not used by virtue of the fact that they are also characterized by distorted contents of other oxides, resulted from hypergene processes.

South African Province. Here some kimberlite fields can be distinguished, such as Pretoria, Kimberly and Jagersfontein. In each of these fields the presence of population successions of kimberlite bodies was established. The resemblance of these successions allows to consider them jointly. As shown from Table 7, the population succession of kimberlite diatremes is expressed in full measure.

Lesotho Province. Because of small quantity of the collected analyses of kimberlites, the province is considered as a whole. The presence of a population succession here is expressed rather definitely (Table 7).

Table 7. *Succession of relative proportions (%) of modal populations in some kimberlite bodies of South Africa and Lesotho*

Diatreme	Population						
	1	2	3	4	5	6	7
South Africa (83 analyses)							
Kalkfontein							100
Frank Smith							100
Kop'esfontein							50
Wesselton						25	70
Premier					37	29	
New-Elands					67		
Lion Hil					75		
Yagersfontein					100		
De Beers			25	68			
Bultfo ntein			33	67			
Ebeneiser			60				
Snt.Augustin			67	33			
Koffifontein			68				
Dutoitspain			100				
Loxtondal			100				
Anomalia №1			100				
Finsh		17	71				
Anomalia №2		100					
Belsbank		60					
Klipfontein		50					
Lesotho (37 analyses)							
Monastery							100
Thaba Putsoa							100
Pipe 200							60
Matsoku						100	
Kao						50	
Letseng-la-terae						29	
Bytha-Buthe					50		
Lemphane					40		
Lighobong				67			
Mothae				50			

Note. *The references of chemical compositions of African kimberlites used in the present work, can be presented on special demand.*

Table 8. *Relative abundance (%) of kimberlite populations in African provinces*

Province	Population						
	1	2	3	4	5	6	7
South Africa(83)*	-	9.6	18.0	13.2	15.7	13.2	29.0
Wood Guinea (48)	-	-	29.0	27.0	14.5	10.4	18.8
Lesotho (37)	-	-	-	16.2	18.8	18.8	43.2

Note. ** the quantity of analyses*

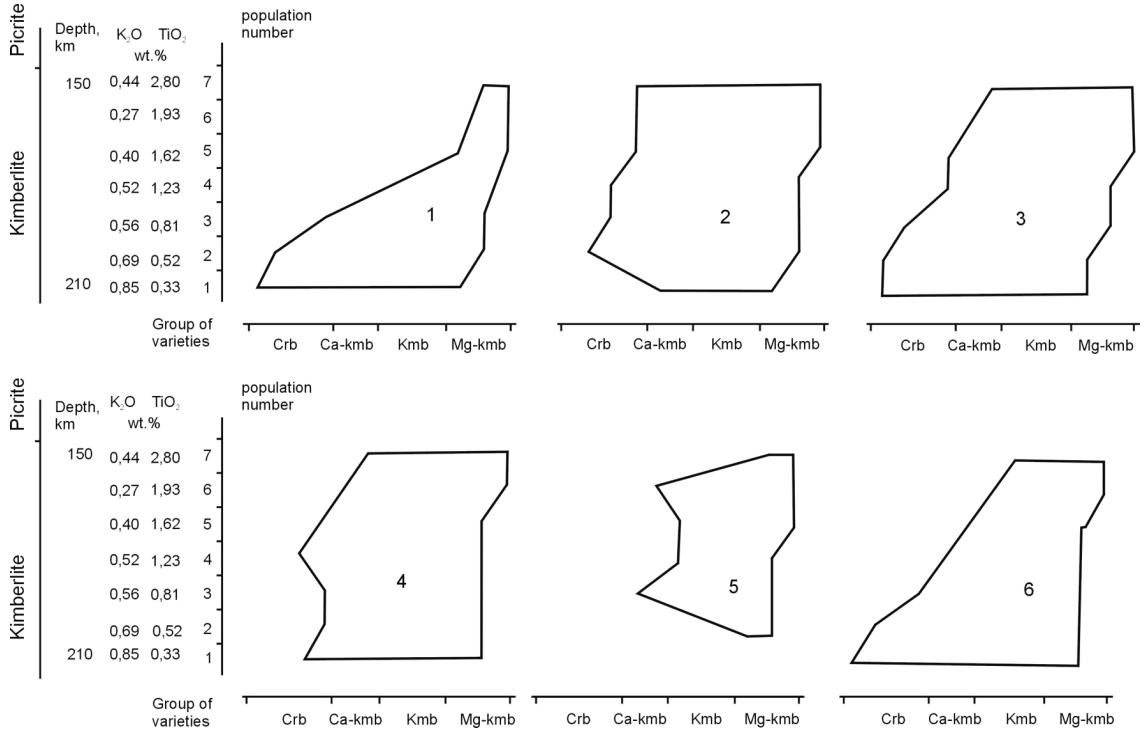

Fig. 3. *Range of chemical compositions of kimberlites of the Vilyui subprovince.*

The fields: 1 - Nakyn, 2 - Mirny, 3 – Alakit-Markha, 4 - Daldyn, 5 – Verkhne-Muna, 6 - the subprovince as a whole.

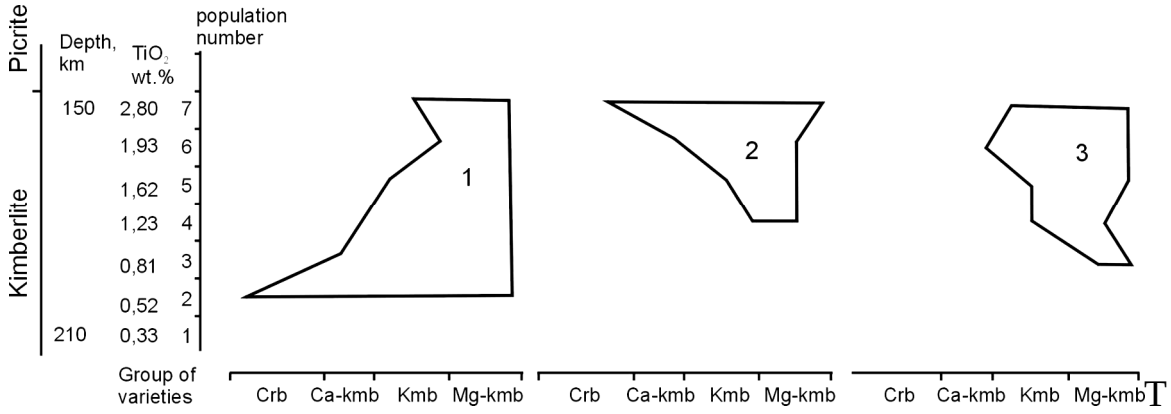

Fig. 4. *Range of chemical compositions of kimberlites of the South African Province (1), Lesotho (2) and Wood Guinea (3).*

he important distinctions of kimberlites from South Africa, Lesotho and Wood Guinea are seen in Table 8. They are the following: in South Africa there are no kimberlites of population 1; populations 1 and 2 are absent in Wood Guinea, and there are no populations 1, 2 and 3 in Lesotho. The sequential lack of the deepest populations is apparently connected with different thickness of lithosphere under separate blocks of the African continent. The distribution patterns of kimberlite

compositions in the diagram "population - variety" display different configuration for the provinces (Fig. 4). For South African Province this pattern coincides in general with such distribution for the Vilyui subprovince of Yakutia (Fig. 3), though it begins from population 2. The ranges of distributions of kimberlite compositions from Lesotho and Wood Guinea are characterized by increasing of carbonate varieties in less deep populations.

The comparison of distribution features of chemical kimberlite compositions between the kimberlite fields and between the diatremes of separate fields in the Yakutian Province and in provinces of the African continent suggests that they are of the same type.

DISCUSSION

The petrological interpretation of obtained results is based on the thesis on baric nature of distinguished series [19] of kimberlite populations. The reliability of this thesis is confirmed by experimental and geologic data, the presence of strong correlation between diamond grade of kimberlites and petrochemical indicators of these rocks formation depth. The major mechanism of titanium distribution in selective smeltings at different depths is the distribution of titanium in clinopyroxene of mantle peridotites. Experimental investigations [1, 2, 5, 13] showed that titanium passes from clinopyroxene passes in garnet structure with increasing pressure. In this case, at selective melting of clinopyroxene-olivine cotectics the melt will be depleted in titanium. The sequential realization of this mechanism at depths of 150-230 km has stipulated originating a series of kimberlite populations with different levels of titanium content. An estimate of melting depths of kimberlites of 1-7 populations, calculated using the petrochemical barometer by Vaganov [17], showed [19] that the depth interval of 150 to 230 km, which is located within the field of crystallization of natural diamonds, is the most probable [15]. The other types of alkaline picrites, associated with kimberlites, were generated at depths of less than 100 km [3, 12].

Based on the analysis of location of fields of diamondiferous kimberlites and picrites in the Yakutian Kimberlite Province relative to isopach lines of lithosphere thickness, which was estimated from seismic data [20], it was shown that the lithosphere thickness under diamondiferous kimberlite fields exceeds 200 km, but under fields with alkaline picrites decreases up to 150 km. The considerable lithosphere thickness under fields of diamondiferous kimberlites is confirmed by data on xenoliths and REE contents in garnets from kimberlites [4], showing that the lithosphere thickness under the Daldyn area in the Palaeozoic can be estimated approximately in 220-230 km.

The establishment of the statistical dependence between chemical composition of kimberlites and their diamond grade [21] is important for comprehension of kimberlite formation processes. This work, in particular, showed that diamond grade of kimberlites increases with an increase in K_2O and MgO contents and a decrease in TiO_2 and CaO contents. The contents of TiO_2 make a

Table 9. *Diamond grade of kimberlite populations from Yubileinaya pipe*

Population	**2**	**3**	**4**	**5**	**6**
TiO_2 content, wt.%	0.53	0.83	1.20	1.53	2.01
Diamond grade, ct/10 t	8.38	4.39	3.92	3.24	2.60

major contribution to description of diamond grade variability. This is harmonically coordinated with the thesis on decreased contents of titanium in the deepest populations. The existing opinion that all rocks of diamond-pyrope subfacies are uniformly saturated with diamonds, is far from actual pattern. Experimental works on diamond synthesis [10, 11] suggest that the amount of diamonds depends on kinetic activity of medium and nucleation rate. It is reasonable that the kinetic activity of diamond formation processes and diamond grade of kimberlites increase with increasing pressure. The effective evidence of this statement is the diatribution of diamonds in populations of Yubileinaya pipe (Table 9).

The above-mentioned arguments allow to consider that the population analysis of kimberlites gives a possibility to reconstruct kimberlite formation conditions to a good approximation to real processes.

Ensuring that the accepted methodology describes harmonically connections between different properties of kimberlites, let’s analyze the obtained results concerning distribution of populations of kimberlites in the fields and between kimberlite fields. We were the first to establish the presence of vertical succession of intrusive bodies from the deepest kimberlites to less deep ones in each studied field. This phenomenon is observed in different regions and does not depend on a number of the deepest population. It is possible to suspect with confidence, that the bodies of the deepest kimberlites were the earliest intrusions, and the further formation of kimberlite field proceeded as a result of a series of sequential intrusions. In a closing stage the bodies of the least deep magmatic rocks were intruded. In connection with the considered model, it should be noted that each sequential intrusion could anneal rocks of the previous intrusions. This should be taken into account, when using the geochronological data.

The formation process of kimberlite fields proceeded at vertical uplift of magma generation zones and their growth laterally from the centers of originating of the deepest populations (Fig. 2). Such phenomena could take place on the assumption of continuos inflow of energy and fluids from deep sources. According to interpretation by Letnikov [7]: "an energy potential of deep fluid systems, resulting in melting of rocks, is of decisive importance for development of magmatic systems, except for composition of initial matrix... Fluid systems separated as plumes from liquid Earth core are of special importance."

Kimberlite fields are formed as a result of divergent rise of mantle plume fluids at depths up to 150-120 km. Investigation of alkaline picrites and other mantle formations will allow, probably, to describe an existing connection between kimberlites and alkaline basalts. The difference between separate fields is

determined not by a qualitative change of mantle plumes, but by depth, where mantle plumes come into contact with lithosphere peridotites. In this connection, it is important to trace petrochemical models of kimberlite fields in the Yakutian Province from Mirny field to West-Ukukit field. The succession of these fields is characterized by steady decreasing of proportion of deeper kimberlite populations and increasing of proportion of less deep populations. This can be a consequence of a gradual decrease of lithosphere thickness from southwest to northeast. Thus, the relief of lithosphere bottom under kimberlite provinces determines a depth interval for zones of generation of kimberlite melts, their composition and diamond grade in places, where fluids of mantle plumes penetrate the lithosphere.

From the foundations of geodynamics, the number of mantle plumes should be less than the number of kimberlite fields. The peculiarity of location of kimberlite fields within the Siberian province can be explained by the hypothesis on lithosphere plate motion over a hot spot during a period of approximately 240 millions years [6]. The palaeomagnetic data on a motion of the Siberian Platform from the Middle Paleozoic to the Early Cretaceous [9] do not contradict such supposition. According to an opinion by Khramov [9], in the Early Cambrian the Siberian Platform was located in the southern hemisphere. From the Late Cambrian up to the present the Siberian Platform has been moving as a major plate. Just this fact determined a steady linear character of distribution of kimberlite fields, originated during a passing of the platform above a hot spot.

CONCLUSIONS

1. The infiltration of fluids of mantle plumes into lithosphere is a principal condition for the beginning of selective melting of mantle peridotites and generating of protokimberlite melts.
2. The melting of lithosphere rocks proceeds at gradual uplift of magma generation zones.
3. Within the kimberlite fields the intrusive bodies were formed successively: the deepest melts were the first to intrude and subsequently they gave way to less deep melts.
4. The kimberlite fields are usually zonal. Zones of the deepest kimberlites are successively surrounded by zones of less deep kimberlites. The least deep rocks are natural borders of kimberlite fields.
5. The kimberlite fields differ in assemblages of chemical types of rocks, if the lithosphere thickness under these fields are different.
6. The hypothesis on the plate moving over a hot spot can be used for explanation of originating of the linear elongation of fields in the Yakutian Kimberlite Province.

ACKNOWLEDGMENTS

The authors thank Dr. L.G. Kuznetsova and Dr. N.I. Volkova for help in preparing the manuscript.

REFERENCES

1. **Gasparik T.** Transformation of enstatite-diopside-jadeite pyroxenes to garnet // Contr. Miner. Petrol., 1989. V. 102. P. 389-405.
2. **Gasparik T. A** petrogenesis grid for the system $MgO-Al_2O_3-SiO_2$ // J. Geol., 1994. V. 102. P. 97-109.
3. **Green D.H.** Composition of basalt magmas as a criterion of their formation conditions at oceanic volcanism // Petrology of magmatic and metamorphic rocks of a sea floor - Moscow: Mir, 1973. P. 242-261.
4. **Griffin W.L., Kaminsky F.V., Ryan C.G., O'Reilly S.Y., Win T.T., Ilupin, I.P.** Thermal state and composition of the lithospheric mantle beneath the Daldyn kimberlite field, Yakutia // Tectonophysics, 1996. V. 262. P. 19-33.
5. **Herzberg C.** Solidus and liquidus temperatures and mineralogy for anhydrous garnet-lherzolite to 15 Gpa // Earth Planet. Int., 1983. V. 32. P. 193-202.
6. **Krivonos V.F.** Relative and absolute age of kimberlites // Otechestvennaya geologiya, 1997. N 1. P. 41-51.
7. **Letnikov F.A.** Fluid regime of endogenic processes in continental lithosphere and a problem of genesis and metallogeny of magmatic formations // Modern problems of formation analysis, petrology and metallogeny of magmatic formations. - Novosibirsk: P.H. SB RAS, branch "GEO", 2003. P. 196-197.
8. **Milashev V.A.** Kimberlites and plutonic geology. - Leningrad: Nedra, 1990. 167 p.
9. **Khramov A.N.** (Ed.) Paleomagnitology - Leningrad: Nedra, 1982. 312 p.
10. **Pal'yanov Yu. N., Sokol A.G., Borsdov Yu. M. Khokhryakov A.E., Shatsky V.S., Sobolev N.V.** The diamond growth from Li_2CO_3, Na_2CO_3, K_2CO_3 and Cs_2CO_3 solvent-catalysts at P=7 GPa and T=1700-1750^oC // Diamond and Related Materials, 1999. V. 8. P. 1118-1124.
11. **Pal'yanov Yu. N., Sokol A.G., Borsdov Yu. M., Khokhryakov A.E., Sobolev N.V**. Diamond formation from mantle carbonate fluids // Nature, 1999. V. 400. P. 417-418.
12. Orlov D.M. (Ed.) Petrochemistry of magmatic formations. Reference book. – Leningrad: Nedra, 1991. 229 p.
13. **Ringwood A.E., Kesson S.E., Hibberson W., Ware N.** Origin of kimberlites and related magmas // Earth Planet. Sci. Lett., 1992. V. 113. P. 255-263.
14. **Scott B.H.** Petrogenesis of kimberlites and associated potassic lamprophyres from Central West Greenland // Kimberlites, diatremes and diamonds: The Geology, Petrology and Geochemistry (Ed. F.R. Boyd, H.O.A. Meyer). - Washington, D.C. 2000_6: Am. Geophysical Union. 1979. P. 190-205.
15. **Sobolev N.V.** Deep seated inclusions in kimberlites and the problem of the composition of the upper mantle. Novosibirsk, Nauka, 1974. 263 pp.
16. **Taylor L.A., Keller R.A., Snyder G.A. et al.** Diamonds and their mineral inclusions, and what they tell us: a detailed "pull-apart" of a diamondiferous eclogite // International Geology Review, 2000, V. 41. P 959-983.
17. **Vaganov V.I.** Plutonic evolution of alkaline ultrabasic magmas // Mantle xenoliths and a problem of ultrabasic magmas. - Novosibirsk: Nauka, 1983. P. 57-62. (in Russian)
18. **Vasilenko V.B., Zinchuk N.N., Kuznetsova L.G., Serenko V.P.** Petrochemistry of subalkaline carbonatite-bearing complexes in Siberia. - Novosibirsk: Nauka, 1994. 232 pp.
19. **Vasilenko V.B., Zinchuk N.N., Kuznetsova L.G.** Petrochemical models of diamond deposits in Yakutia.- Novosibirsk: Nauka, 1997. 574 pp.
20. **Vasilenko V.B., Zinchuk N.N., Kuznetsova L.G.** Geodynamic control of kimberlite field locations in the central and the northern parts of Yakutian Kimberlite Province // Bulletin of Voronezh State University, 2000. N 3. P. 37-55.
21. **Vasilenko V.B., Zinchuk N.N., Krasavchikov V.O., Kuznetsova L.G., Khlestov V.V., Volkova N.I.** Diamond potential estimation based on kimberlite major element chemistry // J. Geochemical Exploration, 2002. V. 76. P. 93-112.

Experimental investigation of fluid-magmatic differentiation of alkaline systems with the connection of carbonatite genesis problem

Suk N.

Institute of Experimental mineralogy RAS, Chernogolovka, Moscow district,
E-mail: suk@iem.ac.ru

Silicate-carbonate liquid immiscibility was experimentally studied with application to the modeling of carbonatite melt separation from foid silicate magmas. Main attention was paid to modeling silicate-carbonate liquid immiscibility and partitioning of REE, Ba, Sr, Nb and Ta between the immiscible phases at T=1100 and 1250^{o}C and P=2 kbar. A wide field of initial melt layering into two liquids – silicate and carbonate – was estimated. At T=1100^{o}C a correlation between the partition coefficients of rare earth elements (La, Ce, Y) and initial composition of the system was observed. The partition coefficients of rare earth elements are also temperature-dependent. Nb and Ta are mainly concentrated in the silicate melt, but Ba and Sr – in carbonate one.

There is a heterogeneity in experimental carbonate and salt-carbonate (phosphate-, fluoride-, chloride-, sulfate-carbonate) melts which is likely to suggest that the salt phase may undergo further evolution after its separation from silicate melt. The experimentally observed regularities are consistent with those revealed in natural carbonatite complexes.

INTRODUCTION

The layering intrusive complexes (including carbonatite) are the products of complicated evolution of heterogeneous fluid-magmatic systems, containing aluminosilicate melt and fluid phase, which can transform into high concentrated salt liquid. Carbonate complexes represent the fluid-magmatic systems, in which high concentrated salt melt, separating from aluminosilicate melt, can directly form own nonsilicate rocks (carbonatites).

The geochemical characteristics of natural carbonatite complexes revealed a close relationship between deposits and ore occurrences of rare and rare earth element and complex REE-Y-Nb deposits with intrusions of carbonatite type, which can be exemplified by the Tomtor layered massif in Siberia and ore occurrences of barium-strontium carbonatites in western Transbaikalia. Thus an urgent task is the investigation of genesis of carbonatites and associated rocks. Furthermore, the specific geochemistry of carbonatites results in the occurrence of apatite, sulfides, phlogopite and other accessory minerals in them. For instance, in the Tomtor massif apatite-polycarbonate eruptive dikes and pipes and tuff-lavas of

phosphate compositions were found [7]. These facts suggest the enrichment of late-stage carbonatites in fluid (salt) components (phosphorus, sulfur and, probably, halogens).

In western Transbaikalia the barium-strontium carbonatite occurrences were found. They associate with basic alkaline silicate rocks (shonkinites and peralkaline syenites) of the high-alkali ultrapotassic series (Na_2O/K_2O=0.3-0.4). The isotopic signatures of carbonatites and shonkinites from the Khalyutinskoe field suggest a single mantle source and probable genetic relationships, which are supported by a number of common geochemical characteristics and similar ages of rock formation [14]. The carbonatites build up dikes and covers containing lenses and bands of barytocelestite and strontium-bearing barite, which show sharp boundaries with the carbonate matrix resembling boundaries between immiscible liquids. The isotopic and geochemical systematics of carbonatites and their country rocks from this region rule out the metasomatic formation of the carbonatites at the expense of limestones and silicate rocks. Moreover, geochemical and REE characteristics including Eu/Eu* suggest that the carbonatites are products of liquid immiscibility rather that the crystallization differentiation of alkaline basic rocks [14]. This allows us to suppose that these carbonatites were formed at an early stage within a parental magma reservoir through melt separation into immiscible silicate and carbonate-sulfate phases. The latter unmixed in turn and produced carbonate and sulfate liquids.

Such melt layering was described also in the carbonatite-bearing alkaline complex Mushugai-Khuduk in southern Mongolia, which belongs to a Late Mesozoic volcanoplutonic association of potassic alkaline and subalkaline rocks and carbonatites [1]. The thermometric investigation of magmatic inclusions in the minerals of the complex revealed the presence of two immiscible phases in a single inclusion. The sharp boundary between them is indicative of silicate-salt liquid immiscibility and suggests the formation of the series of rocks studied under conditions of silicate-phosphate-carbonate liquid immiscibility. The data obtained from the investigation of inclusions of salt melts demonstrated that the differentiation of alkaline magmas may produce not only phosphate and carbonate melts but also sulfate melts with elevated concentrations of fluorine and chlorine. The high homogenization temperatures (1200^oC) of melt inclusions (silicate-phosphate, phosphate-carbonate, and silicate-sulfate) support the separation of the salt melts during early stages of alkaline magmatism [1].

These facts witness about formation of layered carbonatite complexes under high fluid saturation conditions, i.e. enrich of them by different salt components, which during the origin of liquid immiscibility can separate from foid silicate magmas forming high concentrated salt phase.

The possible significance of liquid immiscibility for the formation of carbonatites and related rocks was pointed out by a number of authors [11, 12, 16]. These experimental investigations demonstrated the existence of a wide field of liquid immiscibility of carbonate and silicate melts at various temperatures and

pressures [8, 10], but experiments were mainly carried out at too high TP parameters (up to 15 kbar).

We have experimentally studied the silicate-carbonate melt layering modeling the carbonatite melt separation from foid silicate magmas at real parameters (T=1100 and 1250^{o}C and P=2 kbar which corresponds to the superliquidus region of the systems considered). Special emphasize was placed on the character of some ore element (such as REE, Nb, Ta, Ba and Sr) distribution between immiscible phases. The influence of added fluid components (phosphate, halogenides, sulfate) on the silicate-carbonate immiscibility and distribution of ore elements between immiscible phases has been also studied.

EXPERIMENTAL METHOD

The experiments were carried out in a high gas pressure vessel in sealed platinum capsules (3 mm in diameter) at a duration of 6 h with subsequent quenching at an average rate of 200^{o}C/min. Dry systems were investigated. The initial mixtures consisted of natural minerals (albite, diopside, and potassium feldspar) with addition of sodium carbonate (Na_2CO_3), its mixture with calcite (Na_2CO_3 + $CaCO_3$) and (or) potassium carbonate (K_2CO_3), and, in some experiments, chloride (NaCl), fluoride (NaF), phosphorus salt ($NaPO_3$) or sulfate (Na_2SO_4). Ore elements were introduced as oxides La_2O_3, CeO_2, Y_2O_3, Nb_2O_5, Ta_2O_5 and barium and strontium as carbonates $BaCO_3$ and $SrCO_3$. The initial charge was 100 mg in weight and was preliminary dried at T=100^{o}C for 18-20 h. The experimental samples were analyzed on a Camebax X-ray microanalyzer with an energy-dispersive system Link. Carbon was not analyzed on the microprobe, and the totals of the chemical analyses deviate from 100%.

EXPERIMENTAL RESULTS

Silicate-carbonate systems

The experimental investigation of silicate-carbonate systems at T=1100 and 1250^{o}C and P=2 kbar shows the wide field of liquid immiscibility with separation of starting materials into two phases – silicate and carbonate [13, 15]. The silicate liquid quenches into homogeneous glass in contrast to carbonate phase, which forms a finely dispersed microcrystalline quench aggregate. Both carbonate droplets in a silicate matrix and silicate droplets in a carbonate matrix were observed. Sharp phase boundaries between the melts are remarkable (Fig. 1). In the potassium-rich systems, the silicate melt coexisting with carbonate liquid shows Na_2O/K_2O=0.27-0.34. The obtained carbonate liquids (Table 1, phase II) showed heterogeneities in the form of separation into alkaline (mainly, sodic) and calc-alkaline (mainly, calcic) fractions (Table 1, phases III and IV). Such fractions were observed in all experiments, but they were difficult to analyze and their compositions were determined only in some samples. The heterogeneity can be

Table 1. *Compositions of phases (wt %) in immiscible carbonate-silicate melt systems. (I - silicate melt; II - carbonate melt; III - calcium-rich carbonate phase; IV - sodium-rich carbonate phase). 1-5 - T=1250°C, P=2 kbar; 6-18 - T=1100°C, P=2 kbar.*

N		SiO_2	Al_2O_3	MgO	FeO	Na_2O	K_2O	CaO	La_2O_3	Ce_2O_3	Y_2O_3	Nb_2O_5	Ta_2O_5	Summa
1	**I**	47.09	6.53	6.44	0.05	15.54	0.08	5.22	1.29	1.59	5.23	-	-	89.06
	II	2.50	0.44	1.38	0.12	24.52	0.36	11.49	0.74	0.73	0.61	-	-	42.89
2	**I**	37.10	4.78	5.49	0.02	12.63	0.06	18.64	1.38	1.92	3.16	-	-	85.18
	II	2.33	0.01	1.68	0.00	21.27	0.10	26.82	0.42	0.62	0.70	-	-	53.95
3	**I**	40.40	0.60	12.96	0.02	10.87	0.13	12.90	1.24	1.04	2.53	1.85	1.79	86.33
	II	2.22	0.02	1.87	0.08	22.16	0.15	19.21	0.55	0.28	0.11	0.28	0.20	47.13
4	**I**	31.06	3.71	5.08	0.20	9.52	0.07	24.61	1.03	1.43	2.32	1.21	2.17	82.41
	II	1.93	0.14	0.85	0.00	20.41	0.11	31.80	0.51	0.56	0.36	0.21	0.24	57.12
5	**I**	34.62	4.16	5.41	0.16	9.91	0.06	22.56	1.07	1.17	2.27	1.93	1.85	85.17
	II	1.18	0.09	0.86	0.14	21.76	0.14	27.93	0.21	0.06	0.06	0.02	0.26	52.71
6	**I**	51.45	10.27	4.04	0.09	17.04	0.19	5.04	0.84	1.38	-	-	-	90.34
	II	1.66	0.42	2.17	0.09	28.27	0.19	16.55	1.13	1.54	-	-	-	52.02
	III	0.65	0.17	2.17	0.05	14.66	0.14	22.12	1.72	2.27	-	-	-	43.95
	IV	0.75	0.12	1.88	0.11	34.97	0.16	9.93	0.46	0.66	-	-	-	49.04
7	**I**	50.29	8.18	6.62	0.16	16.11	0.13	7.80	0.91	1.32	-	-	-	91.52
	II	0.60	0.18	5.26	0.10	19.29	0.22	19.70	2.14	2.35	-	-	-	49.84
	III	1.14	0.80	5.97	0.26	12.85	0.36	17.95	3.62	3.17	-	-	-	46.12
	IV	0.48	0.20	0.85	0.00	37.68	0.03	7.28	0.56	0.62	-	-	-	47.70
8	**I**	47.60	5.47	8.67	0.29	15.80	0.14	10.22	0.89	0.87	-	-	-	89.95
	II	0.41	0.03	4.30	0.00	24.09	0.18	25.17	1.21	0.91	-	-	-	56.30
	III	0.26	0.21	4.75	0.00	15.99	0.18	23.05	1.95	1.47	-	-	-	47.86
	IV	0.54	0.29	0.23	0.22	28.76	0.13	0.65	0.00	0.00	-	-	-	30.82
9	**I**	42.60	6.70	5.41	0.52	12.81	0.45	8.56	0.82	1.22	-	-	-	79.09
	II	0.27	0.09	2.42	0.18	19.05	0.13	18.79	1.55	1.45	-	-	-	43.93
10	**I**	42.48	5.06	6.87	0.81	13.44	0.43	11.32	0.52	1.68	-	-	-	82.61
	II	0.50	0.32	2.97	0.26	16.63	0.13	18.30	1.16	1.78	-	-	-	42.05
11	**I**	41.13	4.02	3.89	0.07	9.99	0.10	14.01	1.04	1.66	3.96	-	-	79.87
	II	1.24	0.01	0.90	0.04	17.62	0.11	28.19	0.41	0.44	0.73	-	-	49.69
12	**I**	45.06	0.77	13.06	0.15	10.43	0.09	9.70	0.81	1.28	2.77	-	-	84.12
	II	1.45	0.06	1.85	0.06	11.16	0.17	21.26	0.73	0.66	0.23	-	-	37.63
13	**I**	28.05	5.66	2.01	0.14	9.50	0.15	31.68	1.26	2.11	-	-	-	80.56
	II	0.78	0.10	0.21	0.11	10.95	0.22	38.21	0.18	0.24	-	-	-	51.00
14	**I**	47.08	0.86	13.37	0.20	11.20	0.24	11.53	-	-	-	2.10	2.26	88.84
	II	0.36	0.08	2.04	0.01	20.89	0.27	27.48	-	-	-	0.00	0.06	51.19
15	**I**	47.93	2.30	10.16	0.06	14.20	0.11	14.67	-	-	-	1.45	1.64	92.52
	II	0.50	0.21	0.94	0.14	14.36	0.29	17.86	-	-	-	0.18	0.38	34.86
16	**I**	47.13	3.75	11.28	0.07	11.49	0.17	14.99	-	-	-	1.49	1.36	91.73
	II	0.56	0.00	3.06	0.00	25.20	0.15	32.92	-	-	-	0.00	0.00	61.89
17	**I**	27.36	2.96	5.77	0.04	7.36	0.07	36.76	1.68	3.02	-	-	-	85.02
	II	1.38	0.05	0.11	0.00	7.56	0.10	31.40	0.00	0.05	-	-	-	40.65
18	**I**	26.46	4.46	2.48	0.01	8.10	0.09	38.54	-	-	-	1.49	1.51	83.14
	II	5.10	0.37	0.87	0.07	6.85	0.08	37.33	-	-	-	0.40	0.37	51.44

Note. *The experimental samples were analyzed on a Camebax X-ray microanalyzer with an energy-dispersive system Link, IEM RAS, in 1998-2000.*

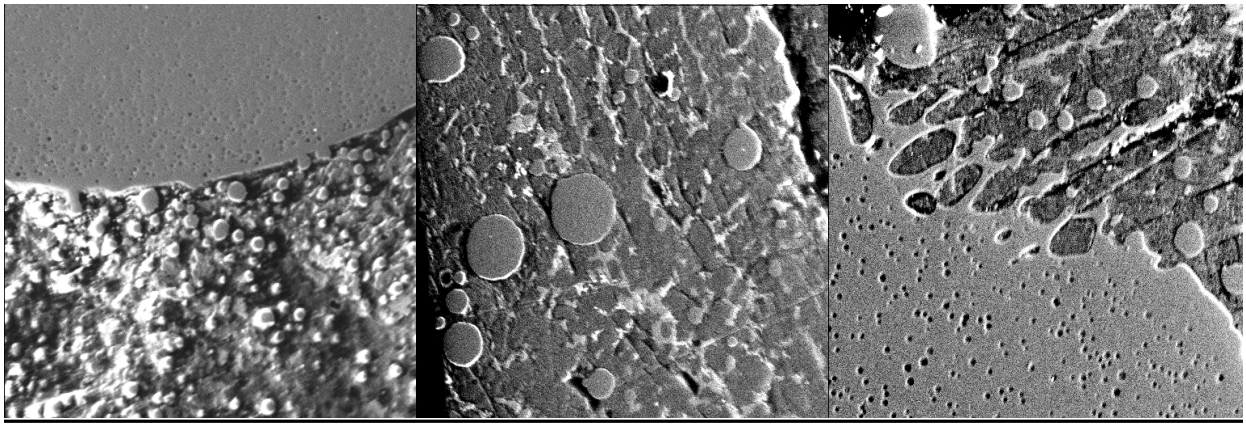

(a) 15 kV x 400 10 µ (b) 15 kV x 200 100 µ (c) 15 kV x 200 100 µ

Fig. 1. *Liquid immiscibility in the carbonate-silicate systems (a) and in sulfate-carbonate-silicate systems (b, c) at T=1250°C and P = 2 kbar.*

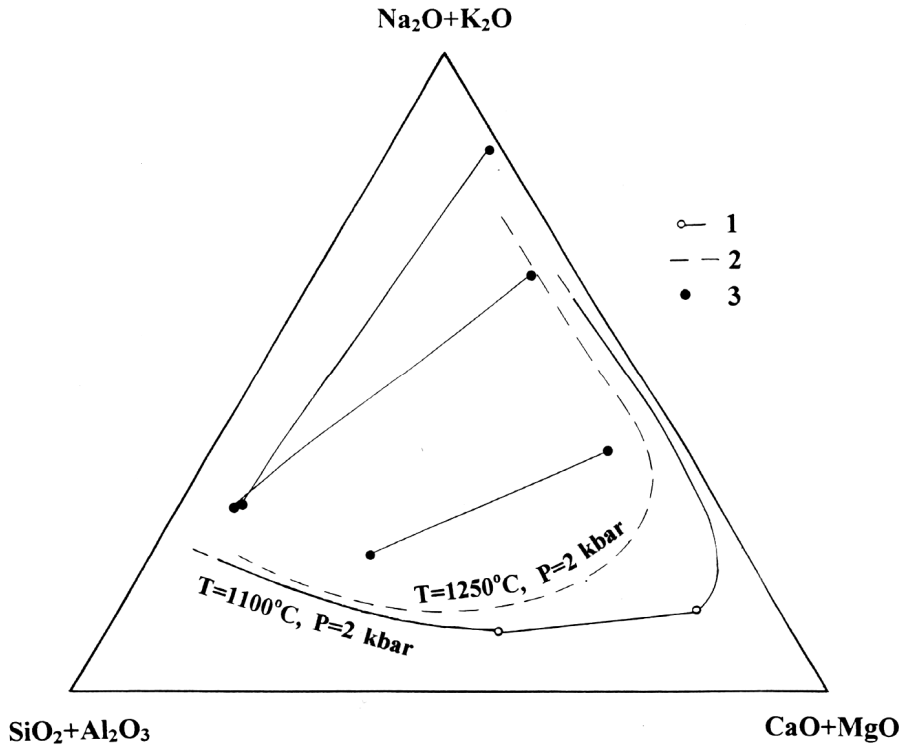

Fig. 2. *Experimental results on silicate-carbonate liquid immiscibility, wt %. 1 - silicate-carbonate systems of sodium specialization at T=1100°C and P=2 kbar [15]; 2 - silicate-carbonate systems of sodium specialization at T=1250°C and P = 2 kbar [15]; and (3) silicate-carbonate systems of potassium specialization at T=1250°C and P = 2 kbar. The tie-lines connect compositions of coexisting phases.*

observed in photomicrographs (Fig. 1) within large segregations of carbonate melt. It can be supposed that this heterogeneity occurred in a liquid state as a result of immiscibility of alkalic and calcic carbonate melts and was subsequently affected by the processes of quench crystallization. Because of the heterogeneity of the salt phase in this case and in more complex systems, its composition was analyzed in

the small droplets (no larger than 10-20 μm), which appeared to be most homogeneous. Figure 2 shows liquid immiscibility fields in silicate-carbonate systems at T=1100 and 1250°C and P=2 kbar. The liquid immiscibility field is somewhat wider at 1100°C as compared with that of 1250°C, however, at high calcium contents it is probably cut by the calcite and calcium silicate crystallization field. This obscures the processe of liquid immiscibility in these systems. Experiments in the potassium-rich systems showed a narrower liquid immiscibility field in comparison with the sodium-rich systems.

The investigation of rare earth element partitioning between immiscible carbonate and silicate phases in the systems studied at T=1100°C and P=2 kbar demonstrates that the character of their extraction depends on the initial melt composition [13, 15]. In alkalic silicate-carbonate systems, rare earth elements (La and Ce) are accumulated in carbonate phases, their partition coefficients ($K=C^{REE}_{carb}/C^{REE}_{sil}$) are greater than one (Fig. 3). Moreover, they are predominantly concentrated in the calcium-rich varieties of carbonate phases, whereas the sodium-rich fractions are essentially free of rare earth elements (Fig. 3, Tabl. 1). In the lime silicate-carbonate systems rare earht elements are accumulated in the silicate melt, which is also calcium-rich in these systems. The silicate melt also concentrates Nb and Ta.

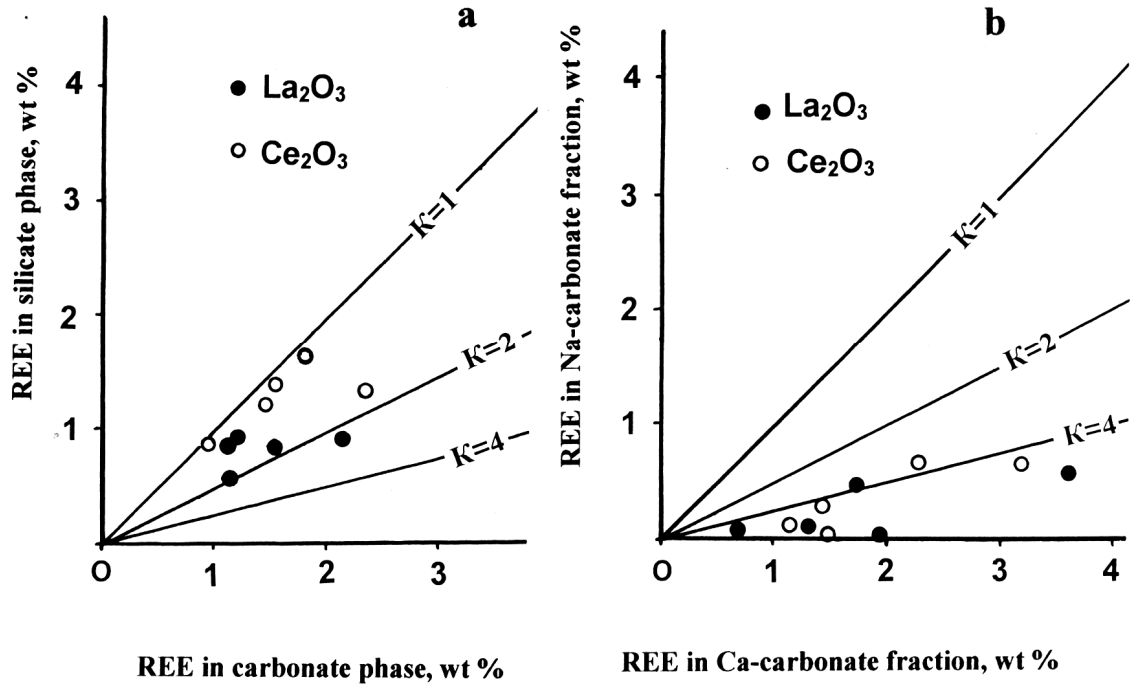

Fig. 3. *Partition coefficients ($K=C_{carbonate}/C_{silicate}$) of rare earth elements between silicate and carbonate melts (a) and between Na-carbonate and Ca-carbonate fractions (b) at T=1100°C and P=2 kbar.*

The experimental study of REE (La, Ce, Y), Nb, Ta partitioning between immiscible carbonate and silicate phases at T=1250°C and P=2 kbar demonstrated their predominant concentration in silicate melt (Tabl. 1). Figure 4a shows REE partition coefficients , which are lower than one. So, there is revealed the dependence of the character of rare earth partitioning on temperature: an increase from 1100 to 1250°C results in the redistribution of rare eath elements into silicate phase.

The investigation of distribution of Ba and Sr between immiscible carbonate and silicate phases shows that these elements are accumulated in carbonate phases: their partition coefficients ($K=C_{carb}/C_{sil}$) are greater than one (Tabl. 2). They are likely to depend on initial composition of the systems. The tendency of increase of Ba and Sr partition coefficients in potassium-rich systems is observed. These elements are predominantly concentrated in the calcium-rich fractions of carbonate phases as compared with sodium ones (Tabl. 2).

Table 2. *Compositions of phases (wt %) in immiscible sulfate-bearing carbonate-silicate melt systems (I - silicate melt; II - salt melt; III - calcium-rich phase; IV - sodium-rich phase; V – potassium-rich phase). T=1250°C, P=2 kbar.*

N		SiO_2	Al_2O_3	MgO	FeO	Na_2O	K_2O	CaO	SO_3	BaO	SrO	Summa
1	**I**	49.59	6.61	5.38	0.05	5.66	20.76	1.85	-	1.13	0.01	91.04
	II	0.85	0.02	0.88	0.06	32.76	13.90	6.47	-	3.72	2.50	61.16
	III	0.36	0.09	2.06	0.06	10.65	21.42	16.02	-	4.52	5.91	61.09
	IV	0.98	0.21	2.30	0.22	23.39	20.52	3.15	-	2.89	1.15	54.81
2	**I**	48.59	6.17	4.70	0.02	6.35	18.72	1.70	-	0.97	0.04	87.26
	II	2.43	0.19	1.17	0.07	9.91	18.57	11.33	-	5.77	4.94	54.38
3	**I**	49.27	5.94	5.20	0.05	7.08	16.10	1.89	0.51	0.60	0.20	86.84
	II	1.15	0.08	1.23	0.04	16.82	15.77	9.73	6.58	2.70	4.23	58.33
	III	0.33	0.00	0.93	0.06	13.26	20.03	15.53	3.80	2.05	6.19	62.18
	IV	0.03	0.01	1.19	0.00	41.12	8.07	1.79	1.04	0.85	0.84	54.94
	V	0.17	0.00	0.16	0.10	3.40	46.93	0.00	36.61	0.24	0.30	87.91
4	**I**	47.72	5.78	5.94	0.08	7.38	17.88	2.55	0.54	1.48	0.25	89.60
	II	1.36	0.09	1.05	0.04	11.42	14.05	11.79	2.61	6.85	6.16	55.42
	III	0.22	0.03	0.38	0.04	11.48	17.86	19.79	1.72	3.82	9.36	64.70
	IV	2.01	0.09	1.03	0.03	20.54	27.27	1.61	15.78	2.33	0.89	71.61
5	**I**	34.34	5.08	4.93	0.05	5.33	12.53	17.73	-	2.58	0.57	83.14
	II	5.55	0.08	1.66	0.10	7.72	12.96	27.18	-	4.46	2.23	61.97
	III	7.07	0.16	2.32	0.00	2.15	4.90	35.46	-	7.48	3.88	63.42
	IV	2.39	0.06	0.66	0.00	7.91	15.98	23.86	-	2.27	1.33	54.46
6	**I**	44.59	5.53	6.82	0.05	12.69	1.20	5.44	-	3.95	3.07	83.34
	II	0.93	0.04	0.95	0.05	26.86	1.06	7.75	-	6.12	6.97	50.73
	III	0.32	0.05	1.10	0.06	11.20	2.38	15.39	-	11.02	13.86	55.38
	IV	0.06	0.01	1.72	0.10	38.55	1.04	3.94	-	0.22	1.16	46.80
7	**I**	51.63	6.98	7.06	0.07	12.62	0.07	5.73	0.83	3.94	2.32	91.25
	II	1.78	0.19	0.58	0.08	12.35	0.24	8.62	7.87	8.26	8.77	48.74
	III	1.06	0.05	1.10	0.10	23.12	0.87	9.73	7.77	14.31	11.01	69.12
	IV	0.18	0.00	0.53	0.04	43.50	0.88	3.95	13.79	0.24	0.97	64.08

Table 2. *(end)*

N		SiO_2	Al_2O_3	MgO	FeO	Na_2O	K_2O	CaO	SO_3	BaO	SrO	Summa
8	**I**	49.66	6.37	7.13	0.05	14.32	0.07	5.00	-	3.98	2.01	88.59
	II	0.89	0.10	1.17	0.02	26.21	0.11	9.07	-	9.77	7.77	55.11
	III	0.72	0.09	1.72	0.06	15.85	0.12	12.63	-	15.22	12.17	58.58
	IV	0.59	0.11	2.27	0.05	31.61	0.13	7.80	-	1.28	2.19	46.03
9	**I**	29.35	3.72	4.87	0.05	10.09	0.07	21.72	-	4.36	3.12	77.35
	II	6.18	0.17	1.58	0.06	13.42	0.12	26.11	-	4.58	4.78	57.00
	III	5.46	0.13	1.89	0.03	2.12	0.03	29.50	-	13.40	10.46	63.02
	IV	1.85	0.13	0.87	0.02	15.50	0.16	28.85	-	2.15	3.59	53.12
10	**I**	30.03	3.74	4.99	0.00	9.60	1.09	21.01	-	3.16	3.03	76.65
	II	7.27	0.34	1.87	0.00	12.98	1.91	25.12	-	3.56	4.50	57.55
	III	12.21	0.71	3.13	0.06	2.94	0.37	27.36	-	10.01	8.06	64.85
	IV	2.46	0.04	0.74	0.05	12.16	2.31	27.68	-	1.78	3.89	51.11
11	**I**	45.89	4.93	6.82	0.15	15.18	0.12	16.86	0.89	1.61	1.40	93.85
	II	0.82	0.01	0.87	0.02	22.35	0.40	22.24	10.36	2.92	3.99	63.98
	III	0.66	0.05	1.54	0.09	23.05	0.23	22.96	8.13	2.89	3.76	63.38
	IV	0.21	0.03	0.87	0.02	40.17	0.33	7.49	23.42	0.90	1.64	75.08
12	**I**	56.33	4.88	8.17	0.12	18.04	1.18	4.15	0.46	2.14	0.71	96.18
	III	0.17	0.02	3.81	0.04	17.40	1.36	16.86	2.62	11.16	8.35	61.79
	IV	0.05	0.03	1.55	0.02	44.35	0.57	5.05	12.75	1.23	1.93	67.53

Note. *The experimental samples were analyzed on a Camebax X-ray microanalyzer with an energy-dispersive system Link, IEM RAS, in 2000-2002.*

Phosphate-carbonate-silicate systems

The influence of phosphorus on the silicate-carbonate liquid immiscibility and distribution of ore metals between immiscible phases is successful illustrated [15] by our experimental results at T=1250^{o}C and P=2 kbar with addition of phosphorus salt $NaPO_3$ (8 and 15 wt.%, which correspond to 5.6 and 10.4 wt.% P_2O_5) into silicate-carbonate systems studied. In the compositional range studied , the addition of phosphorus does not affect significantly the extent of silicate-carbonate liquid immiscibility. However, there is probably a slight increase in compositional contrast between the coexisting phases. The salt phase in the systems studied has phosphate-carbonate composition (Tabl. 3). The partition coefficients of rare earth elements between immiscible phases increase with addition of phosphate into the system (Fig. 4). In alkaline systems we can observed even their predominant concentration in the salt melt (K>1). An increase of the phosphorus content in the system resulted in the appearance of a heterogeneity in the salt phase, which is manifested in the presence of areas with carbonate and phosphate compositions. The phosphate phase is more effective in REE concentrating and significantly enriched in rare earth elements as compared with the carbonate phase (Fig 4c). Thus, the experiments show that phosphorus promote rare earth element extraction by salt melts in the systems studied.

Table 3. *Compositions of phases (wt %) in immiscible phosphate-carbonate-silicate melt systems. (I - silicate melt; II - phosphate-carbonate phase; III - phosphate phase; IV - carbonate phase). T=1250°C, P=2 kbar.*

N		SiO_2	Al_2O_3	MgO	FeO	Na_2O	K_2O	CaO	P_2O_5	La_2O_3	Ce_2O_3	Y_2O_3	Nb_2O_5	Ta_2O_5	Summa
1	**I**	53.80	5.83	7.74	0.06	14.21	0.20	1.14	3.22	0.16	0.55	2.32	3.79	4.01	97.03
	II	2.01	0.25	2.82	0.07	31.10	0.17	10.31	23.38	0.76	1.25	1.85	0.70	0.20	74.87
2	**I**	42.04	5.05	7.50	0.30	11.39	0.13	15.58	1.99	0.56	1.38	1.76	2.30	2.88	92.86
	II	1.89	0.03	3.47	0.05	19.70	0.11	25.57	21.63	0.57	0.69	1.09	0.98	0.23	76.82
	III	3.03	0.02	0.42	0.00	6.70	0.06	42.89	27.67	1.86	2.58	1.51	0.68	0.16	87.58
	IV	1.47	0.00	1.72	0.09	16.31	0.17	34.90	6.37	0.72	0.86	0.72	0.22	0.00	63.55
3	**I**	41.72	4.83	6.16	0.17	8.23	0.17	12.64	1.91	1.08	1.48	2.94	3.43	2.43	87.19
	II	1.36	0.04	2.03	0.08	20.86	0.08	27.27	23.09	0.75	0.80	0.92	0.75	0.09	78.12
4	**I**	49.96	6.22	7.61	0.05	14.37	0.14	2.94	2.37	0.78	2.32	1.77	-	-	88.53
	II	0.18	0.00	2.67	0.03	35.58	0.23	9.50	13.01	0.79	1.67	0.46	-	-	64.12
5	**I**	38.76	5.59	5.60	0.04	8.00	0.09	14.96	3.43	0.89	0.92	2.33	-	-	80.61
	II	4.35	0.30	1.50	0.03	17.37	0.12	26.90	11.83	0.32	0.22	0.41	-	-	63.35
	III	4.35	0.05	0.57	0.00	4.74	0.09	29.62	17.50	1.66	1.50	1.24	-	-	61.32
	IV	2.89	0.20	1.49	0.08	14.16	0.08	26.39	2.83	0.10	0.08	0.13	-	-	48.43
6	**I**	39.39	5.26	6.23	0.03	11.11	0.12	11.87	2.70	0.85	2.46	2.74	-	-	82.76
	II	1.09	0.11	1.08	0.01	23.62	0.10	24.92	11.01	0.39	0.84	0.45	-	-	63.62
7	**I**	35.08	5.25	5.30	0.07	7.91	0.11	17.36	1.71	0.41	0.63	1.67	-	-	75.50
	II	7.79	0.41	1.99	0.05	12.80	0.15	28.85	5.24	0.29	0.26	0.48	-	-	58.31
8	**I**	47.06	0.89	12.39	0.05	10.83	0.17	7.53	1.87	0.75	1.09	2.82	-	-	85.45
	II	0.91	0.02	2.54	0.06	33.50	0.06	14.64	14.16	0.35	0.33	0.32	-	-	66.89

Note. *The experimental sam ples were analyzed on a Camebax X -ray microanalyzer with an energy-dispersive system Link, IEM RAS, in 1998-2000.*

Table 4. *Compositions of phases (wt %) in immiscible carbonate-silicate melt systems with fluorine. (I - silicate melt; II –fluoride-carbonate phase;*
III - fluoride phase; IV - carbonate phase) 1-4 - T=1250°C, P=2 kbar; 5 - T=1100°C, P=2 kbar.

N		SiO_2	Al_2O_3	MgO	FeO	Na_2O	K_2O	CaO	La_2O_3	Ce_2O_3	Y_2O_3	F	Summa
1	**I**	32.41	3.89	5.40	0.02	12.76	0.03	22.59	1.54	2.34	1.62	5.14	87.74
	II	2.17	0.02	1.53	0.05	17.44	0.07	30.16	0.34	0.30	0.04	12.58	64.70
	III	8.69	0.33	6.97	0.01	12.75	0.04	28.52	1.00	1.46	1.19	16.71	77.67
	IV	1.19	0.04	0.47	0.04	19.64	0.11	33.07	0.33	0.43	0.19	1.13	56.64
2	**I**	38.68	4.05	6.96	0.09	13.76	0.08	19.03	1.25	1.28	1.61	3.94	90.73
	II	2.67	0.08	1.80	0.00	18.69	0.14	29.26	0.44	0.38	0.12	13.64	67.22
3	**I**	40.64	5.10	6.40	0.07	11.92	0.08	17.55	1.84	2.25	1.89	4.62	92.36
	II	2.53	0.03	1.85	0.02	19.02	0.12	28.97	0.83	0.82	0.24	13.67	68.10
	III	8.56	0.20	4.74	0.06	12.29	0.07	36.56	2.31	2.33	1.02	19.44	87.58
	IV	1.19	0.02	0.36	0.04	21.30	0.11	35.54	0.41	0.52	0.09	1.70	61.28
4	**I**	48.72	5.92	7.25	0.03	16.48	0.06	5.70	1.84	2.20	1.71	3.89	93.80
	II	2.13	0.09	2.33	0.03	40.54	0.08	8.37	0.96	0.76	0.13	9.41	64.83
	III	8.37	0.04	9.14	0.05	16.13	0.16	21.59	3.65	3.51	1.48	16.29	80.41
	IV	0.23	0.03	0.30	0.08	31.36	0.07	6.52	0.10	0.10	0.02	3.64	42.45
5	**I**	49.48	4.74	8.92	0.02	13.02	0.13	7.08	1.05	1.45	-	4.31	90.20
	II	2.87	0.36	4.26	0.18	15.83	0.18	21.60	1.41	1.26	-	12.47	60.42
	III	4.35	0.15	9.51	0.06	14.58	0.22	27.44	2.12	2.08	-	22.62	83.13
	IV	0.72	0.10	1.25	0.00	31.77	0.08	6.19	0.24	0.26	-	1.35	41.96

Note. *The experimental samples were analyzed on a Camebax X-ray microanalyzer with an energy-dispersive system Link, IEM RAS, in 1998-2000.*

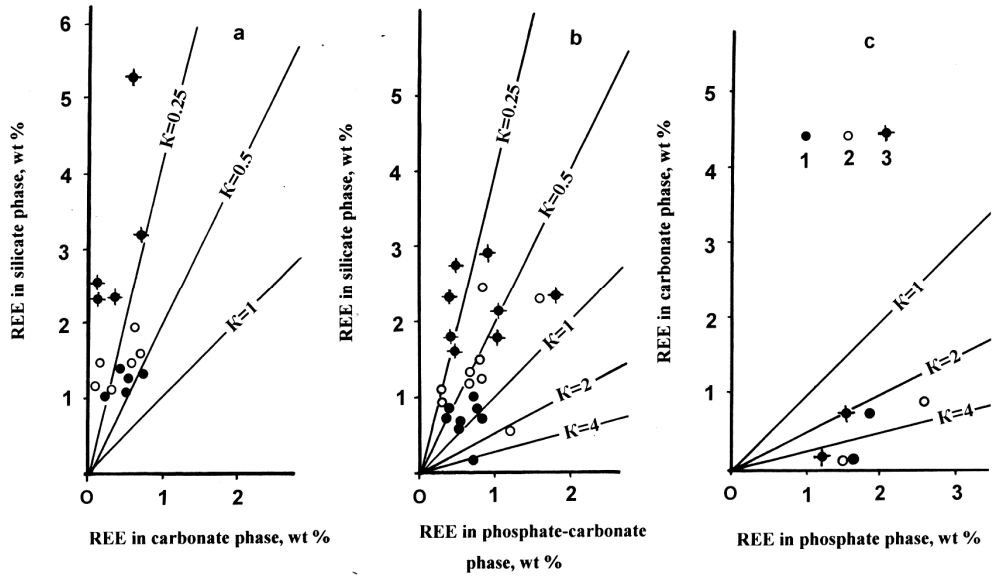

Fig. 4. *Partition coefficients ($K=C_{carbonate}/C_{silicate}$) of rare earth elements between silicate and carbonate melts (a), between silicate and salt (phosphate-carbonate) melts (b) and between carbonate and phosphate phases (c) at T=1250°C and P = 2 kbar. 1 – La_2O_3; 2 – Ce_2O_3; 3 – Y_2O_3.*

Fluoride-carbonate-silicate systems

The influence of fluorine on the silicate-carbonate liquid immiscibility was studied at T=1250°C and P=2 kbar by addition of sodium fluoride (NaF) into the system [15]. The separated salt phase had a carbonate-fluoride composition and formed either a separate layer or droplets in silicate melt. The compositions of the immiscible phases are shown in Table 4. Similar to phosphorus, the addition of fluoride into the system results in an increase in the partition coefficients of rare earth elements between immiscible liquids in the alkalic systems (Tabl. 4, an. 3, 4). The salt liquid is heterogeneous and consists of areas of carbonate and fluoride compositions. It is suggested that the heterogeneity of the salt phases in the phosphate-carbonate-silicate and fluoride-carbonate-silicate systems existed in the liquid state and was subsequently quenched. This is supported by the fact that in these systems, very small (up to 10-15 μm) individual droplets compositionally corresponding to carbonate melts were sometimes observed in the silicate phase. The fluoride phase is significantly enriched in rare earth elements in comparison with the carbonate phase (Tabl. 4). Thus, we can conclude that the addition of fluorine to the silicate-carbonate system also promotes rare earth element extraction by salt melts.

Chloride-carbonate-silicate systems

The influence of chlorine on silicate-carbonate immiscibility was studied at T=1100°C and P=2 kbar by introduction of sodium chloride (NaCl) into the

systems [15]. The separation of chloride-carbonate liquids from silicate melts was observed in these systems. The salt phase form a layer in the upper portion of the sample and droplets in silicate melt. The salt liquid is compositionally heterogeneous and separates into chloride (NaCl with minor Ca and Mg) and carbonate fractions. The compositions of the phases are shown in Table 5. Rare earth elements, niobium and tantalum are predominantly accumulated in the silicate melt. However, there is a slight increase in the concentration of rare earth elements in carbonate phases in comparison with chloride ones. Thus, the presence of chlorine does not promote the extraction of ore elements by salt melts. Moreover, in alkaline systems at 1100°C the addition of chlorine results in the depletion of salt phases in rare earth elements, which are concentrated in the silicate melt. This is in contrast to rare earth elements extraction by carbonate liquids in pure silicate-carbonate systems.

Table 5. *Compositions of phases (wt %) in immiscible carbonate-silicate melt systems with chlorine. (I - silicate melt; II – chloride-carbonate phase; III - carbonate phase) T=1100°C, P=2 kbar.*

N	SiO_2	Al_2O_3	MgO	FeO	Na_2O	K_2O	CaO	Cl	La_2O_3	Ce_2O_3	Y_2O_3	Nb_2O_5	Ta_2O_5	Summa
I	40.21	0.81	10.73	0.22	15.05	0.11	13.51	1.22	0.64	1.44	-	2.26	1.16	87.36
1 II	0.25	0.01	1.70	0.01	29.23	0.16	18.82	13.90	0.12	0.18	-	0.02	0.22	64.62
III	0.35	0.04	2.62	0.02	24.03	0.20	16.73	1.34	0.16	0.41	-	0.09	0.23	46.22
I	31.57	3.57	1.94	0.03	9.01	0.11	22.13	1.54	2.52	2.73	-	3.93	4.19	83.27
2 II	0.91	0.10	0.33	0.00	18.46	0.12	34.82	10.19	0.00	0.11	-	0.00	0.01	65.05
III	0.59	0.15	0.24	0.08	22.08	0.16	28.42	0.90	0.54	0.49	-	0.00	0.10	53.75
I	50.84	5.70	8.84	0.21	9.79	0.06	11.05	1.35	1.15	1.41	-	2.21	1.88	94.49
3III	0.21	0.03	3.61	0.01	29.83	0.27	22.48	1.33	0.53	0.57	-	0.00	0.00	58.87
I	42.38	0.73	11.98	0.49	12.79	0.03	16.63	1.22	0.70	1.38	1.39	-	-	89.72
4 II	0.70	0.24	1.12	0.13	17.65	0.28	7.46	17.69	0.00	0.04	0.00	-	-	45.31
III	1.85	0.20	2.79	0.01	18.73	0.40	17.11	3.71	0.28	0.37	0.05	-	-	45.50
I	49.43	6.14	7.93	0.18	9.19	0.08	10.37	1.07	0.98	1.72	2.20	-	-	89.29
5 II	1.39	0.63	1.34	0.34	18.74	0.31	6.64	10.33	0.26	0.24	0.10	-	-	40.22
III	1.11	0.41	3.26	0.27	11.77	0.28	20.54	1.19	0.98	1.45	0.87	-	-	42.13

Note. *The phase of NaCl occurs in all experiments. The experimental samples were analyzed on a Camebax X-ray microanalyzer with an energy-dispersive system Link, IEM RAS, in 1998-2000.*

Sulfate-carbonate-silicate systems

Separation into silicate and salt phases was observed in the systems studied, and the salt phase has a sulfate-carbonate composition (Tabl. 2). In the potassium-rich systems, the silicate melt shows Na_2O/K_2O=0.41-0.44. Both in sodium-rich and potassium-rich systems, salt melts are enriched in barium and strontium, and their partition coefficients are again higher in the potassium-bearing systems. The salt melts are heterogeneous, which is manifested in the coexistence of phases enriched in calcium and sodium or sodium and potassium. More calcic phases show elevated contents of barium and strontium in comparison with alkaline richer phases, which are enriched in sulfur (Tabl. 2).

DISCUSSION

Since the pioneering studies of Wyllie and Tuttle [16], Koster van Groos and Wyllie [11, 12] and Freestone and Hamilton [8], a number of authors investigated liquid immiscibility in carbonate-silicate systems. This work revealed the role of carbon dioxide pressure, which stabilizes carbonate melts and expands the range of their immiscibility with silicate melts. The separation of carbonatite melts at high pressure was experimentally studied at P=5 kbar [10] and at P=15 kbar [2]. The comparison of previous experimental results with our experimental data suggests that the immiscibility field expands slightly at increasing pressure and decreasing temperature.

Our experimental results on REE partitioning between immiscible liquids in alkalic systems at T=1100^{o}C and P=2 kbar demonstrate the extraction of these elements by carbonate melts. This allows us to conclude that the carbonatite deposits of rare earth elements could be formed in connection with alkalic (agpaitic) magmatism only. The results on the partitioning of barium and strontium between immiscible phases in the systems studies are compatible with those revealed in natural carbonatite complexes, where barium--strontium ore occurrences are directly related to carbonatites, for example, in the Khalyutinskoe barium-strontium ore occurrence in western Transbaikalia [14], which is related to carbonatites enriched in sulfate sulfur.

The heterogeneity of carbonate and salt-carbonate (phosphate-, fluoride-, chloride- or sulfate-carbonate) liquids that was observed in the experimental products suggests the possibility of a further evolution of the salt phase after its separation from silicate melt. It can be supposed that the calcium-alkali separation of melts occurred in a liquid state or originated upon a temperature decrease. The alkaline-lime separation of carbonate melts probably played a certain role in the formation of carbonatites in intrusive ijolite-urtite complexes, where they are represented by calcite and dolomite types. During the emplacement of them alkaline carbonates probably migrated with fluids into the enclosing rocks, which were affected by alkaline metasomatism (fenitization). For instance, the sodium-bearing carbonate mineral burbankite was found in the carbonatites of the Khibinskii massif, which allows one to suggest the appearance of alkalic carbonate liquid at the final stages of the formation of the carbonatite complex in this massif [6]. In the Khalyutinskii ore occurrence, it has been reported [9] about the separation of carbonate melt into two phases, one of which contained phosphorus and fluorine and the other was represented by carbonate-sulfate melt. The concentrations of Ba, Sr, Ca, and sulfate sulfur showed positive correlations at the analysis of their distribution in calcic and alkalic carbonate phases.

The comparison of our experimental results with natural objects shows that the compositions of carbonate phases in experiments at the highest agpaitic coefficient of initial melt are corresponded to the compositions of the carbonatite lavas of Oldoinyo Lengai (Tanzania), and the compositions of silicate phases are comparable with silicate lavas and nephelinites from the same volcano [4, 5] and

urtites, ijolites and nephelinites from different carbonatite complexes [10]. In addition, the compositions of extrusive carbonatites of Oldoinyo Lengai volcano are comparable with lime fractions of the experimental carbonate phases. Calc-alkalic carbonate magmas chemically similar to experimental melts could retain their primary composition only in volcanic environments at a rapid eruption and quenching on the surface.

Our results on the partitioning of rare earth elements between silicate and carbonate phases at 1100^{o}C and 2 kbar in alkaline systems (partition coefficients are from 1.5 to 2.5) are consistent with the data on the rocks of natural carbonatite complexes. For example, similar estimates of REE partition coefficients were obtained from carbonatite droplets and lamprophyre from Callander Bay, Ontario (partition coefficients are 2-3) and carbonatites and coexisting ijolites (K=2.1) of Seabrook Lake, Ontario [3].

The results of investigation of phosphate-carbonate and fluoride-carbonate systems can be applied for the explanation of widespread apatite mineralization in carbonatite-type deposits.

Thus, our study supports the significance of silicate-carbonate liquid immiscibility in the formation of carbonatite deposits, distinguishing geochemical factors favorable or unfavorable for the development of mineralization, which must be taken into account at the construction of genetic models. Thus, the experimental systems studied can be regarded as a simplified model for the formation of ore-bearing carbonatite complexes associating with silicate igneous rocks of sodic and potassic series.

This study was financially supported by the Russian Foundation for Basic Research, projects №№ 97-05-64158, 99-05-64435 and 01-05-64839.

REFERENCES

1. **Andreeva I.A.** Silicate, silicate-salt and salt magmas of alkaline carbonatite-bearing complex Mushugai-Khuduk, Southen Mongoliya (data of melt inclusion investigation). Cand. Sci. (Geol) Dissertation, Moscow IGEM RAS. 2000. 27 p.
2. **Brooker R.A., Hamilton D.L.** Three-liquid immiscibility and the origin of carbonatite. Nature. V. 346. N. 6283. pp. 459-462.
3. **Cullers R.L., Medaric L.G.** Rare earth elements in carbonatite and cogenetic alkaline rocks: Examples from Seabrook Lake and Callander Bay, Ontario. Contrib. Mineral. Petrol. 1977. V. 65. pp. 143-153.
4. **Dawson J.B.** Sodium carbonate extrusions from Oldoinyo Lengai, Tanzania. Implications for carbonatite complex genesis. In “Carbonatites. Genesis and evolution”. Bell K.,Ed., London: Unwyn Hyman, 1989, pp. 255-277.
5. **Dawson J.B., Garson M.S. and Roberts B.** Altered former alkalic carbonatite lava from Oldoinyo Lengai, Tanzania: Inferences for calcite carbonatite lavas. Geology, 1987, V. 15, pp. 765-768.
6. **Dudkin O.B.** Geochemical regularities of Khibinskii massif carbonatites and their place in the sequence of similar formations. Geokhimiya. 2001. N 7. pp. 785-790.

7. **Entin A.R., Zaitsev A.I., Nenashev N.I., et.al.** On the sequence of geologic events connected with the emplacement of the Tomtor massif of alkaline ultramafic rocks and carbonatites. Geol. Geofiz. 1990. N 12. pp. 42-51.
8. **Freestone J.C., Hamilton D.L.** The role of liquid immiscibility in the genesis of carbonatites - An experimental study. Contrib. Mineral. Petrol. 1980. V. 73. N 3. P.105-117.
9. **Kobylkina O.V.** Regularities of quality composition and conditions of formation of barium-stroncium carbonatites in Khaluta ore occurrences. Cand. Sci. (Geol) Dissertation, Ulan-Ude GIN SO RAS. 2002 . 25 p.
10. **Kjarsgaard B.A., Hamilton D.L.** Liquid immiscibility and the origin of alkali-poor carbonatites. Miner. Magaz. 1988. V. 52. pp. 43-55.
11. **Koster van Groos A.F., Wyllie P.J.** Liquid immiscibility in the system Na_2O-Al_2O_3-SiO_2-CO_2 at pressures up to 1 kilobar. Amer. Jour. Sci. 1966. V. 264. pp. 234-255.
12. **Koster van Groos A.F., Wyllie P.J.** Liquid immiscibility in the join $NaAlSi_3O_8$-$CaAlSi_2O_8$-Na_2CO_3-H_2O. Amer. Jour. Sci. 1973. V. 273. pp. 465-487.
13. **Marakushev A.A., Suk N.I.** Carbonate-silicate magmatic layering and the genesis of carbonatites. Dokl. RAS. 1998. V.360. N 5. pp. 681-684.
14. **Ripp G.S., Kobylkina O.V., Doroshkevich A.G., Sharakshinov A.O.** Late-mezozoic carbonatites of western Transbaikalia. Ulan-Ude. Buryatskii Scientific Center SO RAS. 2000. 230 p.
15. **Suk N.I.** Experimental investigation of immiscibility of silicate-carbonate systems. Petrologiya. 2001. V. 9. N 5. pp. 547-558.
16. **Wyllie P.J., Tuttle O.F.** The system CaO-CO_2-H_2O and origin of carbonatites. Jour. Petrol. 1960. V. 1. pp. 1-46.

Chemical composition of carbonatites of Tamil Nadu massif (South India) and problem of "benstoonite" carbonatites

Vladykin N.V.[1], Viladkar S.G.[2], Miyazaki T.[3], Ram MohanV.[4]

[1]Institute of geochemistry SB RAS,Russia, Irkutsk-33, Box 4019, E-mail: vlad@igc.irk.ru
[2]Geology Department, St. Xavier's college, Mumbai 400 001, India, E-mail: viladkar@bom2.vsnl.net.in
[3]Gruate School of Science and Technology, Niigata University, Niigata 950-2181, Japan
[4]Department of Geology, University of Madras, Chennai 600 025, India

"Benstonite-Ba-Sr carbonatites are found only on two sites in the world: the Murun massif in Siberia and South India. The specific feature about those carbonatites is high BaO (20-35%) and SrO (to 10% in the Murun carbonatites) concentrations. They contain the following minerals: high-temperature Ba, Ca, Sr-carbonate benstonite (which decomposes into 12 mineral phases [8], K-Fsp, pyroxene and amphibole. We take "benstonite" in inverted commas, as the decomposed mineral has not been found in carbonatites. " Benstonite" carbonatites are natural ore for Ba and Sr found as carbonates. These carbonatites jointly with calcite varieties occur in K-alkaline complexes of Siberia and South India. However, carbonatites of South India and Siberia are different in terms of the chemical composition. In South India (Tamil Nadu area), carbonatites are found in three alkaline massifs: Samalpatti, Koratti, Elagiri. All carbonatite varieties (calcite, calcite-dolomite, dolomite, ankerite) occur here. "Benstonite" carbonatites are distributed only in the Samalpatti massif as a small dyke. In the Murun massif carbonatites are separated from the silicate rocks and occur as a residual silicate-carbonate complex. It comprises microclinites, pyroxene-microclines, quartz-microcline-pyroxene-calcites, which contain calcite carbonatites and charoite rocks as schleiren and dykes. Benstonite carbonatites form a horizontal body of 40 m thick in the southwestern part of the complex. Benstonite and calcite carbonatites of India and Siberia are different in terms of TR contents and TR spectrum. The data on Nd and Sr isotopes indicate that carbonatites of both areas formed from an enriched EM-1 source. The Indian carbonatites crystallized in the mesoabyssal part of the earth's crust, while Siberian ones formed in the near-surface area and effused on the Earth's surface.

INTRODUCTION

The "benstonite" carbonatites were firstly discovered in the South India (Tamil Nadu complex) by E. I. Semenov [7] as scarce occurrences. Similar carbonatites were found later in the ultra-potassium Murun massif as a large veined body up to 30 m thick [15]. That discovery allowed distinguishing a specific type

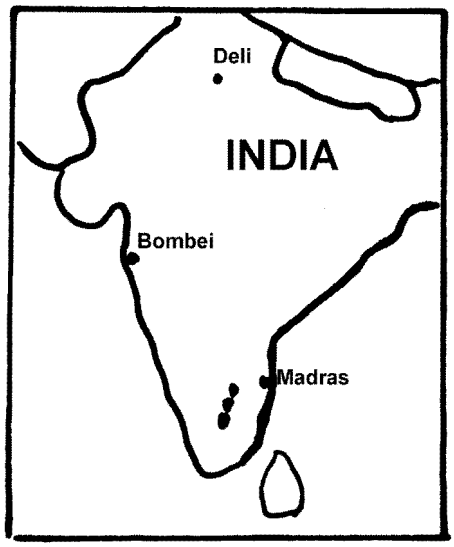

Fig.1. *Location of alkaline massifs of South India.*

of high-Ba and high-Sr carbonatites. These carbonatites formed jointly with unique charoite rocks: a residual silicate carbonate melt-fluid delaminated in the near-surface conditions of crystallization. We were hoping to find the charoite rocks together with "benstonite" carbonatites of South India. However, the studies of those carbonatites showed that they were crystallized from carbonatite magma differentiation at a greater depth. At present "benstonite" carbonatites in Russia find application in the steel industry, thus the present study is of great importance for the South India, as the steel factory in Salem city is located in 50 km away from those alkaline massifs.

GEOLOGIC STRUCTURE OF MASSIFS ALKALINE PROVINCE TAMIL NADU

The Proterozoic alkaline province Tamil Nadu in the South India (Fig.1) occurs in the rift zone and is located along a major northeast lineament [9]. The province includes main massifs (Elagiri, Samalpatti, Koratti) and smaller occurrences of alkaline rocks. The Proterozoic alkaline complex (720-800 Ma) [6] is emplaced within the gneiss terrain and cuts the Proterozoic gneisses. Massifs stretch as a chain from the northeast to southeast and are located at a distance of 10-25 km from each other. The northernmost massif is Elagiri.

Elagiri Massif

The massif (14 x 10 km) cuts biotite-amphibole gneisses (Fig.2). It mainly contains leucocratic syenites, in cases pegmatoid-like ones. Small pyroxenite and peridotite outcrops are found in the south. Shonkinite and pyroxenite dykes occur in the north near-contact part. Carbonatites are found in the center as a small outcrop.

Koratti Massif

The massif (22 x 10 km) stretches from the north to the south. The northwest site is sometimes described as a separate occurrence (Sevathur). The massif is composed mainly of different syenites (pyroxene, biotite, amphibole). The texture of rocks varies from porphyritic to coarse-grained leucocratic. The oldest rocks are pyroxenites, feld spar pyroxenites and biotite pyroxenites in the carbonatite occurrence. They occur in the west and south endocontacts as elongated bodies,

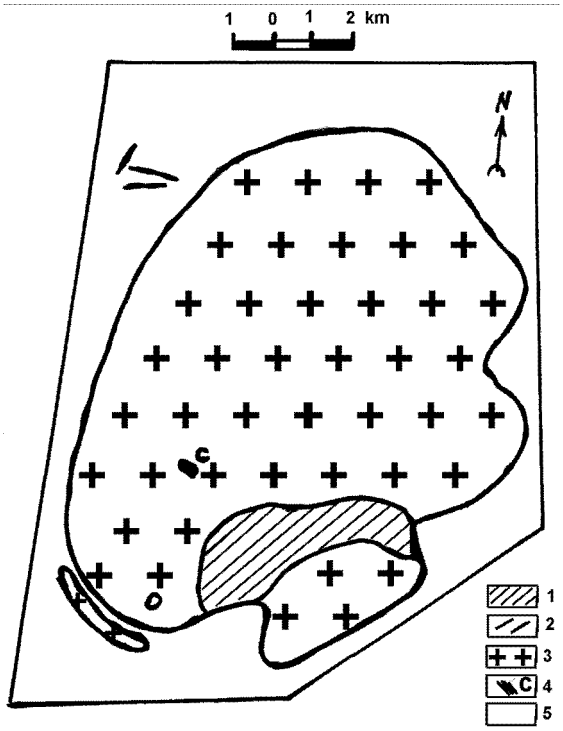

Fig. 2. *Geologic scheme of Elagiri massif:*

1-dunites, 2- pyroxenites, 3-pyroxenite dykes, 4- carbonatites, 5- hosting rocks.

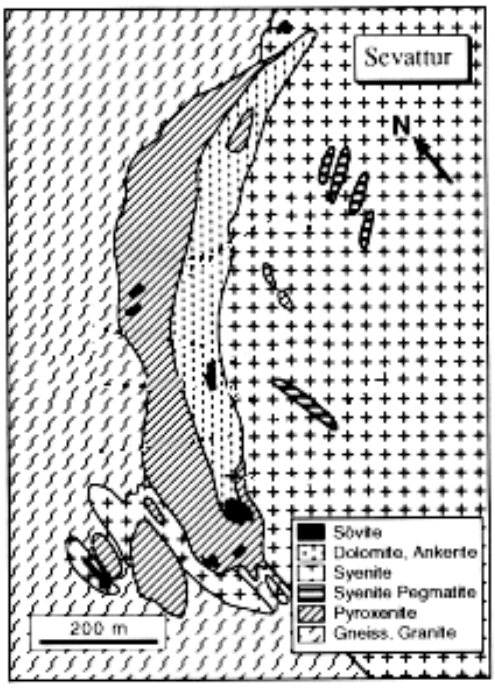

Fig. 3. *Geological scheme of Koratti massif (Sevathur site):*

1 - pyroxenites, 2- syenites, 3- carbonatites, 4- hosting rocks.

and are scarce in the center (Fig.3). Carbonatites are distributed in the north-west (Sevathur site) as a big body (100 x 800 m). The body includes dolomite and ankerite carbonatites with calcite carbonatite (sevites) occurrences. In the south of the Sevathur occurrence sevites form separate bodies in pyroxenites. The biotite pyroxenites are abundant in the carbonatite occurrence.

Samalpatti Massif

It is the most differentiated massif of Tamil Nadu alkaline province. The massif is 20 x 12 km in size, it slightly elongates from the north-east to south-west. It cuts amphibole gneisses. The most ancient rocks include altered dunites and peridotites. These rocks occur as large relics in pyroxenites in the southeast and west. Pyroxenites compose 1/3 of the massif. They are found as a semi-ring in the west, south and east (Fig.4). Syenites (alkaline and nepheline) are distributed in the central part and occupy 2/3 of the massif's area. In the south-west nepheline syenites are enriched in garnet and pectolite. The dyke of alkaline granite-pegmatites with alkaline amphibole and quartz cuts the nepheline syenites. Pyroxenites of the north part contain syenite-pegmatites dykes. Carbonatites occur in different parts of the massif. They have specific names. Benstonite carbonatites are found in the east [7,9]. They are emplaced within syenites (Gorgipatti) as a block pile of stones in the garden (the Indian geologists say that they form a small

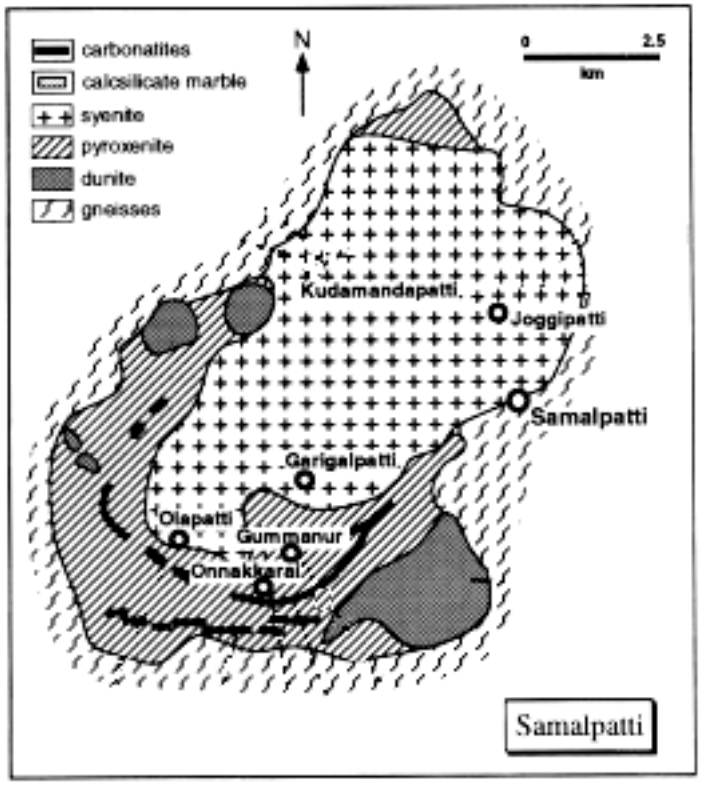

Fig. 4. *Geological scheme of Samalpatti massif*

1-Dunites, peridotites, 2- pyroxenites, 3- syenites, 4-syenite-pegmatites, 5- carbonatites (C), benstonite carbonatites (CB), 6- hosting rocks.

Fig.5. *Photo of carbonatite breccia.*

dyke). A bedrock outcrop of marbles (2x 3 m), containing blue calcite, garnet, wollastonite is found close by. Similar scarnoids occur on the contact of syenites and marbles in the northern part (Table 3, analyses N 40-47). The south part of the massif contains bedrock outcrops of carbonatite breccia (Fig. 5) composed of syenite xenoliths cemented by sevites. Another carbonatite dyke of calcite composition is found as well. The central part of this dyke contains large dolomite phenocrysts (to 2 cm). This carbonatite is crossed by finer-grained carbonatite of the ankerite composition. The massif's western part contains carbonatite dykes, enriched in alkaline amphibole and biotite (to 40-50%). Pyroxenites are cut by veined albitite bodies. So, alkaline massifs of Tamil Nadu are significantly different from the magmatism of the Murun volcanic-plutonic complex [12,14,15].

GEOLOGY AND MAGMATISM OF THE MURUN-MASSIF

The Murun volcanic-plutonic complex is localized in the northeast of the Irkutsk Region, this is the largest alkaline massif in the West Aldan province. Space surveys have revealed a circular structure in the pluton area. The complex includes two exposures of the Murun Massif the Bol'shoi (Large) Murun and Malyi (Small) Murun Massifs, separated by a short bulkhead of country rocks, and a few small trachyte outcrops at the northern, western, and southern exocontacts of the massif. The intrusion of the complex proceeded at the intersection of two regional faults of Precambrian age during the Mesozoic magmatic activity. The complex is 150 km^2 in area. Its western part is made up of K-Na-nepheline, alkaline, and quartz syenites of the Bol'shoi Murun Massif, and its eastern part, of ultrapotassic rocks of the Malyi Murun Massif. Below, we will discuss the Malyi Murun exposure of the Murun volcanoplutonic complex, dated to 145-120 Ma [4]. There are virtually no bedrocks in the Malyi Murun Massif. At the same time, there are serious hydrothermal transformations in abundant tectonic zones as well as surficial weathering and intense horizontal layering of rocks. Therefore, it is impossible to reliably depict the massif structure on a geological map. This structure is schematically shown in Fig. 6. We comprehensively studied the cores from more than 100 boreholes (both new and earlier studied) and proposed a scheme of magmatism that proceeded in the Malyi Murun Massif [10,12,14].

The early phase makes up the northeastern part of the massif (the so-called Mart geophysical anomaly). It includes the following rocks:

(1) Cumulose formations: olivine-spinel rock segregations with zones of melilite-bearing olivine-pyroxene-phlogopite-monticellite rocks, which occur as xenoliths in biotite pyroxenites. According to data of thermobarogeochemical studies [2], these rocks underwent crystallization at T = 1500-1200C. It is not ruled out that the olivine-spinel rocks are mantle xenoliths.

(2) Layered complex of ultrabasic ultrapotassic rocks composed of Bt-pyroxenites (Ap + Bt + Py), olivine lamproites (Ol + Bt + Py + Psdlc + Fsp), K-ijolites (Gr + Bt + Py + Ks), leucitic fergusites (Psdlc + Bt + Py), and shonkinites (Fsp + Bt + Py). (Designations: Ap - apatite, Bt - biotite, Py - pyroxene, Ol - olivine, Psdlc -pseudoleucite, Fsp - K-feldspar, Gr - garnet, Ks - kalsilite.)

The major phase occupies the central part of the massif. It is made up of a horizontally layered complex of various pseudoleucitic, Fsp-kalsilitic, and Bt-Py-bearing K-feldspathic syenites, whose crystallization terminated in the formation of quartz syenites and dykes and stocks of alkali granites. The pseudoleucitic syenites (synnyrites) in the northeast of the massif form a large body no less than 600 m in thickness.

The volcanic phase composes the central and northern parts of the massif. This is a layered flow of leucitic melaphonolites, leucitites, and leucitic lamproites [13] with zones of their tufflavas and tuff breccias. The dyke complex of this phase is formed by leucitic tinguaites, richterite-sanidine lamproites,

trachyte-porphyries, syenite-porphyries, and eudialyte lujavrites. The effused volcanic phase might be

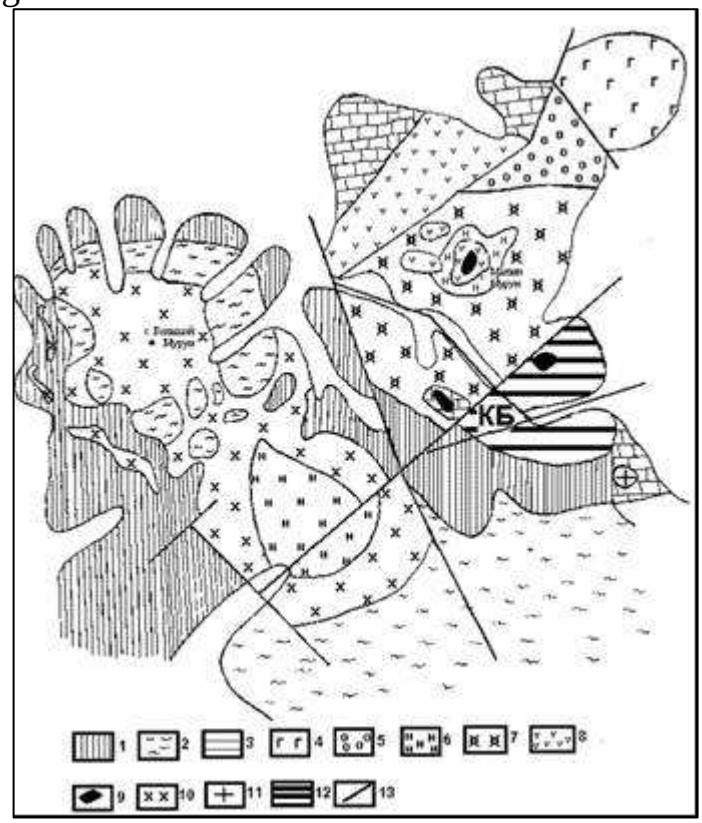

Fig. 6. *Schematic geologic structure of the Murun Massif.*

Country rocks: 1 *– Archean granite-gneisses,* 2 *– Proterozoic quartz sandstones,* 3 *– dolomites. Intrusive rocks:* 4 *– layered complex of Bt-pyroxenites,* 5 *– pseudoleucitic syenites,* 6 *– nephelite syenites,* 7 *– alkali syenite,* 8 *– effusive complex of leucite and sanidine lamproites,* 9 *– aegirinites,* 10 *– alkali and quartz syenites,* 11 *– alkali granites,* 12 *– rocks of the charoite complex,* 13 *– faults, BC – site of occurrence of "benstonite" carbonatites.*

the upper part of a volcanoplutonic complex whose block is subsided along the faults to the hypsometric level of the major phase, which crystallized in magma chamber. This is suggested from the similar petrochemical characteristics of rocks of the volcanic and intrusive phases.

The late phase crystallized from a residual fluxed melt. It occupies the southeastern part of the massif, 10 km^2 in area, and is made up of a banded layered complex of potassic silicate-carbonate rocks which form 1 to 20-30 m wide bands [10,12,14]:

(1) white microgranular K-feldspathic rocks consisting of K-feldspar with minor admixtures of pyroxene and tinaksite;

(2) quartz-calcite-pyroxene-microcline rocks with calcite contents varying from 5 to 20%;

(3) pyroxene-K-feldspathic rocks with widely varying contents of both components. The rocks have diverse structures and textures: banded, spherolitic (for pyroxene), equigranular, fine- and coarse-grained, etc.;

(4) essentially pyroxene rocks, which seem to be a specific case of the previous rocks enriched in pyroxene.

This layered banded substrate contains carbonatites and charoite (silicate) rocks, which are represented by veined bodies - dykes, veins, sill-like formations (horizontal dykes), and schlieric bodies having no sharp contacts with the silicate-carbonate rocks. The latter form a block subsided relative to the major-phase rocks along the feathering faults.

In tectonic zones and fractures, all the above rocks were subjected to intense sulfidization and quartzing at the hydrothermal stage of the massif formation. The hydrothermal processes gave rise to all Cu, Au, Ag, U, Th, Mo, Pb, Nb, and Ti shows (in bornite, thorite, galenite, sphalerite, molybdenite, brookite, etc.)

The chemical composition of silicate rocks of the Murun Massif is given in (tabl. 1). The petrochemical and geochemical characteristics of the massif rocks are presented in Fig.7,8. As seen from the binary and ternary correlation diagrams of petrochemical components, there is a single composition trend for all rocks, i.e., the rocks of the complex are homodromous. We have first discovered a complete series of differentiates in the potassic rocks from ultrabasic-alkaline through basic and normal to acid ones (alkali granites). This series is the result of differentiation processes and magmatic segregation, which are widely developed in all rocks of the complex [12,14]. The intense differentiation was favored by a broad temperature range (1500-700C) in which crystallization from early to late phase took place [2]. Study of the composition of melt inclusions in the early rocks [3] showed that the parental magmas from which the rocks crystallized correspond to basaltoids and are similar to lamproitic magmas. The geochemistry of Sr, Nd, O, C, and Pb isotopes [12] testifies to a deep-level mantle source of matter for the magma that gave rise to the Murun rock complex.

CARBONATITE OCCURRENCES OF THE MALYI MURUN MASSIF

The compositional spectrum of the massif carbonatites is rather diverse but is limited to K-series. We have recognized six varieties of these rocks [12,15]:

1. Calcite carbonatites, the most widespread variety. They are present at all sites of silicate-carbonate rocks but the Yuzhnyi (Southern) one, where only “benstonite” carbonatites have been found. Calcite carbonatites occur as elongate (3 x 10 m) schlieren in silicate-carbonate rocks (Korennoi site) as well as veins and horizontal bodies 1 to 30 m thick and up to 1 km long. The carbonatites are composed of calcite, K-feldspar, pyroxene, and, in smaller amounts, quartz. The secondary and accessory minerals are charoite, pectolite, tinaksite, thorite, dellaite, sulfides, etc. Also, all compositions intermediate between calcite and charoite rocks occur.

Table 1. *Chemical Composition of Silicate Rocks of the Murun Massif (wt.%.)*

№	1	2	3	4	5	6	7	8	9	10	11	12	13	14
SiO2	40.80	45.60	43.06	44.07	42.76	48.95	48.93	55.55	52.10	57.83	61.84	82.59	53.96	47.44
TiO2	0.08	0.56	0.74	1.05	0.82	0.60	0.53	0.56	1.60	0.25	0.14	0.41	0.81	1.34
Al2O3	0.97	4.55	6.40	6.26	10.32	9.77	10.69	16.10	11.10	16.38	18.05	5.46	14.80	9.63
Fe2O3	3.68	3.73	3.52	6.03	3.15	4.04	4.43	4.60	6.62	3.98	1.24	2.81	3.91	8.10
FeO	4.52	1.65	3.41	4.50	5.74	2.12	4.04	2.15	5.28	0.90	0.90	0.54	3.69	4.10
MnO	0.26	0.07	0.10	0.15	0.17	0.06	0.14	0.08	0.19	0.07	0.02	0.01	0.15	0.17
MgO	45.13	20.29	13.04	16.78	14.37	10.65	9.33	0.80	3.40	0.85	0.19	0.62	1.79	6.45
CaO	2.62	19.47	15.85	9.89	12.21	11.31	8.26	3.30	5.00	2.08	0.39	0.61	4.30	3.81
BaO	0.13	0.34	0.12	0.11	0.87	0.19	0.35	0.34	0.76	0.81	1.07	0.01	0.33	1.43
SrO	0.01	0.03	0.40	0.20	0.03	0.19	0.22	0.18	0.17	0.07	0.06	0.04	0.21	0.21
K2O	0.62	2.54	5.84	6.20	6.84	8.65	9.02	14.22	9.96	14.29	15.19	5.12	10.73	8.86
Na2O	0.03	0.10	0.40	1.11	0.45	0.73	0.80	0.31	1.66	1.03	0.30	1.41	0.28	3.16
P2O5	0.01	0.02	4.06	1.47	0.04	1.62	1.07	0.02	0.04	0.04	0.01	0.15	0.26	1.90
H2O	0.99	0.18	2.82	1.13	1.50	1.45	1.40	1.40	1.60	0.98	0.77	0.12	0.96	2.20
CO2	0.31	1.03	0.30	0.44	0.30	0.00	0.26	0.10	0.00	0.20	0.10	0.40	3.15	1.45
F	0.05	0.10	0.70	0.12	0.5	0.40	0.30	0.20	0.02	0.04	0.05	0.20	0.21	0.90
Total	100.18	100.22	100.46	99.46	99.86	100.06	99.64	99.83	99.49	99.78	100.30	100.42	99.46	100.25

Note. *Early phase: 1 – olivine-spinel xenoliths, 2 – olivine-monticellite-phlogopite-pyroxene rocks, 3 – biotite pyroxenite, 4 – olivine lamproite, 5 – kalsilitic ijolite, 6 – leucitic fergisute, 7 – K-feldspar-shonkinite. Major phase: 8 – leucitic syenite, 9 – Bt-Py-Fsp-syenite, 10 – Ks-Fsp-syenite, 11 – Fsp-syenite, 12 – alkali granite. Effusive phase: 13 – leucitic phonolite, 14 – leucitic lamproite. Data were obtained by chemical analysis (analyst L.N. Matveeva, Institute of Geochemistry, Irkutsk, 1985-95).*

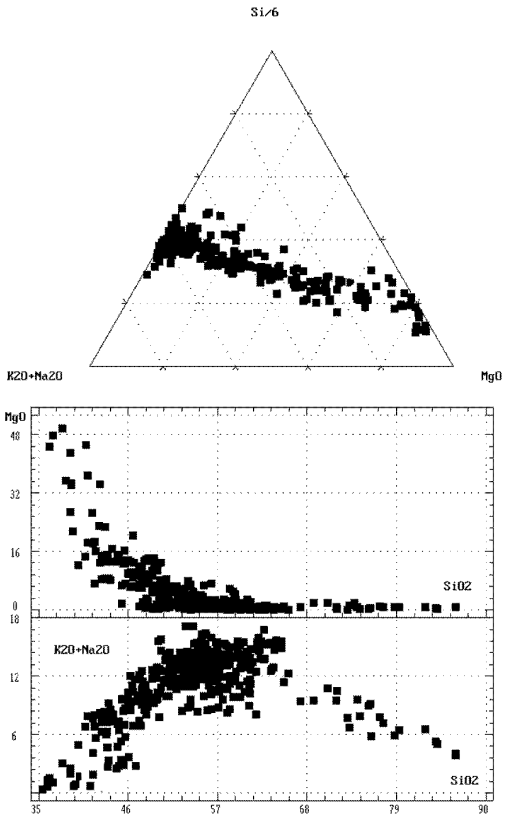

Fig. 7. *Binary and ternary correlation diagrams for rock-forming elements of the Murun Massif. Silicates (wt.%).*

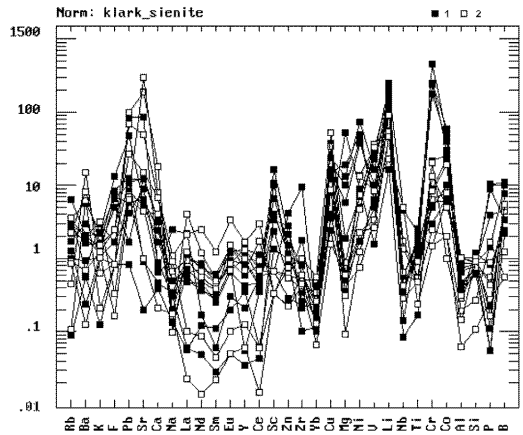

Fig. 8. *Spectra of major and trace elements in the Murun Massif rocks (normalized by clarke in syenites).*

1 – silicate rocks, 2 – silicate-carbonate rocks of the charoite complex. Elements are arranged in order of increasing ionic radius.

2. "Benstonite" carbonatites, next in abundance after calcite varieties. These carbonatites have been found in a large amount at the Yuzhnyi site only, where they form a large 30 m thick body. They consist of "benstonite", pyroxene, K-feldspar, and, occasionally, K-richterite. The secondary and accessory minerals re

quartz, charoite, sphene, wadeite, sulfides, and, rarely, apatite. These carbonatites will be considered in detail below. No intermediates between calcite and "benstonite" carbonatites have been found in the body.

3. Calcite veins with quartz-benstonite core and calcite-benstonite carbonatites of the stockwork zone. They form a 2 m thick and 10 m long veined body at the Korennoi site. The body is made up of calcite, tinaksite, pyroxene, K-feldspar, and quartz. In the vein core, it gives way to macroblock quartz with large "benstonite" crystals up to 10 cm in size. In places, these intergrowths look like graphic. The thickness of the quartz core is about 20 cm. The stockwork zone of calcite-"benstonite" carbonatites has been discovered 500 m east of the Korennoi site, in the core from BH-107 drilled at the Andreevskii site at a depth of 20<196>60 m. Alkali syenites are cut by abundant meeting 1<196>10 cm wide veinlets of leucocratic carbonatite. The carbonatites are composed of calcite, "benstonite", and K-feldspar. In places pyroxene occurs. The thickest veinlets have a chill zone made up of an extremely fine-grained microcline-"benstonite" aggregate.

4. Carbonatite veins composed of graphic quartz-calcite intergrowths. The major minerals are quartz and calcite, which form graphic intergrowths throughout the carbonatite body. They can be both coarse- and fine-grained. Sometimes, rounded quartz-calcite aggregates occur in the calcite mass. The secondary minerals are pyroxene, K-feldspar, richterite, sphene, and sulfides (the latter are present in a large amount). These carbonatites are widespread in the silicate-carbonate rock complex and cut the older calcite carbonatites.

5. Calcite carbonatites with lepidomelane and magnetite. These varieties have been found as veinlets up to 20 cm thick in syenites of the core from BH-107. The veinlets are composed of fine-grained calcite and larger lepidomelane and magnetite segregations. Some of them contain fluorite (up to 20%).

6. Pyroxene-phlogopite-calcite carbonatites have been discovered in country rocks at the southern exocontact of the Murun Massif, in the cores from BH-1026 and BH-1052. They consist of foliated calcite imparting a trachytoid texture to the rocks as well as pyroxene, tetraferriphlogopite, and quartz. The accessory minerals are apatite, brown zircon, and ilmenite (geikielite). The 20-30 m thick carbonatite body cuts the host gneisses. In the upper part, it gives way to an eruptive breccia of rounded tetraferriphlogopite-K-feldspar "xenoliths" cemented with calcite aggregate.

All the above carbonatite varieties are concentrated in the southeast of the massif (the area of the charoite deposit) in the silicate-carbonate rock complex and around it. Moreover, in the northeast of the massif, in the Mart anomaly region, we have discovered a large block of charoite-calcite rocks having no analogs among the rocks of the carbonatite complex; the cores from some boreholes here contain small veinlets of calcite and calcite-barite carbonatites. Note that calcite-

tetraferriphlogopite-K-richterite rocks are also considered carbonatites by some researchers Others [4] assign these rocks to skarns developed after dolomites of the roof pendant of the massif above the silicate-carbonate rock complex. Despite the great thickness of the rocks (more than 400 m along the core), they are persistent in composition and are characterized by fine banding (monomineral bands of K-richterite-asbestos and tetraferriphlogopite) and lack of less altered dolomite relics. Perhaps, these rocks might be considered metasomatic carbonatites(?) as they differ little from carbonatites in mineral and trace-element compositions.

GEOLOGIC OCCURRENCE OF "BENSTONITE" BA-SR-CARBONATITES MURUN MASSIF

In the earlier works, "benstonite" carbonatites found in deluvial rock debris were described, and the structure of the carbonatite body itself was interpolated in depth in different ways. The geologic occurrence of carbonatites was revised after examining the cores from six boreholes drilled by a Sosnovgeologiya Enterprise team under the supervision of I.I. Tsaruk in 1993. Both the parameters of the body itself and the specifics of its internal structure were studied [15].

"Benstonite" carbonatites are the oldest members of the Malyi Murun carbonatite family. They have been found solely at the Yuzhnyi site in the western part of the silicate-carbonate (charoite-carbonatite) rock occurrence. They also occur in small amounts in other types of Murun carbonatites (see the description of carbonatites above). Carbonatites make up a horizontal sill-like dyke body that intruded along the contact between quartz sandstones (base) and older pyroxene-feldspathic rocks (roof) of the silicate-carbonate phase of the charoite-carbonatite complex (fenites, according to [4]). The latter rocks are strongly crushed, cemented with carbonatite matter, and cut by small carbonatite tongues branching off the body. The carbonatite body reaches 30 m in thickness (Fig. 9). Its horizontal bedding with a distinct rhythmic layering of carbonatites into leucocratic and melanocratic bands is in conformity with the horizontal dips and strikes of the most abundant calcite carbonatites. In the west and in the east, the body is cut by later tectonic zones and appears to be subsided, judging from the outcrops of quartz sandstones at its base. Analogous sandstones also occur at a hypsometrically higher level and are a host-rock bulkhead between the Bol'shoi Murun and Malyi Murun Massifs west of the Yuzhnyi site. In addition to pyroxene-feldspathic rock xenoliths, the near-roof part of the carbonatite body bears fine and coarse sill clastics of richterite-sanidine lamproites and quartz sandstone relics. The carbonatite body itself is brecciated by a large tectonic zone (and is subjected to quartzing. The small carbonatite outcrop is cut by fine veinlets of charoite rocks.

The internal structure of the carbonatite body is rather intricate and cannot be shown schematically. The body consists of rhythmically alternating horizontal beds of differently melanocratic rocks and their blocks. The major rock-forming minerals here are white-gray microcline, dark-green pyroxene, and light-yellow

disintegrated benstonite. The bands (rhythms) are composed of one or two minerals. These are most commonly microcline, microcline-"benstonite", pyroxene, and pyroxene-"benstonite" beds with a thickness of 2-5 cm and, locally,

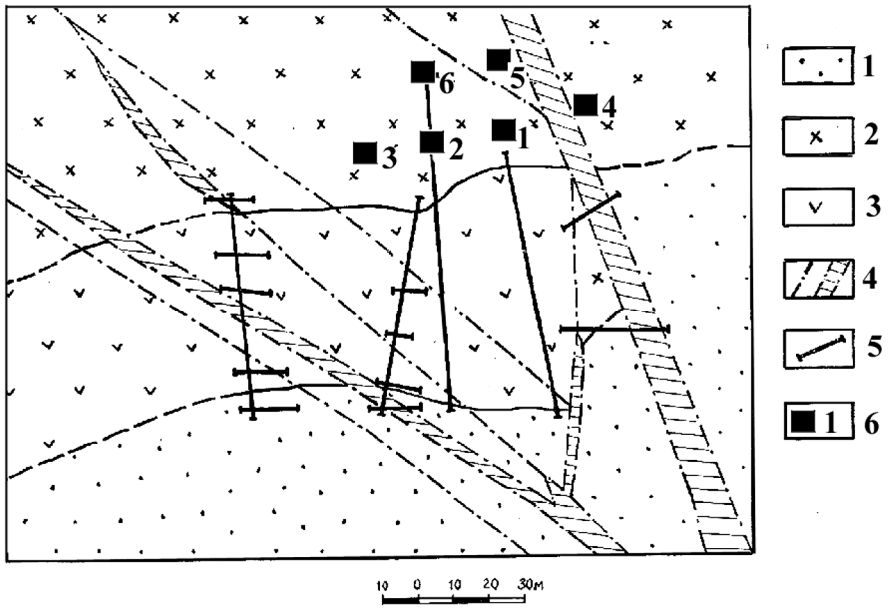

Fig. 9. *Schematic structure of the site of "benstonite" carbonatite occurrence.*

1 – quartz sandstones, 2 – Fsp-Py rocks of the charoite complex, 3 – "besntonite" carbonatites, 4 – faults (a) and tectonic crush zones (b), 5 – ditches, 6 – locality and number of borehole.

up to 50 cm. The size and morphology of the beds can be estimated from the photo in Fig. 6 showing bands of rounded microcline grains (white), aggregates of pyroxene crystals and their spherolites (black), and the groundmass of disintegrated benstonite (gray) hosting microcline and pyroxene bands and their segregations. The left sample in Fig. 6 contains only large microcline crystal aggregates in the "benstonite" mass. The section of the carbonatite body includes up to 100-150 beds of different compositions. The microcline intercalations are composed of faceted crystals 0.5-1 cm in size and their aggregates which form 1-2 cm bands in the "benstonite" mass. The crystals and their fragments are evenly dispersed in the carbonate substance. The pyroxene intercalations consist of ingrown aggregates of elongate crystals that form incomplete "suns". There are also bands formed by sticked complete spherolites of pyroxene composition. The bands are 1 to 10 cm thick. These intercalations and bands also occur in the e "benstonite" mass. Moreover, the latter contains bands consisting of "benstonite" only, which sometimes reach 20-30 cm in thickness. Sphene segregations are most often localized among pyroxene accumulations, and wadeite occurs as grains in the carbonate mass. The silicate-to-carbonate ratio in the carbonatites varies within a small site from 5 to 95%. Silicate minerals crystallize somewhat earlier than carbonate ones and therefore often form faceted crystals and their aggregates. The real structure of the body is difficult to depict because of the small sizes of the bands, but we can evaluate the relative quantities of microcline, pyroxene, and

carbonate, which shows variations in concentrations of Ba, Sr, K, and Na in the recognized blocks of the carbonatite body. As K is concentrated mainly in microcline, Na in pyroxene, and Ba and Sr in disintegrated benstonite, the contents of these elements can provide information on the amounts of the minerals.

CHEMICAL COMPOSITION OF BA-SR-ORE - "BENSTONITE" CARBONATITES

The Ba-Sr-ore is represented by a horizontally striking veined body of "benstonite" carbonatite up to 30 m thick and 1 km long. It is exposed by six boreholes to a depth of 40 m. The orebody has sharp contacts with the host rocks: with quartz sandstones in the base and with microcline-pyroxene rocks of the charoite complex in the roof. It is subjected to magmatic segregation and consists of bands of "benstonite", "benstonite"-microcline, and pyroxene-microcline-"benstonite" compositions. In places, nearly monomineral (pyroxene and microcline) bands 2 to 10 cm in thickness occur. The section of the body contains more than a hundred bands of variable composition; therefore, on mapping boreholes, blocks were recognized by a predominant leucocratic or melanocratic component.

The major rock-forming minerals in the ore are "benstonite", microcline, and pyroxene.

According to chemical composition (Table 2, № 33), "benstonite" is Ba,Sr,Ca-carbonate disintegrated into several carbonate phases: barytocalcite, calcite, strontianite, and, to a lesser degree, barite [8].

Microcline is represented by its potassic variety only, which is specific for all feldspars of the massif. Sometimes, microclines from "benstonite" carbonatites have elevated contents of BaO up to 1-2%, which may be due to the presence of "benstonite" microinclusions. Pyroxene of persistent composition contains 50% aegirine (Na-Fe), 25% diopside (Ca-Mg), and 25% hedenbergite (Ca-Fe) end-members.

The chemical composition of carbonatites is given in Table 2. All its variations depend on the content of the above three major minerals. Runs 151 and 157 for 30 kg samples characterize the average compositions of the major carbonatite varieties - leucocratic and melanocratic, run 33 is the analysis of pure "benstonite", and run 143 is analytical data for calcite carbonatite given for comparison. The other runs characterize samples of differently melanocratic rocks from different parts of the carbonatite body. They were carried out for carbonatites from the borehole cores (the numerator shows the borehole number, and the denominator, the depth of sampling). Analyzing a sample of 180 runs, we have revealed a distinct direct correlation between Ba and Sr concentrations. This also confirms that "benstonite" is the major carrier of Ba and Sr in the carbonatite and indicates stable crystallization conditions expressed as constant concentrations of Ba and Sr in the mineral despite the disintegration of the initial benstonite. Runs 4/47a and 44/31a revealed fine veinlet tongues in the above-carbonatite host rocks.

The elevated Si and Ti contents in the tongue carbonatites evidence a predominance of microcline, tinaxite, and, to a lesser degree, "benstonite" silicates

Table 2. *Chemical Composition of «Benstonite» Carbonatites (wt.%) of the Murun*

Component	151	157	141/3	141/8	3/15	1/30	6/32	1/33
SiO2	28.90	16.55	31.92	9.07	37.64	36.82	32.87	30.08
TiO2	0.64	0.28	0.30	0.08	0.24	0.47	0.66	0.42
Al2O3	1.00	3.20	1.90	2.10	3.93	2.94	2.07	2.65
Fe2O3	8.98	1.39	7.10	0.26	7.69	9.85	10.43	8.22
FeO	2.87	0.72	3.02	0.10	2.96	2.87	2.60	1.98
MnO	0.22	0.05	0.22	0.03	0.22	0.22	0.22	0.18
MgO	1.33	0.41	3.11	0.01	2.35	1.82	1.56	1.29
CaO	15.67	20.10	17.49	21.12	14.15	12.59	14.46	14.25
BaO	15.96	23.80	13.72	29.40	10.85	11.77	14.09	16.98
SrO	3.76	5.93	3.18	7.23	2.60	3.27	3.43	4.45
K2O	1.11	3.06	1.85	1.90	3.93	2.91	1.93	2.67
Na2O	3.86	0.51	2.75	0.35	2.73	3.66	3.65	3.04
F	0.02	0.10	0.01	0.01	0.05	0.07	0.05	0.10
CO2	15.24	23.42	12.88	28.35	10.68	10.12	10.79	13.46
P2O5	0.07	0.30	0.56	0.10	0.23	0.74	0.76	0.38
S	0.12	0.23	0.11	0.12	0.10	0.15	0.11	0.12
Total	99.75	100.05	100.12	100.23	100.20	100.27	100.33	100.27

Component	4/47a	4/31a	3/30	3/20	2/20	1/10	33	143
SiO2	62.19	55.00	26.27	22.46	16.19	6.02	0.21	6.83
TiO2	1.15	1.69	0.22	0.30	0.88	0.20	0.15	0.14
Al2O3	2.33	2.80	4.09	4.10	2.35	0.88	0.22	1.03
Fe2O3	4.49	5.94	4.31	2.96	2.50	0.49	0.12	0.74
FeO	0.27	0.45	1.17	0.63	1.00	0.10	0.12	0.50
MnO	0.22	0.23	0.10	0.06	0.06	0.03	0.07	0.10
MgO	1.33	1.28	0.91	0.85	0.89	0.28	0.14	0.09
CaO	6.65	6.87	15.36	16.19	19.54	21.67	28.16	46.86
BaO	7.38	8.54	19.99	23.03	26.67	33.29	37.00	1.06
SrO	1.77	2.17	5.61	6.52	7.11	10.99	9.57	3.94
K2O	3.38	3.80	4.17	3.91	2.19	0.84	0.14	1.01
Na2O	1.95	2.43	1.49	0.93	0.87	0.37	0.37	0.34
F	0.02	0.03	0.05	0.10	0.12	0.15	0.01	0.04
CO2	6.59	8.22	15.67	17.51	19.36	19.89	23.96	36.97
P2O5	0.57	0.05	0.44	0.60	0.65	4.29	0.03	0.05
S	0.20	0.25	0.16	0.08	0.10	0.10	0.10	0.10
Total	100.49	99.69	100.43	100.17	100.48	99.41	100.25	99.80

Note. *Averaged samples (20 kg) of Ba-Sr-carbonatites: 151 – melanocratic, 157 – leucocratic. Ore lump samples: 141/3 – melanocratic carbonatite, 141/8 – leucocratic carbonatite, 33 – pure "benstonite"; 143 – calcite carbonatite; other samples: numerator – borehole number, denominator – depth of sampling, m; 4/47a and 4/31a – silicate-carbonate rocks from fine veinlets (tongues from "benstonite" carbonatites). Data of chemical and photometric analyses (analysts L.N. Matveeva and A.L. Finkel'shtein, Institute of Geochemistry, Irkutsk, 1990-95). The total of components is given without conversion to F and S.*

in them. Such constant high concentrations of Ba and Sr in carbonate form were not earlier found in other carbonatites; therefore, it is reasonable to separate "benstonite" carbonatites into an individual type of carbonate rocks.

As for trace elements the Ba-Sr-carbonatites are rich in V and Cu, which occur in sulfide form. The concentrations of these elements exceed those in the calcite carbonatites (run 143). The "benstonite" carbonatites have low concentrations of typical elements Nb, Ta, Zr, and Hf (ppm): Nb = 5-10, Ta << 1, Zr = 165-300, and Hf = 2.5-3.6 (data of chemical-spectral analysis after the element concentration). The calcite carbonatites are also poor in these elements: Nb = 5, Ta << 1, Zr = 115, and Hf = 1.3.

The spectrum TR is dominated by LREE. A minor fractionation of Eu is observed, which is due to the predominance of layering processes over crystallization differentiation of mineral phases. The REE patterns of barium-strontium and calcite carbonatites differ insignificantly. In general, "benstonite" carbonatites are a unique natural Ba-Sr-carbonate ore that can be used without dressing for oreing down in steel industry.

CHEMICAL AND MINERAL COMPOSITION OF SOUTH INDIAN CARBONATITES

Calcite,calcite-dolomite, dolomite, ankerite and ore types of "benstonite" carbonatites are found in Tamil Nadu (South India).The ore variety is distributed in the Murun massif as well [15].

The chemical composition of 'benstonite" Ba-Sr-Ca carbonatites is given in Table 3. As the crystallization temperature of "benstonite" is high (840-650oC) [5,11]when the rock cools down the mineral is decomposed into several (to 12) phases [8]. The primary non-decomposed "benstonite" is not available in these carbonatites. Thus, we take the name of carbonatites as benstonites in inverted commas. The hydrothermal benstonite from Arkansas [1] contains 1.7% of MgO and only 4% of SrO. The "benstonites" of India and Murun massif doesn't contain any MgO. The Murun and Indian "benstonites" are different in terms of SrO and TR2O3 concentrations. The Indian mineral contains up to 1.8% of SrO and 4.5% of Tr2O3, while carbonatites proper exhibit from 1 to 3.5% of TR2O3 (table 3) and from 0.2 to 1.3% of SrO. The bulk composition of the "Murun" benstonite" (Table 1, analysis N 33) shows 10 % of SrO and no TR2O3.

BaO and SrO contents vary significantly depending on abundances of microcline and pyroxene (diopside-egirine-hedenbergite)in "benstonite" carbonatites. However, there is a clear linear correlation between Ba and Sr [15]. BaO concentrations in Murun microcline are insignificant (to 0.5%). A clear correlation between Ba and Sr in carbonatites indicated that the main concentrator of these elements is "benstonite". Indian "benstonite" carbonatites don't exhibit

a

Table 3. Chemical Composition in Carbonatites Tamil Nadu (wt.%)

	1	2	3	4	5	6	7	8	9	10	11	12	13	14	15	16
SiO_2	0,54	0,07	0,07	1,29	12,15	7,59	2,66	2,46	1,22	0,15	20,47	5,89	6,48	8,77	11,02	9,74
TiO_2	1,64	0,02	0,04	0,66	0,41	1,24	0,32	1,2	0,07	0,21	1,65	2,32	0,71	0,42	2,99	0,19
Al_2O_3					1,85	1,59	0,3		0,3		4,88	1,51	0,85	1,75	2,87	1,34
Fe_2O_3	17,46	0,51	0,63	8,73	2,73	6,67	2,54	2,13	0,84	1,62	9,65	15,18	5,85	5,41	17,82	1,71
FeO	6,71	0,72	3,13	3,13	1,8	3,59	0,99	2,07	0,1	1,7	6,96	7,45	1,98	2,69	11,01	1,26
MnO	0,26	0,26	0,53	0,25	0,15	0,18	0,16	0,32	0,14	0,32	0,15	0,25	0,11	0,15	0,17	0,19
MgO	2,6	3,7	17,2	2,3	4,87	4,4	2,22	4,42	1,01	5	10,49	2,52	2,93	5	5,16	3,03
CaO	37,92	50,01	32,31	44,81	41,48	39,57	48,94	44,85	52,4	46,82	21,93	35,29	41,88	38,62	25,5	45,71
BaO	0,13	0,16	0,05	0,15	0,22	0,12				0,14	0,19	0,08	0,15		0,11	0,33
SrO	0,59	0,79	0,79	0,66	0,31	0,45	0,42	0,05	0,04	0,75	0,07	0,08	1,32	1,12	3,56	2,85
Na_2O	0,11	0,12	0,09	0,21	0,47	0,19	0,21	0,34	0,08	0,1	0,49	0,29	0,28	0,27	0,3	0,49
K_2O	0,02	0,01	0,01	0,07	1,04	1,43	0,21	0,07	0,13	0,03	3,47	0,52	0,63	1,64	1,72	0,36
P_2O_5	1,39	2,82	2,06	2,65	2,07	10,99	3,6	3,32	1,23	0,84	12,94	16,49	20,04	8,06	13,05	0,01
F	0,26	0,4	0,25	0,25	0,18	0,73	0,22	0,23	0,08	0,15	1,01	1,01	1,2	0,57	0,89	0,03
S	0,01	0,01	0,01	0,01	0,31	0,4	0,68	0,04	0,05	0,01	0,95	0,42	2,75	2,05	0,49	0,09
SO_3													0,71	0,37	0,71	0,37
CO_2	28,96	37,82	41,28	31,89	30,03	20,83	36,67	37,77	41,67	40,24	3,18	10,39	11,97	23,85	6,24	35,08
H2O	1,42	2,2	1,67	2,99						1,44	1,66	0,76	0,82	0,91	0,86	
∑	99,77	99,27	99,92	99,9	99,74	99,3	99,44	99,75	99,49	99,41	99,19	99,96	97,78	99,8	99,69	99,81
∑TR	0,17	0,23	0,09	0,2	0,19	0,36				0,14	0,38	0,45				0,59

Table 3 (Continued)

	17	18	19	20	21	22	23	24	25	26	27	28	29	30	31	32
SiO_2	7,18	2,98	10,93	19,66	2,98	38,82	2,46	17,09	15,34	41,23	18,92	43,57	36,92	44,31	49,56	19,04
TiO_2	0,01	0,04	0,01	1,82	1,08	0,05	0,07	0,61	0,11	0,16	0,53	0,28	0,32	0,71	0,35	0,11
Al_2O_3	1,7	1,2	2,5	1,7		10,52	0,63	0,71	1,47	0,7	4,26	0,7	9,47	7,8	11,58	0,3
Fe_2O_3	0,52	0,02	0,12	12,02	6,03	1,66	1,18	10,93	4,72	3,38	2,63	3,12	3,94	3,67	4,42	8,9
FeO	0,26	0,26	1,34	0,8	2,59	1,98	3,95	3,41	4,58	0,54	3,14	1,52	0,18	0,9	0,99	0,63
MnO	0,01	0,01	0,03	0,24	0,13	0,81	1,54	1,1	0,17	0,08	1,45	0,07	0,07	0,07	0,05	0,23
MgO	1,8	1,1	15,9	3,1	1,7	6,22	16,41	10,81	13,98	14,4	9,4	16,2	4,2	3,04	2,64	1,6
CaO	50,93	52,05	38,61	29,73	47,79	13,64	28,62	20,37	22,22	19,77	23,59	17,32	36,07	37,1	21,97	17,98
BaO	0,2	0,074	0,05	0,57	0,05	0,35	0,3	2,91		0,07					0,05	20,75
SrO	0,1	0,1	0,11	0,32	0,47	0,45	0,41	0,44	0,54	0,06	0,4	0,05	0,21	0,63	0,65	0,65
Na_2O	0,16	0,26	0,07	3,62	0,16	6,4	0,4	2,21	2,24	3,38	3,22	3,77	0,08	0,05	0,1	3,83
K_2O	0,15	0,09	0,01	0,01	0,02	0,12	0,05	0,05	0,11	1,3	0,08	1,57	0,15	0,21	5,97	0,16
P_2O_5	0,03	0,03	0,06	9,87	1,1	0,05	0,02	0,09	0,03	0,01	0,06	0,03	0,02	0,13	0,18	0,42
F	0,17	1,1	0,45	0,8	0,19	0,09	0,01	0,03	0,03	0,06	0,01	0,1	0,07	0,01	0,02	0,13
S	0,24	0,02	0,45	0,14	0,02	0,07	0,02	0,59	0,02	0,01	0,02	0,01	0,01	0,03	0,12	0,09
CO_2	35,08	39,33	29,2	13,09	35,2	18,87	43,4	27,13	33,95	12,76	31,91	9,68	6,69	1,41	1,64	20,4
H2O	1,75	2,07	0,71	2,38	0,77	0,35		0,43		1,69		1,88	1,03	0,29	0,35	
∑	100,1	100,25	100,08	99,28	100,24	99,99	99,19	98,46	99,35	99,48	99,74	99,83	99,25	99,74	99,95	97,02
∑TR	0,32															

Table 3 (End)

	33	34	35	36	37	38	39	40	41	42	43	44	45	46	47
SiO_2	14,7	33,58	41,91	11,24	6,42	18,17	19,21	28,36	10,09	3,05	33,48	26,29	32,48	25,23	10,62
TiO_2	0,02	0,47	0,07	0,11	0,13	0,26	0,22	0,3	0,16	0,19	0,45	0,36	0,6	0,34	0,22
Al_2O_3	2,94	4,4	9,62	2,4	1,6	3,2	1,3	7,9	2,4	3,1	7,9	6,3	7,1	6,9	3,3
Fe_2O_3	2,08	8,51	4,45	1,74	0,52	1,52	2,62	1,82	1,52	1,52	4,32	2,62	4,52	4,52	1,12
FeO	0,18	2,51	0,45	4,38	0,17	0,8	1,25	0,53	0,08	0,17	0,26	0,26	0,89	0,62	0,35
MnO	0,17	0,23	0,11	1,72	0,02	0,04	0,05	0,06	0,04	0,04	0,08	0,06	0,1	0,08	0,02
MgO	0,7	3,08	0,8	12,8	10,4	3,4	6,3	1,8	7	5,1	1,8	1,6	3,9	2,3	11,2
CaO	19	15,8	8,95	22,45	41,84	43,1	40,67	36,6	42,86	48,38	38,78	43,29	37,62	30,5	40,23
BaO	25,86	9,02	10,35	5,9	0,046	0,03		0,01			0,03			0,02	0,1
SrO	0,21	0,51	1,32	0,62	0,05	0,11	0,09	0,11	0,09	0,07	0,09	0,09	0,09	0,12	0,08
Na_2O	0,81	3,88	1,92	1,79	0,02	0,21	0,25	0,74	0,02	0,01	0,18	0,17	0,22	7,32	0,02
K_2O	2,47	2,27	7,82	0,12	0,03	1,04	0,04	2,16	0,01	0,02	1,31	0,46	0,06	0,17	0,03
P_2O_5	0,5	0,45	0,21	0,01	0,03	0,1	0,14	0,05	0,01	0,01	0,47	0,11	0,28	0,12	0,02
F	0,13	0,22	0,06	0,03	0,03	0,13	0,13	0,31	0,12	0,1	0,1	0,1	0,07	0,05	0,05
S	0,1	0,31	0,05	0,76	0,21	0,02	0,01	0,01	0,01	0,05	0,02	0,01	0,02	0,16	0,04
CO_2	23,97	12,62	10,08	32,77	36,15	26,75	25,5	18,19	32,71	37,27	10,23	17,33	11,5	20,02	31,14
H2O		0,39	0,27	0,58	2,3	1,4	2,66	1,45	2,84	0,97	0,49	1	0,37	1,74	1,6
∑	97,1	98,62	98,39	99,03	99,81	100,19	100,38	100,26	99,91	99,98	99,91	100,01	99,78	100,09	99,95

Note. *Name of rocks: Koratti (Sevathur) massif – carbonatites № 1-21, массив Salampatti massif –carbonatites № 22-39 (benstonite Joggipatti carbonatites № 32-35), near-contact scarns № 40 -47ю Data of chemical analyses, analyst - Matveeva L.N., Institute of Geochemistry, SB RAS, 2002.*

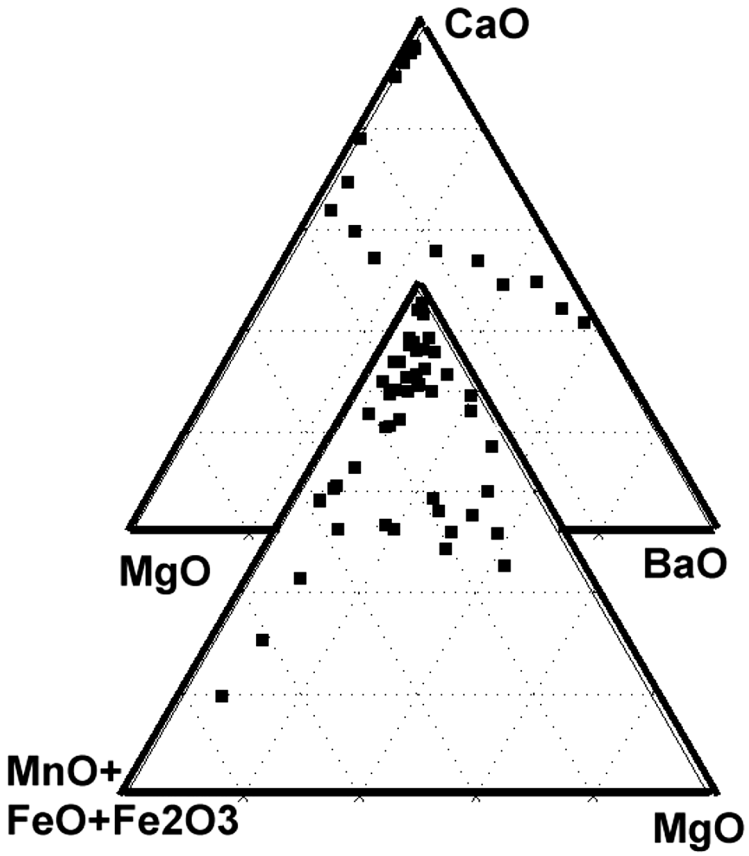

Fig. 10. *Plot of ternary element correlation in carbonatites.*

clear correlation between Ba and Sr contents, as the second concentrator of these elements is microcline, containing up to 5% of BaO [9].

On diagrams of ternary correlation of rock-forming elements the "benstonite" carbonatites form composition trends, different from those of calcite, dolomite and ankerite carbonatites (Fig. 10).

The mineral composition of "benstonite" carbonatites is rather simple. In addition to carbonate the rock-forming minerals include pyroxene-egirine (50%)-diopside (25%)- hedenbergite (25%) and in cases potassic microcline, containing to 5 % of BaO in Indian carbonatites. Alkaline amphiboles (K-richterite on the Murun and arfvedsonite in India) are scarce.

Other carbonatite varieties of India and Murun are thoroughly described in [9].

Alkaline massifs (Salamatti and Koratti (Serathur site) contain abundant calcite, calcite-dolomite carbonatites, which are cut by ankerite carbonatites. All transition varieties between Ca, Mg and Fe carbonatites are distinguished in terms of the chemical composition(Table 3). In cases Salampatti calcite carbonatites contain abundant alkaline amphibole of arfvedsonite-richterite series, while these carbonatites from Derethur site (Koratti massif) contain pyroxene, mica, magnetite and apatite. These minerals form bands in calcite carbonatites, indicating significant magmatic layering in carbonatites. These carbonatites contain separated

layers (to 20 cm thick) of micaceous-apatite-magnetite composition (nelsonites) . These rocks contain up to 20% of P_2O_5.

On triangle diagrams of carbonatites composition (Fig. 10) there is a complete trend of compositions between calcite and ankerite carbonatites. In composition carbonates correspond to calcite, Fe-calcite, dolomite, Fe-dolomite and ankerire. Structures of dolomite decay in calcite and Fe-calcite are found. In cases ankerire corks contain abundant albite and insignificant microcline and amphibole. Silicate-carbonate rocks originate when carbonatites contain abundant amphibole or albite.

RARE EARTH ELEMENTS IN CARBONATITES PROVINCE TAMIL NADU

TR_2O_3 concentrations in carbonatites are given in Table 4. Total concentrations of rare earth elements vary from 0.01 to 3.5%.

The highest TR_2O_3 contents are found in "benstonite' carbonatites and apatite-magnetite bands in calcite carbonatites. The least TR_2O_3 concentrations are typical of near-contact carbonate scarns.

Spectra of rare-earth elements are given on Fig. 11. They are similar of carbonatites with different composition, have a similar inclination of plots and are different only in total TR_2O_3 concentrations. All carbonatite types exhibit almost a complete absence of Eu fractionation. It indicates the genetic similarity of all types of Tamil Nadu carbonatites. *ankerite*

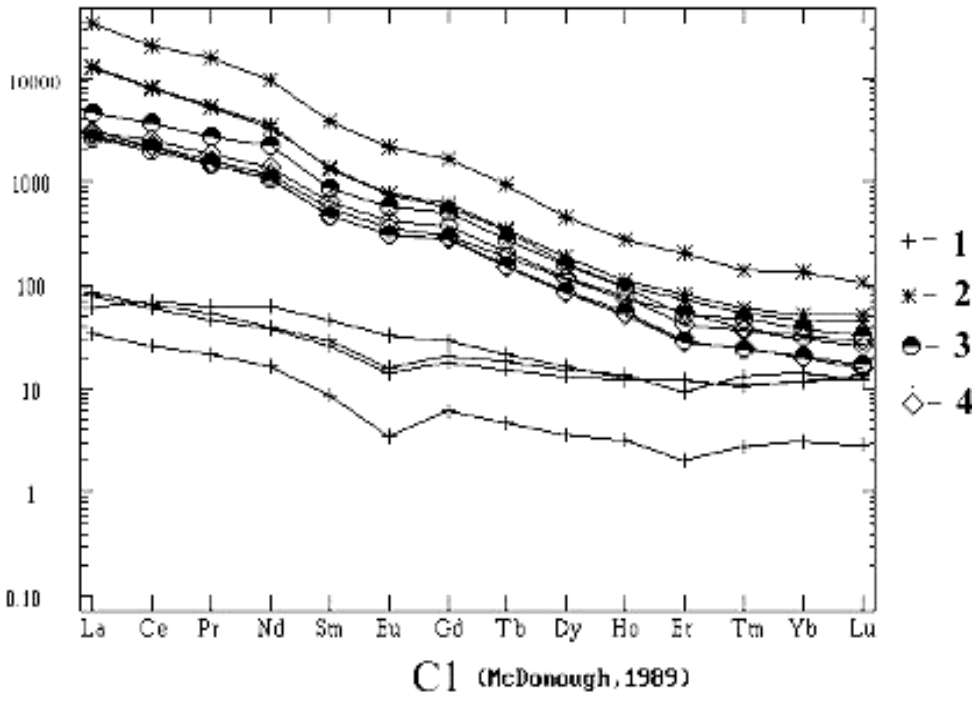

Fig. 11. *TR spectra in south Indian carbonatites.*

1-near-contact scarns; carbonatites: 2 - benstonite, 3 - calcite, 4 –

Table 4. *Rare-Earth Element Contents (ppm) in Carbonatites Tamil Nadu*

№ п/п	1	2	3	4	5	6	10	11	12	13	15	16	18	19	20	21
La	290	412	155	336	447	697	281	769	892	1091	608	820	2,62	11,23	363	252
Ce	617	844	334	758	770	1355	605	1560	1839	2241	1231	1213	5,18	22,21	768	540
Pr	71,51	98,54	42,59	82,29	64,55	149,79	68,15	138,99	173,30	253,43	138,38	113,34	0,55	2,54	100,37	57,14
Nd	276	382	168	323	234	545	266	513	631	1029	490	365	2,16	9,40	386	219
Sm	47,47	66,16	28,87	56,68	36,17	82,93	47,56	73,44	92,39	134,29	73,24	48,82	0,32	1,62	70,27	35,75
Eu	12,45	17,21	7,20	14,33	9,68	21,14	12,25	17,10	22,54	32,61	17,87	12,77	0,08	0,30	18,57	9,91
Gd	38,82	54,03	20,69	45,27	3,56	61,04	39,32	5,96	7,92	88,82	50,50	36,60	0,34	1,43	51,05	29,49
Tb	4,51	6,49	2,37	5,44	29,52	6,90	4,72	53,08	71,83	10,22	5,77	4,53	0,05	0,22	6,12	3,58
Dy	20,25	28,11	9,27	23,47	14,88	29,21	20,69	21,06	29,46	37,61	20,80	20,27	0,33	1,18	24,83	15,91
Ho	3,25	4,35	1,30	3,65	2,45	4,17	3,41	2,99	4,35	5,49	3,11	3,29	0,06	0,22	3,83	2,55
Er	7,35	10,19	2,70	8,64	5,81	9,30	7,92	6,62	9,50	11,93	6,42	8,04	0,16	0,69	8,29	6,06
Tm	0,93	1,20	0,32	1,01	0,68	1,00	0,95	0,67	1,00	1,22	0,62	0,97	0,03	0,08	0,89	0,71
Yb	5,47	7,29	1,76	6,17	3,97	5,49	5,78	3,66	5,46	6,53	3,53	5,83	0,19	0,71	4,99	4,12
Lu	0,77	0,98	0,23	0,85	0,54	0,74	0,79	0,42	0,66	0,80	0,43	0,84	0,03	0,09	0,60	0,58
$\sum TR_2O_3$ (%)	0,17	0,23	0,09	0,20	0,19	0,36	0,16	0,38	0,45	0,59	0,32	0,32	0,001	0,01	0,22	0,14
№ п/п	23	24	26	29	32	33	34	35	36	37	38	39	40	41	43	46
La	36,1	85	28	6,60	6587	8017	2943	3023	20,88	3,40	15,31	3,23	28,27	7,85	20,29	13,96
Ce	118	266	86	17,12	10351	12654	4767	4967	79,00	7,62	29,60	6,90	54,82	16,05	40,02	42,90
Pr	17,31	39,98	13,11	2,41	1063	1460	498	511	12,87	0,96	3,42	0,97	6,37	1,93	4,74	6,38
Nd	73	167	56	10,24	3413	4373	1559	1625	57,61	3,66	13,21	4,33	25,44	7,58	18,37	28,65
Sm	15,71	32,16	13,13	2,68	453	591	211	203	13,44	0,75	2,65	1,01	5,15	1,31	4,38	6,68
Eu	4,49	8,11	3,75	0,64	98,10	123,99	44,33	42,78	3,13	0,17	0,57	0,26	1,09	0,24	0,95	1,91
Gd	10,79	19,60	9,90	0,51	273	334	126	118	9,65	0,73	2,37	0,84	5,08	1,31	4,01	5,60
Tb	1,44	2,34	1,35	2,91	28,37	34,44	12,98	12,28	1,33	0,12	0,31	0,11	0,73	0,17	0,68	0,79
Dy	7,05	10,14	6,87	3,01	94,92	115,29	47,10	41,73	6,15	0,68	1,92	0,60	4,34	0,95	3,74	4,16
Ho	1,16	1,58	1,19	0,59	12,82	15,47	6,34	5,63	1,06	0,12	0,36	0,10	0,82	0,18	0,78	0,72
Er	2,98	4,31	3,23	1,85	28,11	34,03	13,42	12,26	2,66	0,38	1,03	0,21	2,38	0,49	2,32	2,01
Tm	0,44	0,58	0,43	0,27	2,99	3,61	1,54	1,39	0,40	0,07	0,14	0,02	0,34	0,07	0,34	0,28
Yb	3,09	4,00	2,70	1,75	17,10	22,48	8,90	7,86	2,85	0,35	0,93	0,19	2,07	0,52	2,43	1,96
Lu	0,51	0,64	0,35	0,24	2,21	2,69	1,27	1,10	0,44	0,05	0,14	0,02	0,28	0,07	0,32	0,34
$\sum TR_2O_3$ (%)	0,04	0,08	0,03	0,01	2,69	3,33	1,23	1,27	0,03	0,002	0,01	0,00	0,02	0,00	0,01	0,01

Note. *order № from Table 3. ICP MS data, analyst - Mitrophanova A.Yu., Institute of Geochemistry, SB RAS, 2002.*

GEOCHEMISTRY OF SR AND ND ISOTOPES IN CARBONATITES

Geochemistry of isotopes in carbonatites of South India and Murun massif were considered earlier in [6,9]. Additional data for Serathur calcite and calcite-dolomite carbonatites are presented in Table 5. The Serathur and Murun carbonatites are characterized by negative Nd epsilon. Sr ratio isotope values very from 0.705 to 0.709.

Earlier, we studied the geochemistry of Sr, Nd, C, O, and Pb isotopes in the Murun Massif rocks [12, 14]. As seen from the carbon-oxygen isotope diagram, the composition points of the massif carbonatites fall into the mantle square. The points of Pb isotopes form a field near the field of the USA lamproites [14]. The age of the mantle substratum from which the Murun magma melted out was calculated from Pb isotopes in galenites - 3.2 Ga [12,14]. According to the isotope ratios of Nd and Sr, the Murun Massif silicates and carbonatites fall into the field of enriched mantle EM-1 and have the greatest values of Eepsilon Nd among all alkaline rocks (Fig. 12). As Figure shows South Indian and Murun carbonatites originated from the enriched EM-1 mantle source. It is characteristic of alkaline carbonatite complexes, originated in rift zones of ancient shields. These ratios are nearly equal for the silicates and carbonatites, which indicates that these rocks were generated from the same parental magma.

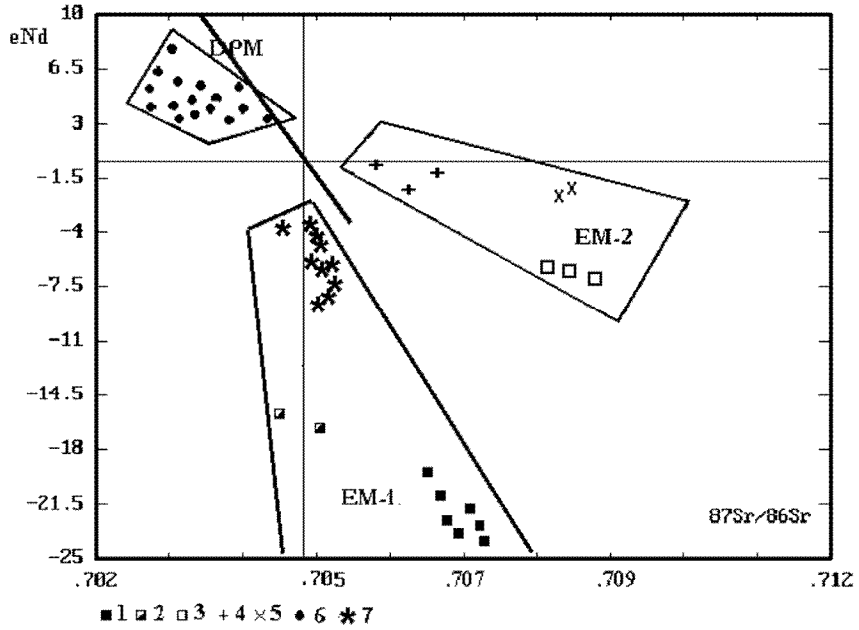

Fig. 12. *Nd-Sr isotope diagram for carbonatites.*

Massifs: 1 *– Murun,* 2 *– Khani,* 3 *– Darai-Pioz,* 4, 5 *– Mongolian province,* 6 *– Sayan province, Guli, and Kola carbonatites, 7- South Indian carbonatites. DPM – depleted mantle, EM-1 and EM-2 – enriched mantle. Black line shows the mantle sequence.*

Table 5

Isotopic Composition of C, O, Sr, and Nd in rocks of the Tamil Nadu

№ п/п	Rb (ppm)	Sr (ppm)	Sm (ppm)	Nd (ppm)	$^{87}Rb/^{86}Sr$	$^{87}Sr/^{86}Sr$	$^{87}Sr/^{86}Sr$ (760Ma)	εSr	$^{147}Sm/^{144}Nd$	$^{143}Nd/^{144}Nd$	$^{143}Nd/^{144}Nd$ (760Ma)	εNd
1	0,08	7212	45,7	227	0,00003	0,705281	0,705281	23,8	0,1217	0,511954	0,511347	-6,1
2	0,05	8292	50,6	232	0,00002	0,705192	0,705192	22,6	0,1320	0,512017	0,511359	-5,8
3	0,05	8304	52,9	272	0,00002	0,705313	0,705313	24,3	0,1176	0,511973	0,511387	-5,3
4	0,07	8173	51,3	265	0,00002	0,705251	0,705251	23,4	0,1169	0,511905	0,511323	-6,6
5	0,24	8806	9,80	66,3	0,00008	0,705103	0,705102	21,3	0,0894	0,511877	0,511432	-4,4
6	0,57	8779	7,70	49,7	0,00019	0,705107	0,705105	21,4	0,0937	0,511853	0,511386	-5,3
7	0,53	8571	9,75	63,1	0,00018	0,705108	0,705106	21,4	0,0935	0,511840	0,511374	-5,6
8	1,15	8353	11,4	71,7	0,00040	0,705085	0,705081	21,0	0,0959	0,511879	0,511401	-5,0
9	0,39	9609	25,5	159	0,00012	0,705146	0,705145	21,9	0,0972	0,511854	0,511369	-5,6
	$\delta^{13}C$		$\delta^{18}O$		$^{87}Rb/^{86}Sr$	$^{87}Sr/^{86}Sr$	$^{87}Sr/^{86}Sr$ (800Ma)	εSr	$^{147}Sm/^{144}Nd$	$^{143}Nd/^{144}Nd$	$^{143}Nd/^{144}Nd$ (800Ma)	εNd
10	-5,63		7,51		0,00003	0,70529	0,70529	24,65	0,1231	0,511912	0,511266	-6,65
11	-5,03		9,32		0,00035	0,70511	0,70510	21,97	0,1039	0,5118	0,511255	-6,86
12					0,00022	0,70500	0,70500	20,53	0,101	0,51857	0,511327	-5,45
13					0,00059	0,70521	0,70521	23,45	0,117	0,511801	0,511187	-8,19
14	-4,85		9,19		0,0035	0,70509	0,70505	21,19	0,126	0,51184	0,511179	-8,35
15	2,08		18,54		0,287	0,71288	0,7096	85,89	0,1072	0,511691	0,511129	-9,33
16	-4,87		8,87		0,00004	0,70514	0,70514	22,53	0,0986	0,511727	0,51121	-7,75
17	-5,81		9,29		0,00005	0,70513	0,70513	22,42	0,111	0,511928	0,511345	-5,1
18	-6,47		9,42		0,00008	0,70455	0,70454	14,06	0,1509	0,512186	0,511394	-4,15
19					0,27	0,70815	0,70507	21,51	0,117	0,511834	0,51122	-7,54
20					1,157	0,72097	0,70775	59,62	0,144	0,511748	0,510993	-11,99
21					0,75	0,71457	0,70599	34,68	0,1179	0,511412	0,510793	-15,89

Note: Data by authors (№1-9): Sevathur massif –calcite carbonatites - № 1-4, dolomite carbonatites - № 5-9. Data [6] : Sevathur massif–carbonatites № 10-14, near-contact scarns №15, Salampatti massif- carbonatites (Joggipatti)- №16-18, pyroxenites ;№19-21.

CONCLUSIONS

1. Potassic alkaline complexes of South India (Tamil Nadu) and Murun (South West Aldan) are significantly different in terms of crystallization conditions. The Murun massif was crystallized close to the surface, while the South Indian one originated in hypomesoabyssal conditions. Thus, leucite syenites were crystallized on the Murun while microcline syenites originated in the South India.
2. Both complexes exhibit a unique type of "benstonite" carbonatites, most likely having different genesis. The magmatic layering is abundant on the Murun massif. "Benstonite" carbonatites originated from layering of the residual silicate-carbonate melt-fluid during an early stage of carbonate formation. On the Samalpatti massif the "benstonite" carbonatites formed from differentiation of the carbonatitic liquid.
3. In terms of the chemical composition the South India exhibits a complete series of carbonatites, markedly Ca-carbonatites (calcite), Ca-Mg-carbonatites (dolomite); Ca-Mg-Fe-carbonatite (ankerite) and Ba-Sr-carbonatite ("benstonite). Carbonatites, enriched with silicate minerals (over 50%), alkaline ampbibole, albite, microcline, mica are also observed. In addition, the apatite-magnetite (with mica) rocks (nelsonites) are distinguished among mesocratic calcite carbonatites. Intermediate (in composition) carbonatites are also found.
4. TR spectra of the South Indian carbonatites exhibit a similar inclination of plots. They do not show Eu fractionation. It indicates a genetic similarity of carbonatites of the region.
5. Isotope ratios and Nd epsilon in south Indian and Murun carbonatites indicate the deep sources from the EM-1 enriched mantle.
6. "Benstonite" carbonatites are native ore for Ba and Sr found as carbonates and can be used without enrichment in the steel industry.

Research was perfomed under a support of Russian Foundation of Basic Research, grants № 03-05-64146 and Integration Projects of RAS № 6-2-1, SB RAS № 67.

REFERENCES

1. **Lippmann F.** // Benstonite $Ca_7Ba_6(CO3)_{13}$, a new mineral from the barite deposit in Hot Spring County, Arkansas // Amer. Mineral. 1962.V. 47. P. 585-598.
2. **Panina, L.I., I.V. Motorina, V.V. Sharygin, and N.V. Vladykin.** Biotitic pyroxenites and melilite-monticellite-olivine rocks of the Malo-Murun alkaline massif, Geologiya i Geofizika (Soviet Geology and Geophysics), **30**, 12, 41-50 1989.

3. **Panina, L.I., and I.V. Motorina.** Alkaline high-calcium sulfate-carbonate melt inclusions in melilite-monticellite-olivine rocks of the Malyi Murun alkaline massif, Petrologiya, **7**, 6, 653-669, 1999.
4. **Potassic alkaline magmatism of the Baikal-Stanovoy rift system** (ed. Kostyuk V.P.)in Russian], 237 pp., Nauka, Novosibirsk, 1990.
5. **Prokof'ev, V.Yu., and Vorob'ev E.I.** Geokhimiya, 10, 1444-1452, 1991.
6. **Schleicher H. et al.** // Enriched Subcontinental Upper Mantle beneath Southern India: Evidence from Pb, Nd, Sr, and C-O Isotopic Studies on Tamil Nadu Carbonatites // Journal of petrology. 1998. V. 39. N.10. P. 1765-1785.
7. **Semenov E.I., Gopal V.** Subramanian V. // A note on the occurrence of benstonite, a carbonate of calcium and barium from the carbonatite complex at Jogipatti, near Samalpatti, Dharmapuri District, Tamil Nadu // Current Science. 1971. V. 40. P. 254-256.
8. **Sokolov S.V. et al.** «On benstonite and benstonite carbonatites»,Geochemistry, 2001, №12, p. 1327-1339 (in Russian).
9. **Viladcar S.G., and Subramanian** // Mineralogy and Geochemistry of the Carbonatites of the Sevathur and Samalpatti Complexes, Tamil Nadu // Journal Geological Society of India. V. 45. May 1995. P. 505-517.
10. **Vladykin, N.V., N.G. Bogacheva, and Yu.A. Alekseev,** New data on charoite and charoite rocks, in Mineralogy and genesis of gemstones of East Siberia [in Russian], 41-57, Nauka, Novosibirsk, 1983.
11. **Vladykin, N.V., V.I. Simonov, and V.S. Sokolov,** The fluid regime and crystallization temperatures of charoite rocks, *in* Thermobarogeochemistry of mineral-forming rocks [in Russian], issue 3, 76-82, Nauka, Novosibirsk, 1994.
12. **Vladykin, N.V.,** Petrology and ore potential of K-alkaline rocks of the Mongolo-Okhotsk magmatic area, ScD thesis [in Russian], 80 pp., IGKh SO RAN, Irkutsk, 1-80 pp.1997.
13. **Vladykin, N.V.,** Geochemistry and genesis of lamproites of the Aldan Shield, Geologiya i Geofizika (Russian Geology and Geophysics), **38**, 1, pp. 123-135 (128-141), 1997.
14. **Vladykin N.V.** Malyi Murun Volcano-Plutonic Complex: An Example of Differentiated Mantle Magmas of Lamproitic Type // Geochemistry International, 2000, v. 38, suppl. 1, pp. 573-583
15. **Vladykin N.V., Tsaruk I.I.** Geology, chemistry and genesis of Ba-Sr-bearing (benstonite»)carbonatites of the Murun massif// Russian Geology and Geophysics, 2003,v 44, № 4, pp325-339

Kovdor apatite-francolite* deposit as an example of explosive and phreatomagmatic endogenous activity in the ultramafic-alkaline and carbonatite complex (Kola Peninsula, Russia)

Krasnova N.I.

Research Inst. of the Earth's Crust, SPbSU, Russia, 199034, St-Petersburg, University Emb. 7/9, E-mail: krasnova@aa5709.spb.edu

Francolite-bearing rocks in Kovdor ultramafic-alkaline and phoscorite-carbonatite complex form a system of structurally complex vein-like bodies extended as a semi-circular zone 3.5 km long. These bodies pinch out at depths of 70-100 m and in some funnel-shaped depressions – about 200 m from the Earth's surface. During the last stage of phreatomagmatic endogenous activity in the Kovdor complex, the accumulating volatile phases enriched in F, P and H_2O components led to the transformation of calcite to francolite. The educed carbon dioxide gave rise to explosions, which took place locally along the semi-circular breaks. The francolite rocks were formed at least in three stages, each of which was accompanied by brecciation of surrounding rocks and cementation of their fragments by various francolite generations under hydrothermal conditions. While calcite, dolomite and apatite from most phoscorites and carbonatites show the low $^{87}Sr/^{86}Sr$ ratios = 0.7032-0.7039, that indicate their origin from the mantle source, this ratio for francolite is about 0.7059-0.7061, which points to crustal contamination during the formation of francolite-apatite rocks.

INTRODUCTION

Francolite-apatite or francolite-magnetite rocks are not very common in carbonatite-bearing complexes and only about 15 occurrences were reported worldwide, which were described in some detail. The most investigated of them are located on the Baltic shield: Sokli (Finland), Kovdor and Vuoriyarvi (Russia); the others – at Siberian platform and in adjacent areas (Russia): Guli, Dalbykha, Essei, Yraas, Tomtor, Tatarskoye II, Chuktukonskoye and Belaya Zima; some occurrences are known in South Africa – Bukusu and Sukulu (Uganda), Tundulu (Malawi), Glenover (R.S.A.) and in Brazil – Angico complex. One of the difficulties for the researchers is the inadequacy of nomenclature of the apatite group of minerals: often fluorapatite and carbonate fluorapatite (= francolite) are not differentiated and both are called apatite. The ambiguous term *secondary phosphate* is also used for description of rock-forming mineral in some of these complexes. The data on the apatite composition frequently are incomplete due to application of the microprobe analytical method, unusable for determination of carbon, hydrogen and sometimes fluorine. In addition, the nomenclature based on

the rule of 50 % boundary between fluorapatite and carbonate apatite varieties does not reflect the natural mineral diversity. Therefore, the term *francolite* will be used for carbonate fluorapatite with a different CO_3 content. This mineral occurs in colloform, microgranular or spherulitic and radial fibrous kidney-shaped aggregates; compared to fluorapatite its refractive indexes are lower: ω = 1.620-1.628, ε = 1.615-1.621 and in the contrary higher $\omega - \varepsilon$ = 0.004-0.007.

The paper provides the geological and mineralogical description of the Kovdor apatite-francolite deposit, which is the best exposed and investigated worldwide.

LOCATION AND GEOLOGY

The apatite-francolite deposit is located in the southeastern part of the Kovdor alkaline-ultrabasic intrusion, the Kola Alkaline Province [8]. This deposit was explored and investigated during the period from 1970 to 1977, but it has not been as yet mined because the dressing of these phosphorous ores requires a special concentrating mill. The dressing technology of the Kovdor francolite-bearing rocks seems to be similar to that of Sokli phosphorus ores, as was shown earlier [17]. These ores both in Kovdor and Sokli could been classified as a new phosphorus ore type with such good characteristics as a low strontium, rare earth elements and magnesium content and they undoubtedly could be utilised in future as a raw material for the fertiliser production. This seems feasible in case of united efforts of Russia and Finland and only after the construction of the railway road between Kovdor and Sokli.

Many types of holes were drilled and trenches were made during the exploration of the Kovdor francolite deposit and therefore this deposit could be considered as the best investigated. The resources of apatite-francolite ores are estimated at approximately 100 million tons including 50 million tons of ores with the P_20_5 content 15-20 wt. % and 50 million tons of ores with the P_20_5 content 5-10%. The apatite-francolite ores were first described by N.A. Volotovskaya [20], and also were investigated by other geologists [3, 6, 8, 9, 11, 13, 14].

The deposit lies in country rocks composed by fenites, ijolites, jacupirangites (clinopyroxenites) and calcite carbonatites. The francolite-bearing rocks form a system of a structurally complex vein-like bodies occupying a semi-circular zone 35 km long (Fig. 1). These bodies are 15-20 to 150-300 m thick and they pinch out at depths of 70-100 m and in some funnel-shaped depressions – at about 200 m from the surface (Fig. 1, 2). At depth the mouths of these funnel-shaped bodies are not connected with each other. The lying contact of the bodies dips at low angles to the centre of the semi-circular system of fractures controlling their arrangement. The common focus of these conical fractures lies at a depth of approximately 200-

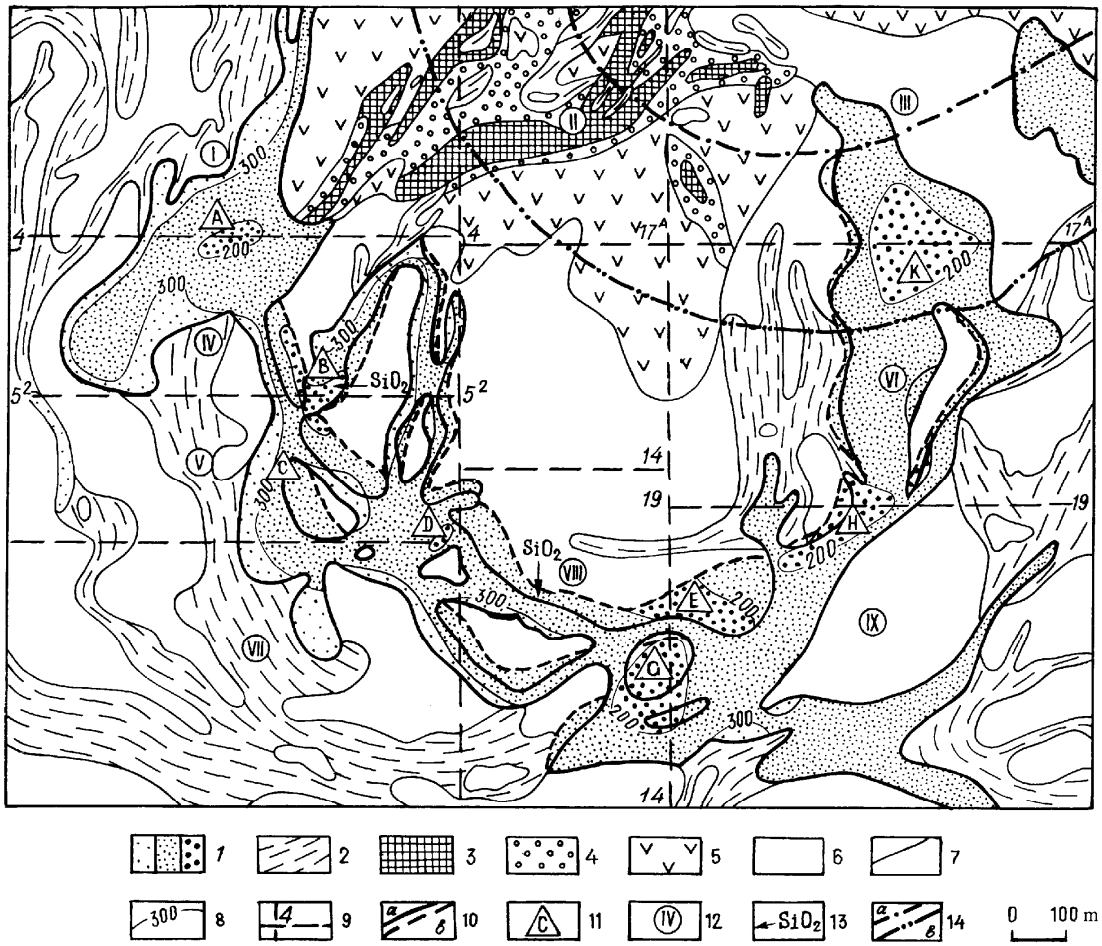

Fig. 1. *Geological structural map of the Kovdor apatite-francolite deposit (prepared by the author, using data of Kovdor Geological Exploration Group).*

1 – apatite-francolite rocks, dismembered according to the bedding depth of the francolite bodies foot: a) more than +300 m, b) from +200 up to +300 m, c) less than +200 m; 2 – calcite carbonatites; 3 – magnetite phoscorites; 4 – apatite-forsterite rocks; 5 – ijolites; 6 – fenites; 7 – geologic boundaries; 8 – isolines of the foot of francolite bodies (meter above the see level); 9 – boundary of blocks, shown on Fig. 2 and the number of profiles; 10 – projection of the boundary of apatite-francolite bodies a) on the surface, b) on the depth; 11 – index of the individual funnels; 12 – number of blocks; 13 – zones of rock silication; 14 – the mining pit boundaries a) recent, b) projecting.

250 m to the Southeast from the main stockwork column of the phoscorite deposit. Noteworthy that in Kovdor one can see a gradual raising of the common focus of the conical fractures controlling the emplacement of the calcitic carbonatites – at a distance of about 2 km, that of dolomite carbonatites lies at 1.5-1.3 km and at least of the mentioned bodies of francolite rocks – at 200-250 m from the surface [7].

The bodies of francolite-bearing rocks are often related to the hanging contacts of carbonatites, but some of them occur among fenites, ijolites, jacupirangites and magnetite phoscorites. The location of francolite-bearing rocks

in magnetite ores (with sky-blue francolite) is now completely worked out. The

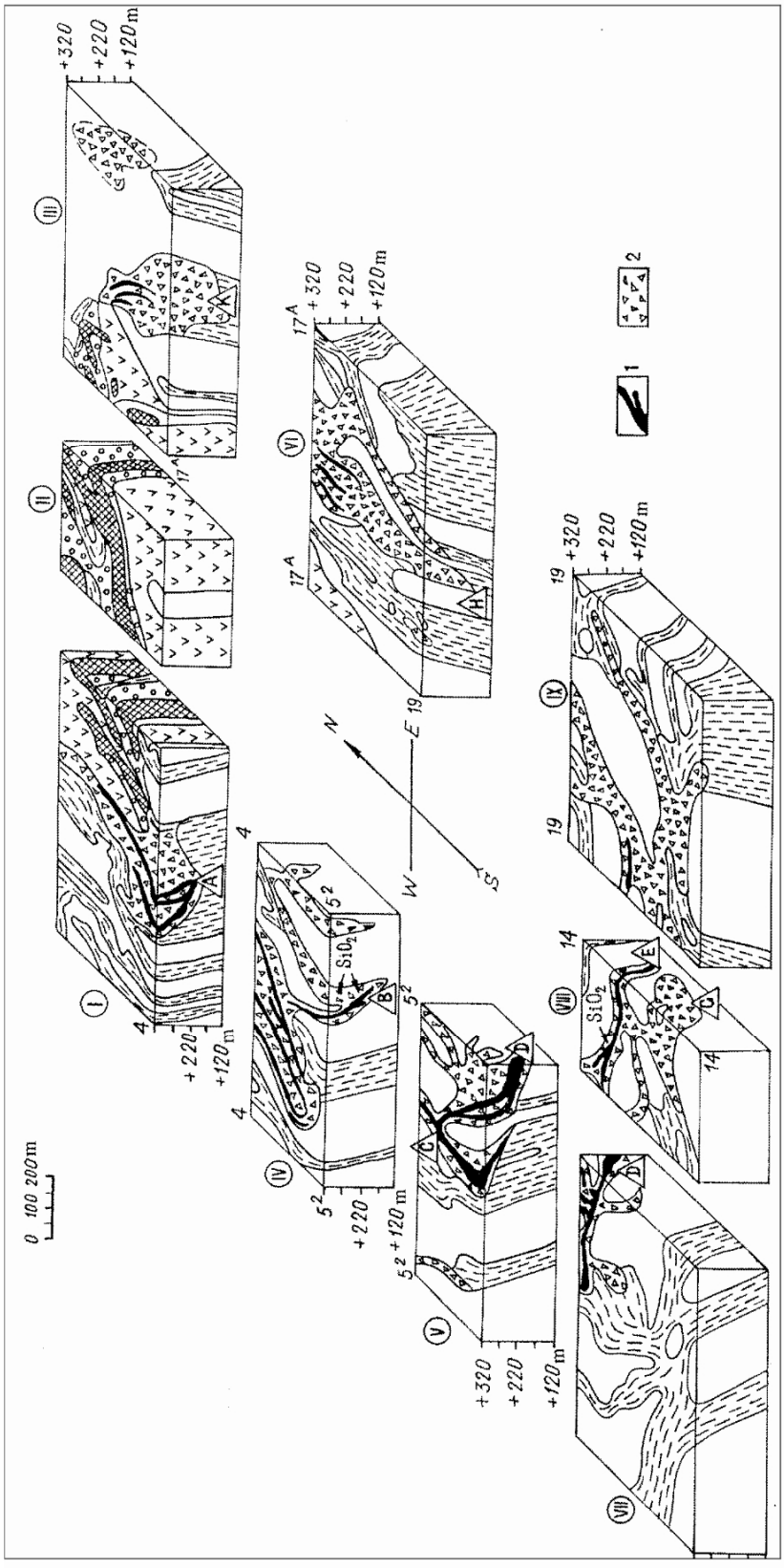

Fig. 2. *Block-diagram of the Kovdor apatite-francolite deposit.*

1 – apatite-francolite brecciform stony phosphate-rich rocks; 2 – francolite-vermiculite bad-cemented and loose phosphate-ordinary rich rocks; all else see Fig. 1.

morphology of the apatite-francolite deposit resembles the semi-circular thick lace collar with some carrot- or cone-like pipes (hoppers) overlaying different country rocks. Zones of rock silication are located near the two of these cone-like pipes (Fig. 2), under which the fenitized granitic pegmatites were found in cores. The bodies of francolite-bearing rocks are similar in shape to extrusions and they exhibit tuff- or breccia-like textures.

TYPE OF FRANCOLITE-BEARING ROCKS

Among the diversity of francolite-bearing rocks following varieties may be distinguished: 1) host rocks replaced by francolite (calcite carbonatites and calcite-bearing phoscorites) or cut by thin francolite veinlets (fenites, ijolites and clinopyroxenites); 2) francolite-vermiculite loose rocks; 3) – massive apatite-francolite brecciform rocks; 4) – vermiculite-psilomelane brecciform rocks.

Some clear evidence of replacement of calcite by francolite shows the presence of shadowy relics of rhombohedral calcite cleavage (grating on Fig. 3) sometimes preserved in fine-grained francolite aggregate, as it was described by Kurbatova and Gannibal [9]. This grating locally is also discernible on a weathered surface of porous francolitized carbonatite. At one funnel mouth calcite carbonatite was transformed to a brown felt-like aggregate of chrysotil-asbest with limonite and wad. Not-cemented residual stable mineral grains (magnetite, apatite, and baddeleyite) were found in this funnel mouth and the other carbonatite fragments were very extensively leached out from the surface and looked like a pumice-stone.

A remarkable outcrop was found in the upper part of the apatite-magnetite open-pit mine. Here the zone of carbonatite replaced by francolite stretches along the calcite carbonatite vein (Fig. 4). There are no signs of brecciation in this francolite-bearing rock and the size and the pattern of magnetite, apatite and mica grains or their aggregates are similar to that of the carbonatite. The colour of both rocks does not differ greatly – the zone of francolitization is much yellow than carbonatite. The shadowy relics of calcite cleavage are preserved in francolitized carbonatite, which supports the metasomatic origin of this rock [5]. The zone of zeolitization and halloysitization of host ijolites occur mainly near the hanging contact of the francolite vein.

Francolitized magnetite rocks lie only within the phoscorite deposit and they are mainly worked out. These rocks exhibit cavernous structure caused by leaching of calcite and partly, by forsterite alteration products. The inner lining of the caverns is incrusted with kidney-shaped aggregates of francolite. A system of branching francolite veinlets, cutting all primary minerals, is very common in this type of rocks. Forsterite in the francolitization zones is replaced by earthy brown aggregate containing hydrochlorite, montmorillonite and iron hydroxides and, locally, by antigorite (sungulite). Phlogopite and tetra-ferriphlogopite are altered into vermiculite, and magnetite was first replaced by hematite and, later, by limonite.

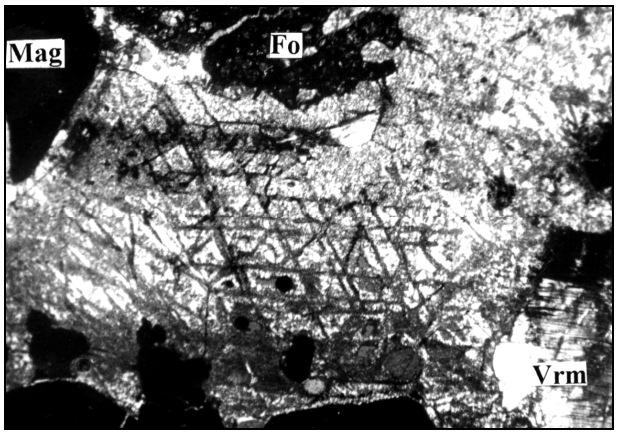

Fig. 3. *Shadowy relics of rhombohedral cleavage of calcite, entirely replaced by microgranular francolite aggregate (light coloured) in francolitized calcite-forsterite-magnetite phoscorite.*

Fo – forsterite, Mag – magnetite, Vrm - vermiculite. Photomicrographs of a thin section (width of field of view is 6.4 mm). Plane-polarised light.

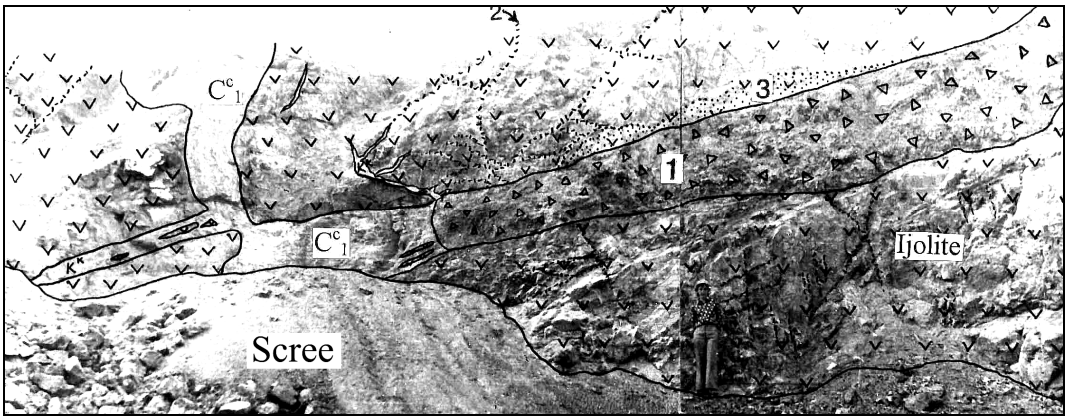

Fig. 4. *Veins of calcite carbonatites (C^c1) cut coarse-grained ijolite, which is also cut by thin hydro-biotite veinlets (2). The upper part of the carbonatite vein is completely altered to apatite-francolite massive (partly porous) rock (francolitized carbonatite – 1). Zone of ijolite is zeolitized near the hanging contact with francolitized carbonatite (dotted zone – 3).*

The francolitized ijolites, jacupirangites (clinopyroxenites) and fenites are represented by brecciated rocks cut by a system of thin branching francolite or chabasite-francolite veinlets (locally with fine-scale vermiculite). The P_20_5 content in this type of francolite poor ores is less than 4-8 wt. %. Many caverns incrusted with the kidney-shaped aggregates of francolite occur in these rocks in zones of intense brecciation. Nepheline of ijolites or urtites at first is replaced by cancrinite, and then by natrolite and chabasite and finally by halloysite.

The francolite-vermiculite loose not unigranular or friable rocks are common in this deposit. Some stratification and stream-like texture subparallel to the bodies' contacts is typical of this type of rocks. The stratification caused by alternation of

pale-coloured and dark-coloured brown limonite-bearing or black pyrolusite- and wad-bearing layers. Some fragments of all types of country rocks including calcite carbonatites modified to various degrees could be found in these francolite-vermiculite rocks.

Brecciform apatite-francolite massive rocks fill up veins, whose location is controlled by breaks stretching from the funnels mouths or wedging outlines of the francolite bodies (Fig. 1, 2). Some apatite-francolite bodies do not reach the Earth surface. The highest content of both francolite and relict apatite occur mainly near the hopper mouths but not close to the surface. These brecciform rocks cross the primary stratification of the earliest francolite-vermiculite loose rocks. Apatite-francolite massive rocks also contain many angular fragments of all earlier formed rocks or their relict minerals, mainly magnetite, apatite, vermiculite and baddeleyite (Fig. 5-7). The fragments of calcite carbonatites and calcite grains can be found occasionally in these apatite-francolite rocks.

The veins of vermiculite-psilomelane brecciform rock with carbonatite fragments crosscut the loose francolite-vermiculite rock types and thin psilomelane stringers cut locally apatite-francolite breccias.

So we can distinguish at least three francolite-bearing rock types of different age: 1 – francolite-vermiculite loose rocks; 2 – massive apatite-francolite brecciform rocks; 3 – vermiculite-psilomelane brecciform rocks. All types of francolitized host rocks formed concurrently with the emplacement of rocks of the first or second rock type. Table 1 shows the chemical composition of the first two rock types. Massive francolite-bearing rocks are enriched mainly in phosphorus – P_20_5 concentration is above 20 wt. %. Loose francolite-bearing rocks have lower P_20_5 content (8 to 20 wt. %) and are enriched in SiO_2, MgO and H_2O primary due to the presence of vermiculite.

MINERALOGY

Relict minerals from various types of country rock as well as minerals of francolitization and the weathering stages are typical of all the francolite-bearing rocks (Tab. 2). Relict minerals occur as fragments of grains or their aggregates. The formation of francolite and some associated minerals is attributed to a low temperature hydrothermal process known as the francolitization stage. Some minerals primarily crystallised together with francolite and lately could occur at the weathering stage. It is very difficult to precisely distinguish between hydrothermal and exogenous minerals.

Francolite assigned to four generations is the most common mineral of the francolite-bearing rocks. The first generation of francolite *Fr-1* is represented by homoaxial pseudomorphs surrounding apatite grains (rim is 0.05-0.1 mm thick; Fig. 6). Francolite of second generation – *Fr-2* (and partly CO_3-OH-F-apatite) forms fine-grained aggregates, which compose more than 50 % of the apatite-francolite breccia matrix (Fig. 5-7). These aggregates often are dark and even

Table 1. *Chemical composition of apatite-francolite rocks, wt.%.*

Rock types	Massive francolite-bearing								Loose francolite-bearing		
	Carbonatite replaced by francolite	Mainly francolite		Francolite breccia	Francolite-magnetite breccia	Francolite-apatite-magnetite vermiculite			Francolite-vermiculite		Mainly francolite
#	1	2	3	4	5	6	7	8	9	10	11
SiO_2	6.97	0.82	7.95	6.20	2.88	1.02	3.01	5.98	20.00	26.80	12.81
TiO_2	0.50	0.42	0.50	0.10	0.25	0.35	0.37	0.00	0.17	0.29	0.51
Al_2O_3	1.27	0.29	1.10	1.46	0.64	0.80	1.12	0.26	2.10	2.18	5.43
Fe_2O_3	9.76	10.70	9.55	1.10	7.14	10.09	8.15	7.65	7.23	6.23	16.12
FeO	3.52	3.51	4.64	0.54	2.16	3.31	1.81	1.26	1.58	0.78	1.38
MnO	0.13	0.13	0.13	0.05	0.13	0.21	0.10	0.18	0.22	0.19	0.64
MgO	4.70	1.41	2.14	4.50	1.68	2.70	2.39	2.60	12.40	23.11	6.81
CaO	40.62	43.67	42.45	47.00	44.89	46.60	45.24	45.20	29.00	17.60	27.13
Na_2O	0.40	0.30	0.30	0.20	0.20	0.20	0.43	0.40	0.30	0.30	0.25
K_2O	0.30	0.20	0.30	0.10	0.20	0.00	0.24	0.20	0.20	0.20	0.20
P_2O_5	26.61	35.20	26.91	33.80	33.90	31.41	32.40	32.25	19.32	11.61	19.58
CO_2	1.54	1.10	1.84	2.02	2.20	0.50	2.07	1.05	0.22	0.43	0.65
H_2O^-	0.61	0.20	0.23	0.54	0.00	0.28	0.32	0.50	1.10	2.07	2.23
H_2O^+	3.23	1.26	1.56	2.29	2.75	1.70	1.16	1.20	5.66	8.59	5.65
F	0.96	0.85	0.80	0.91	1.21	1.50	1.65	1.90	0.28	0.33	0.60
Total	101.12	100.06	100.40	100.81	100.23	100.67	100.46	100.63	99.78	100.71	99.99
$– O=F_2$	0.40	0.36	0.34	0.39	0.50	0.63	0.69	0.79	0.11	0.14	0.25
Total	100.72	99.70	100.06	100.42	99.73	100.04	99.77	99.84	99.67	100.57	99.74

Note. *After [11]. Wet chemical analyses were made in the Chemical laboratory of the Tajik Geological Survey, 1974.*

Table 2. *Mineral composition of francolite-bearing rocks*

Rocks		Francolitized rocks		
		Fenites	**Ijolites, melteigites**	**Phoscorites, carbonatites**
Minerals	**relict (most common)**	***Main***: microcline, albite, oligoclase, aegirine-augite, aegirine	nepheline, aegirine-augite, diopside, phlogopite, biotite	magnetite, apatite, forsterite, calcite
		Secondary: nepheline, biotite, richterite, quartz, calcite	Hastingsite, cancrinite, wollastonite, sodalite, K-feldspar, zeolites (natrolite, chabasite)	phlogopite, tetra-ferriphlogopite, chlorite, dolomite, clinohumite, richterite, serpentine,
		Accessory: titanite, apatite	apatite, titanite, schorlomite	baddeleyite, pyrochlore, zirkelite, zircon, spinel, ilmenite, hematite
	of francolitization and weathering stages	***Main:*** francolite, vermiculite, chabasite		Francolite, vermiculite, hydrophlogopite
		Secondary: hydrophlogopite, vermiculite, chlorite, montmorillonite, nontronite, halloysite, hydrochlorite (?), crandallite, secondary calcite, iron hydroxides, quartz		lizardite, nontronite, montmorillonite, calcite, collinsite, secondary hydrochlorite, malachite, vivianite, hematite, iron and Mn- hydroxides, barite, pseudomalachite

Note. *The underlined minerals are expected to be utilised by a complex ore dressing.*

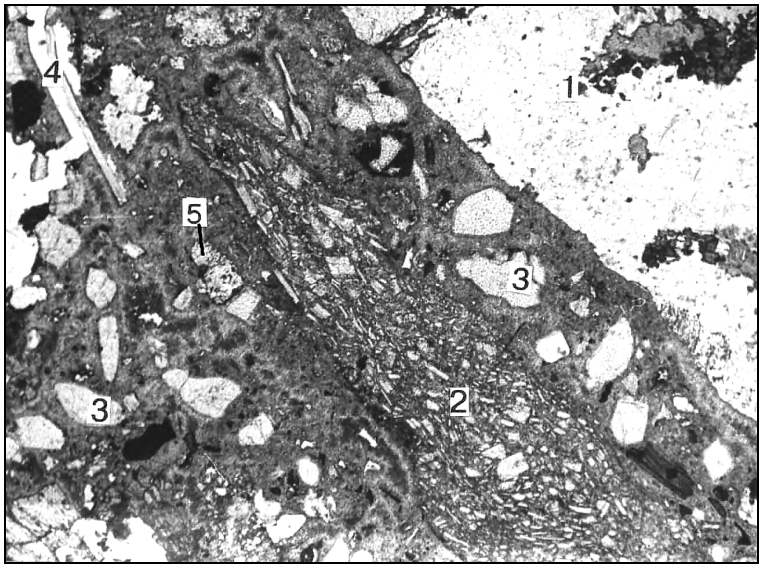

Fig. 5*. Sharp contact of brecciform apatite-francolite vein with fenite (1).*

The vein shows fragments of francolite-vermiculite rock (2), apatite (3), vermiculite (4), forsterite (5), and magnetite (black isodiametric grains). Photomicrographs of a thin section (width of field of view is 2.2 mm). Plane-polarised light.

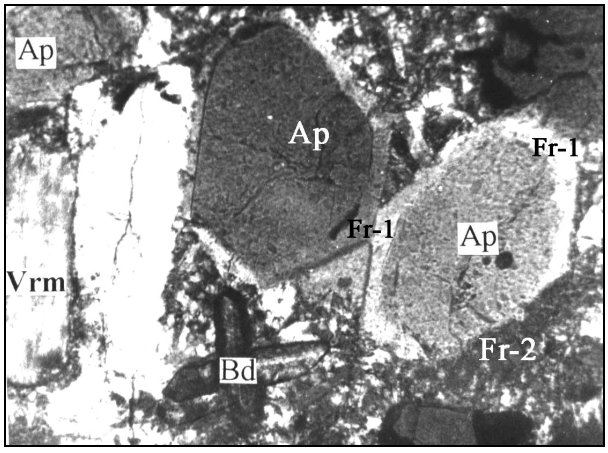

Fig. 6. *Homo-axial pseudomorphs of francolite-1 (Fr-1) after apatite (Ap) in brecciform apatite-francolite rock with grains of relict minerals: baddeleyite (Bd), vermiculite (Vrm) and magnetite (black isodiametric grains) cemented by francolite-2 (Fr-2). Photomicrograph of a thin section (width of field of view is 1 mm). Crossed polars.*

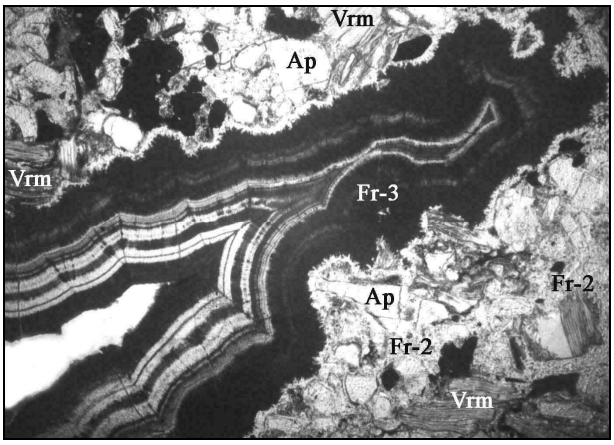

Fig. 7. *Typical brecciform apatite-francolite rock with grains of relict minerals: apatite (Ap), vermiculite (Vrm) and magnetite (black isodiametric grains) in francolite-2 (Fr-2) matrix. The caverns in the rock are filled by kidney-like rhythmic zoned aggregate of francolite-3 (Fr-3). Photomicrograph of thin section (width of field of view is 6 mm). Plane-polarised light.*

opaque due to the presence of fine-grained limonite and manganese hydroxide impurities; the latter sometimes form dendrites. Such apatites seem to be similar to those referred as *brown hydroxyl fluorapatites* associated with dolomite carbonatites [8].

The third best-known francolite generation *Fr-3* forms zonal crust- and kidney-like aggregates (Fig. 7), spherolites and veinlets. Thin micro-zones differ from each other in a content of fluorine and carbon dioxide hence their optical constants are different. The transparent zones contain 4-4.5 mass % of F and about 3 % of CO_2, and opaque, slightly weathered zones contain 0.45 % of F and 1.30 % of CO_2. Francolite of the third generation is usually white and a rare sky-blue

colour of this mineral is caused by copper impurity (0.44-0.55 wt. %). The crust of small chabasite crystals locally covers the surface of francolite-3.

The fourth francolite generation *Fr-4* occurs as the porcelain-like aggregates, filling caverns or axial zones of veinlets growing over francolite 3. Francolite-4 is opaque and white or pale yellow in colour. Francolite-4 can also lining the bottom of some caverns and its zoning here is parallel to the water level.

The chemical composition of francolite 3 and 4 was investigated by many authors [4, 8, 10]. These data show that contents of P_2O_5 (37.43 – 40.00 wt. %), CaO (53.00 – 55.35%), SrO (0.02 – 0.25%), Mg0 (0.10 – 0.50%), H_2O (1.13 – 2.32%), F (1.55 – 3.28%) and CO_2 (1.75 – 3.61 wt. %) are relatively constant. Our analyses revealed an inversely proportional dependence between the refractive index (ω, Fig.8) and cell dimension (a_o, Fig. 9) and the CO_2 concentration (Tab. 3).

Table 3. *Refractive indexes, cell dimensions (Å) and F and CO_2 content (wt. %) in various zones of francolite kidney-like aggregates*

#	Type of francolite	ω	ε	a_o	c_o	F	CO_2
1	**Transparent**	1.626	1.617	9.353	6.894	4.3	3.10
2	**Non-transparent**	1.606	1.603	9.356	6.892	3.3	2.26
3	**White, matt**	1.623	1.617	9.369	6.881	0.45	1.32

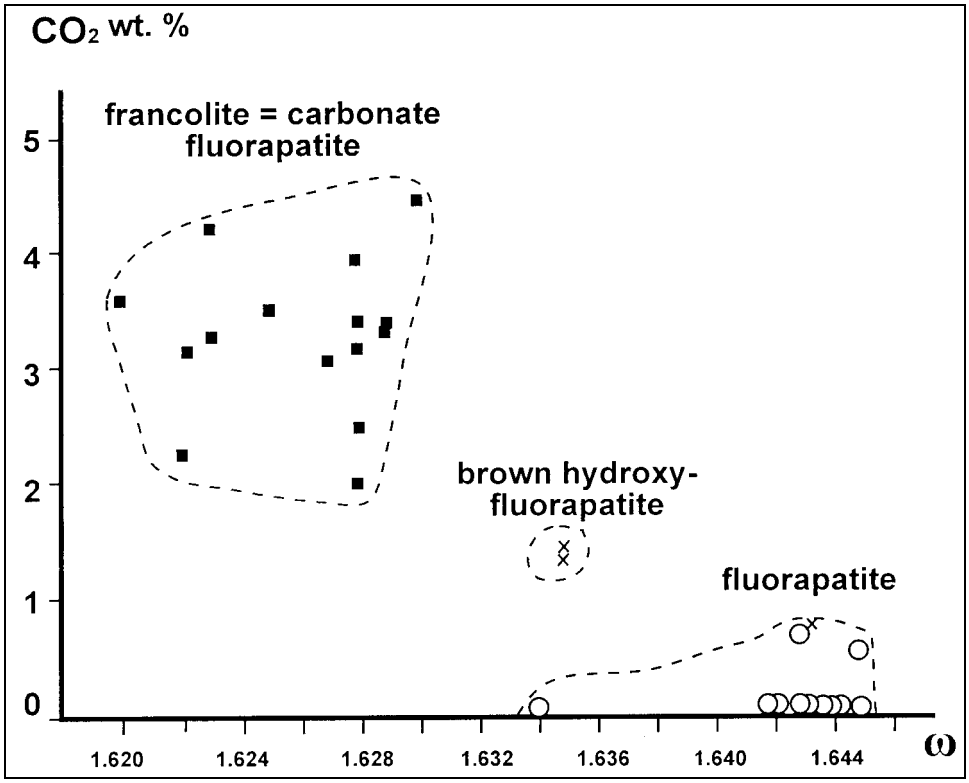

Fig. 8. *Refractive index ω minerals of apatite group from Kovdor phoscorite and apatite-francolite deposits versus CO_2 content.*

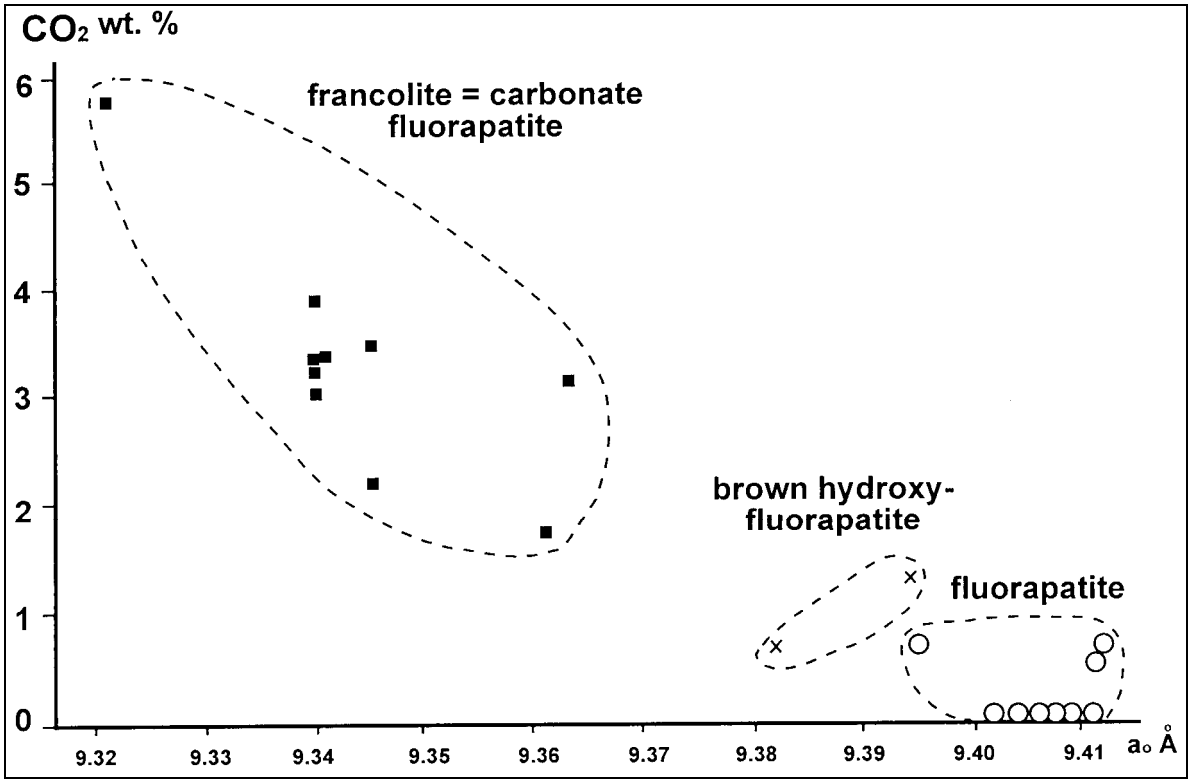

Fig. 9. *a_o of apatite group minerals from Kovdor phoscorite and apatite-francolite deposits versus CO_2 content.*

It is remarkable that fluorine content in apatites of the phoscorite-carbonatite rock series increases from 0.87–0.97 wt. % in the oldest apatite-forsterite rocks to the 1.77–2.08 % in younger dolomite carbonatites. Fluorine content in francolites gradually increases faster considerably – to 2.0–4.3 wt. % [12].

PETROGENETIC MODEL

Different hypotheses were proposed to explain genesis of francolite deposit [1, 2, 3, 8, 6, 10, 14, 15, 16, 18, 19, 22]. Despite of numerous genetic models many problems dealing with the francolite rock formation remain to be resolved.

Following statements made in this paper should be taken into consideration to highlight on the origin of apatite-francolite deposit.

1. Francolite-bearing rocks are genetically related to alkaline-ultrabasic intrusions and in all known deposits they followed the formation of carbonatites and are associated with carbonatite bodies.

2. Francolite-bearing rocks sink to depths of 10 to 150m (rarely to 200m). Bodies of these rocks are vein-, funnel-, mushroom-like or bed-like in shape branching downwards. These bodies in Kovdor are related to a system of semi-circular faults very typical of the central type intrusions. The morphology of francolite-bearing bodies is similar to that of tuff breccias, agglomerates and zones of alumstone-bearing rocks located in the vicinity of volcanoes [23].

3. Breccia and cavernous texture, crustified cement structures are typical features of francolite-bearing rocks.

4. No signs of karst formation have been found in the country carbonatites bedding or surrounding the francolite bodies; leaching of carbonate substance and subsequent redeposition, as lime tuffs have not been reported from rocks of this deposit.

5. All the minerals associated with francolite (zeolites, crandallite, antigorite, vermiculite, montmorillonite, halloysite, hydroxides of iron and manganese etc.) could form at low-temperature conditions. It is remarkable that the process of rock silication is developed near the mouths of two of hopper-shaped francolite bodies located in fenites.

6. The various types of francolite-bearing rocks were formed at least in three stages accompanied by the repeated rock brecciation and crushing followed by cementation of the fragments by francolite of different generations.

7. According to Zaitsev and Bell [21] all calcites, dolomites and apatites from most rocks of Kovdor UAPC complex show the low $^{87}Sr/^{86}Sr$ ratios = 0.7032-0.7039, suggesting their origin from the mantle source. On the contrary, this ratio = 0.7059-0.7061 for francolite from the apatite-francolite rocks of the latest formation stage seems to point to the crustal contamination.

All the above data and considerations lead to suggest the following scheme of apatite-francolite deposit formation illustrated by Fig. 10. The volatile phases F, H_3PO_4 and some H_2O accumulated at the last stages of endogenous magmatic carbonatite formation has transformed calcite to francolite (first and second generations in francolitized carbonatites). A possible chemical reaction is:

$$5CaCO_3 + 3H_3PO_4 + HF \rightarrow Ca_5(PO_4)_3\,(OH,F) + 5H_2O + 5CO2\uparrow.$$

The released carbon dioxide caused explosions, which took place in some local sites along semicircular breaks to which mouths of the funnel-shaped bodies are related now. The strongest explosions probably could take place when volatile emanations reached the level of the ground water table. In this case, the surface water undoubtedly was enriched in acidic components and this solutions could boil. Both volatile and these hydrothermal solutions transformed the country rocks surrounding these hot pipes and this process gave rise to the development of low-temperature mineral associations. The composition of rock fragments in francolite-bearing breccias was fully controlled by that of surrounding country rocks.

In this funnel-shaped bodies the stable residual minerals of carbonatites (magnetite, apatite and baddeleyite) were accumulated due to the calcite dissolution and, therefore apatite-francolite breccias got enriched in these minerals. The cementation of all the rock and mineral fragments affected by phosphorous hydrothermal low-temperature (< 150-180^o C) solutions. These solutions probably were strongly supersaturated and became colloidal. It is this process, which is responsible for the formation of the massive apatite-francolite brecciform rocks. Light mineral particles could been transported during the explosions for a long distance whereas the lack of hydrothermal solutions caused the formation of loose

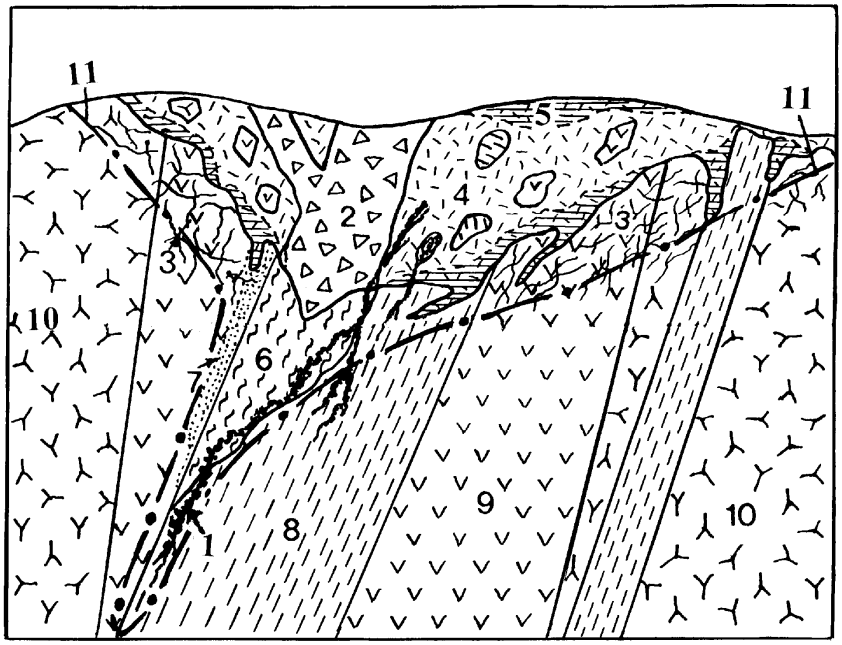

Fig. 10. *Schematic diagram of Kovdor apatite-francolite geological section.*

1 – vermiculite-psilomelane brecciform veins; 2 – apatite-francolite brecciform massive rocks; 3 – francolite and chabasite-francolite veinlets; 4 – francolite-vermiculite loose rocks; 5 – limonite-rich loose rocks; 6 – francolitized calcite carbonatite; 7 – zone of ijolite zeolitization; 8 – calcitic carbonatite; 9 – ijolite; 10 – fenite; 11 – ground water table.

or poorly cemented francolite-vermiculite rocks. Many stages of rock brecciation were accompanied by cementation of all the earlier minerals and rock types by different francolite generations. The latest fractions of hydrothermal solutions were enriched in iron and manganese. The process responsible for the formation of francolite deposit resembles in emplacement of phreatomagmatic eruptive centres, often located near the volcanic edifices (Fig. 11).

The source of P, F, partly H_2O, and Fe, Mn seems to be of deep-seated origin similar to that of ore- and carbonatite-forming liquids. The greater part of H_2O is ground water, as indirect evidenced by low $^{87}Sr/^{86}Sr$ ratios in francolite samples. The part of Fe and Mn hydroxides, montmorillonite, hydro-chlorite, malachite etc. could be formed due to the exogenous processes. Is very difficult to distinguish between exogenous minerals and those formed at the hydrothermal stage. Unfortunately, the age of this francolite mineralisation has not been defined as yet.

Thus, the francolite-bearing rocks of Kovdor complex could be regarded as a multistage polygenetic formation similar to hydrothermal explosive breccias or rocks of the phreatomagmatic eruptive origin. It is very likely to find some analogy in the genesis of other francolite deposits for instance in Sokli (Finland), Glenover (Transvaal, South Africa), Bukusu and Sukulu (Uganda), Tundululu (Malawi) etc.

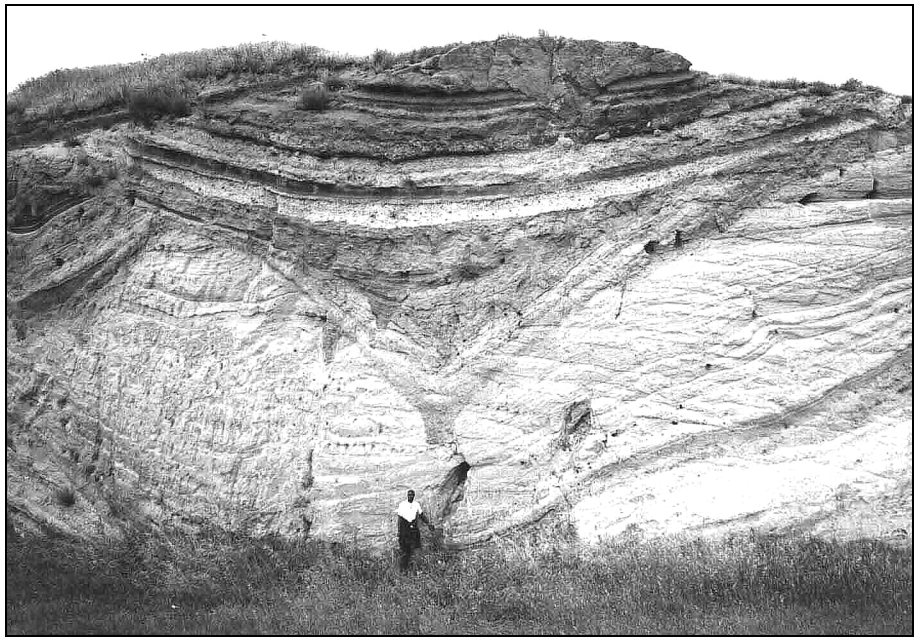

Fig. 11. *Outcrop of a small lacustrine basin filled by the phreatomagmatic ash-tuff and accretionary lapilli deposits, Rionero area, the Mt. Vulture Volcano, Italy. The outcrop is 12 m high.*

ACKNOWLEDGEMENTS

The author is grateful to A. Chakhmouradian and R. Sorkina who tried improve my English.

REFERENCES

1. **Afanasiev, A.P.** Mineralogy of the preglacial weathering crust of Kola Peninsula and connected vermiculite deposits. Moscow-Leningrad, Nauka Press: 1966, 170 pp. (In Russian).
2. **Egorov, L.S.** Apatite in Maimecha-Kotui ultrabasic alkaline rock complex. Pp. 227-233 in: Apatite. Moscow, Nedra Press: 1968, (In Russian).
3. **Kapustin, Yu.L.** Mineralogy of the carbonatite weathering crust. Moscow, Nedra Press: 1973, 198 pp. (In Russian).
4. **Kapustin, Yu.L.** Mineralogy of carbonatites. D.K. Biswas (trans.) New Delhi Amerind: 1980, 259 pp.
5. **Krasnova N.I.** Diagnostic features of metasomatism. // Intern. Geol. Review. 1988, **30,** pp. 1070-1083.
6. **Krasnova, N.I.** Geology, mineralogy and the questions of apatite-francolite rocks genesis of Kovdor massif. Pp. 164-172 in: Material composition of phosphorites. Novosibirsk, 1979, (In Russian).
7. **Krasnova, N.I. and Sokolova, V.B.** Tectonics and mechanism of formation of the Kovdor alkaline-ultrabasic intrusive complex. // Vestnik Leningr. Univ., 1978, No. 6, pp. 16-21. (In Russian).
8. **Kukharenko, A.A., Orlova, M.P., Bulakh, A.G., Bagdasarov, E.A., Rimskaya-Korsakova, O.M., Nefedov, E.I., Ilinskiy, G.A., Sergeev, A.S. and Abakumova, N.B.**

Kukharenko, A.A. The Caledonian ultramafic alkaline rocks and carbonatites of the Kola Peninsula and Northern Karelia. Moscow, Nedra Press: 1965, 772 pp. (In Russian).

9. **Kurbatova, G.S. and Gannibal, L.F.** Geochemistry of phosphorus and the main apatite mineralization types in Kovdor massif. Pp. 78-86 in: Perspective of Kovdor mining complex development, 1972, Apatity (In Russian).
10. **Kurbatova, G.S. Gannibal, L.F. and Dudkin O.B.** The material composition and genetically peculiarities of francolite breccia of Kovdor massif. // Dokl. Akad. Nauk SSSR, Earth Sci. Sect., 1972, **207**, No. 5, pp. 1208-1211. (In Russian).
11. **Rimskaya-Korsakova, O.M. and Krasnova, N.I.** Geology of the deposits of Kovdor massif. Saint-Petersburg, Saint-Petersburg University Press: 2002, 146 pp. (In Russian).
12. **Rimskaya-Korsakova, O.M., Krasnova N.I. and Kopylova L.N.** Typochemical peculiarities of apatites of Kovdor complex deposit. Pp. 58-70 in: Mineralogy and geochemistry. LGU Press: 1979, No. 6. (In Russian).
13. **Ternovoy, V.I.** Carbonatite massifs and their mineral resources. Leningrad, LGU Press: 1977, 168 pp. (In Russian).
14. **Ternovoy, V.I., Chuyeva M.N., Yevangulova E.B. and Belova A.N.** On the genesis of Kovdor apatite-francolite deposit. // Zap. Vses. Mineral. Obshchest., 1976, Part **105**, No.2, pp. 241-147. (In Russian)
15. **Vartiainen, H.** The petrography, mineralogy and petrochemistry of the Sokli carbonatite massif, northern Finland. Geol. Surv. of Finland, Bull., 1980, **313**, 126 pp.
16. **Vartiainen, H. and Paarma, H.** Geological characteristics of the Sokli carbonatite complex, Finland. // Econ. Geol., 1979, **74**, pp. 1296-1306.
17. **Vartiainen, H., Melnikov I. and Sulimov B.** The francolite ore deposit of Kovdor and Sokli. // Proc. of Finnish-Soviet Symposium held in Helsinki, Finland, Nov. 14-15, 1990. Otaniemi, 1991, pp. 7-14.
18. **Verwoerd, W.J.** The carbonatites of South Africa and South West Africa. // Geol. Survey, Handbook, 1967, **6**, 452 pp.
19. **Verwoerd, W.J.** Mineral deposits associated with carbonatites and alkaline rocks. // Mineral Deposits of Southern Africa, 1986, **1**, pp. 2173- 2191.
20. **Volotovskaya, N.A.** The Kovdor massif. Pp. 419-428 in: Geology of USSR, 1958, **27**, Part 1, Leningrad (In Russian).
21. **Zaitsev, A. and Bell, K.** (1995) Sr and Nd isotope data of apatite, calcite and dolomite as indicators of source, and the relationships of phoscorites and carbonatites from the Kovdor massif, Kola peninsula, Russia. // Contrib. Mineral. Petrol., **121,** 324-335.
22. **Zanin, Yu.N. and Zhirova, L.T.** On the question of the formation conditions of phosphate breccias in Maimecha-Kotui province of ultrabasic-alkaline rocks. // Dokl. Akad. Nauk SSSR, Earth Sci. Sect., 1972, **205**, No 3, pp. 692-695. (In Russian).
23. **Zelenov, K.K.** The volcanoes as a source of ore-forming components of sedimentary deposits. Moscow, Nauka Press: 1972, 214 pp. (In Russian).

Ultrapotassic rhyolites of Southern Kamchatka : geochemical and petrological evidence

Perepelov. A.B. [1], AntipinV.S. [1], Kablukov A.V. [1], Filosofova T.M. [2]

[1]*Institute of Geochemistry SB RAS, Irkutsk, Russia, E-mail: region@igc.irk.ru*
[2]*Institute of Volcanology FEB RAS, Petropavlovsk-Kamchatsky, Russia*

The calculations of geothermometers show the crystallization temperatures of albite, occurring as phenocrysts along with Kfs and Pl, to vary from 774 to 554 °C. The calculated mass balance points out that UPR might have formed after fractionation from highly potassic rhyolites Ab (~ 28,2-33,7%), Pl (~ 0–0,5%), Mgt (~ 0-0,8%), Ap (~ 0,2-0,3%), Ilm (~ 0-0,3%). Thus, albite represents the main mineral phase involved in differentiation process.

Plotting within coordinates K_2O-SiO_2 with the trends of composition displacement, while Ab, An, Cpx, Mgt, Bt and Kfs were fractionating displays similar results.

Crystallization differentiaton with albite involved is the main mechanism responsible for UPR formation.

INTRODUCTION

Ultra-potassic rhyolites (UPR) represent fairly specific magmatic formations. They show anomalously high concentrations of silicic acid (SiO_2 to 80-81%) and K_2O (from 5-6 to 9-11%). These rocks are depleted in Na_2O (1-2 mass %) and some other petrogenic and rare lithophyle components. The ratios K_2O/Na_2O vary from 2-5 to 25-35. UPR are found in different geological units and geodynamic settings and have an exclusively wide age range of formation within Proterozoic sequences of the Voronezhsky crystalline massif and Sinay Peninsula, in the Paleozoic magmatic formations of the Urals, Kazakhstan, Middle Asia, Rudny Altay, within Mesozoic depressions of Trans-Baikal, Primorye, Caucasus, Mongolia, in the Okhotsk-Chukotka volcanic belt They are hosted by the geological units of South and North America, East Europe and elsewhere. Common features of the geological and petrogenetic status of UPR are as follows.

Such rocks are normally derived in the geological units in the end of volcanic activity or at the late stages of their development. While forming, they approach the subsequent post-magmatic processes; UPR make up subvolcanic bodies and dykes; produce lava flows fairly seldom; associate closely within the structures with the other types of acid volcanic rocks. As regards the pattern of petrogenetic indicator elements distribution UPR display common features with every concrete magmatic rock series.

The existing models of UPR formation may be conventionally divided into: (i) magmatic and (ii) amagmatic. The latter are responsible for high concentrations

of K_2O in UPR by post-magmatic adularization of primarily glassy matrix of rhyolites of the calc-alkaline series, polar redistribution of potassium and sodium in the zone of catagenesis resulting from low-T regional metamorphism or ion-exchange interaction of glassy matrix of volcanics with the fluids of endogenous and exogenous origin. The magmatic model accounts for the UPR origin due to partial melting of K-enriched crystalline substance of the crust, and concentration of acid magmaic melts of potassium which are derived by differentiation or liquation separation of acid melts of the normal series into sodium and potassium phases. The petrological and geochemical lines of evidence on this rock type were earlier reported by some authors, e.g. Fromberg [3].

When developing the models of formation of ultrapotassic rhyolites, as magmatic formations, the important task was posed to search the main petrogenetic factors in the evolution of acid melts leading to formation of fairly stable petrogenetic type of UPR irrespective of the place, time, geological setting of their origination and the type of parent magmas, which precondition inheritance of UPR with the evidence of associated rocks.

UPR of the island arc system of Kamchatka have been selected as the study object characterizing ultrapotassic rhyolites of the "ocean-continent" transition zones. Any mineralogical or geochemical investigations of these formations have not been accomplished so far, and the ultra-potassic acid rocks have not been discovered within magmatic formations in the region. As an exception, we may refer to Volynets and Flerov [10] who earlier had found pegmatoid quartz feldspar veins amongst Paleogene assemblages of gabbro-syenite-trachyandesites (Central Kamchatka) similar to UPR in chemical composition (K_2O=8,56%).

GEOLOGICAL SETTING, MINERALOGICAL AND PETROGRAPHIC TRAITS OF ULTRAPOTASSIC RHYOLITES

Ultrapotassic rhyolites represent a rare petrogenetic type within the rocks of magmatic formations of the recent island system of Kamchatka. Such formations are now distributed locally within the Neogene-Quaternary volcanic belt lying in the northern part of Southern Kamchatka. Structurally, the UPR are distributed through the Malko-Petropavlovsk zone of transcurrent fault dislocations, near its southern flank (Fig. 1). The magmatism of this zone through the entire time span of formation of island arc volcanogenic sequences from Oligocene to Holocene, along with predominance of moderately potassic types of rocks, are also typified by development of highly-potassic (HP) volcanic series differentiated from HP basalts to HP rhyolites [2, 6, 7]. In this connection, the available type of petrochemical zonation of island arc volcanism within the transverse zone is disturbed due to distribution of HP rocks in the frontal part of island arc.

Geological survey revealed UPR within the Neogene volcanogenic sequences on the left bank of the Bannaya river midstream. In 1987, these formations were

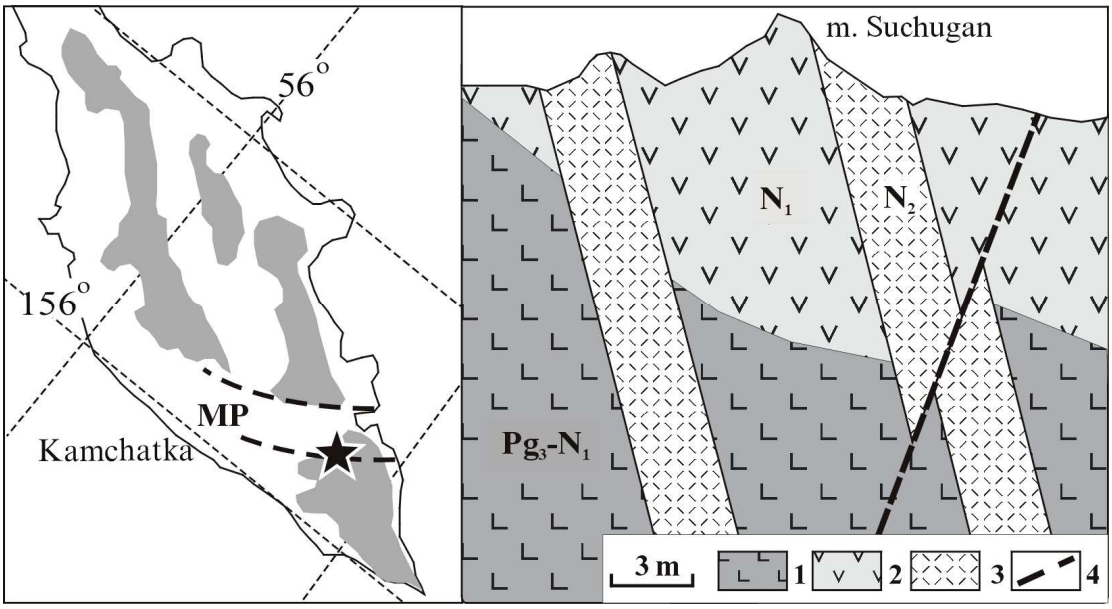

Fig. 1. *Scheme of geological cross-section of ultra-potassic rhyolites (southern slope – Suchugan Mt, left side of Bannaya river, Southern Kamchatka).*

On the map: star shows location of ultra-potassic rhyolites in volcanic belts of Kamchatka, MP – conventional boundaries of Malko-Petropavlovsk zone of fault dislocations.

Legend: 1 – tuff-sedimentary sequence of the Paratunsky suite (Pg3-N1), 2 – volcanogenic-sedimentary sequence of the Berjozovsky suite (N_1), 3 – dykes of ultra-potassic rhyolites (N_2), 4 – fault.

studied in terms of project "Geochemistry of HP volcanism of Kamchatka" at the Institute of Geochemistry, Irkutsk. UPR make up two large subparallel dykes of steep occurrence striking northeast, their thickness varying from 3 to 10 meters on the southwestern slopes of Suchugan Mt (Fig. 1). The dykes have been dated from geological data to be Pliocene. They cut the rocks of the tuff-sedimentary sequence of the Upper Oligocene – Lower Miocene Paratunsky suite ($Pg_3 – N_1$) which consist of tuffites, tuffs, tuff-breccias, tuff siltstones, argillites, sandstones and conglomerates and volcanogenic-sedimentary sequence of the Upper Oligocene – Middle Miocene Berezovsky suite (N_1, andesites, andesite-dacites, dacites, rhyolites and their tuffs, tuff breccias, ignimbrites, tuffites, tuffogenic sandstones and siltstones and conglomerates). Younger volcanogenic formations are referred to the Pliocene Alney series and Quaternary volcanic units. The lava-pyroclastic sequences of the Alney series (N_2) consist of basalts, andesite-basalts, andesites and their tuffs, tuff breccias, lying ubiquitously as nappe outliers or eroded volcanic chambers. Numerous extrusions of HP dacites and rhyolites, reaching 300-400 m in diameter, cut volcanogenic sequences of the Paratunsky and Berezovsky suites and show themselves at the final stage of formation of the Alney series. UPR occur in a close spatial position with HP rhyolites, however no direct geological relationships have been found. The closest extrusive body of HP

rhyolites is located about 300 m from ultrapotassic rock dykes. The UPR dykes are cut by the fault with oblique displacement of rocks of subvolcanic body for 2-2.5 m (Fig. 1). Even if in this paper the age of UPR of South Kamchatka is accepted to be Pliocene, their age is to be checked. It is known that albite-bearing acid magmatic rocks and albite-porphyries of the adjacent territories of the South-East Kamchatka belong to volcanogenic sequences of Pg_3-N_1 age interval of formation [6].

UPR are white milky, white-yellowish rhyolite porphyries with block-like separations. They are hosted by the lavas of almond-shaped andesite basalts and tuffs of similar composition. In the dyke bodies the rocks do not bear any traces of propilitization, however in deluvial piles such varieties are the case.

UPR include porphyry structures. The porphyry and fine-grained mass, composed of microlites of Na-sanidine (Fsp), sanidine (Kfs) and quartz (Qtz) containse idiomorphic phenocrysts, clasts and ingrowths of albite crystals (Ab), Fsp, Kfs and Qz of 2-3 mm size (Table 1). The dark color minerals are represented by fine single crystals of mica, ore minerals and orthite are accessory. Inclusions of quartz consist of clasts and idiomorphic grains of mineral, often resorbed through cracks. There are also traces of dissolution and melting of large phenocrysts of quartz with formation of “shirt” from crystallized glass and “filling in” of glass into crystals. In places quartz encloses tiny resorbed crystals of Kfs and Fsp looking as perthite. Some grains show sectorial decay. The agglomerate ingrowths of fine quartz grains of lenticular shape, appearing as the late generation of this mineral, are present.

The K-Na feldspars of UPR may be subdivided into three generations: large phenocrysts and subphenocrysts Kfs ($Ab_{2.5\text{-}4.1}$ – $Or_{95.9\text{-}97.4}$); - phenocrysts and subphenocrysts Fsp ($Ab_{33.4\text{-}33.5}$ – $Or_{66.4\text{-}66.5}$) often being in aggregate with Qtz; and microlites Kfs ($Ab_{2.1\text{-}7.4}$ – $Or_{92.5\text{-}97.9}$), making up (along with quartz) the fine-grained the bulk rock (Fig. 2). Subphenocrysts Fsp are discovered in aggregates with albite.

Albite, being idiomorphic at the level of subphenocrysts and large phenocrysts, is saturated in inclusions of magmatic glass. Those albites, which are “saturated” in glass, are available in aggregates with crystals Fsp ($An_{4.8\text{-}5.1}$ – $Ab_{93.9\text{-}94.8}$). Albite, forming aggregates with Kfs have purely “clean” compositions (An_0 – $Ab_{99.2\text{-}99.3}$).

The petrographic observations indicate that formation of feldspar and quartz phenocrysts for UPR are arranged as follows: Fsp - (Ab + Fsp) - (Ab+Kfs+Qtz) - (Kfs+Qtz). It is confirmed by the fact that Fsp in aggregate with “pure” San are not discovered. The process is completed in the bulk rock mass as aggregates of small crystals.

Orthite, its composition not defined, forms short-prismatic separations with grain size 0.05-0.1 mm, found in aggregates with Kfs as small inclusions in Kfs and albite, as well as tiny separations in the bulk rock mass. It remarkable that rare and small grains of orthite are often confined to the boundaries of quartz and Kfs

Table 1. *Representative microprobe analyses for rhyolites of Pliocene extrusions of Malko-Petropavlosvk fault dilocations (Southern Kamchatka)*

# sample	BT1121												
Mineral	Pl	Pl	Pl	Pl	Fsp	Kfs	Fsp	Gl	Cpx	Cpx	Bt	Mt	Ilm
Phases	c	r	m	m**(Pl2)**	c	m	r	gl	m	m	bt	m	m
SiO_2	49,44	55,31	62,12	**63,45**	65,53	66,97	68,18	73,44	45,28	**52,87**	37,81	0,04	0,00
TiO_2	0,00	0,01	0,03	**0,01**	0,00	0,00	0,01	0,10	1,45	**0,47**	3,99	9,48	43,81
Al_2O_3	32,16	28,33	23,44	**22,31**	19,40	17,51	19,57	12,22	8,75	**1,80**	13,30	2,39	0,31
Cr_2O_3	0,03	0,03	0,00	**0,00**	0,00	0,03	0,00	0,00	0,05	**0,00**	0,05	0,04	0,04
Fe_2O_3	0,00	0,00	0,00	**0,00**	0,16	0,00	0,00	-	3,72	**0,00**	-	49,00	19,92
FeO	0,88	0,64	0,30	**0,43**	0,00	0,10	0,39	0,64	11,11	**12,02**	15,92	37,08	32,74
MnO	0,00	0,00	0,04	**0,00**	0,00	0,03	0,01	0,02	0,30	**0,56**	0,59	1,53	3,91
MgO	0,00	0,06	0,00	**0,01**	0,00	0,00	0,01	0,00	10,69	**17,12**	14,17	1,17	1,63
CaO	15,00	10,73	5,11	**3,87**	0,23	0,06	1,97	0,48	18,12	**15,15**	0,01	0,08	0,01
Na_2O	2,61	4,96	7,40	**7,61**	3,92	2,40	7,93	0,53	0,38	**0,19**	0,59	0,01	0,00
K_2O	0,16	0,34	1,39	**1,52**	11,14	13,60	2,71	2,79	0,00	**0,00**	9,51	0,00	0,00
Total	100,28	100,41	99,83	**99,21**	100,38	100,70	100,78	90,22*	99,85	**100,18**	99,94*	100,82	102,37
An (Wo)	75,32	53,36	25,35	**19,90**	1,12	0,29	10,08		40,92	**31,33**			
Ab (En)	23,72	44,63	66,44	**70,80**	34,46	21,09	73,41		33,59	**49,26**			
Or (Fs)	0,96	2,01	8,21	**9,30**	64,42	78,62	16,51		25,49	**19,41**			

Table 1. (end)

# sample	BT1120.1							BT1103				
Mineral	Pl	Fsp	Fsp	Bt	**Ilm**	Mt	Sph	Kfs	Kfs	Fsp	Ab	Ab
Phases	r	c	m	c	**c**	**c**	sph	c	c	c	c **(Pl1)**	c
SiO_2	64,02	65,06	67,08	36,72	**0,00**	**0,00**	28,69	62,32	64,29	64,99	**66,99**	67,16
TiO_2	0,00	0,00	0,00	3,83	**45,71**	**4,33**	33,81	0,00	0,00	0,00	**0,03**	0,00
Al_2O_3	22,12	18,69	18,82	13,24	**0,14**	**0,87**	1,40	18,73	19,20	19,17	**20,86**	20,68
Cr_2O_3	0,00	0,00	0,02	0,03	**0,06**	**0,04**	0,00	0,00	0,06	0,00	**0,07**	0,04
Fe_2O_3	0,00	0,09	0,00	-	**16,67**	**63,79**		0,00	0,00	0,12	0,00	0,00
FeO	0,12	0,00	0,28	16,80	**33,47**	**33,86**	2,17	0,00	0,00	0,00	**0,00**	0,01
MnO	0,00	0,03	0,01	0,76	**4,79**	**1,83**	0,29	0,00	0,00	0,01	**0,02**	0,00
MgO	0,00	0,00	0,00	13,93	**1,63**	**0,79**	0,02	0,00	0,00	0,00	**0,00**	0,00
CaO	3,61	0,20	0,54	0,00	**0,00**	**0,00**	25,87	0,00	0,00	0,00	**0,00**	1,00
Na_2O	8,61	4,10	5,47	0,54	**0,00**	**0,00**	0,00	0,45	0,53	3,86	**10,58**	10,91
K_2O	1,27	11,09	8,31	9,62	**0,00**	**0,00**	0,00	17,03	17,01	11,67	**0,11**	0,10
Sum*	99,75	99,26	100,53	99,41*	**102,47**	**105,51**	92,25	98,53	101,09	99,82	98,66	99,90
An (Wo)	17,44	0,96	2,66					0,00	0,00	0,00	0,00	4,79
Ab (En)	75,26	35,63	48,68					3,86	4,52	33,45	99,32	94,64
Or (Fs)	7,30	63,41	48,66					96,14	95,48	66,55	0,68	0,57

Note. *Sample # BT1121 – hughly-potassic rhyodacite, 1121.1 – HPR, 1103 – UPR..*

Mineral designations: *Pl - plagioclase, Fsp –Na-sanidine, Kfs - K- feldspar, Ab - albite, Cpx – clinopyroxenes, Bt – biotite, Mt – magnetite, Ilm – ilmenite, Sph – sphene. Gl – glass of bulk mass. Phase mineral designations: c – central and r – marginal zones of phenocrysts, m – microlytes, in – sphene inclusions in feldspar. Solid font shows mineral compositions which were use d in calculating the models of crystallization differentiation by the method of mass balance (see Table 3. Sum* - in biotite analyses H_2O contents (1121 – 4,00%, 1120.1 – 3,94%) were considered. Distribution of Fe_2O_3 and FeO is calculated after stoichiometry. In Bt, Sph, Gl ferrum is present as FeO. Minals: An, Ab, Or –for feldspars, Wo, En, Fs –for pyroxenes. The mineral compositions are defined by « CAMEBAX» microprobe analyser (Institute of Volcanology, FEB RAS) with current 40 nA and accelerating volt age 20 kV. Oxide contents were calculated by ZAF-correction method using "Correx" program upgraded by V.M.Chubarov. Analysts: Ponomarjov G.P., T.M. Filosofova.*

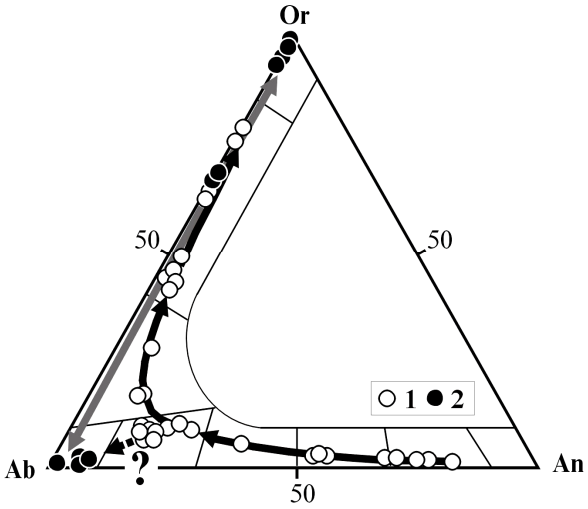

Fig. 2. *Compositions of feldspars of highly- and ultra-potassic rhyolites (HPR and UPR) on the plot Ab-An-Or.*

1 – points of HPR compositions, 2 – the same for UPR. Lines with arrows indicate the evolutionary trends for feldspar compositions: black lines – for HPR, gray – for UPR. The evolutionry trend with question mark denotes the tendency for increase of albite and decrease of orthoclase components in the marginal zones of oligoclase phenocrysts from HPR.

aggregates, in places this mineral fills thin interstitial zones between phenocrysts and subphenocrysts of feldspars and quartz. The amount of orthite, as well as rare and small separations of ore mineral (magnetite, ilmenite?) are not abundant. Besides, at the microlevel among UPR mineral components the method ICP-MS detected minerals bearing Ca, La, Ce and minor amounts of Si, Fe, Mn.

Thus, the principal mineralogical features of UPR are presence of plentiful phenocrysts of magmatic Ab and Kfs, as well as accessory orthite with extremely small distribution of dark color minerals.

The HP rhyolites associated with UPR are dominated by acid Pl (oligoclase $An_{10.1\text{-}20.0}$ – $Ab_{70.8\text{-}77.2}$; rarely andesine $An_{22\text{-}1\text{-}36.8}$ – $Ab_{58.4\text{-}68.1}$) and less widespread are labradorite ($An_{53.3\text{-}68.0}$-$Ab_{30.1\text{-}44.6}$) and bitovnite ($An_{70.1\text{-}81.7}$ – $Ab_{17.6\text{-}28.6}$) (Fig. 2). K-Na feldspars in HP rhyolites contain Fsp both at the level of phenocrysts ($Ab_{32.1\text{-}37.1}$ – $Or_{61.9\text{-}69.9}$), as well as microlytes ($Ab_{48.7\text{-}54.8}$ – $Or_{41.1\text{-}48.7}$). Microlytes in HP rhyolites contain triple feldspars ($Ab_{64\cdot8}Or_{27.5}$) and Na-sanidines enriched in potassium ($Ab_{21.1\text{-}24.3}$ – $Or_{75.6\text{-}78.6}$). It should be marked that in evolving of oligoclase compositions from central to marginal zones of phenocrysts in HP rhyolites there is a tendency towards reducing orthoclase and increase of albite component (Fig. 2, Table 1). Ferruginous biotites (Bt) and rare clinopyroxenes (Cpx) of augite composition are less abundant, while Ab and “pure” sanidines are not discovered. Among other mineralogical features of HP rhyolites it is necessary to mark increased contents of MnO in ilmenite and titanium magnetite (to 4.7%), as well as presence of accessory sphene or inclusions of this mineral in feldspars. Compositions of magmatic glass from HP rhyolites demonstrate redistribution of alkaline components in the residual melt in favor of potassium (Table 1). Structures of HP rhyolites vary from perlite to essentially porphyric depending on the facial type of rocks (dykes, central and marginal zones of extrusions).

GEOCHEMISTRY OF ULTRAPOTASSIC AND HIGHLY POTASSIC RHYOLITES

Ultrapotassic rhyolites (Table 2) represent silicic magmatic formations (sample # BT-1103: SiO_2=78.60%; K_2O=7.54%) with extremely low Ti, Fe, Mg, P, Na and besides, essentially impoverished in Ba, Sr, Zr and rare-earth elements (REE). HP-rhyolites show higher contents of Al_2O_3, Na_2O, MgO, FeO, as well as Ba and Sr. It should marked that any noticeable values of volatiles (F, B) and water are observed. Position of point for UPR composition on diagram K_2O-SiO_2 demonstrate its separation from the evolutionary series of dacites and rhyolites of Neogene volcanogenic sequences in the study region. If the points of rock compositions in the series "dacites-rhyolites" produce a general trend of potassium content increase with increasing their silicic acid concentration in the field of HP series, at the UPR level the potassium alkalinity increases. However, there are no any changes of K/Rb ratio values (Table 2). On the contrary, in the acid volcanic rocks of the region some rhyolite varieties display reduction of alkalinity with formation of the group of compositions lying below the main trend of composition evolution on the plot K_2O-SiO_2 (Fig. 3).

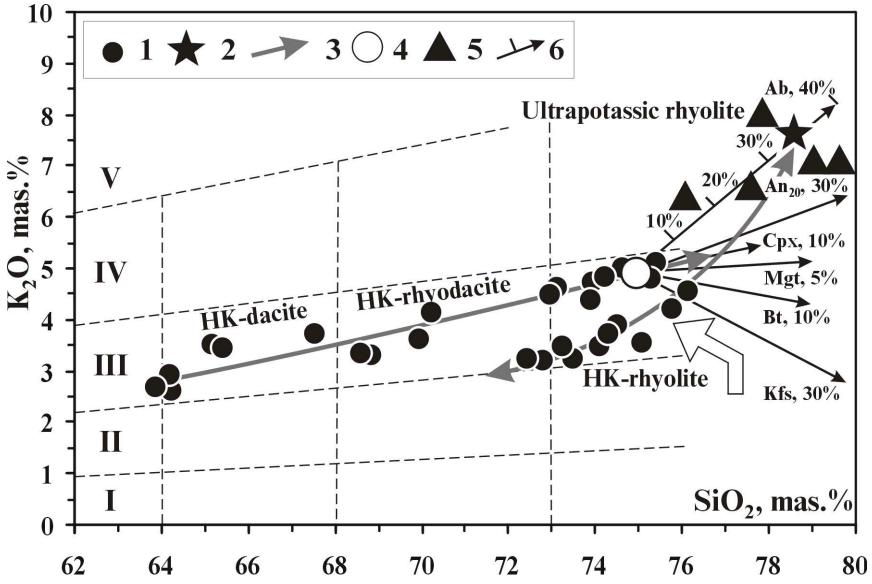

Fig. 3. *Classification diagram K_2O-SiO_2 for dacites and rhyolites of Neogene volcanogenic sequences of Malko-Petropavlovsk zone of transverse fault dislocations (Southern Kamchatka).*

Designations: 1 – points of highly-potassic dacites and rhyolites, 2 – point of UPR composition, 3 – conventional trends of evolution of acid volcanic rock compositions, 4 – UPR composition calculated for fractionation of minerals (SiO_2=75 wt.%, K_2O=4,5 wt %), 5 – trends of UPR composition evolution (4) in fractionating major rock-forming minerals (the plot shows abbreviation of minerals and calculated per cent fractions of their fractionation). The composition fields of rock series: I – low-potassic, II – moderately potassic, III – highly-potassic, IV – subalkaline shoshonite-latite, V –potassic alkaline series. Vertical lines represent the boundary of rock composition fields.

Table 2. *Compositions of highly- and ultra-potassic rhyolites of Southern Kamchatka*

# sample	BT-1121	BT-1120/1	BT-1120/2	BT-1113/1	BT-1100	BT-1103	# sample	BT-1121	BT-1120/1	BT-1120/2	BT-1113/1	BT-1100	BT-1103
SiO_2	69,98	73,14	75,33	75,37	76,13	78,60	V	15,76	28,75	6,23	8,88	11,29	6,14
TiO_2	0,17	0,26	0,15	0,15	0,16	0,12	Sc	3,53	4,20	2,34	2,11	3,11	1,59
Al_2O_3	12,51	13,68	13,17	13,14	12,82	10,76	Ga	14,19	17,78	13,45	14,03	14,24	8,49
Fe_2O_3	0,56	1,35	0,77	0,58	0,59	0,30	Ge	1,55	1,59	1,34	1,60	1,73	0,64
FeO	0,68	0,83	0,39	0,50	0,57	0,65	Ta	0,53	0,29	0,58	0,56	0,42	0,18
MnO	0,08	0,05	0,05	0,03	0,06	0,01	Nb	8,60	7,94	8,24	8,07	9,38	6,13
MgO	0,23	0,26	0,12	0,09	0,14	0,05	Zr	106,95	46,92	106,37	98,71	77,39	43,58
CaO	1,16	0,73	0,57	0,56	0,61	0,18	Hf	4,74	1,92	4,37	3,84	4,08	2,42
Na_2O	4,04	3,96	4,17	4,09	3,90	1,20	La	23,60	21,75	23,79	22,93	20,93	14,93
K_2O	3,61	4,55	4,81	5,06	4,50	7,54	Ce	49,23	48,53	47,63	44,20	44,87	18,48
P_2O_5	0,03	0,03	0,02	0,02	0,02	0,02	Pr	6,38	5,91	6,08	5,76	5,43	2,00
LOI	6,87	1,12	0,41	0,35	0,44	0,46	Nd	21,54	21,03	19,70	18,30	18,38	6,05
Total	99,92	99,96	99,96	99,94	99,94	99,89	Sm	4,43	3,81	3,81	3,67	3,91	1,23
K_2O/Na_2O	0,89	1,15	1,15	1,24	1,15	6,28	Eu	0,54	0,58	0,54	0,53	0,36	0,08
Rb	127,81	153,81	134,08	165,90	154,29	241,61	Gd	3,86	3,45	3,32	3,09	3,52	1,05
Cs	46,34	5,58	4,28	4,23	3,15	2,90	Tb	0,56	0,50	0,49	0,45	0,54	0,16
Ba	377,80	427,95	710,09	774,03	200,77	317,26	Dy	4,17	3,47	3,24	3,35	3,75	1,17
Sr	187,66	71,42	40,46	41,80	34,30	58,95	Ho	1,02	0,73	0,74	0,73	0,97	0,38
Zn	39,91	39,74	21,06	31,27	43,51	14,58	Er	2,44	1,75	2,10	1,85	2,44	0,79
Pb	15,48	15,71	13,09	14,93	12,41	12,60	Tm	0,37	0,32	0,34	0,30	0,44	0,16
Sn	1,95	1,71	2,10	1,77	1,90	1,58	Yb	2,68	1,97	2,32	1,93	2,61	0,96
Cu	12,32	25,22	9,55	5,70	7,11	9,03	Lu	0,49	0,37	0,35	0,36	0,45	0,28
Mo	3,32	1,31	1,05	1,97	0,85	2,07	Y	26,21	21,46	21,14	19,44	23,14	7,76
Co	1,05	2,45	0,43	0,38	0,64	0,32	Th	10,30	8,26	9,94	9,14	12,20	8,03
Ni	3,62	5,85	2,79	3,93	2,08	4,88	U	3,93	3,38	3,59	3,36	4,91	3,13

Note. BT-1121 – UPR (perlite, extrusion, right side of Bannaya river, altitude 1289,8 м), BT-1120.1 – UPR (extrusion, the same), BT-1120.2 – UPR (fluidal extrusion, the same), BT-1113.1 – UPR (rock clast of subvolcanic origin from Pliocene tuff, right side of Maly Klyuchik river), BT-1100 – UPR (extrusion, Mt. Two Brothers), BT-1103 – UPR (dyke, southern slope of Mt. Suchugan, left side of Bannaya river). Analytical methods: petrogenetic elements – RFA; rare elements – (ICP-MS), device - Plasma Quad PQ II Turbo Plus (VG), control: after international standards of rocks (Institute of Geochemistry, SB RAS).

The plots of normalized distribution of rare-earth elements for rhyolites studied are characterized by a significant Eu minimum. The ultrapotassic rhyolites have the deepest Eu-minima (Eu/Eu*=0.19) against HP (Eu/Eu*=0.28-0.46). The most significant degree of differentiation of ultrapotassic rhyolites relative to HP rhyolites is also indicated by the low summary content REE (REE=47.72 ppm, against 107.43-121.33 ppm in HP rhyolites). One should also mark a fairly high degree of REE fractionation in rhyolites (La/Yb=15.48 for UPR and 8.01-11.87 for HP rhyolites). When analyzing the plots of distribution of normalized REE concentrations it was found that HREE contents in ultrapotassic and HP rhyolites is significantly lower than in moderately potassic. Comparison of plots for HP rhyolites and moderately potassic rhyolites of Kamchatka indicates that the degree of REE fractionation in the latter is lower than in highly potassic (La/Yb = 2.6-5.7) with low values of Eu minima (Eu/Eu*=0.26-0.82). The sums of rare earths in moderately potassic rhyolites ranges from 46.1-131.7 ppm, i.e. they are comparable with such for UPR and HP rhyolites.

The main feature of UPR, expressed in the distribution of petrogenic and rare elements is their extremely high degree of differentiation, while their specifics in general corresponds to rhyolites of highly-potassic calc-alkaline series of island arcs.

TEMPERATURES OF FELDSPAR CRYSTALLIZATION OF ULTRAPOTASSIC AND HIGHLY POTASSIC RHYOLITES

Experimental geothermometers may be used to verify the temperature regime of crystallization in rhyolites of the main rock-forming minerals, namely feldspars, defined from petrographic observations and relative estimation of the temperature regime. Some specifics have been revealed in estimating the temperatures of feldspar crystallization for highly- and ultra- potassic rhyolite melts. They will be considered in developing the model of UPR formation. Well-known constructions by Kudo and Weil [5] and Stermer [9] are chosen as alternative and supplementing each other geothermometers. The first method is applied to evaluate the temperature of crystallization of feldspars of Ca-Na series (plagioclase) as well as anorthoclase and An-bearing Na-sanidines from the magmatic melt of known composition. The other method provides the opportunity to calculate the temperatures of joint crystallization of plagioclases with potassium feldspars. For a correct correlation of calculated temperatures of crystallization of all investigated rock compositions the value of total pressure is accepted to be equal to 1 kb. Such a value of pressure is commonly used in modeling of low-depth magmatic systems. Similarity in evaluating crystallization temperature obtained in the calculations indicate a fairly good agreement of the geothermometers (Table 3).

According to calculations (Table 3, Fig. 4), plagioclase is crystallized in HP rhyolites as phenocrysts at T °C-1190-967 (microlytes because of a high dispersion of calculated temperature are not considered). In addition to plagioclases,

anorthoclases and triple feldspars show up in the melt within the temperature range 975-988°C. Further, when temperatures are dropping, within the range 916-844 °C crystallization proceeds jointly between Pl phenocrysts of oligoclase composition

Table 3. *Results of temperature (^{o} C) calculation on feldspars from HP and UP rhyolites of Southern Kamchatka*

Compositions for calculation, sample #	**BT-1121**	**BT-1120.1**	**Compositions for calculation, sample #**	**BT-1103**
Pl-Fsp	888-916 897	884-912 894	**Ab-Fsp**	776-799 791
Pl-R*	1077- 1190 1144	967-979 971	**Ab-Kfs**	532-576 554
Fsp-R*	857-890 878	798-843 819	**Ab-R***	772-776 774

Note. *Tthe calculation of T^oC for Pl-R*, Fsp-R*, Ab-R* (mineral-rock pairs, R - rock) are made (Kudo and Weill, 1970). The calculation of T^oC for Pl-Fsp, Ab-Fsp, Ab-Kfs (mineral-mineral pairs) are made by (Stermer, 1975). The numerator is the calculated temperatures interval, the denominator is the mean for intervals.*

and Fsp. As soon as the system approaches the temperature range 890-798°C, crystallization of plagioclase comes to an end and Fsp (Na-sanidines) may serve the only crystallizing phase of feldspar phenocrysts. However, within the interval T=871-878 °C crystallization of high Ab is feasible. The calculation show that within the range 776-799 °C Ab and Fsp phenocrysts may be crystallized jointly starting from he temperature interval 733-776 °C crystallization of Fsp should cease. Only at the level T=532-756 °C association of Ab-Kfs phenocrysts may be formed, which is observed in ultrapotassic rhyolite.

Thus, within the interval of average temperatures from 744 to 544 °C albite could be the dominant crystallization phase of feldspars in the UPR melt.

ULTRAPOTASSIC RHYOLITES OF KAMCHATKA RESULTING FROM CRYSTALLIZATION DIFFERENTIATION OF MELTS WITH ALBITE INVOLVED

Participation of albite in formation of volcanic rocks was shown earlier for ongonites [4], in which the temperatures of mineral crystallization varied from ~750 to 550 ^{o}C. An effort was made to define the compositions of UPR from compositions of highly-potassic rhyodacites and rhyolites by mass balance method. The calculation required application of the real compositions of minerals from rhyolites (Table 2). The results of calculations point out that in highly potassic rhyodacites and rhyolites the UPR rhyolite is calculated with minimum discrepancies. It follows from calculations that obtaining UPR requires removal of

Ab (~ 28,2 - 33,7%), and insignificant amount of Pl (~ 0 - 0,5%), Mt (~ 0 -0,8%), Ap (~ 0,2 - 0,3%), Ilm (~ 0 - 0,3%) (Table 4).

Thus, albite is the main mineral phase involved in the process of differentiation. Fractionation of these minerals with transition to the UPR

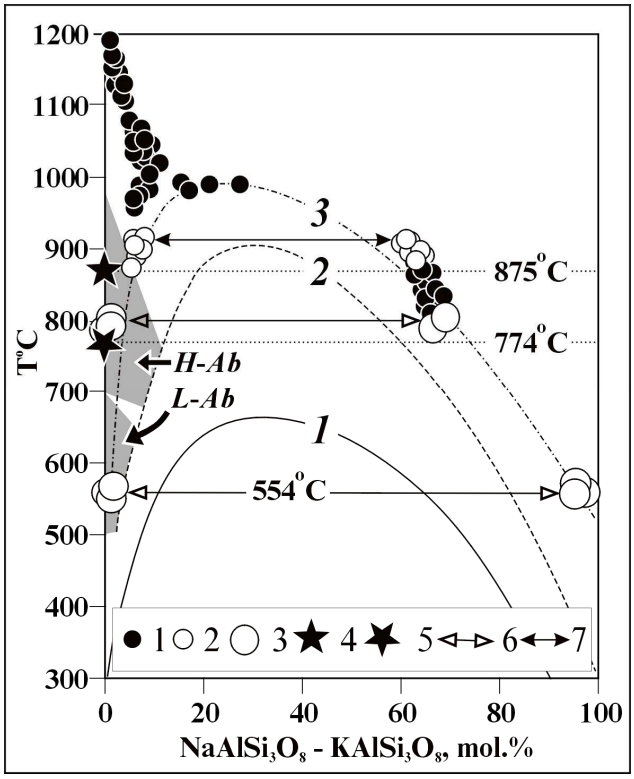

Fig. 4. *Calculated temperatures of crystallization Pl, Ab, Fsp u Kfs in UPR at P=PH$_2$O=1 kb.*

Designations: 1, 4, 5 – calculated temperatures of crystallization Pl, anorthosites and Fsp (1), as well as Ab from HPR (4) and UPR (5) melts after geothermometer [5]. 2, 3 –temperatures of joint crystallization of feldspar phenocrysts calculated after geothermometer [9] for HPR (2) and UPR (3). Solvus curves on the diagram: 1 - low Ab-Kfs, 2 - high Ab-Kfs after (Senderov, 1990), 3 – conventional curve for system of HPR. Composition fields: H-Ab – low albite, B-Ab –high albite. Connodes (6, 7) unite compositions of co-existing feldspars for UPR (6) and UPR (7). T °C thresholds: ~875 °C – possible initial temperature Ab from HPR melt, ~774° – the same from UPR melt after [5], ~554°C – temperature of joint crys-ta-lization Ab and Kfs in UPR melt after [9].

Table 4. *Calculating the model of UPR formation in crystallization differentiation of HPR by mass balance (Southern Kamchatka)*

Initial compositions of melts and minerals					
Initial melts	**BT-1120.1**	**BT-1121n***	**BT-1120.2**	**BT-1113.1**	**BT-1100**
SiO_2	73,14	75,21	75,33	75,37	76,13
Number of minerals involved in differentiation					
Ab ($Ab_{99,3}Or_{0,7}$)	31,76	33,73	29,21	28,19	27,29
Pl ($An_{19,9}Or_{9,3}$)	0,49	0,00	0,00	0,00	0,00
Cpx	1,88	3,78	1,61	0,92	2,24
Mt	0,76	0,00	0,00	0,00	0,00
Ap	0,24	0,29	0,00	0,03	0,00
Ilm	0,28	0,00	0,31	0,00	0,00
Sum	35,41	37,80	31,13	29,14	29,53
Compositions and conventional volumes of residual melts					
Melt (Rock)	**BT-1103**	**BT-1103**	**BT-1103**	**BT-1103**	**BT-1103**
V (%)	64,25	64,20	69,67	71,10	71,83
S*	0,41	3,88	1,22	0,79	2,87

Note. *In calculations HPR compositions are used as initial melts. BT-1121n* – perlite composition, BT-1121 is calculated for water-devoid variant. Compositions of minerals from*

rocks (Table 1): BT-1121 (Cpx, Pl – sub-phenocrysts), BT- 1103 (Ab - phenocryst), BT-1120.1 (Mt, Ilm –microlites). Apatite composition is calculated from the ideal formula. V (%) – sum of components (residual melt volume in mass% from the initial melt volume, S - mran quadratic deviation from differences of oxides between initial and calculated compositions (at S < 1 – satisfactory solution). Calculations were fulfilled with the program «Crystal» applied [8].*

composition causes sharp increase in K_2O content and decrease in TiO_2, Al_2O_3, FeO, MgO, Ca_2O, Na_2O и P_2O_5 on the background of silicic acid content increase. Calculations were made with "Crystal" program (Peretyazhko, 1996) applied, and by the mass balance method for melts. Constuctions on the diagram K_2O-SiO_2 with shift of compositions in fractionation Ab, An, Cpx, Mgt, Bt and Kfs (Fig. 4) display similar results. Only in fractionation ~ 34 % Ab UPR may originate. The mean composition of HPR was accepted as initial.

ACKNOLEDGMENTS

The authors thank T.V. Bounaeva for translating the manuscript.

Research was perfomed under a support of Russian Foundation of Basic Research, grants № 01-05-64206.

REFERENCES

1. **Anders, E., Grevesse, N.**, 1989. Abundances of the elements: meteoric and solar. Geochemica and Cosmochimica Acta 53: 197-214.
2. **Baluev, E.Yu., Perepelov, A.B.**, 1988. Mineralogical and geochemical features of highly-potassic andesites of the frontal part of island arc (Kamchatka). Journal Geochemistry, 813-823. (in Russian)
3. **Fromberg, E.D.**, 1993. Ultra-potassic rhyolites: geology, geochemistry, petrology. Thesis, Moscow, 45. (in Russian)
4. **Kovalenko, V.I., Kovalenko, N.I.**, 1976. Ongonites. Topaz-bearing quartz keratophyres as the analogs of rare-metal Li-F granites. Moscow, Nauka, 124. (in Russian)
5. **Kudo, A.M., Weill, D.F.**, 1970. An igneous plagioclase thermometer. Contribs. Mineral. Petrol., 25, 1.52-65.
6. **Perepelov, A.B., Bazanova, L.I., Florenskiy, I.V., Baluev, E.Yu.**, 1986. Geochemical evolution of the Late Cenozoic magmatism of the south-eastern flank of Malko-Petropavlovsk zone of transcurrent fault dislocations (Kamchatka). In: Kuzmin, M.I., Almukhamedov, A.I. (Ed.), Geochemistry of volcanics of different geodynamic settings. Novosibirsk. Nauka, pp. 165-179. (in Russian).
7. **Perepelov, A.B.**, 1989. Geochemistry of Late Cenozoic highly-potassic volcanic series of island arc system of Kamchatka. Thesis. Univ. Publ. P. 394. (in Russian).
8. **Peretyazhko, I.S.**, 1996. CRYSTAL – applied software for minelogists, petrologists, geochemists. Journal Zapiski VMO 3, pp. 140-148 (in Russian).
9. **Stermer, J.C.**, 1975. A practical two-field spar geothermometer. Amer. Miner. 60, 7-8, pp.664-674.
10. **Volynets, O.N., Flerov, G.B.**, 1967. Petrochemical features of the Upper Cretaceous-Tertiary plutonic and volcano-plutonic assemblages of Central Kamchatka. In: Rudich, K.N. (Ed.) Optic and petrochemical studies of magmatic formations of Central Kamchatka. Moscow, Nauka, pp. 1131-1186.

Jurassic meymechite-picrite complexes of Primorye, Russia: comparative study with komatiite and Japanese picrite suites

Shcheka S.A., Vrzhosek A.A., Vysotskiy S.V.

Far Eastern Geological Institute, 100-letya. 159, 690022 Vladivostok, Russia.
Tel: 7-4232-317-132, fax: 7-4232-317-847, E-mail: sashcheka@fegi.ru

Peculiar ultrabasic volcanic rocks represented by lava flows, pyroclastic rocks, diatremes, and subvolcanic intrusions were found in northern Siberia (Russia) in 1939, and were named meymechite. Recent studies established that meymechite is widespread in the Sikhote-Alin' Mountains (Primorye, Russia) and Japan. The meymechite appears to be a member of an alkaline suite including various alkaline basalts, picrite, phonolite, hawaiite and trachyte as well as the ultrabasic rocks. The meymechite is often associa ***Table 2.*** *Average compositions of meymechites, picrites and komatiites* ted with dunite-pyroxenite-syenite-carbonatite complex bearing Fe-Ti and rare-metal deposits. Fine-grained diamonds (carbonado) were found as placers in the area of potassium-rich diatremes. All these meymechite suites are hosted by Jurassic chert-volcanic formation, and K-Ar ages of the youngest intrusions and diatremes are 152-159 Ma. The meymechite is composed of large (up to 30 mm) olivine (Fa_{10-15}) phenocrysts, small grains of Ti-rich Cr-spinel and variolitic Ti-augite groundmass, which grades into dark glass at pillow rim. More crystallized subvolcanic rocks contain phenocrysts of high-Ti, Cr-bearing augite, kaersutite and phlogopite with the groundmass ilmenite and Ti-magnetite. The geochemical features of the "alkaline" ultrabasic rocks (meymechite) as compared with the "tholeiitic" analog (komatiite) are a higher Ti-content at the same Fe/Mg ratio and enrichment in lithophile elements (Zr, Sr, Ba, Rb, K, U) and volatiles (F, P). Spinels are high-Ti and enriched in iron in the alkaline suite. These data indicate that the meymechite-picrite complexes of Primorye and Japan represent an alkaline analog of the komatiite complexes.

INTRODUCTION

Viljoen and Viljoen [42-43] introduced a new term "komatiite" for the unusual ultrabasic rocks with volcanic texture although they were known there since start of the 20th century [44]. As far back as 1943 [19], however, V.K. Kotul'skiy proposed a term "meymechite"* for the subvolcanic olivine-rich rocks from the river Maymecha (Northern Siberia, Russia). The later investigations showed that this area is a new, vast province of alkaline magmatism including various ultrabasic volcanics, alkali-ultrabasic ring intrusions, kimberlite pipes and carbonatite. For a long time, these data were unknown for the foreign specialists, and it seemed that the Siberian province was a unique area of alkaline ultrabasic volcanism. However, the subsequent study showed that ultrabasic volcanics are

* In English publications, one can find other transliterations (meimechite, maimechite), though they designate the same rock.

widespread in the East-Asian margin [28-29, 26]. Detailed descriptions of the Siberian volcanics appeared recently in English [41,2]. So we hope that these volcanics will be found worldwide in future. Terminology for alkali-ultrabasic volcanic rocks is not well established, and in this paper we use the terms meymechite and picrite as volcanic analogs of alkaline wehrlite (CaO, Al_2O_3 bellow 6 wt.%) and clinopyroxenite (Al_2O_3 – 6-10 wt.%), respectively [32].

S. A. Shcheka first found ultrabasic volcanic rocks from Primorye in 1958, a minor pipe-like body near village Ariadnoe in Middle Sikhote-Alin' [27]. The rock consisting of kaersutite, biotite, olivine and ilmenite and including large (up 0,5 m) blocks of wehrlite was named "subalkaline peridotite". In 1964, Zimin et al. [48] have found a pebble of olivine-rich porphyritic rock named meymechite in the Northern Sikhote-Alin' (River Katen). Any special attention was not paid to these findings at that time. After 1977 [28-29, 27, 45], however, it was established that ultrabasic volcanics and associated rocks are widespread over the Sikhote-Alin' Mountains and in the adjacent areas. It was revealed that the volcanics are accompanied by the ring dunite-pyroxenite intrusions with Au-Pt-ilmenite deposits and diamond occurrences as placers.

Sameshima [25] made the first report of the ultrabasic volcanic rocks in Japan from the Pacific coast near Shizuoka City. Later they were described from other places of Central Japan [36-38, 15]. Ultrabasic varieties of the rocks were named "picrite basalt", "ultrabasic picrite basalt" and even "meymechite" [37]. Taking into account similarity of the most pre-Cenozoic geological structures of Japan and Primorye, it may be supposed that ultrabasic volcanic rocks are widespread in Japan and deserve more detailed investigation.

GEOLOGICAL SETTING

The general regularity of geological position of the meymechite-picrite complex in Primorye is its coincidence with the Jurassic clay-chert formations which outcrop at the most lifted portion of the Cenozoic-Mesozoic sequence along the Central Fault of the Sikhote-Alin' (Fig. 1). The volcanic zones adjoin to the Central Fault under angle 60-70^o in accordance with strike of the Jurassic host beds. Thick Cenozoic-Upper Cretaceous formations cover the eastern margin of Primorye, and the meymechite-picrite rocks crop out in rare eroded "windows" of the Lower Mesozoic formations. Along the eastern side of the Khanka massif occurrences of the meymechite-picrite complex are combined with outcrops of the stockpiled Devonian ophiolite complex [31].

Observation of the Jurassic cross-sections from south to north of the Sikhote-Alin' range (Fig. 2) shows that the meymechite-picrite volcanics appear at the lowermost parts of the sections and extend to the uppermost parts of the Jurassic sequence, where they are covered by the Lower Cretaceous sedimentary

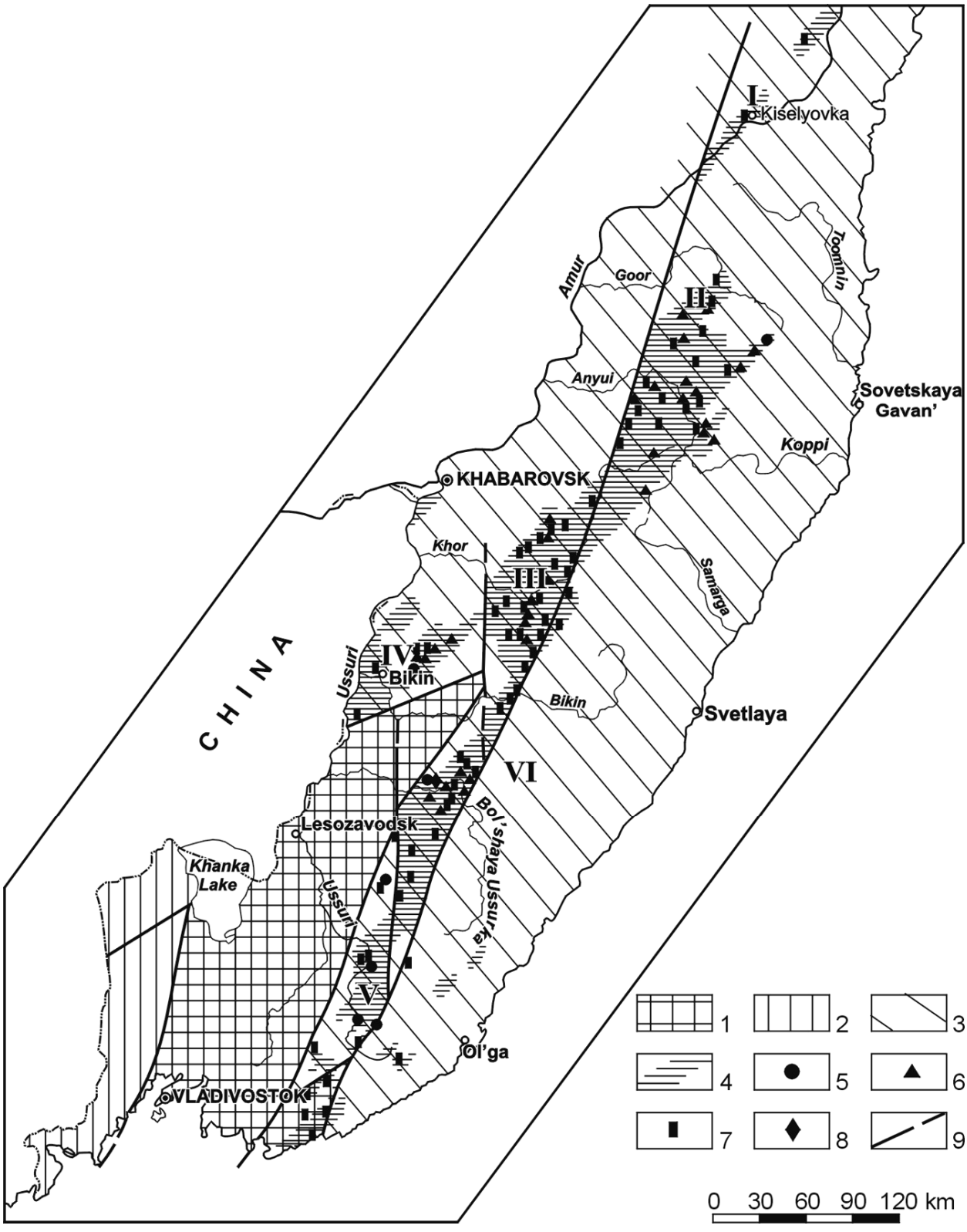

Fig. 1. *Location map of the meymechite-picrite complex in Primorye.*

Compiled by A.A. Vrzhosek. 1 - Khanka crystalline massif; 2 - Late Paleozoic zone; 3 - Mesozoic zone; 4 – volcanic area of the Jurassic volcano-chert series; 5-7 - alkali-ultrabasic complex: 5 - diatremes, 6 - meymechite subvolcanic bodies; 7 - dunite-pyroxenite ring intrusions; 8 - diamond occurence at the placer; 9 - general faults. Roman numerals show location of the studied area: I to V- Fig. 2; VI - Fig. 3.

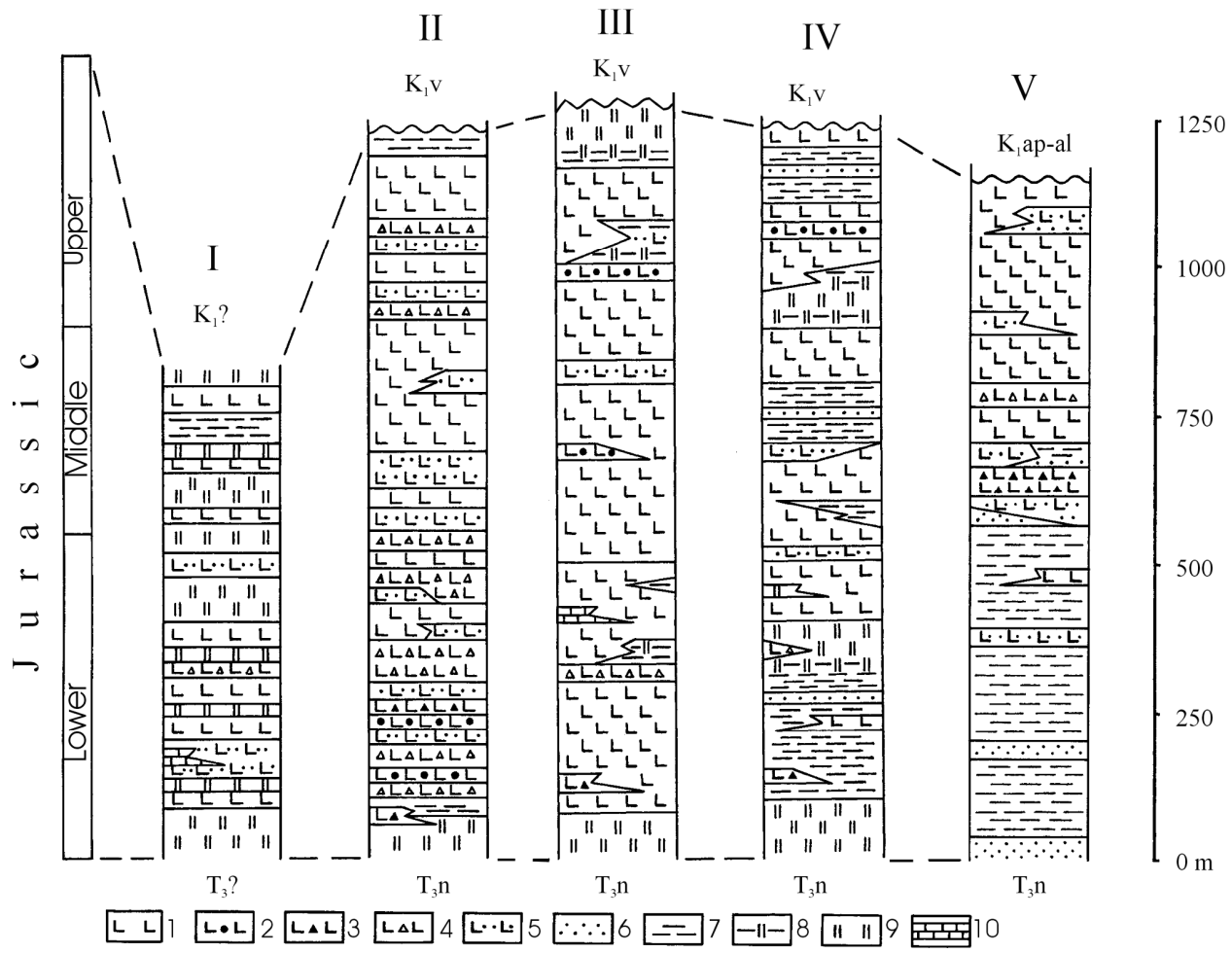

Fig. 2. *Correlation of Jurassic cross-sections of the Sikhote-Alin' Mountains.*

See Fig. 1 for location. 1 - massive lava; 2 - variolitic lava; 3 - autobrecciated lava; 4 - agglomerate tuff; 5 - tuff; 6 - sandstone; 7 - siltstone; 8 - siliceous mudstone, siltstone, 9 - chert, 10 - limestone.

formations enclosing sills of the Apt-Albian trachybasalt (110-112 Ma, K-Ar method, whole rock, our data). The K-Ar data of coexisting kaersutite and Ti-biotite from the latest picrite pipes and from the ring intrusion near village Ariadnoe show a short age interval - 152-159 Ma (159-157 and 157-152 Ma).

Some lateral change of the Jurassic formation are observed from south to north of the Sikhote-Alin' (as same as to northward from Khanka massif) (Fig. 2). A portion of the volcanics and cherts increases in this direction as well as continental sediments are replaced by shallow-water marine sediments. The proper changes are also seen in composition of the magmatic complex. Picrites and leucocratic basaltoids (phonolite, trachyte) with syenite (carbonatite) - pyroxenite ring bodies (villages Koksharovka, Ariadnoe) near margin of the Khanka massif to northward grade into meymechite and non-differentiated dunite-wehrlite intrusions (rivers Katen, Aniuy).

The most typical area of the meymechite-picrite magmatism is shown on Fig. 3. All the mapped series extend along NE direction and are broken by

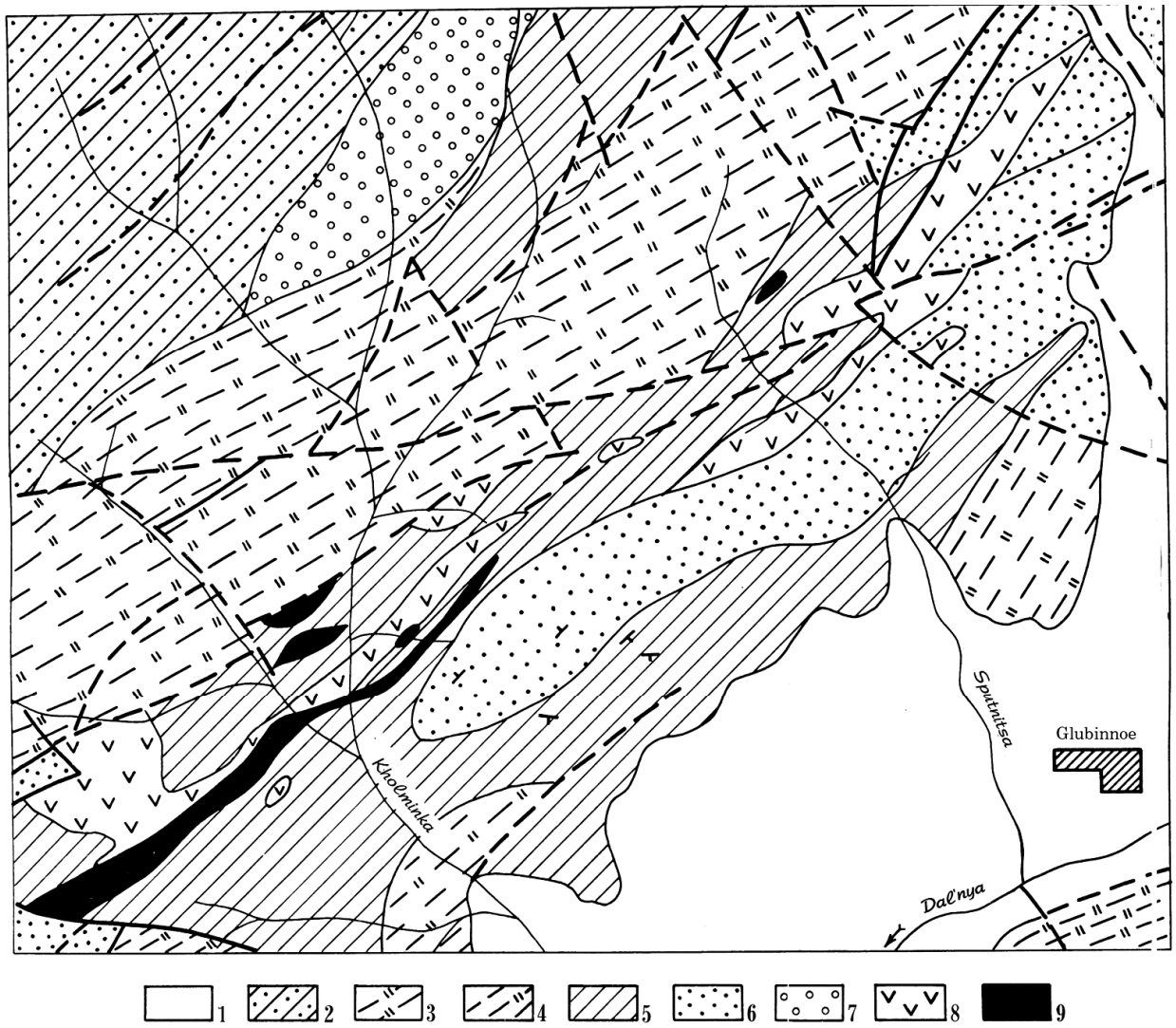

Fig. 3. *Geological map of the typical area of meymechite-picrite magmatism.*

1 - Quaternary sediments; 2-6 - Jurassic formation: 2 - dark grey sandstone, mudstone; 3 - chert; 4 - chert with layers of mudstone and volcanics, 5 - mudstone with layers of chert and volcanics; 6 - siltstones with layers of mudstone and chert; 7 - Upper Permian sandstone; 8- meymechite, picrite, alkaline basalts; 9 - wehrlite, dunite, pyroxenite, serpentinite (not divided).

numerous faults so the blocks are in fault contacts. NW part of the area adjacent to the Khanka massif is composed of terrigenous Upper Permian block unconformably covered by various levels of the Upper Jurassic series of black mudstone and sandstone. The SE part of the area is characterized by siliceous cross-section composed of alternation of light chert and dark mudstone. The base of the siliceous sequence outcropped at the top of anticlinal rise is dated by Radiolarians as Middle Jurassic. To the uppermost this series is covered by chert-rich series of the Upper Jurassic age. The volcanic rocks represented by alternation of picrite, alkaline basalt and sills of meymechite enclosed in the various lower levels of the sequence and are cut by linear clinopyroxenite-wehrlite intrusions.

Marginal parts of the intrusions are composed of quench-textured clinopyroxenite and the volcanics are transformed into pyroxene hornfelses.

Finally, it is necessary to note that the Jurassic terrigenous rocks associated with the volcanics are represented by both greywacke and arkose varieties that may be indication of their formation at the slope of the Khanka massif and onto stockpiled ophiolites.

Occurrences of rocks of the meymechite-picrite complex in Japan are mostly concentrated in Circum-Izu Massif (Setogawa, Kobotoke, Mineoka belts) on the Pacific coast of Central Japan [25, 36, 38, 35, 15-16]. The alkaline basic-ultrabasic volcanics close in details to Sikhote-Alin' ones are represented here by quenched pillow lavas (Mineoka belt), dikes and sills (Setogawa belt) or small mass enclosed by greenish sandstone (Kobotoke belt). The meymechite and picrite are associated here with Hawaii-type basalt. In all places they are hosted by fresh Paleogene sandstone and mudstone and considered to be of Paleogene age but some data contradict this opinion. Ishida et al. [15] have noted that the Paleogene sandstone and mudstone "have clasts derived from picrite basalt and related rocks". The most volcanics are metamorphosed in greenschist facies and crushed at the marginal sides of the bodies. Observations of S.V. Vysotskiy during geological excursion at the Mineoka belt showed that the peridotite and meymechite occur as olistolith within Paleogene matrix. So, it may be supposed that ultrabasic volcanics in Japan are older and may belong to the Jurassic chert-sedimentary formation of the Mikabu belt [18] where that kind of rocks was known before [13]. According to its composition and structure of cross-section and to Radiolarian fauna this belt is identical to Primorye Jurassic formation.

The meymechite-picrite volcanics in Primorye were presumably forming in submarine behavior. This is supported by both a regular association of lava with marine sediments and by presence of pillow-lava with specific quench crusts and by widespread occurrence of autobrecciated lava and hyaloclastite. In addition, in the northern areas (Rivers Bikin, Khor and Aniuy), volcanic activity took place in more deep conditions at the same time with the shallow-water and subaerial volcanism in the southern areas. The latter is characteristic of the meymechite-picrite occurrences associated with the outcrops of Paleozoic ophiolite closer to the boundary of the Khanka massif. However, constituents of the volcanic cross-section are kept constant over the Sikhote-Alin' Mountains. They include psephite vitroclastic tuff and autobrecciated lava intercalated with hyaloclastite, tuffaceous conglomerate and aphyric picrite lava. Above these, it is observed an intercalation of leucocratic and melanocratic (partly picritic) alkaline basalts. They are covered by porphyritic lava of picrite basalt with large phenocrysts of Ti-augite. The uppermost of the section is composed of fluidal picrite lava and picrite basalt enriched in kaersutite. Intercalation of the volcanic rocks with tuffaceous siltstone, sandstone, clay and chert-clay shales is often observed. Upward the section, numerous sills of meymechite and subvolcanic bodies of diabase, gabbro and peridotite are often observed. A thickness of the meymechite and picrite sills is not

more than fifty meters and length is about some hundreds of meters. In the some area, the explosive picrite and alkaline basalt pipes are present, and they are located within or outside the volcanic series. Diameter of the pipes ranges from 0.4 m to some tens of meters. Recently I.P. Voinova and V.S. Prihod'ko [45] have found meymechite pipes which are located near Aniyuy metamorphic block hosted by Mesozoic formation.

Intrusive member of the complex is represented by two kinds of massifs [27]. The first one occurs as small (2-3 - 15 km^2) elongated bodies differentiated from dunite (in interiors) through wehrlite to clinopyroxenite and gabbro sometimes cut by syenite and carbonatite. They are closer to the Khanka massif and are hosted by black shales and cherts and, at the same time, are intruded by the final explosive picrite pipes. They usually bear ores. Gabbro and pyroxenite include iron-titanium deposits with gold and platinum mineralization, and alkaline rocks contain REE mineralization. It is established that Fe-Ti mineral of the massifs emplaced in black shales and cherts (enriched in organic matter) is ilmenite while the ore mineral of massifs hosted by rocks lack in organic matter is Ti-magnetite. Rich ilmenite placers with commercial content of gold and platinum accompany the massifs.

Large (up to 15 km) elongated massifs are placed in volcanic and siliceous bedrocks. They are not differentiated and composed of wehrlite with dunite lenses penetrated by numerous veins of pegmatitic, metasomatic clinopyroxenite. According to bulk chemistry, the massifs are an intrusive analog of the meymechite.

PETROLOGY, MINERALOGY AND GEOCHEMISTRY

According to petrological-mineralogical and geochemical characteristics, meymechite-picrite complexes in Primorye and Japan resemble, and they will be described together. Typical rocks of the complexes are meymechite and picrite, although melanocratic alkaline basalt prevails in volume.

The meymechite is easily recognized on weathered surface due to presence of light grey, well-shaped tablets of olivine within dark interstitial material. The resemblance of olivine tablets to plagioclase often results in confusion of meymechite and porphyric basalt by mapping geologists. The olivine-rich rocks are sometimes similar to intrusive peridotites, and the marginal facies of the subvolcanic intrusions is composed of peridotite with well-shaped olivine grains. However, presence of fibrous laths of Ti-augite and kaersutite as well as of rounded glass inclusions in olivine allows us to distinguish meymechite from peridotite.

The meymechite is coarse-porphyritic rock (Fig. 4) composed of large (from 5-8 up to 30 mm) well-faceted tablets of olivine, which sometimes show a clear lineation. Large (8-30 mm) individuals are distinguished among the granular (3-5 mm) olivine aggregate. An olivine content ranges within 70-85 vol.%. Opaque rhombic inclusions in olivine and in matrix are represented by spinel. At the lava and pyroclastic varieties small (0,5-1 mm) tablets of Ti-augite appear among the

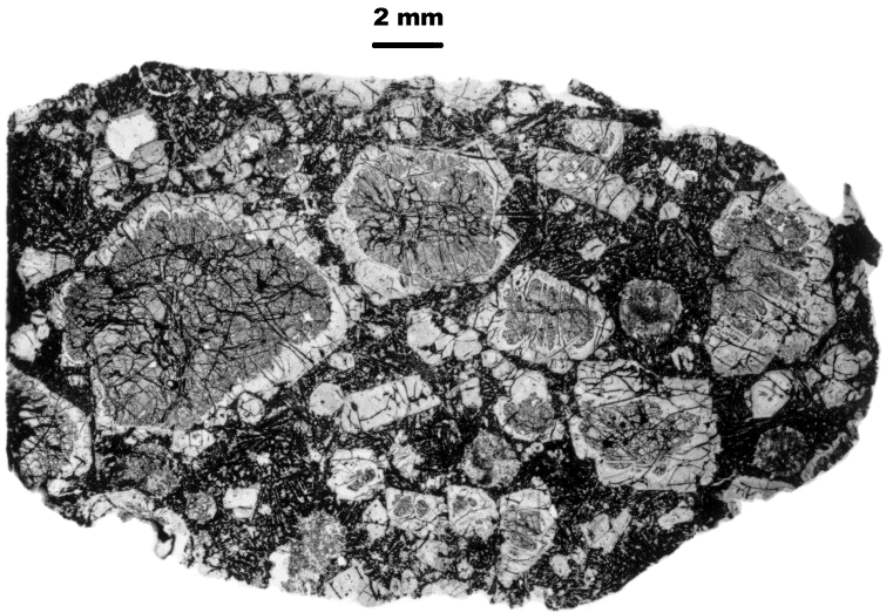

Fig. 4. *Typical microscopic texture of meymechite. Olivine phenocrysts are rimmed by serpentine. Open polar.*

phenocrysts as same as kaersutite and Ti-phlogopite - in subvolcanic bodies. The phenocrysts are surrounded by fine-grained fibrous matrix consisting of fine lathes of Ti-augite, Ti-magnetite, ilmenite and various quantities of glass. In the subvolcanic bodies, Ti-augite and glass are completely displaced with kaersutite and phlogopite. The Ti-augite and kaersutite lathes envelope olivine phenocrysts. The glass content depends on crystallization degree and reaches maximum at the pillow crusts. A disarranged fibrous aggregate of Ti-augite in such areas has the spinifex-like texture.

The picrite differs from the meymechite by displacement of olivine with large (up to 30 mm) Ti-augite phenocrysts within fibrous or spinifex-like groundmass. The last is highly porous that is characteristic of all rocks of the complex. The Ti-augite phenocrysts show a multiply zoning.

The picrite breccia of the explosive pipes differs from the volcanic picrite by the presence of the giant (up to 70 mm) crystals of kaersutite, Ti-phlogopite, megacrysts (8-12 mm) of olivine, magnetite, and clinopyroxene, large (up to 0.5 m) inclusions of wehrlite and host rocks. The groundmass contains calcite, which may be considered to be magmatic.

Among the alkaline basalts melanocratic varieties are prevail but leucocratic ones (phonolite, trachyte) appear near boundary with Khanka massif. The specific feature of the rocks at such areas is widespread occurrence of globular varieties in which glassy spheres are included in glassy groundmass. The globules and the matrix are distinctly different in chemistry (e.g. in K and Na), indicating liquid immiscibility [30].

Compositions of the magmatic minerals from Primorye and Japan are same (Table 1). The liquidus olivine is characterized by the elevated Ca-content with

Table 1. *Chemical composition of selected minerals from rocks of the meymechite-picrite complex of Primorye and Japan*

	1	2	3	4	5	6	7	8	9	10	11	12	13	14	15	16	17	18	19	20
SiO_2	40,58	38,89	40,11	39,59	53,01	43,11	50,83	44,19	38,68	39,18	38,22	n.d.	n.d.	n.d.	n.d.	0,57	0,34	38,63	43,30	37,33
TiO_2	0,02	0,02	0,01	n.d.	0,67	4,27	1,24	4,22	6,97	5,87	6,25	2,31	1,44	20,07	46,62	1,52	13,11	5,77	3,51	5,53
Al_2O_3	0,01	0,01	0,03	n.d.	2,27	10,27	3,68	8,97	14,30	13,04	13,14	13,21	17,09	5,23	0,33	15,32	5,07	11,33	12,57	15,68
Cr_2O_3	0,01	0,01	n.a.	n.a.	0,61	0,12	0,76	n.d.	n.d.	n.d.	n.a.	46,12	40,45	n.d.	n.d.	45,00	27,61	n.d.	n.d.	n.d.
Fe_2O_3	n.a.	n.a.	n.a.	n.a.	n.a.	n.a.	n.a.	n.a.	n.a.	n.a.	n.a.	9,42	10,27	21,88	12,88	6,78	10,81	n.a.	n.a.	n.a.
FeO	10,16	19,10	9,49	13,67	5,67	9,67	6,05	10,73	10,49	12,91	10,05	18,61	19,54	46,20	38,11	20,12	37,06	11,78	11,05	10,14
MnO	0,10	0,10	0,23	0,21	0,12	0,17	0,05	0,09	0,04	0,05	0,05	0,39	0,37	2,17	1,59	0,37	0,52	0,09	0,13	0,05
MgO	48,39	40,65	49,33	46,45	17,42	10,97	15,07	10,12	12,24	15,68	19,05	11,55	10,30	0,78	1,37	9,73	5,10	8,17	13,21	16,36
CaO	0,26	0,42	0,25	0,34	20,19	21,28	21,53	20,18	11,78	0,01	0,07	n.d.	n.d.	n.d.	n.d.	0,07	n.d.	21,92	9,81	0,03
Na_2O	n.d.	n.d.	n.d.	n.d.	0,18	0,40	0,38	0,44	2,86	0,55	0,62	n.d.	n.d.	n.d.	n.d.	n.d.	n.d.	0,59	2,49	0,64
K_2O	n.d.	n.d.	n.d.	n.d.	n.d.	n.d.	0,02	n.d.	0,69	8,85	8,39	n.d.	n.d.	n.d.	n.d.	n.d.	n.d.	0,05	1,87	9,19
Total	99,53	99,20	99,45	99,43	100,14	100,27	99,62	98,94	98,06	96,14	95,84	101,61	99,68	96,33	100,94	99,48	99,62	98,32	97,87	95,17
$Fe^{\#}$	10,5	20,9	9,7	14,0	15,4	31,1	18,3	37,3	32,4	31,6	23,0	56,8	51,6	98,0	94,0	60,2	83,7	44,7	32,0	25,8
$Cr^{\#}$					15,2	0,8	12,2					70,1	61,4			66,3	21,5			
$Fe^{+3\#}$												31,3	32,1	29,9	23,9	23,3	20,8			

Notes. *1-4 olivine; 5-8 - Ti-augite; 9, 19 - kaersutite; 10-11, 20 - phlogopite; 12-13, 16, 17 - Cr-spinel; 14 - Ti-magnetite; 15 - ilmenite. 1-17 - meymechites, 18-20 - picrite. 1-2, 7-10, 12-15, 18-20 - from Primorye (1-2, 7-10 - river Bikin, near IV, Fig. 1; 12-15 - river Katen, near III, Fig. 1; 18-20 - village Ariadnoe southward VI, Fig. 1); others - from Japan [38]. Fe^{+2} and Fe^{+3} in spinels are calculated according to stoichiometry. $Fe^{\#} = Fe/(Fe + Mg)$; $Cr^{\#} = Cr/(Cr + Al)$; $Fe^{+3\#} = Fe^{+3}/Fe_{tot.}$. All ratios in at, %. n.d., n.d - not detected, not analysed.*

Table 2. *Average compositions of meymechites, picrites and komatiites*

	Alkaline suite							Tholeiitic suite					
	1 (17)	2 (1)	3 (1)	4 (9)	5 (2)	6 (21)	7 (16)	8 (35)	9 (3)	10 (5)	11 (15)	12 (8)	13 (6)
SiO_2	42,51	41,73	41,01	43,41	46,57	39,89	41,13	45,14	43,80	47,24	44,36	46,33	45,89
TiO_2	1,24	2,02	3,05	1,14	1,19	2,23	3,23	0,35	0,38	0,40	0,22	0,34	0,23
Al_2O_3	5,39	8,56	9,60	6,24	8,08	2,49	4,79	5,05	7,94	8,52	4,81	3,01	5,40
Fe_2O_3	6,20	10,07	4,25	4,53	2,27	7,04	8,56	4,83	3,88	3,37	5,62	6,27	2,81
FeO	7,58	6,61	8,07	7,80	12,30	6,92	7,26	5,73	6,64	6,87	4,39	4,84	6,49
MnO	0,26	0,23	0,24	0,18	0,19	0,20	0,23	0,19	0,18	0,17	0,17	0,19	0,16
MgO	30,94	18,73	17,45	30,96	21,88	35,71	22,41	32,59	30,92	23,19	36,21	34,04	33,94
CaO	4,85	9,92	15,82	4,69	6,38	4,30	10,63	5,38	5,38	8,14	3,90	4,78	4,64
Na_2O	0,34	1,07	0,55	0,56	0,82	0,11	0,49	0,24	0,39	1,27	0,12	0,17	0,38
K_2O	0,20	0,11	0,22	0,18	0,36	0,32	1,08	0,50	0,20	0,78	0,20	0,03	0,06
Cr_2O_3	0,26	0,18	n.a.	0,35	0,04	0,45	0,09	n.a.	0,21	0,20	n.a.	n.a.	n.a.
NiO	0,19	0,16	n.a.	0,20	0,06	0,27	0,05	n.a.	0,15	n.a.	n.a.	n.a.	n.a.
Total	99,96	99,49	100,26	100,24	100,14	99,94	99,95	100,00	100,07	100,15	100,00	100,00	100,00
f	19,2	31,1	27,7	17,8	26,9	18,9	27,2	14,8	15,5	19,3	12,8	14,7	13,0

Notes. *1, 2 - Sikhote-Alin'; 3 - Sakhalin; 4 - Japan; 5- New Zealand [6]; 6-7 - Maymecha-Kotuy region [39]; 8 - Kamchatka; 9 - Olyutorskiy gulf [12]; 10 - Solomon Islands [34]; 11 -Western Australia [23, 46]; 12 - Komati formation, Africa [42 -43]; 13 - Cyprus [11]. 1, 4, 6 - meymechites; 2,3, 5, 7, 10 - picrites and the others - komatiites. Numerals in brackets - analysis numbers. All analyses are recalculated on volatile free matter. f = Fe/(Fe + Mg) at.%.*

trace amounts of Al, Ti, Cr as usual and Fa content of 10-15 atomic per cent. Even the largest (up 15 mm) phenocrysts do not show compositional zoning. The solidus olivine in matrix is more ferrous (up to 22% Fa). The spinel is enriched in titanium with high Cr# and Fe# and in contrast to olivine shows transition to high Ti-magnetite at the grain margins (Table 1, №s 14, 17). The same transition (from chromium to high Ti) is characteristic of clinopyroxene. In the extrusive picrites it is observed multiply intercalation of Cr and Ti zones within the large phenocrysts of clinopyroxene. High Ti-content is characteristic of hornblende and mica from the subvolcanic bodies. In addition, Al in these minerals occupies an Al^{IV} position, and kaersutite is enriched in potassium. Elevated Mg and Mn content characterize ilmenite and magnetite from the matrix of the more crystallized rocks at the same time. The magnetite is close to ulvospinel (including up to 25 wt.% TiO_2).

According to chemical composition (Table 2), the meymechite corresponds to wehrlite, whereas picrite corresponds to clinopyroxenite, and transitional varieties between them are absent. The higher alkalinity of the rocks is emphasized by their high Ti-content and by coherent with alkalis minor elements (Table 3) and volatiles. Picrite of the explosive pipes are usually enriched in potassium. It would be noted that $^{87}Sr/^{86}Sr$ ratio is the same in melanocratic and leucocratic rocks as well as in globule-groundmass pair or in carbonatite, proving a unity of their initial magma source [30].

Table 3. *Trace elements abundancies (ppm) in the meymechites and komatiites*

	Alkaline suite		**Tholeiitic suite**	
	1 (12)	2 (42)	3 (7)	4 (30)
Cr	2000	3095	2996	3190
Ni	1300	2115	1530	1931
Co	120	142	103	108
V	86	170	120	92
Zr	60	140	15	23
Sr	35	350	19	26
Rb	12	12	0,7	0,9
Ba	40	195	4,7	7
Nb	14	24	1,2	2,0
U	0,26	0,9*	0,03*	0,03*
F	300	420*	< 100*	< 100*
P	440	960	160	110
$^{87}Sr/^{86}Sr$ initial	0,7036-0,7040	0,7031-0,7037	0,7015-0,7025	0,7005-0,7015

Notes. *1 - Sikhote-Alin'; 2 - Maymecha-Kotuy region [41]; 3 - Western Australia [20, 8]; 4 - Southern Africa [33, 17, 8]. Numerals in brackets - analysis number.* -author's data.*

DISCUSSION

Geochemical analyses (Tables 2 and 3) show that two magma types, tholeiitic and alkaline, are clearly distinguished. A low primary alkaline content and a heavy alteration masks an alkalinity difference between ultrabasic members of the complexes, and therefore it is revealed using some correlations of the coherent elements. The most favorable indicator of this is mutual change of Fe/(Mg+Fe) ratio and Ti content (Fig. 5). This demonstrates that the points of all rocks either from the Precambrian komatiite complexes or partly from the younger ones of the Pacific belt (Kamchatka, Olyutorsky gulf, Solomon and New Hebrides Islands) form a single trend slightly inclined towards Fe/Mg axis as distinct from one of the rocks of the alkaline complexes (Primorye, Sakhalin and Japan). The steepest angle shows a differentiation trend of the alkaline complexes of Siberian platform, including kimberlite. Trend of the ophiolite ultrabasic rocks coincides with the komatiite one. Above difference between two magma types is outlined by isotopic and trace element data (Table 3) - the rocks of alkaline suite are richer in Zr, U, Sr, Ba and Rb as compared with the tholeiitic analogs.

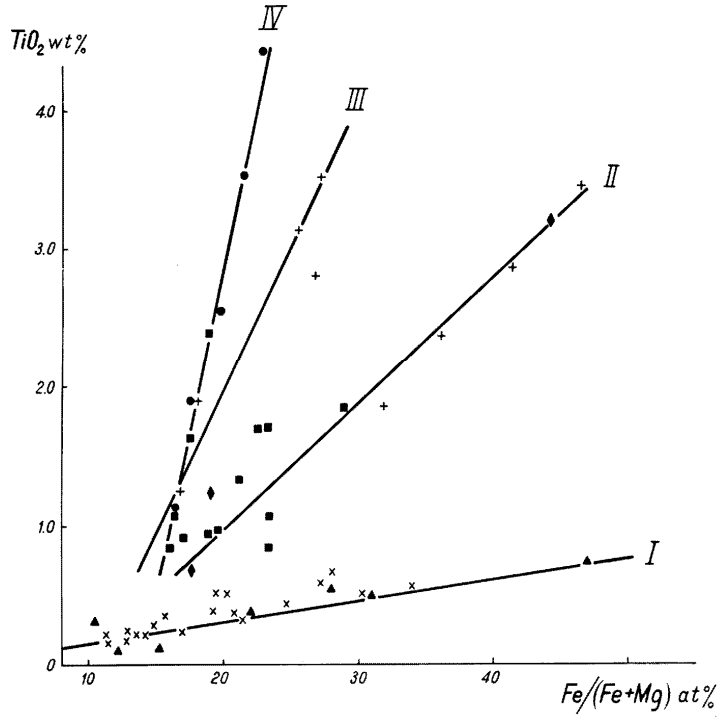

Fig. 5. *TiO_2 vs. Fe/(Fe + Mg) plot for the bulk rock compositions.*

Oblique crosses - lavas and subvolcanic bodies, triangles - intrusions, both from the tholeiitic suite; others - from the alkaline suite: right crosses - lavas, circles - diatremes, squares - subvolcanic bodies, rhombs - intrusions. The lines show trends of chemical evolution of the magmas: I - tholeiitic suite; II-IV - alkaline suite: II - Mesozoic-Cenozoic complexes of the Pacific belt, III - Maymecha-Kotuy region, IV - Siberian kimberlite.

A regular change in composition of liquidus phases of the tholeiitic and alkaline magmas is observed. Fe content of olivine in plagioclase-free komatiites

ranges from 8 up to 12% Fa and from alkaline meymechites - 8-22%. Titanium (0.01-0.05% TiO_2), calcium (0.2-0.5% CaO), aluminum (0.01-0.04% Al_2O_3) and chromium (0.01-0.70% Cr_2O_3) appear in the olivine of both complexes. Liquidus pyroxenes from komatiite have a lower iron, titanium and aluminum content together with slightly higher chromium content. However, most remarkable difference between alkaline and tholeiitic members and ultrabasic rocks of the other complexes is shown by spinel compositions (Fig. 6). Komatiitic spinels from both younger and older complexes fall on the plot in the same areas as ones of tholeiitic basalts and non-ophiolite ultrabasic rocks, whereas the spinels from alkaline analogs are mainly distributed within an area of the lunar (marine) spinels, i.e. they are enriched in chromium and titanium at the same time. In addition, trends of tholeiitic spinels in the "lava flows-subvolcanic bodies-intrusive bodies" sequence are parallel to Al-Cr axis, and Al increases in this order. On the other hand, spinels from the rocks of alkaline suite form a number of individual fields subparallel to Ti-Cr axis. Possibly this may be due to crystallization of the spinel from ultrabasic magma of basalt series (rich in titanium).

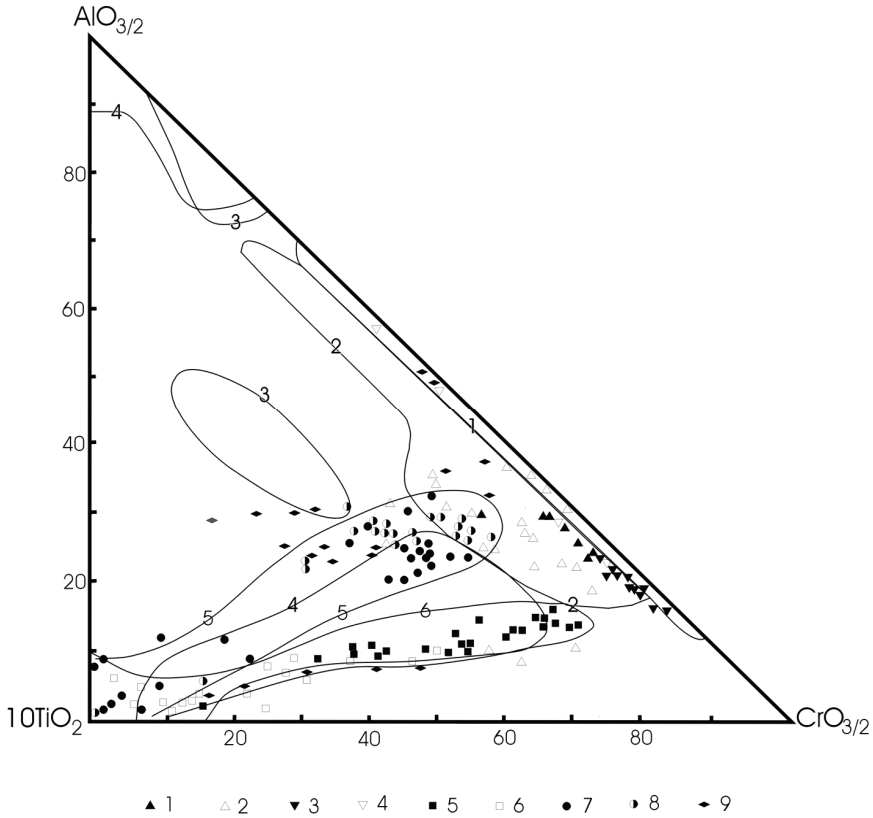

Fig. 6. *Compositions of magmatic spinels from the meymechite, komatiite and other basic-ultrabasic associations.*

1-4 - tholeiitic suite: 1 - komatiite of Canada [1], Australia [22], Africa [24]; 2 - zonal ultrabasic intrusions of Alaska [14, 5]; 3 - meymechite of Kamchatka [3]; 4 - high-level intrusions of Kamchatka. 5-11 - alkaline suite: 5-6 - meymechite (5) and associated high-level intrusions (6) of Maymecha-Kotuy region [40]; 7 - meymechite of Sikhote-Alin`; 8 - meymechite of Japan [36,38, our data]; 9 - dikes of micaceous kimberlites of Canada [46, 21]. Areas of spinel compositions are outlined: I - ophiolitic ultrabasic rocks; 2 - gabbro-peridotite (non-ophiolitic) intrusions and tholeiitic basalts; 3 - ultrabasic inclusions in alkaline basalts and kimberlites; 4 - lunar basalts; 5 - meymechites and picrites of Sikhote-Alin` and Japan; 6 - meymechites of Maymecha-Kotuy region.

Geochemical evolution of the meymechite (komatiite) magmas is accompanied by a regular change of chemistry in the enclosing basalts [29]. The

latter from Precambrian komatiite complexes are represented by typical low-potassium island arc tholeiites with boninite affinity. On the contrary in all the younger zones of komatiite magmatism (Chukotka, Kamchatka, Solomon and New Hebrides Islands) a distinct enrichment of associated tholeiitic basalts in potassium is remarked. Both older (Precambrian) and younger basalts are characterized by low Ti-content, i.e. the complexes of tholeiitic suite are the branches of divergent evolution of a single deep magmatic chamber.

The basalts related to the alkaline meymechite-picrite complexes (Primorye, Sakhalin, New Zealand, Japan, and Maymecha-Kotuy region) are characterized by a contrasting chemistry developed in coexistence of essentially sodium and potassium varieties, enriched in titanium [29, 26].

A number of specific types of ore deposits, which are not characteristic of the other magmatic complexes, are related to meymechite association. Besides kimberlites, the diamonds were recently found in lamproites, which are undoubtedly a member of meymechite-picrite complex. This is supported by occurrence of "carbonado" (fine-grained diamonds) in the Primorye placers. Deposits of disseminated and schlieren ilmenite ores at the differentiated gabbro-peridotite intrusions are known in Primorye. In some intrusions both of tholeiitic and alkaline suite the gold - platinum mineralization are revealed. Alkaline members (syenites) of the association carry a rare-metal mineralization. Hydrated mica (vermiculite) is sometimes formed in zones of alkaline metasomatism in ultrabasic rocks. In contrast to the meymechite association the komatiitic intrusions emplace gold and copper-nickel sulfide deposits only.

All data above allow us to conclude that the meymechite-picrite complex of Primorye and Japan is alkaline analog of the komatiite complex. The higher alkalinity of the meymechite-picrite complex is caused by specific volatiles (F, P) participated in fusion and evolution of the meymechite-picrite melts. There may be some doubts that high magnesium content of the meymechites is due to accumulation of olivine crystals in picrite melt but existence of giant mass of subvolcanic dunite (Guli pluton at the Maymecha-Kotuy region) supports an autonomy of olivine-rich melts.

CONCLUSIONS

(1) More than 100 occurrences of the meymechite-picrite suite are found from Primorye, and most of them are associated with the Jurassic chert-volcanic formation. They occur as pillow lavas, volcanic breccias and associated subvolcanic plutons as well as diatremes.

(2) The meymechite-picrite suite of Primorye resembles in details to ultrabasic volcanics reported from Japanese Mesozoic and Cenozoic accretionary complexes. They show common characteristics in bulk-rock and mineral chemistries, which are distinct from those of komatiite (tholeiitic) suite. Generally the rocks of the same bulk composition of both complexes are common in contents of siderophile elements (Cr, Ni, Co, V) but differ in lithophile elements (Zr, Sr, Rb,

Ba, U) abundances as well as by Sr-isotope ratio that may be explained by enrichment of alkaline melts in F and P volatiles.

(3) The meymechite-picrite suite at the Primorye-Japan area is less in TiO_2 contents of bulk rock, and also poorer in Ti and Cr of spinel than those of typical meymechite at the Maymecha-Kotuy area of northern Siberia. Possibly this is consistent with the different tectonic settings of the two areas: the Circum-Pacific orogenic belt and the margin of continental craton.

(4) The volcanics of both alkaline and tholeiitic suites are accompanied by ring dunite-pyroxenite intrusions with chromite-platinum and ilmenite deposits. Although the komatiite volcanics bear sulphide Cu-Ni deposits, fine-crystalline diamonds are found in the Primorye placers in the area of potassium-rich diatremes.

(5) Spinels of the meymechite-picrite suite are rich both in Ti and Cr resembling to those from lunar (marine) basalts. These spinels are clearly different from those of komatiite-basalt suite, and this may be due to deep mantle origin of the meymechite-picrite melts.

ACKNOLEDGMENTS

The authors are thankful to Dr. A. Ishiwatari for useful advices and corrections of our manuscript.

REFERENCES

1. **Arndt N.T.** (1977) Thick, layered peridotite - gabbro lava flows in Munro Township, Ontario. Can. Jour. Earth Sci., 14: 2620-2637.
2. **Arndt N.T., Lennert V. and Vasiliev Yu.R.** (1995) Meimechites: highly magnesian litosphere-contaminated alkaline magmas from deep subcontinental mantle. Lithos, 34: 41-59.
3. **Bagdasarov E.A., Landa E.A. and Markovskiy B.A.** (1979) Chemical composition and crystallization behavior of chromian spinels in the volcanic ultramafics and in other rocks of mafic-ultramafic series. Zap. V.M.O., 108: 524-535.*
4. **Beliy V.F. and Gel'man M.L.** (1980) Meymechites in the Penginskiy Range. Ac. Sci. USSR. Dokl., 250: 928-932.*
5. **Bird M.L. and Clark A.L.** (1976) Microprobe study of olivine chromitites of the Goodnews Bay ultramafic complex, Alaska, and the occurrence of platinum. Jour. Geophys. Res. U.S. Geol. Surv., 4: 717.
6. **Challis G.A.** (1971) Chemical analyses of New Zealand rocks and minerals with C.I.P.W. norms and petrographic descriptions, 1917-57. N.Z. Geol. Surv. Bull., 84: 178 p.
7. **Colley H. and Warden A.J.** (1974) Petrology of the New Hebrides. Geol. Soc. Amer. Bull., 85: 1635-1646.
8. **Condie R.C.** (1981) The Archean green stone belts. Elsevier Sci. Publ. Comp. Amsterdam - Oxford- New York. 390 p.
9. **Echeverria L.M.** (1980) Tertiary or Mesozoic komatiites from Gorgona Island, Colombia: field relations and geochemistry. Contrib. Mineral. Petrol., 73: 253-266.
10. **Gansser A., Deitrich V.J. and Cameron W.E.** (1978) Paleogene komatiites from Gorgona Island. Nature, 278: 545-546.
11. **Gass I.G.** (1958) Ultrabasic pillow lavas from Cyprus. Geol. Mag., 95: 241-251.

12. Geologiya SSSR (1970) V. XXX, II. Nedra, Moscow, 536 p.*
13. **Inomata M. and Tazaki K.** (1974) Phlogopite and kaersutite bearing ultramafic rocks from the Mikabu zone, Central Japan. Jour. Japan. Assoc. Min. Petr. Econ. Geol., 69: 205-214.
14. **Irvine T.N.** (1967) Chomian spinel as a petrogenetic indicator. Can. Jour. Earth Sci., 4: 71-103.
15. **Ishida T., Arai Sh. and Takahashi N.** (1988) The occurrence of picrite basalt in Kobotoke group, the Hatsu-Kari arrea, Yamanashi Prefecture, Central Japan. Jour. Japan Assoc. Mineral. Petrol. Econ. Geol., 83: 43-50.
16. **Ishida T., Arai Sh. and Takahashi N.** (1990) Metamorphosed picrite basalts in the nothern part of the Setogawa belt, Central Japan. Jour. Geol. Soc. Japan, 96: 181-191.
17. **Jan B.J. and Shih C.Y.** (1974) Onthe age of rthe Onverwacht Group, Swaziland Sequence, South Africa. Geochim. Cosmochim. Acta, 38: 873-875.
18. **Kimura G.** (1997) Cretaceous episodic growth of the Japanes Islands. The Island Arc., 6: 52-58.
19. **Levinsson-Lessing F.Y. and Strouve E.A.** (1963) Petrographic dictionary. Gosgeoltekhizdat, Moscow. 448 p.*
20. **Markovskiy D.A. and Rotmann V.K.** (1975) Geochemistry of the Kamchatka ultrabasic volcanic province. Soviet. Geol., № 1: 70-82.*
21. **Mitchell R.H.** (1978) Composition of spinels in micaceous kimberlite from the Upper Canada Mine, Kirkland Lake, Ontario. Can. Mineral., 16: 591-595.
22. **Moeskops P.G.** (1977) Volume increase serpentinization in Archean quench texture ultramafic rocks near Kalgoorlie, Western Australia. Geol. Mag., 114: 41-46.
23. **Nesbitt R.W. and Sun Sh.-S.** (1976) Geochemistry of Archaean spinifex-textured peridotites and magnesian and low-magnesian tholeiites. Earth. Planet. Sci. Lett., 31: 433-453.
24. **Nisbet E.G., Bickle M.J. and Martin A.** (1977) The mafic and ultramafic lavas of the Belingwe green stone belt, Rhodesia. Jour. Petrol., 18: 521-566.
25. **Sameshima T.** (1960) Picrite basalt dikes in the Paleogene formation in Central Japan. Rept. Liberal Art Sci. Fac. Shizuoka Univ., Sec. Nat. Sci. № 3: 77-80.
26. **Shcheglov A.D.** (ed) (1984) Volcanic belts of the Eastern Asia. Nauka, Moscow, 504 p.*
27. **Shcheka S.A. et.al.** (1973) The general regularities of evolution of basic-ultrabasic magmatizm in the Primorye. In: Shcheka S.A. (ed) Magmatic rocks of the Far East. Ac. Sci. USSR, Far East Centre, Vladivostok, 9-61.*
28. **Shcheka S.A.** (1977) Meymechite-picrite complex of the Sikhote-Alin'. Ac. Sci. USSR. Dokl., 234: 444-447.*
29. **Shcheka S.A. and Vrzhosek A.A.** (1983) Ultrabasic volcanism of the Pacific Belt and problem of definition of the meymechites and komatiites. Vulcanologiya i Seismologiya (Volcanology and Seismology), № 2: 3-15.*
30. **Shcheka S.A., Vrzhosek A.A., Grebennikov A.V. and Sawada Y.** (1999) Again on liquid immiscibility of the natural silicate melts. In: Khanchuk A.I. (ed) Geodynamics and Metallogeny. Dal'nauka, Vladivostok, 81-92.*
31. **Shcheka S.A., Ishiwatari A. and Vrzhosek A.A.** (2001) Geology and petrology of Cambrian Khanka ophiolite in Primorye (Far East Russia) with notes on its manganese-rich chromian spinel. Earth Science (Chikyu Kagaku), 55: 265-274.
32. **Shcheka S.A., Vrzhosek A.A., Chubarov V.M., Vysotskiy S.V.** (2003) Meymechite, komatiite, picrite: nomenclature, formations, melt composition. In: Polyakov G. V. (ed) Modern problems of the formation analysis, petrology and ore minerialization of magmatic complexes. Acad. Kuznetsov vol. RAS Publ. Novosibirsk, 396-397.*
33. **Smith H.S. and Erlank A.J.** (1982) Geochemistry and petrogenesis of komatiites from the Barberton green stone belt, South Africa. In: Arndt N.T. and Nisbet E.G. (eds) Komatiites.

George Allen and Unwin Publ., Boston-Sydney, 347-397.
34. **Stanton R.L. and Bell J.D.** (1969) Volcanic and associated rocks of the New Georgia Group, British Solomon Islands Protectorate. Overseas Geol. Miner. Resour., 10: 113-145.
35. **Takasawa K.** (1976) Olivine from the Takayama picrite in the Setogawa Group, Shizuoka Prefecture, Central Japan. Jour. Geol. Soc. Japan, 82: 765-771.
36. **Tazaki K.** (1975) Chromian spinels in picrite basalt from Mineoka tectonic belt, Boso Peninsula, Central Japan. Jour. Geol. Soc. Japan, 81: 399-406.
37. **Tazaki K.** (1976) Dendritic titanaugite in ultrabasic picrite basalt from Mineoka tectonic belt, Boso Peninsula, Central Japan. Jour. Geol. Soc. Japan, 82: 573-580.
38. **Tazaki K. and Inomata M.** (1980) Picrite basalts and tholeiitic basalts from Mineoka tectonic belt, Central Japan. Jour. Geol. Soc. Japan, 86: 653-671 (in Japanese with English abstract).
39. **Vasiliev Yu.R. and Zolotukhin V.V.** (1975) Petrology of ultrabasics in the North of Siberian platform and some problems of their genesis. Nauka, Novosibirsk, 272 p.*
40. **Vasiliev Yu.R., Konenko V.F. and Korolyuk V.N.** (1976) Accessory chromian spinels from ultrabasic rocks of the Maymecha-Kotuy region. In: Materiali po experimental'noy i geneticheskoy mineralogii, 10. Nauka, Novosibirsk, 7-16.*
41. **Vasiliev Yu.R. and Zolotukhin V.G.** (1995) The Maimecha-Kotuy alkaline-ultramafic province of the northern Siberia platform, Russia. Episodes, 2: 155-164.
42. **Viljoen M.J. and Viljoen R.P.** (1969a) The geology and geochemistry of the lower ultramafic unit of the Onverwacht Group and a proposed new class of igneous rocks, Spec. Publ. Geol. Soc. S. Africa, 2: 55-86.
43. **Viljoen M.Y. and Viljoen R.P.** (1969b) Evidence for the existence of a mobile extrusive peridotitic magma from the Komati Formation of the Onverwacht Group. Spec. Publ. Geol. Soc. S. Africa, 2: 87-112.
44. **Viljoen R.P. and Viljoen M.G.** (1982) Komatiites - an historial review. In: Arndt N.T., Nisbet E.G. (eds) Komatiites. G. Allen et Unwin, Publ, Boston-Sydney, 5-17.
45. **Voinova I.P. and Prihod'ko V.S.** (2002) Meymechites in the Central Sikhote-Alin'. In: Khanchuk A.I. (ed) Deep-seated magmatism, magmatic sources and the problem of plumes. Dalnauka. Vladivostok, 223-229.
46. **Watson K.D., Bruce G.S.W. and Halladay L.B.** (1978) Kimberlitic dike in Keith Township, Ontario. Can. Mineral., 16: 97-102.
47. **Williams D.A.C.** (1972) Archaean ultramafic, mafic and associated rocks, Mt. Morger, Western Australia. Jour. Geol. Soc. Aust., 19: 163-188.
48. **Zimin S.S., Starkov G.N. and Shcheka S.A.** (1965) On occurrence of meymechite in the Main Sikhote-Alin' Anticlinorium. In: Radkevith (ed) Problems of geology and ore formation of the Far East. Ac. Sci. USSR, Vladivostok, 194-195.*

** in Russian*